

DIAGNOZA - GENEZA - PROGNOZA => PODSTAWA KAŻDEJ DECYZJI

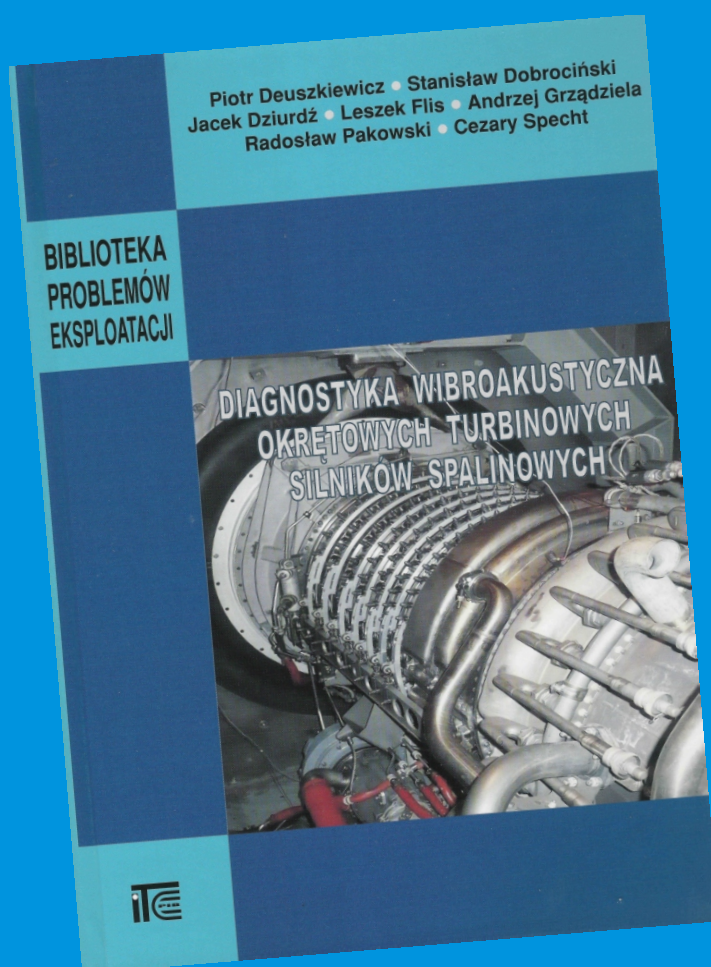


afiliowane przy

Wydziale Nauk
Technicznych
Polskiej Akademii Nauk

Diagnostyka

ISSN 1641-6414



Nr 4(52) / 2009

RADA PROGRAMOWA / PROGRAM COUNCIL

PRZEWODNICZĄCY / CHAIRMAN:

prof. dr hab. dr h.c. mult. **Czesław CEMPEL** *Politechnika Poznańska*

REDAKTOR NACZELNY / CHIEF EDITOR:

prof. dr hab. inż. **Ryszard MICHALSKI** *UWM w Olsztynie*

CZŁONKOWIE / MEMBERS:

prof. dr hab. inż. **Jan ADAMCZYK**
AGH w Krakowie

prof. **Jérôme ANTONI**
University of Technology of Compiègne – France

prof. dr. **Ioannis ANTONIADIS**
National Technical University Of Athens – Greece

dr inż. **Roman BARCZEWSKI**
Politechnika Poznańska

prof. dr hab. inż. **Walter BARTELMUS**
Politechnika Wroclawska

prof. dr hab. inż. **Wojciech BATKO**
AGH w Krakowie

prof. dr hab. inż. **Lesław BĘDKOWSKI**
WAT Warszawa

prof. dr hab. inż. **Adam CHARCHALIS**
Akademia Morska w Gdyni

prof. dr hab. inż. **Wojciech CHOLEWA**
Politechnika Śląska

prof. dr hab. inż. **Zbigniew DĄBROWSKI**
Politechnika Warszawska

prof. **Wiktor FRID**
Royal Institute of Technology in Stockholm – Sweden

dr inż. **Tomasz GAŁKA**
Instytut Energetyki w Warszawie

prof. **Len GELMAN**
Cranfield University – England

prof. **Mohamed HADDAR**
National School of Engineers of Sfax – Tunisia

prof. dr hab. inż. **Jan KICIŃSKI**
IMP w Gdańsku

prof. dr hab. inż. **Jerzy KISIŁOWSKI**
Politechnika Warszawska

prof. dr hab. inż. **Daniel KUJAWSKI**
Western Michigan University – USA

prof. dr hab. **Wojciech MOCZULSKI**
Politechnika Śląska

prof. dr hab. inż. **Stanisław NIZIŃSKI**
UWM w Olsztynie

prof. **Vasyl OSADCHUK**
Politechnika Lwowska – Ukraine

prof. dr hab. inż. **Stanisław RADKOWSKI**
Politechnika Warszawska

prof. **Bob RANDALL**
University of South Wales – Australia

prof. dr **Raj B. K. N. RAO**
President COMADEM International – England

prof. **Vasily S. SHEVCHENKO**
BSSR Academy of Sciences Mińsk – Belarus

prof. **Menad SIDAHMED**
University of Technology Compiègne – France

prof. dr hab. inż. **Tadeusz UHL**
AGH w Krakowie

prof. **Vitalijus VOLKOVAS**
Kaunas University of Technology – Lithuania

prof. dr hab. inż. **Andrzej WILK**
Politechnika Śląska

dr **Gajraj Singh YADAVA**
Indian Institute of Technology – India

prof. dr hab. inż. **Bogdan ŻÓŁTOWSKI**
UTP w Bydgoszczy

WYDAWCA:

Polskie Towarzystwo Diagnostyki Technicznej
02-981 Warszawa
ul. Augustówka 5

REDAKTOR NACZELNY:

prof. dr hab. inż. **Ryszard MICHALSKI**

SEKRETARZ REDAKCJI:

dr inż. **Sławomir WIERZBICKI**

CZŁONKOWIE KOMITETU REDAKCYJNEGO:

dr inż. **Krzysztof LIGIER**
dr inż. **Paweł MIKOŁAJCZAK**

ADRES REDAKCJI:

Redakcja Diagnostyki
Katedra Budowy, Eksploatacji Pojazdów i Maszyn
UWM w Olsztynie
ul. Oczapowskiego 11
10-736 Olsztyn, Poland
tel.: 089-523-48-11, fax: 089-523-34-63
www.diagnostyka.net.pl
e-mail: redakcja@diagnostyka.net.pl

KONTO PTDT:

Bank PEKAO SA O/Warszawa
nr konta: 33 1240 5963 1111 0000 4796 8376

NAKLAD: 500 egzemplarzy

Spis treści / Contents

Amira AMAMOU, Mnaouar CHOUCANE, Sami NAIMI – National Engineering School of Monastir, Tunisia.....	3
Nonlinear Analysis Of The Stability Of Hydrodynamic Bearings	
Lamjed Hadj TAÏEB, Ezzeddine Hadj TAÏEB – Ecole Nationale d'Ingénieurs de Sfax, Tunisia	11
Transient Analysis For Leak Detection In Pipe With Fluid-Structure Interaction	
Said CHKIR, Ivan DOBREV, Patrick KUSZLA, Fawaz MASSOUH – Arts et métiers ParisTech, France.....	17
Unsteady Loads Evaluation For A Wind Turbine Rotor	
Czesław CEMPEL – Poznan University of Technology	23
The Global And Partial System Condition Assessment In Multidimensional Condition Monitoring <i>Całkowita i cząstkowa ocena stanu w wielowymiarowej diagnostyce maszyn</i>	
Marcin JASIŃSKI, Stanisław RADKOWSKI – Warsaw University of Technology.....	35
Examination Of The Impact Of Amplitude-Modulated Vibration On The Course Of A Fatigue Test (HCF) <i>Badanie wpływu amplitudowo zmodulowanych drgań na przebieg testu zmęczenia (HCF)</i>	
Anna BZYMEK, Anna TIMOFIEJCZUK – Silesian University of Technology	41
Estimation Of Welding Process Stability Based On Image Analysis And Recognition <i>Ocena stabilności procesu spawania z zastosowaniem metod analizy i rozpoznawania obrazów</i>	
Tomasz GAŁKA – Instytut Energetyki w Warszawie.....	45
<i>Symptom Limit Value: A Statistical Approach</i> <i>Wartość graniczna symptomu w ujęciu statystycznym</i>	
Jan MONIETA, Karol KROCZYŃSKI – Akademia Morska w Szczecinie.....	51
Application Of The Pressure Process Detector For Diagnosing Injection Apparatus In Marine Diesel Engines In The Injection Pipe <i>Zastosowanie detektora przebiegu ciśnienia w przewodzie wtryskowym do diagnozowania aparatury wtryskowej silników okrętowych</i>	
Bogusław ŁAZARZ, Grzegorz PERUŃ – Silesian University of Technology	55
Identification And Verification Of Simulation Model Of Gears Working In Circulating Power System <i>Identyfikacja i weryfikacja modelu symulacyjnego przekładni zębatach pracujących w układzie mocy krążącej</i>	
Mirosław RODZEWICZ – Warsaw University of Technology, Grzegorz CZERWIŃSKI – Telecommunication Research Institute S.A.....	61
Some Investigations Into Ultrasonic Diagnostics Applicability For Composite Structure <i>Badania nad zastosowaniem diagnostyki ultradźwiękowej w badaniu struktur kompozytowych</i>	
Zbigniew KOZANECKI, Jakub ŁAGODZIŃSKI, Dorota KOZANECKA - Technical University of Łódź.....	65
Failure Diagnosis Of The Gas Compressor Diaphragm Vane <i>Diagnostyka uszkodzeń łopatek kierownicy sprężarki przepływowej</i>	
Zdzisław GOLEC, Maria GOLEC, Maciej TABASZEWSKI – Poznan University of Technology	73
Identification Of Vibroacoustic Field Of Complex Mechanical Structures On The Example Of A Toothed Gear <i>Identyfikacja pola wibroakustycznego złożonych struktur mechanicznych na przykładzie przekładni zębatej</i>	
Józef RYBCZYŃSKI – Institute of Fluid-Flow Machinery in Gdansk.....	77
Diagnostics Of The Turbogenerator Shaft Line Misalignment Based On The Bearing Trajectory Patterns <i>Diagnostyka rozosiowania linii wałów turbogenerators na podstawie obrazów trajektorii łożysk</i>	

Szymon GONTARZ, Marcin JASIŃSKI, Stanisław RADKOWSKI – Warsaw University of Technology	85
Use Of Hilbert-Huang Transform Of A Vibroacoustic Signal In The Research Related To The Gigacycle Fatigue Process <i>Zastosowanie transformaty Hilberta-Huang sygnału wibroakustycznego w badaniach gigacyklowego procesu zmęczenia</i>	
Stanisław RADKOWSKI, Maciej ZAWISZA – Warsaw University of Technology.....	93
Failure Oriented Diagnostic Models In Condition Monitoring <i>Uszkodzeniowo zorientowane modele diagnostyczne w monitorowaniu stanu obiektów technicznych</i>	
Marcin STARNACKI – Przemysłowy Instytut Telekomunikacji S.A.	99
Komputerowe przetwarzanie sygnałów ultradźwiękowych <i>Computer Ultrasounds Processing</i>	
Małgorzata ORCZYK, Franciszek TOMASZEWSKI – Poznan University of Technology	105
Diagnozowanie zmian klimatu akustycznego na odcinku autostrady A2 Komorniki – Krzesiny <i>Diagnosis Of Acoustic Climate Changes At A2 Motorway Distance From Komorniki To Krzesiny</i>	
Sprawozdanie z VII Krajowej Konferencji DIAG'2009 "Diagnostyka techniczna urządzeń i systemów".....	109
Warto przeczytać / Worth to read	111

NONLINEAR ANALYSIS OF THE STABILITY OF HYDRODYNAMIC BEARINGS

Amira AMAMOU*, Mnaouar CHOUCANE**, Sami NAIMI***

* Laboratory of Mechanical Engineering, National Engineering School of Monastir, Tunisia
Avenue Ibn Eljazzar, 5019 Monastir, Tunisia

e-mail: amira.amamou@yahoo.fr

** Laboratory of Mechanical engineering, National Engineering School of Monastir, Tunisia
Avenue Ibn Eljazzar, 5019 Monastir, Tunisia

e-mail: mnaouar.chouchane@enim.rnu.tn

*** Laboratory of Mechanical Engineering, National Engineering School of Monastir, Tunisia
Avenue Ibn Eljazzar, 5019 Monastir, Tunisia

e-mail: naïmisami@yahoo.fr

Summary

The linear analysis of the stability of a hydrodynamic bearing is used to determine the stability boundaries and to predict if the steady state is stable or not. A nonlinear or weakly nonlinear model is used to determine the behaviour of the system near the critical stability boundaries. By applying the Hopf bifurcation theory, the existence of stable or unstable limit cycles in the neighbourhood of the stability boundaries can be predicted depending on the characteristics of the bearing. A numerical integration of the nonlinear equations of motion is then carried out in order to verify the results obtained analytically.

Keywords: hydrodynamic bearing, stability analysis, nonlinear analysis, Hopf bifurcation, limit cycles.

INTRODUCTION

Hopf bifurcation theory is used in the analysis of the stability of a rigid rotor symmetrically supported by two identical journal bearings to determine the nature of instability and the existence of stable or unstable limit cycles near the stability boundaries.

Meyers [4] applied, in 1984, this theory to determine the stability of an infinitely long journal bearing. He identified the existence of three different regions in the parameters space of the steady state eccentricity ratio.

The same analysis is carried out by Hollis and Taylor [3] to identify the stability of a rigid rotor supported symmetrically by two infinitely short journal bearings.

All this work is based on the assumption of lubrication under the laminar flow condition. However, Khonsari and Wang [7] have applied the Hopf bifurcation theory for the analysis of the stability of short journal bearings considering the turbulence effect.

The purpose of this paper is to use nonlinear models for both infinitely short and long journal bearings to analyse the stability of a hydrodynamic bearing using Hopf bifurcation theory in order to determine the nature of instability according to the bearing's parameters. Analytical results are then verified numerically.

The purpose of this paper is to use nonlinear models for both infinitely short and long journal

bearings to analyse the stability of a hydrodynamic bearing using Hopf bifurcation theory in order to determine the nature of instability according to the bearing's parameters. Analytical results are then verified numerically.

The outline of this paper is as follows. First, the equations of motion of the rotor bearing system are presented. Then, a linear analysis of the stability for short and long journal bearings is performed to determine the stability boundaries.

A nonlinear analysis of the stability is then carried out by applying the Hopf bifurcation theory to determine the shape, the size and stability of the periodic solutions of the journal orbit.

A numerical integration of the equations of motion is used to verify the analytical results.

The paper is concluded with the presentation of the implications of these results on the stability characteristics of journal bearing.

1. EQUATIONS OF MOTION

Consider a system of a rigid and perfectly balanced and symmetrical rotor supported by two identical hydrodynamic bearings, figure 1.

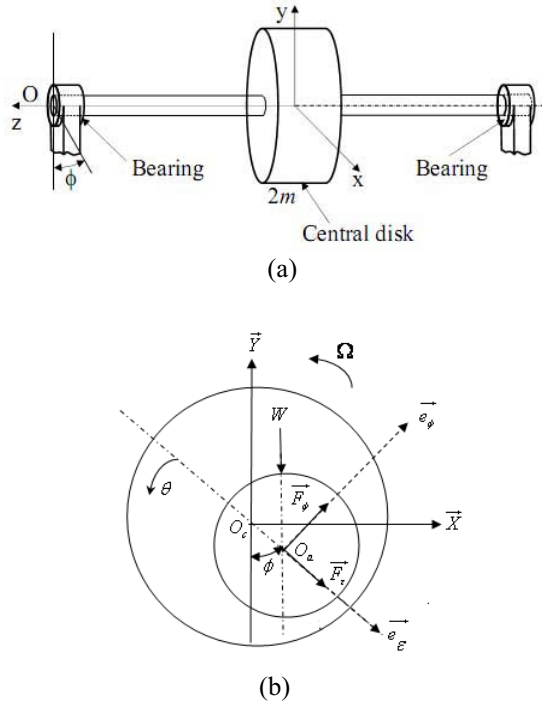


Fig. 1. (a) The model of the symmetric rigid rotor
(b) A section of the hydrodynamic bearing

The equations of motion of this system are:

$$\begin{cases} M\ddot{x} = F_x \\ M\ddot{y} = -W + F_y \end{cases} \Rightarrow \begin{cases} M\ddot{x} = F_\varepsilon \sin \phi + F_\phi \cos \phi \\ M\ddot{y} = -W - F_\varepsilon \cos \phi + F_\phi \sin \phi \end{cases} \quad (1)$$

where

x, y : Cartesian coordinates of the rotor centre

F_ε, F_ϕ : Radial and tangential components of the fluid force applied on the journal

W : Static load applied on the bearing

These equations may be written in polar coordinates as follow:

$$\begin{cases} M\ddot{\varepsilon} - M\varepsilon\dot{\phi}^2 = F_\varepsilon + W \cos \phi \\ M\varepsilon\ddot{\phi} + 2M\dot{\varepsilon}\dot{\phi} = F_\phi - W \sin \phi \end{cases} \quad (2)$$

In a non dimensional form, these equations become

$$\begin{cases} \ddot{\varepsilon} - \varepsilon\dot{\phi}^2 = \frac{F_\varepsilon}{Mc} + \frac{W}{Mc} \cos \phi \\ \varepsilon\ddot{\phi} + 2\dot{\varepsilon}\dot{\phi} = \frac{F_\phi}{Mc} - \frac{W}{Mc} \sin \phi \end{cases} \quad (3)$$

where

- $\left(\frac{\square}{\square} \right) = \frac{1}{\Omega} \frac{d}{dt}$
- $\varepsilon = \frac{e}{c}$
- $\overline{F_\varepsilon} = \frac{F_\varepsilon}{Mc\Omega^2}$
- $\overline{F_\phi} = \frac{F_\phi}{Mc\Omega^2}$

The above system of equations is composed of two 2nd order nonlinear equations. To solve this system, the two 2nd order equations are transformed into four 1st order equations.

Let

$$\mathbf{x} = \begin{Bmatrix} x_1 \\ x_2 \\ x_3 \\ x_4 \end{Bmatrix} = \begin{Bmatrix} \varepsilon \\ \phi \\ \dot{\varepsilon} \\ \dot{\phi} \end{Bmatrix}$$

$$\overline{\Omega} = \Omega \sqrt{\frac{c}{g}}$$

Then the equations of motion become:

$$\begin{cases} \dot{x}_1 = x_3 \\ \dot{x}_2 = x_4 \\ \dot{x}_3 = x_1 x_4^2 + \overline{F_\varepsilon} + \frac{1}{\overline{\Omega}^2} \cos x_2 \\ \dot{x}_4 = \frac{-2x_3 x_4}{x_1} + \overline{F_\phi} - \frac{1}{\overline{\Omega}^2} \sin x_2 \end{cases} \quad (4)$$

For an infinitely short journal bearing, the hydrodynamic force has a radial component F_ε , and a tangential component F_ϕ as shown in Fig. 1.

Assuming the Half-Sommerfeld boundary conditions, the two components of the dynamic oil-film reaction force of the journal are [7]:

$$\begin{cases} \overline{F_\varepsilon} = \frac{F_\varepsilon}{Mc\Omega^2} = -\frac{\mu RL^3}{2Mc^3\Omega} \left[\frac{2(1-2\dot{\phi})\varepsilon^2}{(1-\varepsilon^2)^2} + \frac{\pi\varepsilon(1+2\varepsilon^2)}{(1-\varepsilon^2)^{2.5}} \right] \\ \overline{F_\phi} = \frac{F_\phi}{Mc\Omega^2} = \frac{\mu RL^3}{2Mc^3\Omega\varepsilon} \left[\frac{\pi(1-2\dot{\phi})\varepsilon^2}{2(1-\varepsilon^2)^{1.5}} + \frac{4\varepsilon^2}{(1-\varepsilon^2)^2} \right] \end{cases} \quad (5)$$

Substituting the expression of the film reaction components into equation (4) and using the non

dimensional bearing modulus $\Gamma = \frac{\mu RL^3}{2Mc^{2.5}g^{0.5}}$

which is independent of the rotor speed, we obtain:

$$\begin{cases} \dot{x}_1 = x_3 \\ \dot{x}_2 = x_4 \\ \dot{x}_3 = x_1 x_4^2 - \frac{\Gamma}{\Omega} \left[\frac{(1-2x_4)x_1^2}{(1-x_1^2)^2} + \frac{\pi x_3(1+2x_1^2)}{(1-x_1^2)^{2.5}} \right] + \frac{1}{\Omega} \cos x_2 \\ \dot{x}_4 = \frac{-2x_3 x_4}{x_1} + \frac{\Gamma}{\Omega x_1^2} \left[\frac{\pi(1-2x_4)x_1^2}{2(1-x_1^2)^{1.5}} + \frac{4x_3 x_1^2}{(1-x_1^2)^2} \right] - \frac{1}{\Omega} \sin x_2 \end{cases} \quad (6)$$

For an infinitely long journal bearing approximation, the non dimensional expressions for the hydrodynamic force components are [1]:

$$\begin{cases} \frac{-F_\varepsilon}{Mc\Omega^2} = -\frac{6\mu LR^3}{Mc^3\Omega} \left\{ \frac{2\varepsilon^2(1-2\phi)}{(1-\varepsilon^2)(2+\varepsilon^2)} + \frac{[\pi^2(2+\varepsilon^2)-16]\dot{\varepsilon}}{\pi(2+\varepsilon^2)(1-\varepsilon^2)^{1.5}} \right\} \\ \frac{-F_\phi}{Mc\Omega^2} = \frac{6\mu LR^3}{Mc^3\Omega\varepsilon} \left\{ \frac{\pi\varepsilon^2(1-2\phi)}{(2+\varepsilon^2)(1-\varepsilon^2)^{0.5}} + \frac{4\varepsilon\dot{\varepsilon}}{(2+\varepsilon^2)(1-\varepsilon^2)} \right\} \end{cases} \quad (7)$$

The equations of motion of an infinitely long journal bearing is obtained by substituting equations (7) into equation (4) and using a non

dimensional parameter $s = \frac{\mu LR^3}{Mc^{2.5}g^{0.5}}$,

$$\begin{cases} \dot{x}_1 = x_3 \\ \dot{x}_2 = x_4 \\ \dot{x}_3 = x_1 x_4^2 - \frac{6s}{\Omega} \left\{ \frac{2x_1^2(1-2x_4)}{(1-x_1^2)(2+x_1^2)} + \frac{[\pi^2(2+x_1^2)-16]x_3}{\pi(2+x_1^2)(1-x_1^2)^{1.5}} \right\} + \frac{1}{\Omega} \cos x_2 \\ \dot{x}_4 = \frac{-2x_3 x_4}{x_1} + \frac{6s}{\Omega x_1^2} \left\{ \frac{\pi(1-2x_4)x_1^2}{(2+x_1^2)(1-x_1^2)^{0.5}} + \frac{4x_3 x_1^2}{(2+x_1^2)(1-x_1^2)} \right\} - \frac{1}{\Omega} \sin x_2 \end{cases} \quad (8)$$

2. LINEAR ANALYSIS

A linear analysis in the case of the Half-Sommerfeld boundary approximation can be used to determine the stability boundaries for both short and long bearings.

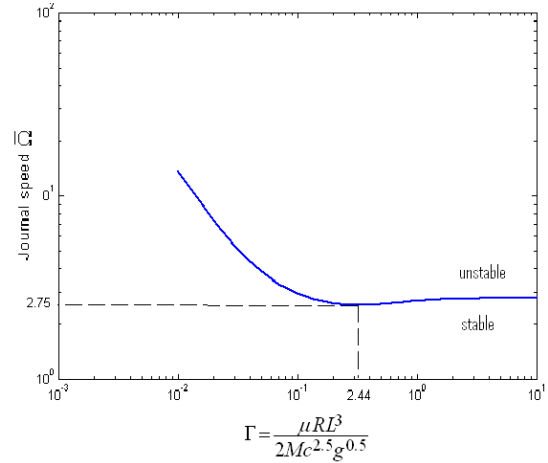


Fig. 2. Stability boundaries for an infinitely short journal bearing

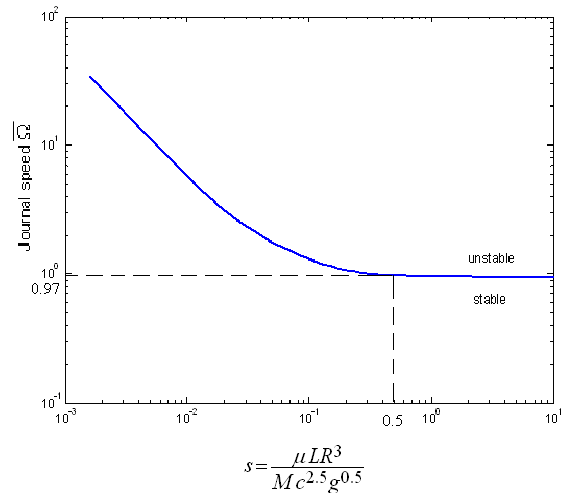


Fig. 3. Stability boundaries for an infinitely long journal bearing

Figures 2 and 3 can be used to determine the stability threshold speed of a bearing.

The non dimensional parameter Γ or s is calculated, then the non dimensional journal speed $\bar{\Omega}$ at the stability boundary is determined.

3. NONLINEAR ANALYSIS

To determine if stable or unstable limit cycles exist in the neighbourhood of the stability boundaries, a nonlinear analysis is applied using Hopf bifurcation theory.

A bifurcation is a qualitative change in the features of a system, such as the number and type of solutions, under the variation of the system parameters [1].

It has been shown that for a nonlinear system, a Hopf bifurcation must appear as the bifurcation

from a fixed point to a limit cycles. The size, shape and stability of the limit cycles have to be determined.

Using Hopf bifurcation analysis, the regions of subcritical and supercritical stability can be predicted in terms of the non dimensional bearing parameter.

3.1. Application of Hopf Bifurcation Theory to a Rotor-Bearing System

The Hopf bifurcation theory (HBT) is concerned with the bifurcation of the periodic orbits from the equilibrium points of a system whose behaviour is described by the system of ordinary differential equation $\dot{x} = F(x, \lambda)$.

Using Hopf bifurcation theory, one can investigate the existence of small amplitude periodic solutions of the equations (6, 8) which describe the motion of a rotor supported in fluid bearings. It is shown that the existence of stable limit cycles for rotor speed in excess of the threshold speed is confined to a specific region of parameter space. Outside this region, unstable limit cycles exist below the threshold speed [6].

Size and Stability of the Periodic Solutions of Journal Orbit

A Hopf bifurcation subroutine developed by Hassard et al. [2] to calculate the typical bifurcation parameters using HBT has been used. This theory is based on six parameters used to determine the shape, size and stability of the periodic solutions close to the bifurcation point.

These parameters are expressed as follow:

γ represents the parameter that gives the range of the existence of the periodic solutions of journal orbit. If $\gamma < 0$, periodic solutions exist for $\bar{\Omega} < \bar{\Omega}_s$; if $\gamma > 0$, periodic solutions exist for $\bar{\Omega} > \bar{\Omega}_s$.

τ is the coefficient in the expansion of the periods of periodic solutions $T(\bar{\Omega})$.

β is the leading coefficient in the expansion of the characteristic exponent $S_p(\bar{\Omega})$ which gives the stability of the periodic solution. If $\beta < 0$, the periodic solution is orbital asymptotically stable. If $\beta > 0$, the periodic solution is orbital-asymptotically unstable.

ω_0 is defined as $\beta(\bar{\Omega}_s)$.

The vector V contains the eigenvector of the Jacobian matrix at the stationary point when $\bar{\Omega} = \bar{\Omega}_s$. It corresponds to the eigenvalue $i\omega_0$.

The approximate periodic solutions can be expressed in the neighbourhood of $\bar{\Omega}_s$ using Hopf parameters [2].

$$x(t, \bar{\Omega}) = x_s(\bar{\Omega}_s) + \left(\frac{\bar{\Omega} - \bar{\Omega}_s}{\gamma} \right)^{0.5} \text{Re} \left(e^{2\pi i t / T} V \right) + \mathcal{O}(\bar{\Omega} - \bar{\Omega}_s) \quad (9)$$

where

$$T(\bar{\Omega}) = \frac{2\pi}{\omega_0} \left[1 + \tau \left(\frac{\bar{\Omega} - \bar{\Omega}_s}{\gamma} \right) + \mathcal{O}(\bar{\Omega} - \bar{\Omega}_s)^2 \right]$$

The characteristic exponent is expressed as:

$$S_p(\bar{\Omega}) = \beta \left(\frac{\bar{\Omega} - \bar{\Omega}_s}{\gamma} \right) + \mathcal{O}(\bar{\Omega} - \bar{\Omega}_s)^2$$

3.2. Infinitely short journal bearing

It is shown that for a journal speeds above a threshold speed; the system can exhibit supercritical bifurcations and so stable limit cycles. Unstable limit cycles however, exist for rotor speeds below the threshold speed.

The nonlinear parameters provided predict that for $\Gamma < 0.588$, there exist supercritical bifurcations for non dimensional speed $\bar{\Omega}$ greater than the critical value $\bar{\Omega}_s$. For $\Gamma \geq 0.588$, subcritical bifurcations exist for $\bar{\Omega}$ less than $\bar{\Omega}_s$ (Figure.4).

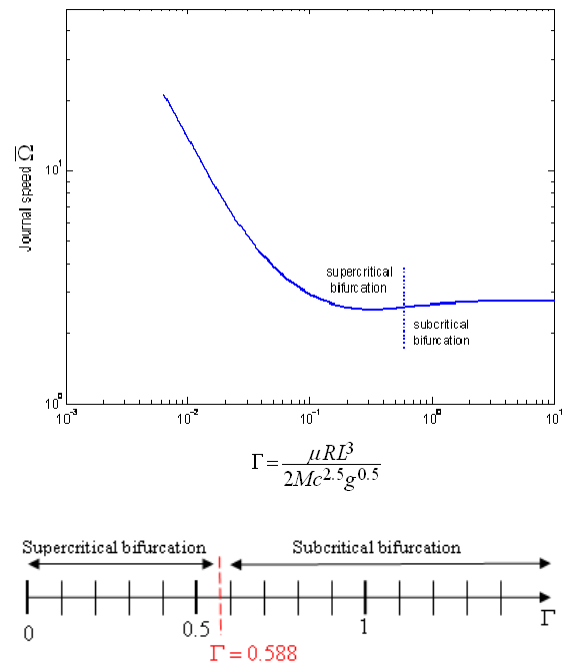


Fig. 4. Supercritical and subcritical bifurcations for short journal bearing

In order to describe the Hopf bifurcation behaviour of the journal bearing, Figure 5 illustrates the supercritical bifurcation profiles for several values of Γ . Stable solutions are shown by solid lines and unstable solutions by dashed lines.

For $\Gamma = 0.4$ with $\bar{\Omega} \leq \bar{\Omega}_s (=2.54)$ the rotor is stable at the position of steady-state eccentricity ratio ε_s . With $\bar{\Omega} > \bar{\Omega}_s$ the supercritical bifurcation appears close to the bifurcation point. Similar features are predicted for $\Gamma = 0.1$ and $\Gamma = 0.2$.

The amplitude of the periodic solution corresponding to a specific running speed $\bar{\Omega}$ is

$$\delta = \varepsilon_s \pm \sqrt{\frac{(\bar{\Omega} - \bar{\Omega}_s)}{\gamma}}$$

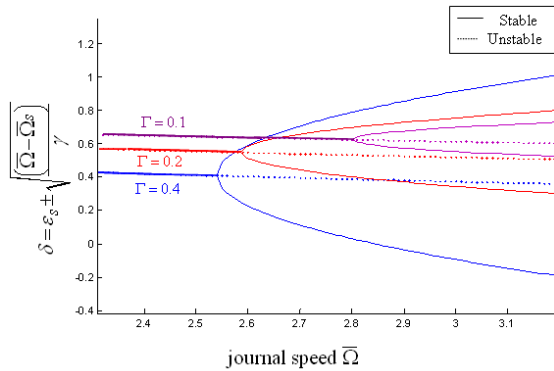


Fig. 5. Supercritical bifurcation profiles for several values of Γ

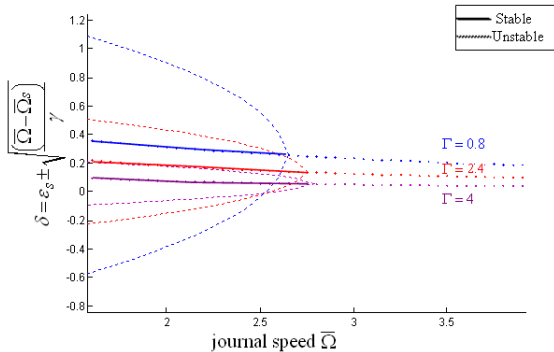


Fig. 6. Subcritical bifurcation profiles for several values of Γ

Figure 6 illustrates the subcritical bifurcation diagrams for several values of Γ . Stable solutions are shown by solid lines and unstable solutions by dashed lines. For $\Gamma = 0.8$ with $\bar{\Omega} > \bar{\Omega}_s (=2.6)$, the equilibrium position of the rotor is unstable. There is unstable periodic solution for $\bar{\Omega} < \bar{\Omega}_s$; this is the subcritical behavior predicted by Hopf bifurcation theory. Similar features are observed for $\Gamma = 2.4$ and $\Gamma = 4$.

3.3. Infinitely long journal bearing

In this case, there are three separate regions of the parameter space s (Figure 7). The Hopf bifurcation analysis, predicted that for $0 < s \leq 0.05$ and $s > 0.79$ subcritical bifurcations appear for $\bar{\Omega} < \bar{\Omega}_s$ and therefore the bifurcated periodic orbit is unstable.

For $0.05 < s \leq 0.79$, supercritical bifurcations occur for $\bar{\Omega} > \bar{\Omega}_s$. The bifurcated periodic orbits are stable.

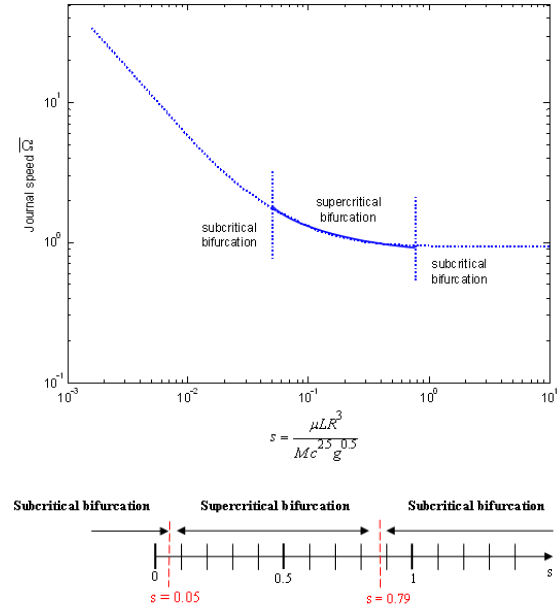


Fig. 7. Supercritical and subcritical bifurcations for long journal bearing

Figures (8-9) show the bifurcation profiles, which depict the amplitudes of the periodic solutions corresponding to running speeds close to the critical speed $\bar{\Omega}_s$ for several values of s .

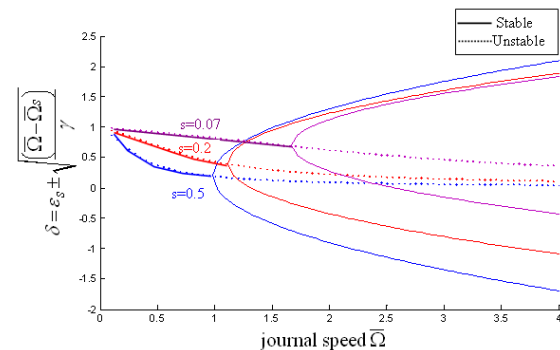


Fig. 8. Supercritical bifurcation profiles for several values of s

Figure. 8 shows the supercritical bifurcation diagrams.

Stable solutions are shown by solid lines and unstable solutions by dashed lines.

The supercritical bifurcation occurs close to the bifurcation point when $\bar{\Omega} > \bar{\Omega}_s$.

The predicted limit cycles grow as the value of s increases.

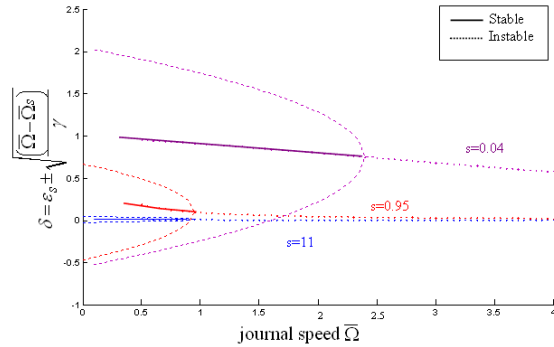


Fig. 9. Subcritical bifurcation profiles for several values of s

In order to describe the subcritical behavior, Figure 9 illustrates the subcritical profiles for several values of s . Below the threshold speed $\bar{\Omega}_s$, unstable limit cycles appear.

The predicted limit cycles grow as the value of s decreases.

4. NUMERICAL INTEGRATION

A numerical integration is carried out to verify the results obtained using HBT and to investigate how the whirl orbits develop at speeds well away from the threshold speed. The equations of motion are integrated using a variable-order Runge-Kutta method. The function ode45 is used to solve the system of ordinary differential equations (6) or (8) under Matlab.

Example 1: A short journal bearing

Consider the rotor-bearing system whose specifications are listed in Table 1 [5]. This rotor-bearing system consists of a rigid rotor symmetrically supported by two identical plain journal bearings. We apply Hopf bifurcation theory to determine its stability.

Table 1. Specification of the rotor-bearing system

μ (Pa.s)	c (m)	D (m)	L (m)	M (Kg)
0.0212	$0.125 \cdot 10^{-3}$	0.25	0.125	1936.8

This rotor-bearing has:

- A journal parameter: $\Gamma = 2.44$
- A threshold speed : 7360 rpm

The Hopf bifurcation parameters were obtained and the results are shown in Table 2.

Table 2. Hopf Bifurcation Parameters

$\bar{\Omega}_s$	γ	τ	β	$\mathbf{x}_s(\bar{\Omega}_s)$	\mathcal{V}
2.744	-19.95	0.14	2.27	0.093 1.452 0 0	1.0+0.0i 0.6-1.1i 0+0.5i 5.52+0.31i

The value of the threshold speed calculated is similar to the value of $\bar{\Omega}_s$ determined by the linear analysis as shown in Fig.2.

In Table 2, $\gamma < 0$ and $\beta > 0$ unstable periodic solutions exist for $\bar{\Omega} < \bar{\Omega}_s = 2.744$.

To understand the behaviour of bearing instability, the journal is released from positions inside and outside the unstable periodic orbit for $\bar{\Omega} < \bar{\Omega}_s$.

Consider the non dimensional running speeds $\bar{\Omega} = 2$ which is less than $\bar{\Omega}_s (=2.744)$.

The equations were integrated for two values of initial conditions. One is located inside the periodic limit orbit close to the equilibrium position. The other one is situated outside the periodic limit cycle (Figure 6).

Figures 10-11 represent the trajectory of the journal centre (the circle at $\varepsilon = 1$ is the clearance circle and represents the orbit of the journal centre when the journal surface is in contact with the bearing side).

According to the definition of the unstable periodic solution, for $\bar{\Omega} = 2 < \bar{\Omega}_s$ if the journal is released from a position inside the unstable periodic solution (Figure. 10), the system tends to asymptotically approach the steady state equilibrium position.

If the journal is released from a position outside the unstable periodic solution (Figure. 11), the orbit of the journal tends to become unstable.

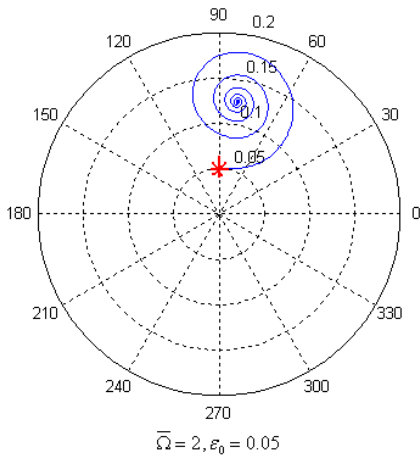


Fig. 10. The periodic solutions of the equations of motion for $\bar{\Omega} = 2, \epsilon_0 = 0.05$

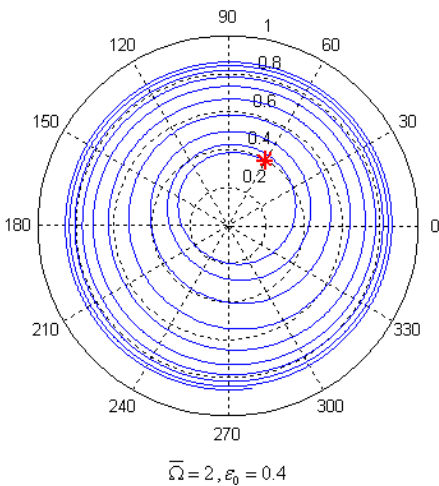


Fig. 11. The periodic solutions of the equations of motion for $\bar{\Omega} = 2, \epsilon_0 = 0.4$

Example 2: A long journal bearing

Consider a bearing with a modulus $s = 0.5$.

In Table 3, $\gamma > 0$ et $\beta < 0$, then stable periodic solutions exist for $\bar{\Omega} > \bar{\Omega}_s = 0.98$.

Table 3. Hopf Bifurcation Parameters

$\bar{\Omega}_s$	γ	τ	β	$x_s(\bar{\Omega}_s)$	ν
0.98	0.9	2.05	-1.12	0.21 1.43 0 0	1.0+0.0i 0.5-2.15i 0+1.1i 2.38+5.9i

The value of the threshold speed calculated $\bar{\Omega}_s = 0.98$ is similar to the value determined by the linear analysis (Figure 3).

For rotor speeds immediately above $\bar{\Omega}$, a stable limit cycles appear, independent of the initial conditions (Figures 12-13).

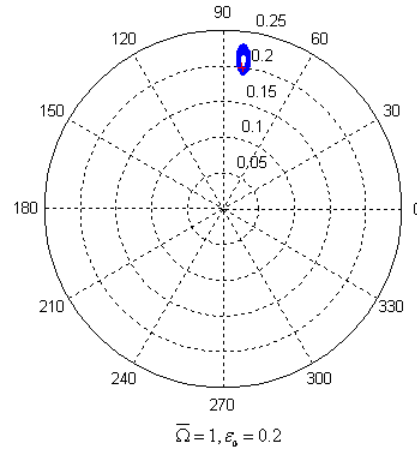


Fig. 12. The periodic solutions of the equations of motion for $\bar{\Omega} = 1, \epsilon_0 = 0.2$

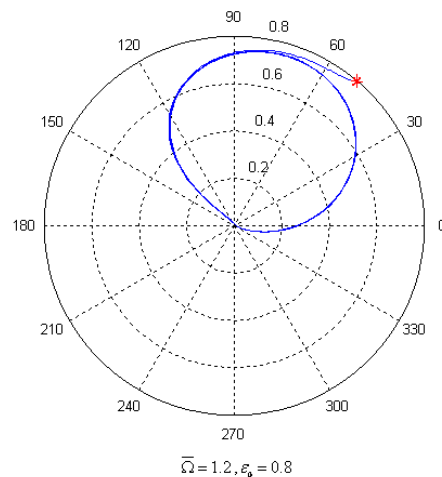


Fig. 13. The periodic solutions of the equations of motion for $\bar{\Omega} = 1.2, \epsilon_0 = 0.8$

It is shown that the size of the limit cycles increase with rotor speed.

5. SUMMARY

The analysis of weakly nonlinear stability of both infinitely short and long journal bearings is presented.

Linear analysis may be used to determine the stability boundaries and the threshold speed for a particular bearing parameter.

Using the Hopf bifurcation theory, the nonlinear behaviours in the neighbourhood of the linear stability boundaries are predicted.

The onset of oil whirl for a rigid rotor bearing system supported by two identical hydrodynamic

bearings is a bifurcation phenomenon. The existence of supercritical limit cycles or subcritical limit cycles can be established for journal speeds close to the threshold speed.

A numerical investigation supported the results of analytical analysis.

For the occurrence of supercritical bifurcation, a stable, small-amplitude whirl orbits appears when the rotor speed exceeds its threshold value and the size of the limit cycles increase with rotor speed.

When subcritical bifurcation occurs, unstable limit cycles with large amplitude are predicted at journal speed below its threshold speed.

For the practising engineer, it is interesting to choose specific operating parameters of a system in a manner that sustain subcritical bifurcation.

The effect of shaft flexibility on the stability boundaries and bifurcation regions is challenging future extension.

REFERENCES

- [1] Dokhane A.: *BWR stability and bifurcation analysis using a novel reduced order model and the system code RAMONA*. Ph.D thesis, polytechnic Federal school of Lausanne, 2004.
- [2] Hassard, B. D., Kazarinoff, N. D., Wan, Y. H.: *Theory and Applications of Hopf Bifurcation*. London Mathematical Society Lecture Notes 41, Cambridge University Press, New York, 1981.
- [3] Hollis P., Taylor D. L.: *Hopf bifurcation to limit cycles in fluid film bearings*. ASME J Tribol, 1986, Vol. 108, pp. 184–9.
- [4] Myers C. J.: *Bifurcation theory applied to oil whirl in plain cylindrical journal bearings*. ASME J Tribol, 1984, Vol. 5, pp. 244–9.
- [5] Stolarski A.: *Tribology in Machine Design*. Butterworth-Heinemann, 2000.
- [6] Wang J. K.: *On the stability of rotor bearing systems based on Hopf bifurcation*. Ph.D thesis, Faculty of the Louisiana State University, 2005.
- [7] Wang J. K., Khonsari M .M.: *Application of Hopf bifurcation theory to rotor-bearing systems with consideration of turbulent effects*. ASME J Tribol, 2006, Vol. 39, pp. 701-14.

TRANSIENT ANALYSIS FOR LEAK DETECTION IN PIPE WITH FLUID-STRUCTURE INTERACTION

Lamjed Hadj TAÏEB*, Ezzeddine Hadj TAÏEB**

*UR Mécanique des Fluides Appliquée et Modélisation, Ecole Nationale d'Ingénieurs de Sfax, B. P. W 3038 Sfax, Tunisia, lamjed@quebecemail.com

**UR Mécanique des Fluides Appliquée et Modélisation, Ecole Nationale d'Ingénieurs de Sfax, B. P. W 3038 Sfax, Tunisia, Ezed.Hadj@enis.run.tn

Summary

The use of fluid transients has the potential to provide insight into effect of leaks in pipeline systems and hence provide leak detection method. This paper presents a technique for detection and location of leaks in a single pipe by means of transient analysis. The method uses transient pressure waves initiated by the sudden closure of an upstream valve. The presence of a leak in a pipe partially reflects these pressure waves and allows for the location and magnitude of leaks. The two constitutive equations of continuity and momentum yield a set of two partial differential equations of hyperbolic type. The computed results obtained by the method of characteristics describe the influence of the leak on head and discharge time-histories. To put in evidence the fluid-structure, interaction the influence of friction and Young modulus of the pipe wall on the leak detection and sizing is also discussed.

Keywords: leak detection, transient analysis , fluid-structure interaction, method of characteristics pipe.

1. INTRODUCTION

The detection and location of leaks in pipeline systems are major problems and leakage control has become high priorities for water supply utilities and authorities [1]. This is not only because there is a greater understanding of the economic and social costs associated with water losses, but there is also an imperative to make best possible use of the natural source that is water.

Several techniques for leak detection in pipe have been presented in the literature using different methods include acoustic technology [2], ground penetration radar or infrared spectroscopy [3], transmission and reflection of pressure waves [4, 5], sequential statistical analysis [6], and transient analysis methods [7, 8, 9, 10, 11].

Some of the current numerical methods for locating and identifying leaks are either complicated or imprecise; most of them are time consuming. These methods usually used the acquisition and the analysis of extensive real-time data. Often, these data are either not available or costly to obtain.

The ideal technology for leak detection and location should be non-intrusive, faster and cheaper and should not require cessation of pipeline operations for long period of time. Since transient test data can give more information about a pipe system than steady state measurements, leak detection methodologies based on transient analysis can achieve this goal.

The purpose of this paper is to detect leaks in a single pipe system using transient event (water hammer signals) generated by the sudden closure of a downstream valve. A pressure wave travels along the system at high speed and is modified by the system during its travel. Leaks within a pipe partially reflect these pressure signals and allow for the accurate location and sizing of a leak by measuring the period of time which the pressure wave takes to travel from the measurement section to the leak and vice-versa.

To apply the procedure of leak detection with confidence and success, special attention has to be given to the dynamic effects related to the energy dissipation, namely the friction and the mechanical behaviour of the pipe wall [12].

The focus here is mainly to study the fluid-structure interaction by analysing the influence of the friction and the Young modulus of the pipe wall on the leak detection and sizing.

2. WATER HAMMER MODEL

2.1. Basic equations

The simplified one-dimensional continuity and momentum equations that describe transient flow in elastic pipe are [13]:

$$\frac{\partial H}{\partial t} + \frac{C^2}{gA} \frac{\partial Q}{\partial x} = 0 \quad (1)$$

$$\frac{\partial H}{\partial x} + \frac{1}{gA} \frac{\partial Q}{\partial t} + \frac{\lambda Q|Q|}{2gDA^2} = 0 \quad (2)$$

where H is the piezometric head, Q is the discharge, C is the pressure wave speed, g is the gravitational acceleration, A is the pipe cross-sectional area, D is the internal pipe diameter, λ is the coefficient of friction, x is the special coordinate and t is the time.

The elastic wave speed, C , is a parameter that depends on the fluid compressibility and on the physical properties and external constraints of the pipe. Assuming linear-elastic behaviour of the pipe wall (described by Hooke's law), wave speed can be estimated by [13]:

$$C = \sqrt{\frac{K/\rho}{1 + \frac{cD}{eE} K}} \quad (3)$$

where E is the Young's modulus of elasticity of the pipe, K is the fluid bulk modulus, ρ is the fluid density, e is the pipe wall thickness and c is a pipe constraint factor.

2.2. Leak modelling

A leak represents a flow loss without head loss. A leak is modelled as an orifice and the discharge, Q_ℓ , through it is assumed to be given by the following equation [7]:

$$Q_\ell = C_d A_\ell \sqrt{2gH_\ell} \quad (4)$$

where C_d is a discharge coefficient, A_ℓ is the orifice area and H_ℓ is the head on either side of the orifice assumed to be equivalent.

3. NUMERICAL RESOLUTION

Equations (1) and (2) can be transformed into a system of ordinary differential equations and solved by the method of characteristics (MOC). The compatibility equations are [3]:

$$Q_{Pi} - Q_{i-1} + \frac{gA}{C}(H_{Pi} - H_{i-1}) + \frac{\lambda}{2DA} Q_{i-1} |Q_{i-1}| \Delta t = 0 \quad (5)$$

along the positive characteristic line ($\Delta x/\Delta t = +C$), and

$$Q_{Pi} - Q_{i+1} - \frac{gA}{C}(H_{Pi} - H_{i+1}) + \frac{\lambda}{2DA} Q_{i+1} |Q_{i+1}| \Delta t = 0 \quad (6)$$

along the negative characteristic line ($\Delta x/\Delta t = -C$) where i is the node number, Δx and Δt are the distance and the time steps respectively (figure 1).

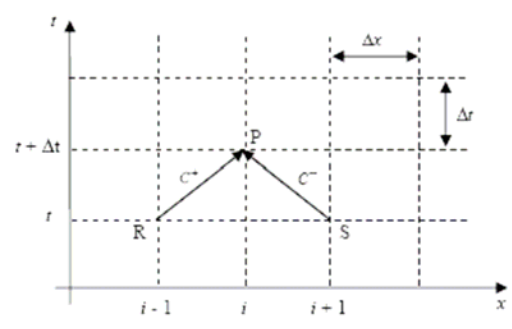


Fig. 1. Characteristic lines: Regular grid

3.1. Initial conditions

In this paper, attention is focused mainly on transients occurring in a single elastic pipe with a constant level reservoir at the upstream end and a rapid closure valve at the downstream end (figure 2). A single leak is supposed to exist at an intermediate section of the pipe located at a distance X from the valve. The pipe with a length L is subdivided in two segments: pipe 1 from the reservoir to the leak and pipe 2 from the leak to the valve.

Initial conditions must be provided at the time 0 in order to solve the problem. These conditions can be determined by computing the solution of the following system of ordinary differential equations deduced from equations (1) and (2):

$$\begin{cases} \frac{dQ_J}{dx} = 0 \\ \frac{dH_J}{dx} = -\frac{\lambda Q_J^2}{2gDA^2} \end{cases} \quad (7)$$

where J refers to the pipe number.

The solution of this system is:

$$\begin{cases} Q_J(0, x) = Q_J(0, 0) \\ H_J(0, x) = H_J(0, 0) - \frac{\lambda Q_J^2}{2gDA^2} x \end{cases} \quad (8)$$

At the leak:

$$Q_1(0, L-X) = Q_2(0, 0) + Q_{\ell 0} \quad (9)$$

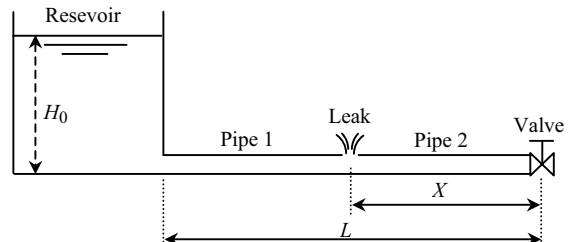


Fig. 2. Reservoir-pipe-valve system with a leak

3.2. Boundary conditions

Transient flow is created by the fast closure of the valve at the downstream end ($x = L$). At this section $Q_2(t, X) = 0$. At the upstream end, $x = 0$ and $t > 0$, the condition is given by the reservoir at fixed level $H_1(t, 0) = H_0$.

At a leak, equation (4) is implemented in the MOC as an internal boundary condition (figure 3). The two relationships that relate the upstream head and flow to the downstream head and flow are:

$$H_{1P, N_1+1} = H_{2P, 1} = H_P \tag{10}$$

$$\begin{aligned} Q_{1P, N_1+1} &= Q_{2P, 1} + Q_\ell \\ &= Q_{2P, 1} + C_d A_\ell \sqrt{2gH_P} \end{aligned} \tag{11}$$

The compatibility equations either side of the leak are given by equations (5) and (6):

$$\begin{aligned} Q_{1P, N_1+1} - Q_{1, N_1} + \frac{gA}{C} (H_{1P, N_1+1} - H_{1, N_1}) \\ + \frac{\lambda}{2DA} Q_{1, N_1} |Q_{1, N_1}| \Delta t = 0 \end{aligned} \tag{12}$$

$$\begin{aligned} Q_{2P, 1} - Q_{2, 2} - \frac{gA}{C} (H_{2P, 1} - H_{2, 2}) \\ + \frac{\lambda}{2DA} Q_{2, 2} |Q_{2, 2}| \Delta t = 0 \end{aligned} \tag{13}$$

Equations (10) to (13) form a set of quadratic equation in $\sqrt{H_P}$ that is solved using the quadratic formula:

$$H_P = \left[\frac{-C_d A_\ell \sqrt{2g} + \sqrt{\Delta}}{4 \frac{gA}{C}} \right]^2 \tag{14}$$

where

$$\begin{aligned} \Delta = & (C_d A_\ell \sqrt{2g})^2 - 8 \frac{gA}{C} \left[(Q_{2, 2} - Q_{1, N_1}) \right. \\ & \left. - \frac{\lambda \Delta t}{2DA} (Q_{2, 2} |Q_{2, 2}| - Q_{1, N_1} |Q_{1, N_1}|) \right. \\ & \left. - \frac{gA}{C} (H_{2, 2} + H_{1, N_1}) \right] \end{aligned} \tag{15}$$

Once H_P is determined the upstream and downstream flows are calculated using the positive and negative compatibility equations (5) and (6) respectively.

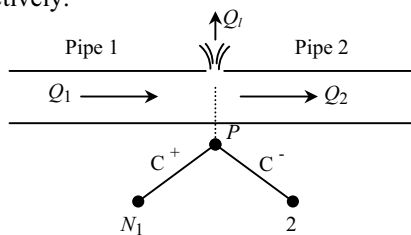


Fig. 3. Leak implementation in the MOC

4. APPLICATION AND RESULTS

4.1. Leak location and sizing

As an example, considering the reservoir-pipe-valve system represented by figure 1 with a leak at an intermediate section and the following characteristics: $D = 0.3048 \text{ m}$, $L = 1600 \text{ m}$, $C = 1200 \text{ m/s}$, $H_0 = 50 \text{ m}$ and $Q_0 = 0.02 \text{ m}^3/\text{s}$. The mean leak discharge Q_{ℓ_0} is $0.002 \text{ m}^3/\text{s}$ which is 10 % of the total mean flow at the upstream end.

Figures 4 (a, b and c) show the head history at the valve obtained by the numerical simulation for leaks located at various positions along the pipe ($X = L/3$, $X = L/2$ and $X = 2L/3$). Figure 5 shows the discharge history at leaks located at the previous positions.

Friction effects are ignored ($\lambda = 0$) to highlight the impact of the leak on the head of pressure evolution.

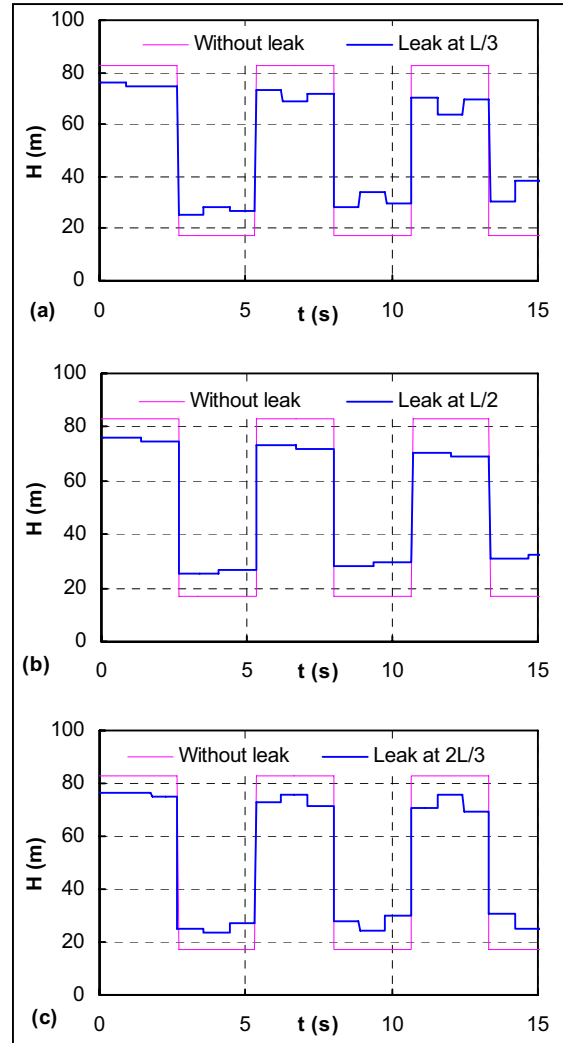


Fig. 4. Comparison of head history at the valve with different leak locations

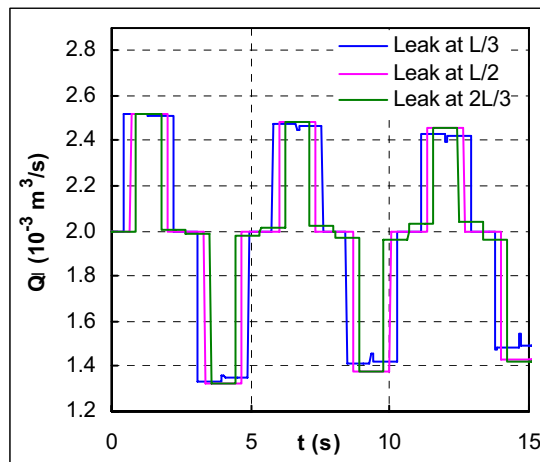


Fig. 5. Discharge history at the leak

The transient event is damped much more rapidly than in the system where the leak does not exist. It can be interpreted by the effect of the leak on the features of the pressure wave propagating along the pipe. Indeed, the leak causes partial reflections of wave fronts that became small pressure discontinuities in the original pressure trace and increase the damping of the overall pressure signal. Hence, through correctly interpreting the head-time history at the valve it is possible to extract information on leak location and leak discharge.

Figure 6, which is an enlargement of the results of figure 4, shows that the location of leak is given by:

$$X = \frac{t_f}{t_0} L \quad \text{and} \quad \frac{X}{L} = \frac{t_f}{t_0} \quad (16)$$

where t_f is the time difference between the initial transient wave and the reflected wave at the leak section (time corresponding to the sudden change of head from ΔH_1 to ΔH_2) and $t_0 = 2L/C$ is the pipe characteristic time. Table 1 summarizes values of t_f for the considered leak locations.

By analysing the head-time transient in figure 5, the leak discharge may be obtained by:

$$Q_{l_0} = \frac{gA}{C} (\Delta H_0 - \Delta H_1) \quad (17)$$

ΔH_0 and ΔH_1 are head rises provoked by the sudden closure of the valve when there is or there is no leak respectively.

Table 1. Leak location ($t_0 = 2.666$ s)

Leak location	$L/3$	$L/2$	$2L/3$
t_f (s)	0.888	1.333	1.777
$X/L = t_f/t_0$	0.333	0.5	0.666

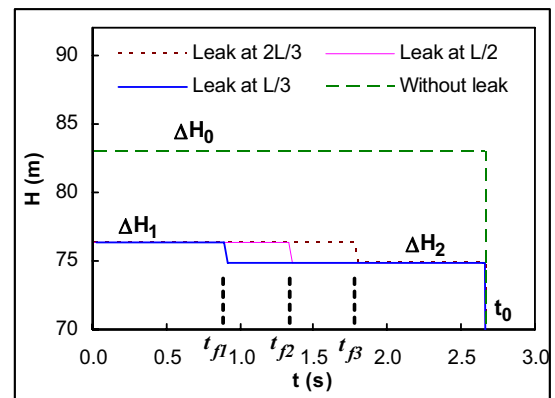


Fig. 6. Head history at the valve with different leak locations

4.2. Influence of the friction

The previous example of reservoir-pipe-valve system is numerically simulated taking in consideration the friction term ($\lambda \neq 0$). Figure 7 shows the effect of friction and leak on the pressure response at the valve.

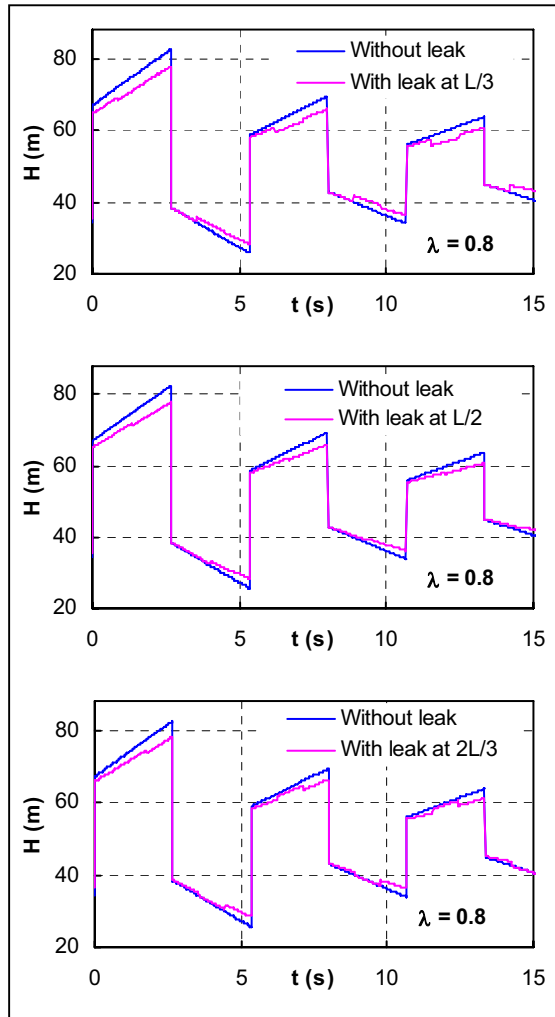


Fig. 7. Head history at the valve ($\lambda = 0.8$)

The friction damps and reduces the overall magnitude of the pressure response. The presence of leak serves to increase the damping in the system. Additionally, the pressure response is more complicated due to the reflection from the leak.

4.3. Influence of Young modulus

Figure 8 represents pressure head at the valve obtained for different values of Young modulus. When the pipe wall elasticity increases the pressure amplitude is reduced and the period increases (the pressure fluctuations are damped more rapidly). This can be interpreted by the effect of the pipe wall deformation on the features of the pressure wave propagating along the pipe. Indeed, the reduction of Young modulus generates a reduction of the celerity (Eq. 3) and consequently the amplitude of this wave is decreased.

Figure 7 shows also that the times t_0 and t_f increases when the Young modulus increases, but the quotient t_f/t_0 remains constant and equal to L/C . Consequently the leak location given by

equation (16) is not affected by the change of Young modulus.

Figure 8 represents the fluctuations of the leak discharge for different values of Young modulus. The amplitude of leak discharge fluctuations is reduced when the Young modulus decreases.

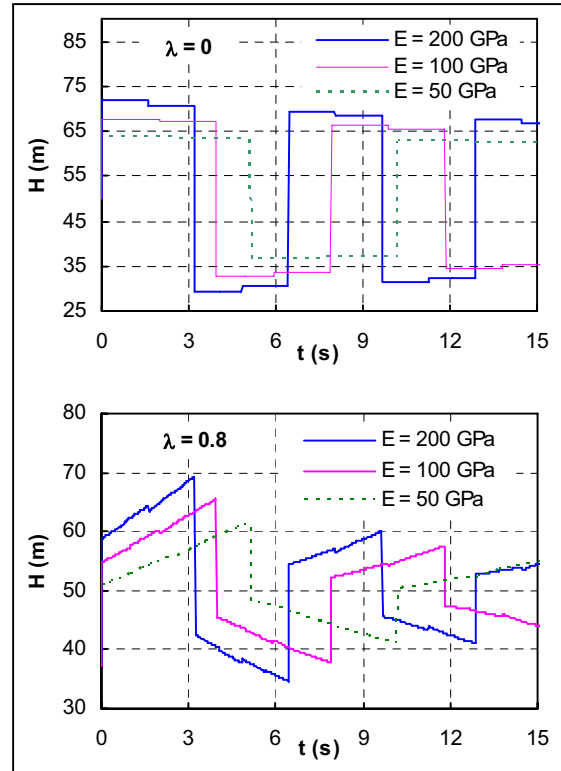


Fig. 8. Head history at the valve for different values of Young modulus

(Leak at $L/2$, $Q_{l_0} = 0.004 \text{ m}^3/\text{s}$)

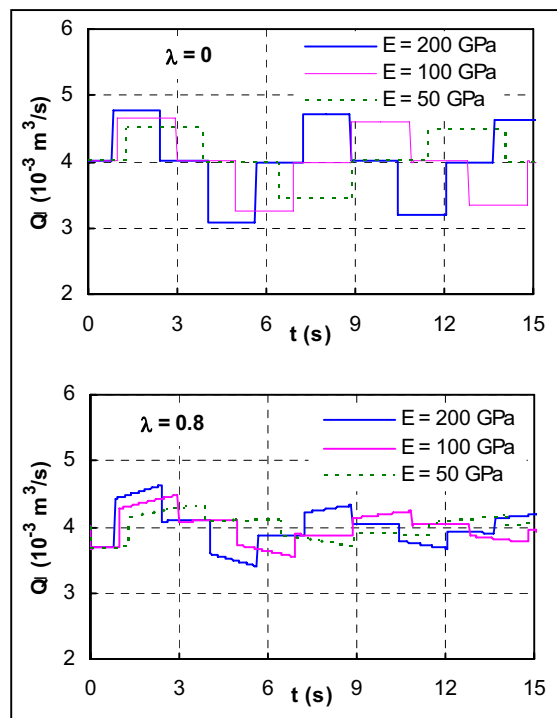


Fig. 9. Leak discharge for different values of Young modulus

(Leak at $L/2$, $Q_{\ell_0} = 0.004 \text{ m}^3/\text{s}$)

5. CONCLUSIONS

In this paper, a technique based on the analysis of pressure wave in a single pipe system to locate and size leaks was investigated. The method of characteristics, which requires less computer cost, is directly used to determine the magnitude of leaks by developing relations between the location and amplitude of the reflected wave at the leak section.

Furthermore, it is necessary to register the pressure time-history in just one section of the pipe (for example the downstream end) and then the proposed technique can strongly reduce leak detection survey costs in safe conditions.

This study shows that pipe-wall elasticity and steady friction affect the leak detection. Further work is needed in order to investigate the effect of the unsteady friction and pipe-wall viscoelasticity.

6. BIBLIOGRAPHIE

- [1] D. Covas, I. Stoianov, H. Ramos, N. Graham, C. Maksimovic: *The dissipation of pressure surges in water pipeline systems*. First Joint Conf. IAHR-IWA on pump, Electromechanical Devices and Systems (PEDS 2003), Valencia, Spain, 2003.
- [2] A. N. Tafuri: *Locating Leaks with acoustic technology*. American Water Works Association Journal, 92 (2000) 57-66.
- [3] O. Hunaidi, P. Giamou: *Ground-Penetrating Radar for Detection of Leaks in Buried Plastic Water Distribution Pipes*. Seventh International Conference on Ground-Penetrating Radar, Lawrence, Kansas, USA, 1998.
- [4] B. Brunone: *Transient Test-Based Techniques for Leak Detection in Outfall Pipes*. Journal of Water Resources Planning and Management, 125 (1999) 302-306.
- [5] D. Misiunas, J. Vitkovsky, G. Olsson, A. Simpson, M. Lambert: *Pipeline Break Detection Using Pressure Transient Monitoring*. Journal of Water Resources Planning and Management, 131 (2005) 316-325.
- [6] S. G. Buchberger, G. Nadimpalli: *Leak Estimation in Water Distribution Systems by Statistical Analysis of Flow Readings*. Journal of Water Resources Planning And Management, 130 (2004) 321-329.
- [7] B. Brunone, M. Ferrante: *Detecting leaks in pressurized pipes by means of transients*. Journal of Hydraulic Research, 39 (2001) 539-547.
- [8] W. Mpesha, S. L. Gassman, M. H. Chaudhry: *Leak Detection in Pipes by Frequency Response Method*. Journal of Hydraulic Engineering, 127 (2001) 134-147.
- [9] M. Ferrante, B. Brunone. *Pipe system diagnosis and leak detection by unsteady-state tests. I harmonic analysis*. Advances in Water Resources 26 (2003) 95-105.
- [10] M. Taghvaei, S. B. M. Beck, W. J. Staszewski, 2006: *Leak detection in pipelines using cepstrum analysis*. Measurement Science and Technologie, IOP Publishing Ltd, UK. 17 (2006) 367-372.
- [11] E. Hadj Taïeb: *Leak detection by using water hammer and impedance methods*. Water Mangement Challenges in Global Change, Ulanicki et al. (eds), Taylor & Francis Group, London, UK, 2007, pp. 345-352.
- [12] A. K. Soares, D. I. C. Covas, L. F. R. Reis: *Inverse transient analysis for leak detection in PVC pipe network*. Water Mangement Challenges in Global Change, Ulanicki et al. (eds), Taylor & Francis Group, London, UK, 2007, pp. 337-344.
- [13] E. B. Wylie, V. L. Streeter, L. Suo: *Fluid transients in systems*. Prentice Hall, Englewood Cliffs, New Jersey, USA, 1993.
- [14] R. Courant, K.O. Friederichs: *Supersonic flow and shock waves*. Interscience publishers Inc., New York, 1948.

UNSTEADY LOADS EVALUATION FOR A WIND TURBINE ROTOR

Said CHKIR*, Ivan DOBREV**, Patrick KUSZLA***, Fawaz MASSOUH****

* Arts et métiers ParisTech, ERDT
 151 Bd de l'Hôpital, 75013 Paris, France, said.chkir@paris.ensam.fr
 ** Arts et métiers ParisTech, LMF
 151 Bd de l'Hôpital, 75013 Paris, France, ivan.dobrev@paris.ensam.fr
 *** Arts et métiers ParisTech, DYNFLUID
 151 Bd de l'Hôpital, 75013 Paris, France, patrick.kuszla@paris.ensam.fr
 **** Arts et métiers ParisTech, ERDT, LMF
 151 Bd de l'Hôpital, 75013 Paris, France, fawaz.massouh@paris.ensam.fr

Summary

This paper presents a method for calculating the flow around a wind turbine rotor. The real flow is replaced by a free stream past a vortex model of the rotor. This model consists of lifting vortex lines which replace the blades and a trailing free vorticity. The vorticity shed from the blade is concentrated in two vortices issued from tip and root. To compute the unsteady forces exerted on the rotor, a free wake method is used. The evolution of the wake is obtained by tracking the markers representing the vortices issued from the blade tips and roots. To solve the wake governing equation and to obtain the marker positions, a time-marching method is applied and the solution is obtained by a second order predictor-corrector scheme. To validate the proposed method a comparison is made with experimental data obtained in the case of a model of wind turbine where the flow field immediately behind the rotor is measured by means of PIV. It is shown that the numerical simulation captures correctly the near wake development. The comparison shows satisfactory accuracy for the velocity field downstream of the rotor.

Keywords: Wind turbine/Unsteady aerodynamics/Vortex/Wake/PIV.

NOMENCLATURE

α : Lamb-Oseen constant
 δ : Effective eddy-viscosity coefficient
 \vec{r} : Position vector of vortex control point
 t_0 : Initial position at time $t = 0$
 ψ_w : Vortex wake age (rad)
 ψ_b : Azimuthal angle (rad)
 V_∞ : Free-stream velocity vector
 Γ : Vortex strength, Circulation (m/s)
 ρ : Density of air
 N : Number of rotor blades
 c : Blade chord
 W : Wind relative velocity
 V_{ind} : Induced velocity vector
 r_t : Blade tip radius, (m)
 r_h : Blade root radius, (m)
 ds : Element of the vortex.
 r_0 : Initial viscous core radius
 r_c : Viscous core radius
 a_1 : Turbulent viscosity constant
 Re_v : Vortex Reynolds number
 Ω : Rotational speed of the rotor (rad/s)

ϕ : Flow angle
 v_i : Self-induced velocity at point i
 Δs : Vortex segment length
 C_L : Lift coefficient
 C_D : Drag coefficient

INTRODUCTION

In the last few decades, wind energy has become the leading contender among the renewable sources of energy. Wind turbines are playing a significantly increasing role in the generation of electrical power that can then be used in various applications. Wind turbines operate in a complex unsteady flow environment composed of various effects such as atmospheric turbulence, ground boundary layer effects, directional and spatial variations in wind shear and the effects of the tower shadow. The estimation of the velocity field and local angle of attack of the blade's profiles could be the key to predict the aerodynamic loads on the rotor and the power generated by a wind turbine.

Improving the capability of the numerical tools to predict the aerodynamic and mechanical forces applied to the rotor, is one of the most important factors to optimize their design, operating and maintenance costs and to verify their reliability.

Generally, methods concerned with the prediction of the aerodynamic loading and performance of wind turbines assume that the fluid is inviscid and incompressible. In the most common method, the Blade Element Momentum Theory (BEM) methods [1], the blade is divided into several segments with cylindrical surfaces and the calculation is performed segment by segment. All blade elements are assumed to operate independently of each other. Accordingly, if lift and drag forces are determined for each element; it will be then possible to evaluate the rotor characteristics. In the present free wake method, the airfoil relative velocity is corrected by the induced velocity. The axial and tangential induced velocities are calculated for each section using the momentum theorem. The BEM methods are simple to use, require little computer time and provide accurate results, however, it contains invalid assumptions which are overcome in practice by empirical adjustments.

In recent years the resolution of the Navier-Stokes equations [2] has become a preferred method in all the domains of fluid mechanics. The advantages of this method are well known, especially the possibility of obtaining a solution in very complex flows cases. Despite the good results in most cases, these methods need huge computational costs and large memory requirements that delayed their practical use for many problems, including helicopter and wind turbine applications.

The vortex methods are potential methods based on the replacement of the real flow through the rotor by an inviscid fluid flow through an equivalent vortex system. This system consists of blade attached vortices and free vortices trailed into the wake. According to the representation manner of the vortex wake, there are two different approaches: prescribed wake and free wake. The prescribed wake method assumes that the wake shape is known, either through testing, or from an approached calculation [3]. In unsteady conditions and if the induced velocity is important, the wake shape varies in time and the prescribed wake method is therefore not applicable. In this case, the free wake method is preferred and we will describe its principles in the following.

1. METHODOLOGY

The free wake method is originally used in the analysis of helicopter rotors [4]. These models created for helicopter rotors have been later adapted for the calculation of wind turbines rotors [5]. In this vortex method, the real flow is replaced by an inviscid fluid flow through an equivalent vortex system.

This system consists of vortex attached to each blade (exerting on the fluid the same forces as those applied by the blades) and a wake consisting of

a strong tip-vortex emanating from each blade tip and root (Fig. 1).

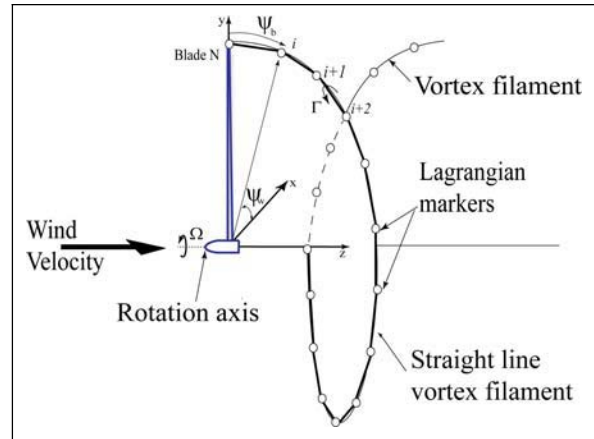


Fig. 1. Representation of the rotor wake

In this work, a Lagrangian description of the flow is used. Lagrangian markers are distributed along each tip-vortex filament (Fig. 2). Thus, tip-vortex filaments are discretized and the markers are linked together, usually with straight line segments. This allows the induced velocity to be determined using the Biot-Savart law:

$$d\vec{V}_{ind} = \frac{\Gamma}{4\pi} \frac{d\vec{s} \times \vec{r}}{|\vec{r}|^3}. \quad (1)$$

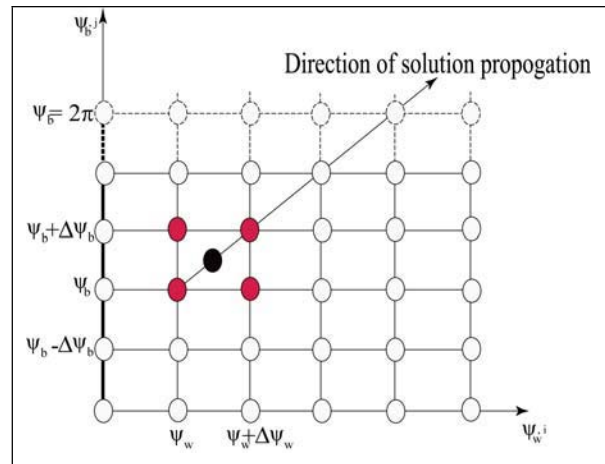


Fig. 2. Five-point central differencing scheme

The spatio-temporal evolution of the markers in the rotor wake can be derived from Helmholtz's law (vorticity transport theorem) by assuming that for each point in the flow the local vorticity is convected by the local velocity. The fundamental equation describing the transport of the filament is:

$$\frac{d\vec{r}}{dt} = \vec{v}. \quad (2)$$

Where \vec{r} is the position vector that can be represented using a function of two variables, which represent the spatio-temporal evolution of the Lagrangian markers position:

$$\vec{r} = \vec{r}(\psi_w, \psi_b). \quad (3)$$

In equation (3), ψ_w is the azimuth angle (wake age) corresponding to the vortex that was trailed from the blade when it was at an azimuth angle ψ_b . Using these two angular variables and a constant angular velocity Ω of the wind turbine, the position vector \vec{r} of a wake element can be expressed as a function of the azimuthal blade position ψ_b and the age of the filament ψ_w relative to the blade when it was introduced into the wake. Equation (2) can, therefore, be written in the non-rotating, hub-fixed coordinate system as:

$$\frac{\partial \vec{r}}{\partial \psi_w} + \frac{\partial \vec{r}}{\partial \psi_b} = \frac{1}{\Omega} \vec{V}. \quad (4)$$

where the velocity \vec{V} is the contribution of the free stream and the highly nonlinear self and mutually induced velocities corresponding to the vortex wake structure. Note that equation (4) is a first-order, partial differential equation. The homogeneous portion of this equation is hyperbolic. However, the right-hand side, which includes the velocity induced by the attached and the free vortex, is highly nonlinear.

The complexity of the solution of equation (4) arises from the nonlinearity and the singularity of the vortex filaments. To simplify the calculation, the blade surface must be replaced by a vortex line with a constant circulation. This simplification can be justified in the case of high aspect ratio blades, as observed in wind turbines. A numerical solution of equation (4) may be made by using a second order predictor-corrector scheme to improve the accuracy and the stability of the numerical algorithm. The discretization of equation (4) is presented in (Fig. 2) using a five-point central differencing scheme.

The predictor step is used to obtain an intermediate solution at the new time step to enable the induced velocity calculation $\vec{V}_{j+\frac{1}{2}}^n$ to proceed by using Biot-Savart law as:

$$\tilde{\vec{r}}_{j+1} = \vec{r}_j^n + \frac{2}{\Omega} \left(\frac{\Delta \psi_w \cdot \Delta \psi_b}{\Delta \psi_w + \Delta \psi_b} \right) \vec{V}_{j+\frac{1}{2}}^n \quad (5)$$

The corrector step is obtained by averaging the predicted induced velocity $\tilde{\vec{V}}_{j+\frac{1}{2}}^n$ with $\vec{V}_{j+\frac{1}{2}}^n$ at (n)th time step as:

$$\vec{V}_{j+\frac{1}{2}}^{n+\frac{1}{2}} = \frac{1}{2} \left(\vec{V}_{j+\frac{1}{2}}^n + \tilde{\vec{V}}_{j+\frac{1}{2}}^n \right). \quad (6)$$

Then, this value is used with the obtained value of (5) in the corrector step as:

$$\tilde{\vec{r}}_{j+1}^{n+1} = \vec{r}_j^n + \frac{2}{\Omega} \left(\frac{\Delta \psi_w \Delta \psi_b}{\Delta \psi_w + \Delta \psi_b} \right) \vec{V}_{j+\frac{1}{2}}^{n+\frac{1}{2}}. \quad (7)$$

The local air velocity relative to the rotor blade consists of the free-stream velocity and the wake induced velocities as:

$$\vec{V} = \vec{V}_\infty + \vec{V}_{ind}. \quad (8)$$

The wake induced velocity is evaluated by the application of the Biot-Savart law (1) as an integral along the complete length of each vortex wake filament. For a vortex segment of length AB (Fig. 3), the induced velocity at a point C can be written as:

$$d\vec{V}_{ind C} = \frac{\Gamma}{4\pi} (\vec{r}_1 \times \vec{r}_2) \frac{1}{|\vec{r}_1| \cdot |\vec{r}_2| + \vec{r}_1 \cdot \vec{r}_2} \frac{|\vec{r}_1| + |\vec{r}_2|}{|\vec{r}_1| \cdot |\vec{r}_2|}. \quad (9)$$

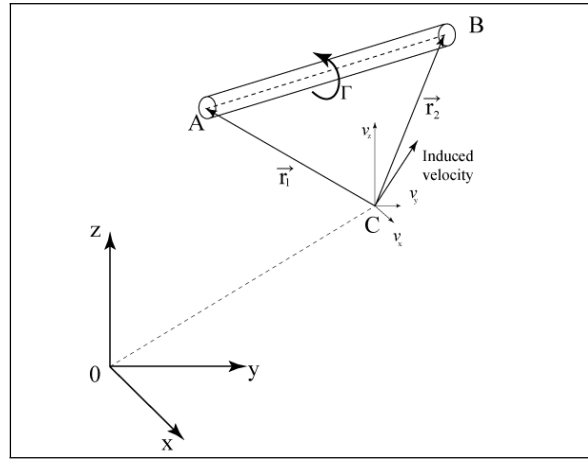


Fig. 3. Induced velocity by a segment vortex

At the control point, where we have to calculate the self induced velocity, equation (9) is singular. However, a straight vortex representation cannot induce a velocity on itself, the contribution of vortex straight-segment at the left and right of the control point is zero, so a curvature correction should be applied [6]. The correction is applied only at the neighboring of the control point, where the self-induced velocity is needed. The theoretical velocity on the vortex line is infinite. But in the real case, a vortex tube is observed. The maximum velocity induced by this tube can be found on the surface of the vortex core of radius r_c . The self-induced velocity can be calculated by an integration of the Biot-Savart law along a curved vortex filament excluding the vortex core (Fig.4).

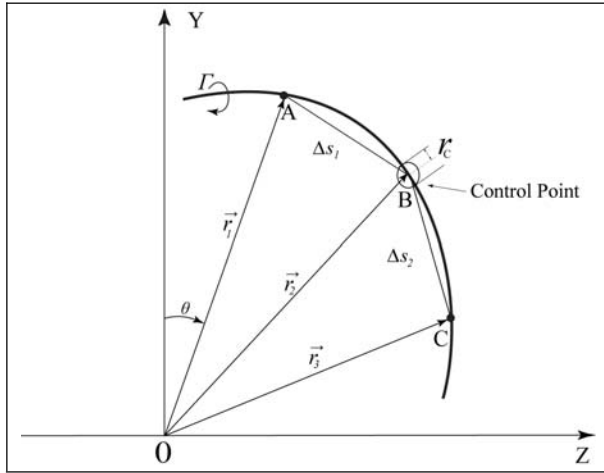


Fig. 4. Calculation of the self-induced velocity

This treatment gives the formula proposed by Hama [7]

$$\vec{v}_i = -\frac{\Gamma \left(\frac{\partial \vec{r}}{\partial s} \right) \times \left(\frac{\partial^2 \vec{r}}{\partial s^2} \right)}{4\pi \left| \frac{\partial \vec{r}}{\partial s} \right|^3} \ln r_c. \quad (10)$$

In our case, the value of r_c is in order of 10 % of the tip airfoil chord. It represents the core radius of the viscous vortex and allows taking into account his actual structure. The radius r_c can be obtained either from experiments or from semi-empirical laws.

Because of the viscous effects, the core radius of the tip vortices does not remain constant and increases as it progresses downstream of the rotor. Leishman and Bhagwat [8] suggested an empirical approach to calculate the growth of the viscous core radius:

$$r_c(\psi_w) = \sqrt{r_0^2 + \frac{4\alpha\delta\nu\psi_w}{\Omega}}. \quad (11)$$

Here, the eddy-viscosity coefficients δ takes into account the diffusion rate of the tip vortex, which must be a function of the Reynolds number as:

$$\delta = 1 + a_1 \text{Re}_v. \quad (12)$$

The experimental values of a and a_1 are given in [9]. It is observed also that the circulation Γ decreases along the vortex filament, this is caused by viscous dissipation. Indeed, this circulation reduction is taken into account from experimental data.

1.1. Numerical algorithm

The calculation is initialized with all the vortex markers located at the tip vortex of the blades. At each time step one vortex segment is emitted and moves with the local fluid velocity. The modified vortex structure changes the induced velocity field. The updated velocities are then used to move the markers using the described predictor-corrector scheme. For the presented calculation, each vortex filament was discretized by 200 segments. A stable

periodic configuration was obtained after 30 revolutions of the rotor.

At each time step, we also calculate the induced velocity along the blades axis. These induced velocities allow us to obtain the relative velocity distribution and the angles of attack along the blade. And finally the updated circulation is obtained using the Kutta-Joukowski lift theorem.

For the steady case, we can calculate the aerodynamic efforts exerted on a wind turbine rotor (the calculations of blade forces F , rotor torque Q , and the power P) by using the formula:

$$F = \int_{r_r}^{r_t} \frac{1}{2} \rho N c W^2 (C_L \cos \phi + C_D \sin \phi) dr \quad (13)$$

$$Q = \int_{r_r}^{r_t} \frac{1}{2} \rho N c W^2 (C_L \sin \phi - C_D \cos \phi) r dr \quad (14)$$

$$P = \int_{r_r}^{r_t} \frac{1}{2} \rho N c W^2 (C_L \sin \phi - C_D \cos \phi) r \Omega dr \quad (15)$$

If the blades circulation does not vary any more, we stop the calculation, and then the aerodynamic characteristics of the wind turbine can be evaluated by (13), (14) and (15).

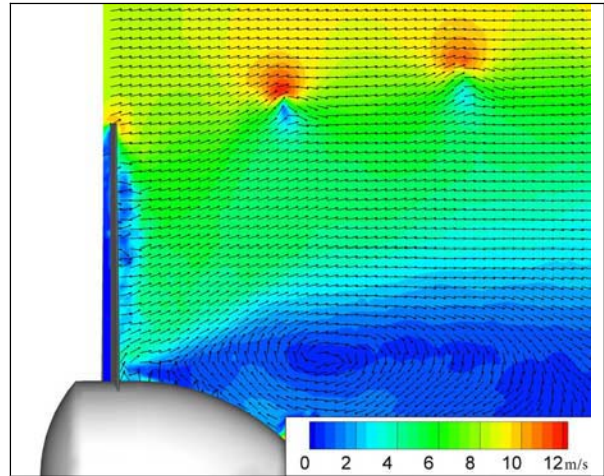


Fig 5. Downstream axial velocity field, Rutland 503 wind turbine (m/s), PIV measurement

2. RESULTS AND DISCUSSION

The calculation results show the robustness of the predictor-corrector scheme proposed. In order to validate this method, we present here only the wake calculation results witch compared with laboratory measurements made with PIV. The study focused on areas where wake modeling requires attention; in particular, to obtained the form trailing tip vortex, vital for the prediction of fluid loading on the rotor blades.

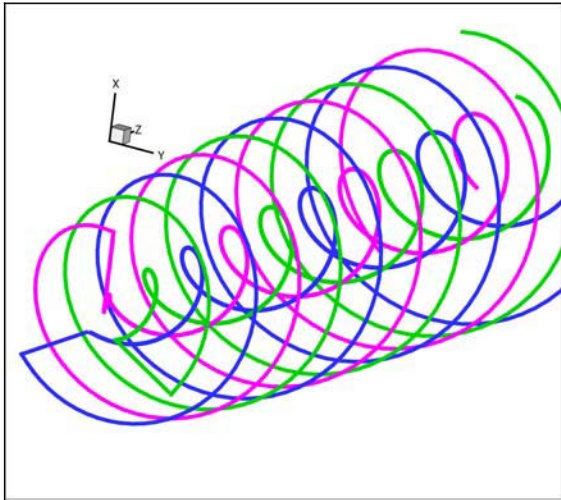


Fig. 6. Downstream wake shape calculated by the present free wake method, Rutland 503 wind turbine

The experimental data used for validation were obtained at the ENSAM-Paris wind tunnel using a modified commercial wind turbine Rutland 503, [10]. The PIV technique is applied to obtain the velocity in the wake downstream of the turbine rotor and also the vortex tip positions.

The horizontal axis wind turbine has a three blades rotor with a diameter of 0.5 m and a hub diameter of 0.135 m. The blades are tapered and untwisted. They have a pitch angle of 10° and a chord of 0.045 m at tip and 0,065 m at root. The rotational speed is 1000 rpm with a free-stream velocity of 9.3 m/s. The wind turbine is mounted on a support tube ensuring a sufficient height in order to allow the lasers fixed above the transparent roof to illuminate the explored plane with an adequate intensity.

The airfoil characteristics are important to calculate the circulation along the blade. Unfortunately the experimental data concerning Rutland airfoil sections is not available. It is possible to carried out CFD calculation and obtain the needed data, but to reduce the influence of blade airfoil characteristics on the calculation, the tip vortex intensity is prescribed. This circulation is the same as in experiments.

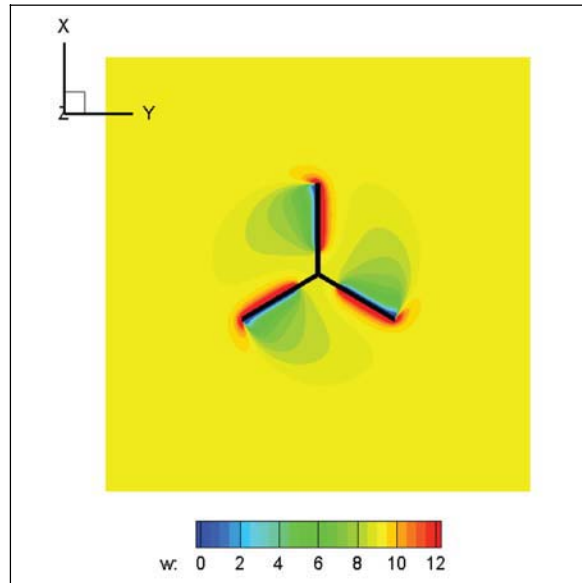


Fig. 7. Face view of the wake calculated by the present free-wake method, axial velocity (m/s)

The wake vortex shape is presented in (Fig.6), it generally fits the experimental wake shown in (Fig. 5). The axial velocity field in the rotor plane and in the azimuth plane is presented in (Fig.7). It may be noted, outside the wake, the wind is accelerated by the axial component of the induced velocity of all the vortices. However, in the wake, the induced velocity by the vortex is decelerating the flow. Accordingly, downstream of the turbine the wake diameter increases as the distance from the rotor increases. After some distance, the diameter remains constant in the simulation as in the experiment.

In the experiment (Fig. 5), we can see that there is a vortex area behind the hub which is not taken into account in our simulation. In fact, in the case of industrial turbines, the hub is much smaller and this stall area and recirculation does not exist.

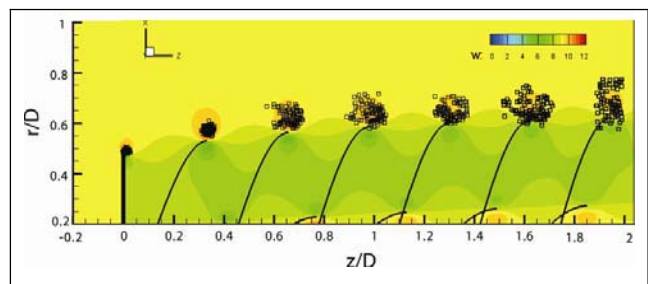


Fig. 8. Comparison of the tip vortex locations obtained from the free wake method and the PIV results

Figure (8) shows a comparison between the tip vortex positions obtained from the PIV experiment and the free wake method for axial (unyawed) flow conditions. The wake expands behind the turbine, and the free wake method captures the tip vortex locations well for younger wake ages. Some differences can be seen in the far wake. The increased uncertainty in defining the tip vortex

positions is partially due to the diffusion of the real vortex cores. In addition, some aperiodicity of the flow may account for the differences in the locations for older wake ages.

3. SUMMARY

This paper has reviewed the theoretical basis and numerical implementation of one class of a free wake method, which was set up to calculate the aerodynamic loadings and performance of a horizontal-axis wind turbine.

In this method, the rotor wake is discretized into vortex filaments defined by a series of Lagrangian markers. The governing equation for this free-wake problem is reduced to a system of first-order, partial differential equations that describe the convection of these markers through the flow.

Unlike the prescribed wake method, we calculate here explicitly the trajectory of vortex markers emitted by blade tips. The calculation results show that the wake has a helical-like form. Furthermore the vortex lines are not located on a cylindrical surface, as suggested by the linear vortex theory. They move outward by increasing the diameter of the vortex tube. A validation study for the prediction of the wake geometry behind a three-bladed wind turbine using a free-wake was performed for axial flow conditions, and was validated against laboratory experiments using the PIV technique. The comparison reveals that accurate results can be obtained, for the operating conditions considered, with substantial savings of computer time, comparing to the CFD method

REFERENCES

- [1] Sørensen, JN., Mikkelsen, R.: *On the validity of the blade element momentum method*, Proceedings of the EWEC, Copenhagen, 2001.
- [2] Sørensen, J N., Michelsen, J., and Schreck, S. *Navier-Stokes predictions of the NREL phase VI rotor in the NASA Ames 80x120 ft wind tunnel*. Wind Energy, pp 151-169, 2002.
- [3] Leishman, G. *Challenges in modeling the unsteady aerodynamics of wind turbines*, Wind Energy, 5(2-3):85-132, 2002.
- [4] Leishman, G., *Principles of helicopter aerodynamics*. Cambridge Aero. Series., 2000.
- [5] Afjeh, A, Keith T.: *A Simplified Free Wake Method for Horizontal-Axis Wind Turbine Performance Prediction*, Journal of fluid engineering vol. 108 pp 400-406. 1986.
- [6] Wood, D. H.: *Generic vortex modeling for horizontal-axis wind turbine*, Wind Engineering, 26(2), pp. 71-84, 2002.
- [7] Hama, F.: *Progressive Deformation of a Curved Vortex by Its Own Induction*, Physics of fluids, pp 1156-1162. 1962.
- [8] Leishman, G., Bhagwat, M.: *Correlation of Helicopter Tip Vortex Measurement*, AIAA Journal, Vol. 38, No 2, pp.301-308, 2000.
- [9] Ramasamy, M., Leishman, G., *Interdependence of Diffusion and Straining of Helicopter Blade Tip Vortices*, Journal of Aircraft, 41(5):1014-1024, 2004/
- [10] Dobrev, I., Maallouf, B., Troldborg N., Massouh, F.: *Investigation of the Wind Turbine Vortex Structure*, 14th Int Symp on App. of Laser Tech. to Fluid Mech., Lisbon, 2008.



Said CHKIR
Researcher, Arts et Métiers ParisTech
France

Research interests: Fluid Mechanics,
Wind energy



Ivan DOBREV
Researcher, Arts et Métiers ParisTech
France

Research interests: Fluid Mechanics,
Wind energy.



Patrick KUSZLA
Qualified Professor, Arts et Métiers
ParisTech, France

Research interests: Aerodynamics,
Numerical simulation, Wind turbines,
Simulation of manufacturing processes,
Unmanned aerial vehicles



Fawaz MASSOUH
Assoc. Professor, Arts et Métiers
ParisTech, France

Research interests: Fluid Mechanics,
Wind energy.

THE GLOBAL AND PARTIAL SYSTEM CONDITION ASSESSMENT IN MULTIDIMENSIONAL CONDITION MONITORING¹

Czesław CEMPEL

Poznan University of Technology, Poland

ul. Piotrowo 3, 60-965 Poznań, Poland, e-mail: czeslaw.cempel@put.poznan.pl

Summary

Machines have many faults which evolve during its life (*operation*). Observing some number of symptoms during the machine operation it is possible to capture needed fault oriented information. One of the methods to extract fault information from such symptom observation matrix (SOM) is to apply the singular value decomposition (SVD), obtaining in this way the generalized fault symptoms. The problem of this paper is to use the total damage symptom, being a sum of all generalized symptoms. Also we will use the first generalized symptom as the dominating fault symptom, to infer better on machine condition. There was some new software created for this purpose, and some cases of machine condition monitoring have been considered as examples. Considering these it seems to the author, that both generalized symptoms should be used for the inference on machine condition. They are complimentary each other in some way, and should be used together to increase the reliability of diagnostic decision.

Keywords: condition monitoring, multidimensional observation, singular value decomposition, generalized fault symptoms, grey models, forecasting, decision reliability.

CAŁKOWITA I CZĄSTKOWA OCENA STANU W WIELOWYMIAROWEJ DIAGNOSTYCE MASZYN

Streszczenie

Maszyny mają wiele uszkodzeń, które ewoluują w trakcie ich pracy. Jeśli obserwujemy pewną liczbę dobranych symptomów w trakcie życia obiektu możemy tą informację o uszkodzeniach wychwycić w zapisie symptomowej macierzy obserwacji (SOM). Ekstrakcja tej informacji uszkodzeniowej jest możliwa za pomocą procedury SVD, która wyodrębnia poszczególne uogólnione symptomy związane z niezależnymi uszkodzeniami w maszynie. Zazwyczaj mamy sytuacje jednego dominującego symptomu i nasze wnioskowanie diagnostyczne może być związane z tym dominującym symptomem, lub też z tzw. uszkodzeniem całkowitym jako suma wszystkich uogólnionych symptomów. Problemem pracy jest właśnie pytanie; czy wziąć pod uwagę jedynie dominujące uszkodzenie, czy też całkowite. Okazuje się z kilku przykładów, że większą pewność decyzji diagnostycznej uzyskamy jeśli w weźmiemy pod uwagę oba symptomy, symptom całkowitego uszkodzenia jak i dominujący symptom.

Słowa kluczowe: nadzorowanie stanu, wielowymiarowa obserwacja, rozkład SVD, uogólnione symptomy, szare modele, prognozowanie, pewność decyzji.

1. INTRODUCTION

The most machines in operation, even performing simple operations, have many modes of failure. Hence their diagnostics have to be multidimensional. From the other side, the contemporary advancement in measurement technology allows us to measure almost any component of phenomenal field, inside or outside of the working machine. The only condition for symptoms in such multidimensional diagnostics is some kind of proportionality to gradual worsening of the machine condition which takes place during it operation. If it is so, we can name the measured component of machine phenomenal field as the **symptom**² of condition. In this way we are measuring a dozen of 'would be' symptoms, and

our condition monitoring is multidimensional from the beginning. Due to this situation, the application of multidimensional machine condition observation is now well established fact, see [1, 4, 5, 6] - for example. Moreover there exist some difference in application and processing of the multidimensional signals and/ or symptom observation matrix. For a diagnostic signals and symptoms one can apply also so called data fusion technique [4, 20, 21], and similar techniques developed lately.

¹Paper presented at ISVR09 Cracow

²Measured physical quantity being proportional to the condition of the machine.

In case of multi symptom observation one can apply principal component analysis (PCA), or singular value decomposition (SVD), looking for principal or singular components, which may have some diagnostic meaning. For the case of SVD method (*Singular Value Distribution*), there exists the body of experimental evidence [2, 19], for example, that singular components and the quantities created from them can be treated as **generalized** fault symptoms having prescribed diagnostic meaning.

All these transformation and symptom processing starts from the data base called symptom observation matrix (SOM) acquired during the on line or off line machine monitoring. Let us explain now how this SOM is structured and how it may be obtained.

During the machine life θ we can observe its condition by means of several symptoms $S_m(\theta)$ physically different and measured at some moments of life $\theta_n, n=0,1,\dots, p > r, \theta_p < \theta_b, (\theta_b - \text{anticipated breakdown time})$. This creates sequentially the symptom observation matrix (SOM), the only source of information on condition evolution of machine in its life time $0 < \theta < \theta_b$. We assume additionally that real condition degradation is also multidimensional, and is described by semi independent faults $F_t(\theta), t=1,\dots, u < r$, which are evolving in the machine body, as the expression of gradual degradation of the overall machine condition. This degradation proceeds from the **not faulty condition**³ up to its near breakdown state. Generalizing, one can say now, that we have m dimensional symptom space for condition observation, and $r < m$ dimensional fault space, which we try to extract from the observation space, by using SVD or PCA.

Moreover, some of 'would be' symptoms contained in SOM are redundant; it means not carrying enough information on the evolving faults during the machine life. But of course there is not unique criterion of the redundancy. During the course of our research, several measure of redundancy has been applied, the volume of observation space (*VolI*), pseudo Frobenius norm (*FrobI*) of SOM [19], and others. But they seem to be not good enough with respect of the quality of the final diagnostic decision. This means additionally, when optimizing the observation space, we should take into account the adequate assessment of the **current** and the **future machine condition**. The paper considers this problem, and it is done on the level of previous SVD works of the author. As the forecasting technique with minimal error, the **grey system model** with rolling window [12] was adopted for diagnostic purposes, and has been applied here according to [19].

But having the multidimensional problem of fault assessment, it is important now what type of generalized symptom we use for the forecasting and condition inference. Do we use the overall degradation symptom of the machine, or some specified generalized symptom proportional to one fault only, or both these symptoms. The results of such new approach to multidimensional diagnosis presented here were verified on the real data of machine vibration condition monitoring. Concerning the software, some modification of last programs for the data processing was needed as well. As a result it was found, that this approach seems to be promising enabling a better understanding of machine condition, and also the better current and future condition assessment.

2. EXTRACTION METHOD OF PARTIAL FAULTS FROM THE SOM

As it was said in the introduction, our information on machine condition evolution is contained in $p \bullet r$ symptom observation matrix (SOM), where in r columns are presented p rows of the successive readings of each symptom, made at equidistant system lifetime moments $\theta_n, t=1,2,\dots,p$. The columns of such SOM are next centered and normalized to three point average of the three initial readings of every symptom. This is in order to make the SOM dimensionless, to diminish starting disturbances of symptoms, and to present the evolution range of every symptom from zero up to few times of the initial symptom value S_{0n} , measured in the vicinity of lifetime $\theta_l = \theta$.

After such preprocessing we will obtain the dimensionless symptom observation matrix (**SOM**) in the form;

$$\mathbf{SOM} \equiv \mathbf{O}_{pr} = [\mathbf{S}_{nm}], \quad \mathbf{S}_{nm} = \frac{\mathbf{S}_{nm}}{\mathbf{S}_{0m}} - 1, \quad (1)$$

where bold non italic letters indicate primary measured dimensional symptoms.

It was said in the introduction, we apply now to the dimensionless **SOM** (1), the Singular Value Decomposition (**SVD**), [22], to obtain singular components (*vectors*) and singular values (*numbers*) of **SOM**, in the form

$$\mathbf{O}_{pr} = \mathbf{U}_{pp} * \mathbf{\Sigma}_{pr} * \mathbf{V}_{rr}^T, \quad (\mathbf{T} - \text{matrix transposition}), \quad (2)$$

where \mathbf{U}_{pp} is p dimensional orthonormal matrix of left hand side singular vectors, \mathbf{V}_{rr} is r dimensional orthonormal matrix of right hand side singular vectors, and the diagonal matrix of singular values $\mathbf{\Sigma}_{pr}$ is defined as below

$$\mathbf{\Sigma}_{pr} = \text{diag}(\sigma_1, \dots, \sigma_l), \quad \text{with nonzero s. v.: } \sigma_1 > \sigma_2 > \dots > \sigma_u > 0, \quad (3)$$

³We assume machine is new, or after the overhaul and repair process.

and zero s. v. ; $\sigma_{u+1} = \dots = \sigma_l = 0$, $l = \max(p, r)$,
 $u \leq \min(p, r)$, $u < r < p$.

In terms of machine condition monitoring the above (3) means, that from the r primarily measured symptoms (*dimension of observation space*) we can extract only $u \leq r$ nonzero independent sources of diagnostic information, describing the evolving generalized faults $F_t(\theta)$, $t=1, \dots, u$, and creating in this way the less dimensional **fault space**. But only a few faults developing currently in a machine are making essential contribution to total fault information (*are enough developed*). The rest of potential generalized faults, symbolized here by small σ_u value, are usually below the standard 10% level of noise. What is important here, that such **SVD** decomposition can be made currently, after each new observation (*reading*) of the symptom vector $[S_m]$; $n = 1 \dots p$, and in this way we can trace the faults evolution, and their advancement, in any operating mechanical system.

3. DIAGNOSTIC INTERPRETATION OF SVD

From the current research and implementation of this idea [2], one can say, that the most important fault oriented indices obtained from **SVD**; is the generalized fault symptom SD_t , $t=1, 2$, and also the sum of all generalized fault symptoms $SumSD_i$, as some equivalent symptom of total (*cumulated*) machine damage. In another way, the generalized fault symptom SD_t can be named also as discriminant, or the generalized symptom of the fault order t , and one can obtain this as the **SOM** product and singular vector v_t , or in general in matrix notation as below:

$$SD = O_{pr} * V = U * \Sigma,$$

and in particular; $SD_t = O_{pr} * v_t = \sigma_t \cdot u_t$,
 $t=1, \dots, u < r$. (4)

We know from **SVD** theory [22], that all singular vectors v_t , and u_t , as the components of singular matrices, are normalized to one, so the energy norm of this new discriminant (*generalized fault symptom*) gives simply the respective singular value σ_t :

$$Norm(SD_t) \equiv //SD_t// = \sigma_t, t = 1, \dots, u. (5)$$

The above defined discriminant $SD_t(\theta)$ can be also named as lifetime fault profile, and the respective singular value $\sigma_t(\theta)$ as a function of the lifetime seems to be its life advancement of damage (*energy norm*) and the same the measure of importance of the fault. That is the main reason why we use dimensional or dimensionless singular values for the ordering of importance of generalized symptoms (*faults*).

The similar fault inference can be postulated to the meaning, and the evolution of summation quantities, the total damage profile $SumSD_i(\theta)$ as below

$$SD_t(\theta) \propto F_t(\theta), \text{ with: } //SD_t(\theta)// = \sigma_t, t=1, 2,$$

$$SumSD_i(\theta) = \sum_{i=1}^u SD_i(\theta) = \sum_{i=1}^u \sigma_i(\theta) \cdot u_i(\theta) \propto F(\theta)$$

with: $//SumSD_i(\theta)// \cong \sum \sigma_i(\theta)$ (6)

Currently it seems to be, that the condition inference based on the first summation damage measure; $SumSD_i$, (*total damage measure*) may stand as the first approach to multidimensional condition inference, as it was lately shown in the previous papers (*see for example* [1, 2, 7]). The similar inference based on the first (*dominating*) generalized fault SD_1 is valuable and complimentary, as it was shown lately [19].

$$SumSD_i(\theta) = SD_1(\theta) + \varepsilon(SumSD_i(\theta)). (6a)$$

Going back to **SVD** itself it is worthwhile to show some mathematical metaphor of (5), that every perpendicular matrix has such decomposition, and it may be interpreted also as the product of three matrices [22], namely

$$O_{pr} = (Hanger) \times (Stretcher) \times (Aligner)^T. (7)$$

This is very metaphorical description of **SVD** transformation, but it seems to be useful analogy for the inference and decision making in our case. The diagnostic interpretation of formulae (7) one can obtain very easily. Namely, using its left hand side part we are stretching our **SOM** over the life (*observations*) dimension, obtaining the matrix of generalized symptoms as the columns of the matrix SD (*see below*). And using its right hand side part of (7) we are stretching **SOM** over the observed symptoms dimension, obtaining the assessment of contribution of every primary measured symptoms in the matrix AL , assessing in this way the contribution of each primary symptom to the generalized fault symptom SD_i .

$$SD = O_{pr} * V_{rr} = U_{pp} * \Sigma_{rr};$$

and $AL = U_{pp}^T * O_{pr} = \Sigma_{rr} * V_{rr}^T$. (8)

This means that SD matrix is stretched along the life coordinate giving us the life evolution of the weighted (σ_i) singular vectors. And AL matrix is aligned along the symptom dimension with the same way of weighting by σ_i , giving the assessment of information contribution of each primary symptom.

We will calculate numerically the above matrices and use them for the better interpretation of monitoring results (SD), and optimization of dimension of the observation space (AL).

4. THE SOM INFORMATION MEASURE AND OPTIMIZATION

Having in mind the redundancy of some primary symptoms, i.e. the primary observation space, some additional considerations should be made concerning SOM information assessment. In terms of previous findings this can be done by calculating the Frobenius norm (*Frob*) of this matrix, and the volume (*Vol*) created by *u*-dimensional generalized fault space identified by application of (SVD). One can calculate easily both information indices as the sum and the product of singular values in the following way:

$$\begin{aligned} \text{Frob}(SOM) &\equiv \{\Sigma \sigma_i^2\}^{1/2}; \\ \text{and Vol}(SOM) &\equiv \Pi \sigma_i, \quad i = 1, \dots, u. \end{aligned}$$

But squaring the small singular values of σ_i (*less than one*) make them much smaller, giving seemingly smaller contributions to the matrix information asset, and to the volume of the observation space. Due to this we can propose to use not the exact Frobenius norm but its modification as below:

$$\begin{aligned} \text{FrobI} &= \Sigma \sigma_i; \text{ and: } \text{VolI} = \Pi \sigma_i. \\ & \quad i = 1, \dots, u. \end{aligned} \quad (9)$$

This will give us possibility to look for the small, just evolving faults, and not omit them when we try to reduce the redundancy of the observation vector. Consequently one can get less redundancy of new optimized SOM, with less number of columns but also keeping in observation the small just evolving fault information (σ_i).

The use of Frobenius measure for a matrix has also mathematical validation. In general, one can understand this as the problem of approximation of matrix *B*, by so called k-rank approximation. Following the paper [9] we can make the quantitative assessment of such k-rank approximation of a matrix *B* as the difference below:

$$\|B - B_k\|_F = \{\sigma_{k+1}^2 + \dots + \sigma_u^2\}^{1/2}, \quad (10)$$

where the subscript *u* stands for maximal dimension of nonzero singular value, i.e. the rank of our primary SOM.

This means also, that instead of (9), we will write simplified measure of approximation of SOM in the form of deviation from primary SOM rank, as below

$$\Delta_k \text{FrobI} \equiv \text{FrobI}_o - \text{FrobI}_k = \{\sigma_{k+1} + \dots + \sigma_u\}. \quad (11)$$

Using this quality index of matrix approximation measure we, can form additional objective measure of the SOM redundancy. And minimization of SOM rank may be carried by excluding some primary measured symptoms S_m with low information contribution, which produce mainly small (*less than one*) singular values σ_u .

Such criteria of redundancy minimization we have used quite recently. But following the last

papers [19], one may notice that after some symptom rejection, which gives expected increase in the volume of information space (*VolI*). Also the rank approximation of SOM gives only some drop in *FrobI* measure, but the result of prognosis is not enough good, *giving erroneous future values*, sometimes less than the previous one. How to avoid such errors in forecasting?

There seem to be one possibility more, to make the symptom rejection more objective and anticipating the goodness of the condition forecast. We have to consider the contribution of primary measured symptoms to the creation of first generalized symptoms SD_j , and also the creation of total damage generalized symptom $SumSD_i$. The first overall information contribution measure, can be calculated separately to each primary symptom, from the correlation matrix of our SOM (*with appended lifetime in the first column*), as the centered and normalized sum of column elements. The second measure one can obtain if we append additionally to the previous matrix the vector $SumSD_i$, as a first column. When calculating covariance matrix from these and in the first row we will have needed information. After needed normalization to the first element of this row this will give us the contribution of every primary symptom to the total damage symptom $SumSD_i$.

5. THE GLOBAL AND PARTIAL FAULT INFERENCE

We have gathered above all necessary analytical and inference knowledge concerning processing of symptom observation matrix, the extraction of fault information, and optimization of SOM rank. So, there is a right moment to validate these finding and proposal by some experimental data taken from real situations of vibration condition monitoring. In order to do this the last Matlab® program `svdopt1gs.m` presented in [19] has been modified to `svdoptInt.m`. The inference basis for the first program was the total damage generalized symptom $SumSD_i$, while in the modified program such inference basis is the first generalized symptom SD_j . Just to catch the the way of inference and the followed diagnostic decision difference we will take some uneasy case of heavy fan (3MW) working in unstable and load uncontrolled regime (*random supply of the air to the mine shaft*), serving as the source of fresh air for ventilation at the deep copper mine. The main troubles with this fan were unbalance and nonalignment between the fan and the driving electric motor, due to that the unit was constantly monitored.

Figure 1 presents below the six pictures as the result of fan data processing by specially prepared program `svdoptint.m` made in the Matlab® environment, where the main stream of inference follows the evolution of the first generalized symptom SD_j . The first top left picture, gives the results of 30 weeks measurements of symptom life

curves of vibration velocity at a five points located on the fan aggregate structure. One may notice here the great instability of symptom readings, symptom No 4 in particular. This is better seen at the picture middle left when data are centered and normalized to the average value of the three initial symptom readings. We can notice here the negative values of symptom as an effect of load instability and normalization. The picture bottom left presents the *generalized symptoms* as the result of SVD processing, indicating also the symptom limit value calculated for the generalized symptom of total damage *SumSD_i* (red line) denoted there as *S_{ic}*, and also symptom limit value *S₁₁* calculated from the first generalized symptom *SD₁*.

The picture top right shows the relative amounts of information obtained as percentage of given singular value σ_i normalized to the sum of all singular values. As it follows from (5) this indicates at the same time the advancement of the given fault evolution in the machine life. As the legend to this

picture we have indication of two redundancy measure, the *Frob1* and the *Vol1*, which will serve as some guidance in the optimization process of the observation space.

The middle right picture presents the contribution of primary measured symptoms (*the first = lifetime*) to the creation of the dominating three generalized symptoms. One can notice here, that symptoms No 4 and 5 give minimal contribution and can be rejected in a process of optimization of the observation space. The last picture, the bottom right, of the Figure 1 shows the evolution of symptom limit value as calculated from the first generalized symptom *SD₁*, indicating also the value of symptom limit value as calculated from the sum of generalized symptoms *SumSD_i*. One can notice from the both bottom pictures, that in this case the difference between symptom limit values is a small one, but the value obtained from *SD₁* gives better indication of the coming machine breakdown.

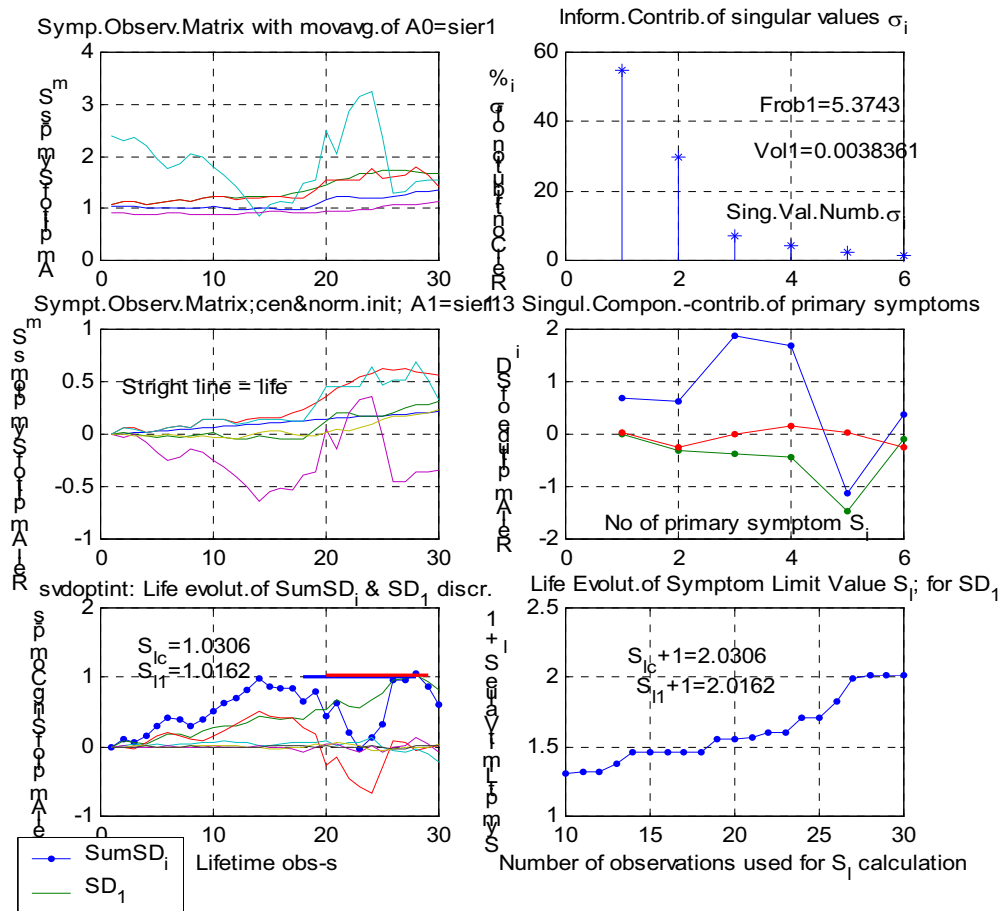


Fig. 1 The results of SVD processing of vibration data of a huge fan pumping air into the copper mine shaft, with the inference according to dominating generalized symptom *SD₁*

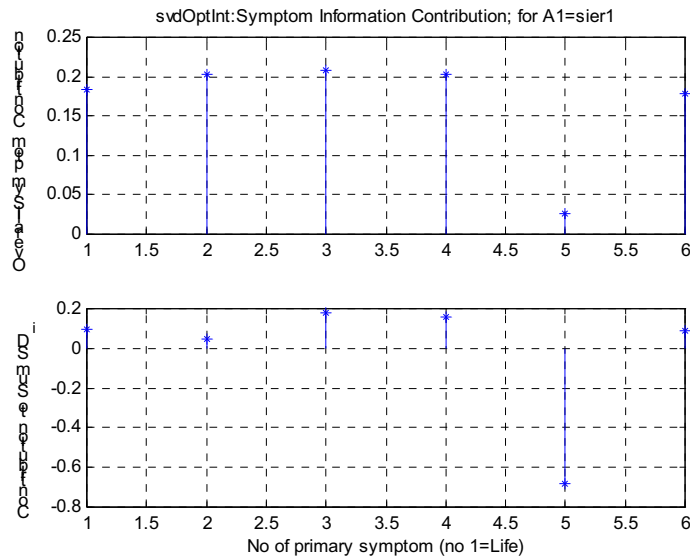


Fig. 2. *The Correlation measure of overall and particular contribution of primary symptoms*

As it was mentioned before, the program **svdoptint.m** contains not only the matrix AL (8) (picture middle left), but also some correlation assessment of individual and overall information contribution of every primary symptom in SOM. Figure 2 presents these data, and we can see there, really symptom No4 has minimal overall contribution, and a negative one to generalized symptom SD_1 .

Having such strong indication of the two symptoms redundancy (No 4 and No 5), let us begin a gradual rejection of these symptoms contained in SOM. As a first step we rejected symptom No 4, however its contribution is not minimal in this case. The effect of such rejection is shown in a Figure 2, organized in the same manner as a previous one. Comparing the both we can notice the radical change in the symptom behavior, mainly we have

rejected the most unstable primary symptom No 4. As the result of such rejection we have much clear situation of symptom evolution, primary symptom (picture top left) and generalized (picture bottom left), and the values of symptom limit values have change slightly, differing more than previously. Also the Frobenius redundancy measure drops significantly, and the volume of the fault space increased a little. But the most important effect of this rejection is the increased stationarity of remaining symptoms, the primary and generalized as well. Looking at the picture middle right one can notice very low contribution of primary symptom No 5. Hence next motion will be the rejection of this symptom together with previously rejected No 4. The results of such double rejection operation and subsequent processing one can find on the Figure 4.

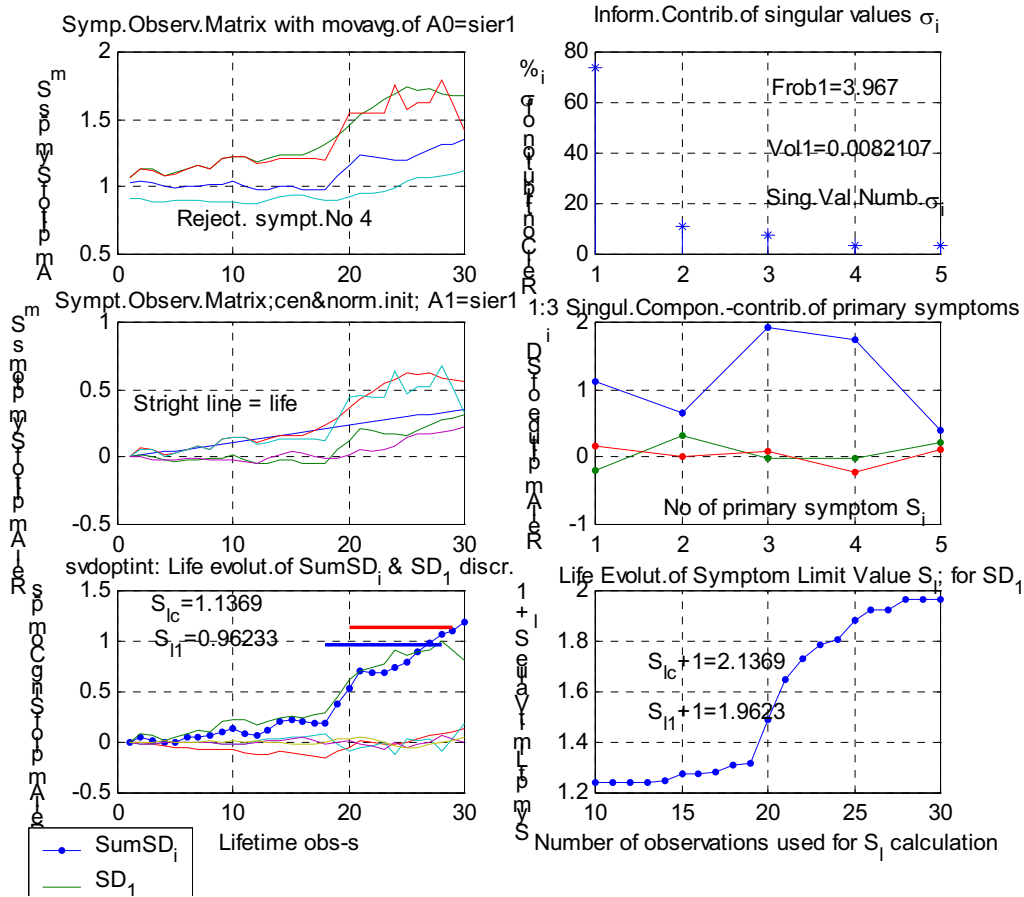


Fig. 3. The vibration symptom observation matrix of the huge fan (see Fig.1) after the rejection of unstable symptom No 4

Looking at the difference between Figures 3 and 4 one can notice much more clear situation on the right hand pictures of Fig. 4. Now we can infer on fan condition using both symptom limit values S_{lc} and S_{l1} , however with S_{l1} diagnosis seems to be more reliable. The top right picture indicate that Frobenius measure does not change much, but the volume of fault space increases almost ten times. This may mean that for the condition inference of the fan we should take into consideration the remaining three primary symptoms No 1, 2, 3, and due to this we will have the relative stable and reliable situation for the inference. This conclusion is validated more by the picture middle right, where

one can see that the contribution of all remaining symptoms and the life symptom to the generalized symptom SD_1 is valuable, being almost of the same order.

One can notice also that the calculation of limit value using first generalized symptom SD_1 gives us lower value and this can give us more safe assessment of lifetime moment for machine shut down and renewal. From the point of view of diagnostic **decision reliability**, this seems to be important to have two different sources of symptom limit vale assessment, and to confront these values and the associated knowledge.

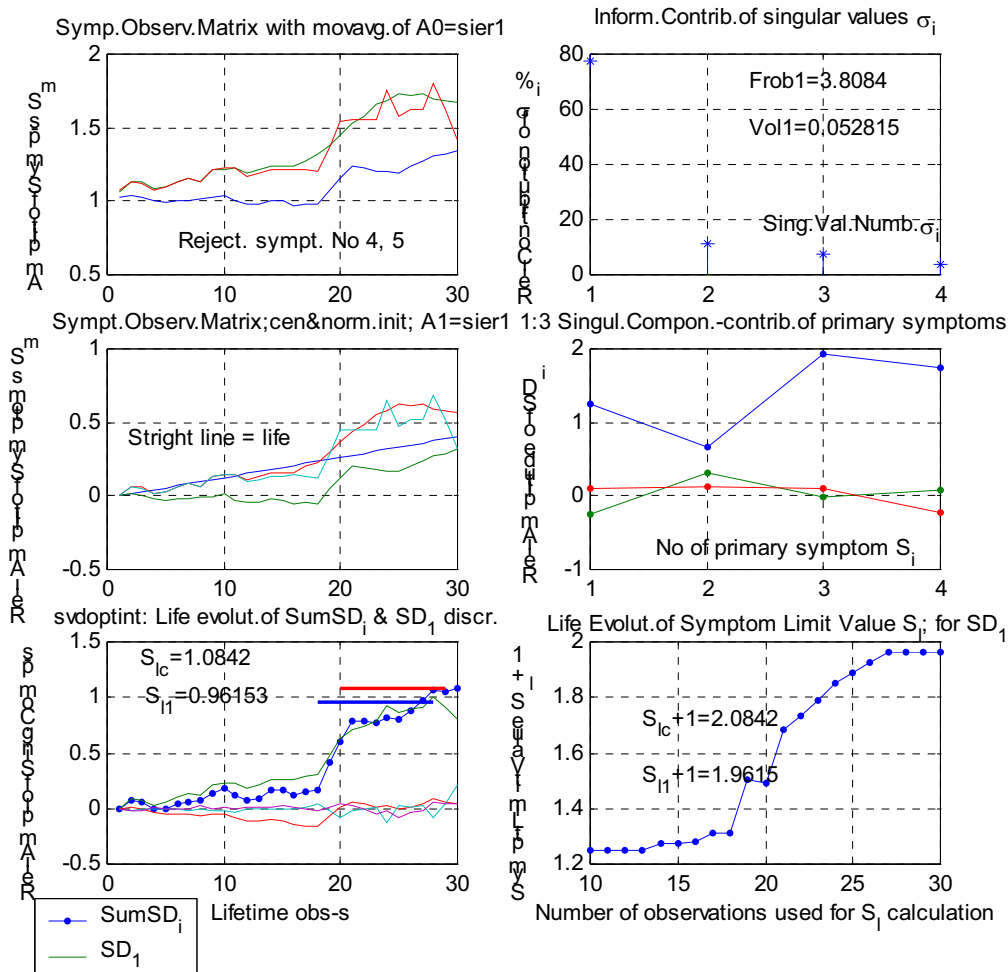


Fig. 4. The vibration symptom observation matrix of the huge fan (see Fig.1) after the rejection of unstable and the redundant symptoms No 4 and No 5

6. FORECASTING OF GLOBAL SYSTEM DAMAGE AND PARTIAL FAULTS ADVANCEMENT

The final quality of diagnostic decision one may judge making the forecast of the future condition in terms of total damage symptom *SumSDi*, and the first generalized fault symptom *SD1*. It was said in the introduction, that the forecast will be made by grey system theory (GST) [13], together with the rolling window method using the first order grey model GM(1,1) [12].

In general GST assumes that our incomplete and uncertain observation can be the output of some dynamic multi input system of high order, described by the grey differential or difference model [20]. In condition monitoring, we assume it is enough to take the first order system described by the grey differential equation, and one forcing or control input only. This simplest case in GST is denoted as GM(1,1), means the grey model of order 1 with one input only. The output of the system is the series of discrete observations (*our symptom readings*) denoted here as:

$$x^{(0)} = \{x^{(0)}(1), x^{(0)}(2), \dots, x^{(0)}(n)\}, \quad (12)$$

where $n \geq 4$ is the number of observation made on a system (*machine*).

We will not present GST theory here, but only using the final formulae for the forecasting, and the rolling window concept, which is implemented into the forecasting software.

The application of GST to the above symptom readings gives the possibility to forecast the future one step symptom value, starting from very small number observation, and using the formula:

$$\hat{x}^{(0)}(k+1) = [x^{(0)}(1) - u/a] (e^{-ak} - e^{-a(k-1)}), \quad k=2,3,\dots,n, \quad (13)$$

where *u* and *a* are parameters to be estimated by special least square matrix procedure using the observed data (12), and the hat ^ in (13) means future value of the forecasted quantity.

This concept was adjusted to the purposes of vibration condition monitoring in one of the earlier paper [18, 19]. One can notice here from the bottom left picture of Fig. 3 and 4, that the total damage generalized symptom *SumSDi* (*line with dots*) is evolved well after rejection the primary symptom No 4 and 5, enabling to undertake good diagnostic decision on the basis of these two symptom limit values (*see Fig. 4 bottom left*). Moreover it enables good forecast even without the rolling window (*see*

fig. 5). But of course, as usually in case of grey system modeling, the rolling windows forecast gives the smallest error. This error can be even smaller if we diminish the span of window (w), as it is clearly seen from the picture bottom right of the Fig. 5. It is worthwhile also to analyze the other pictures of this figure. Picture top left presents clearly, that the rejection of symptom No 4 was a good idea allowing us to determine symptom limit value S_{II} and having this information do act properly to shut down the fan ahead of breakdown time. The top right picture present the total forecast of dominating damage symptom SD_1 with the grey model $GM(1,1)$. It seems to be good forecast with the small average error, but the picture bottom left with the rolling windows forecast, have smaller error and the actual forecast adapts smoothly to the course of SD_1 , (see curve with asterisk on the picture bottom right).

It is seen from the Fig. 5 left top picture, that the course of SD_1 generalized symptom is decreasing at the end of fan life, but the both assessed symptom limit values S_{Ic} and S_{II} warns in advance enough to undertake shut down decision, just on time. However, comparing the both symptom limit values

shown on the picture top right of the last figure, and Fig.4, it is good to know that the global damage symptom limit value S_{Ic} can be used only with a global damage symptom $SumSD_i$, in other case it can give erroneous decision. But the limit value of the first generalized symptom SG_1 (dominating fault) warns us enough in time when to shut down the machine safely. And this is the **most important message** for using partial and global condition inference simultaneously in order to increase the reliability of diagnostic decision, as proposed in this paper.

To illustrate this idea more, let us consider another object, railroad diesel engine monitored by vibration measurement, each ten thousand kilometers of mileage. Here 12 vibration symptoms were initially monitored at the top of one of the engine cylinder. With this data using the software similar as previously (Fig.1-4), two primary symptoms have been found as redundant. As it is seen from the vibration course on the next figure 6, at 210 thousand kilometers of the engine mileage some minor repair was done without overhauling the engine, what reduced greatly the generalized symptom of total engine damage $SumSD_i$.

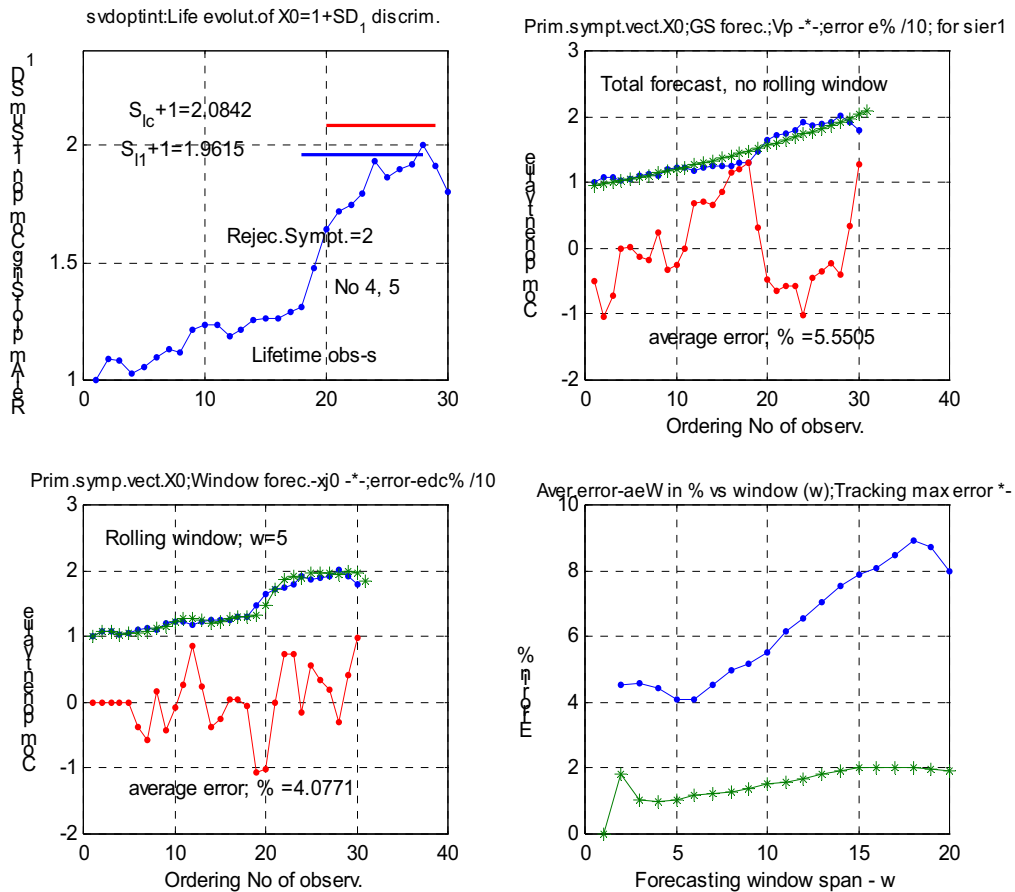


Fig. 5. Grey rolling forecast of the fan condition using the first generalized symptom SD_1 , together with the both symptom limit values and the errors of the forecasts, with and without rolling window

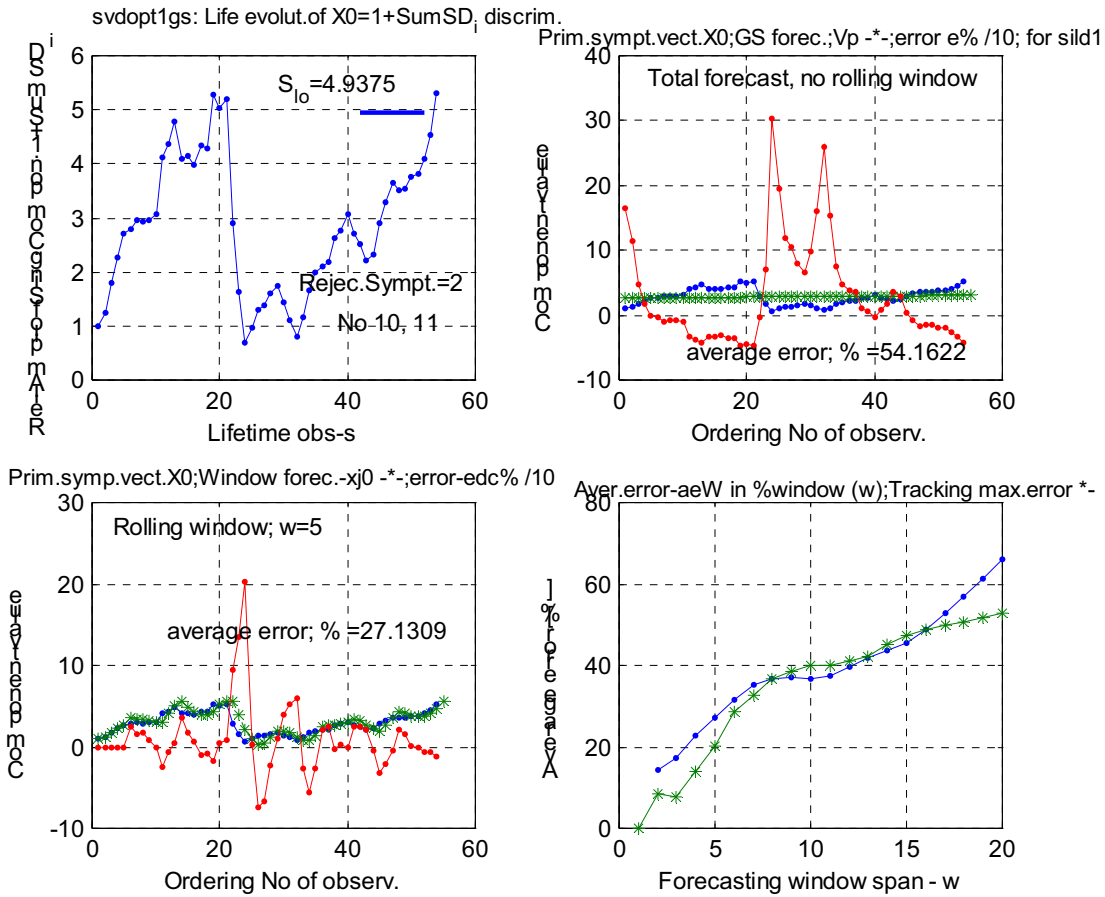


Fig. 6. Vibration based total damage forecast by grey system theory for the railroad diesel engine

The resultant forecast with the use of grey system model **GM(1,1)** has a great jump in the magnitude of error at the vicinity of this point, but assessed symptom limit vale S_{lo} gives enough lead time to warn us on the impending engine failure.

Much better situation with this respect one can note when the same engine data has been processed for the dominating generalized symptom SD_I

instead of total damage symptom $SumSD_i$, as it was done for the fan vibration data (Fig. 1-5). One can see from the figure 7 that symptom limit vale S_{II} calculated for the dominating generalized symptom SD_I gives us much better lead in warning before impending failure. Also the tracking error of the forecast (asterisk curve on picture bottom right) is smaller than its average error.

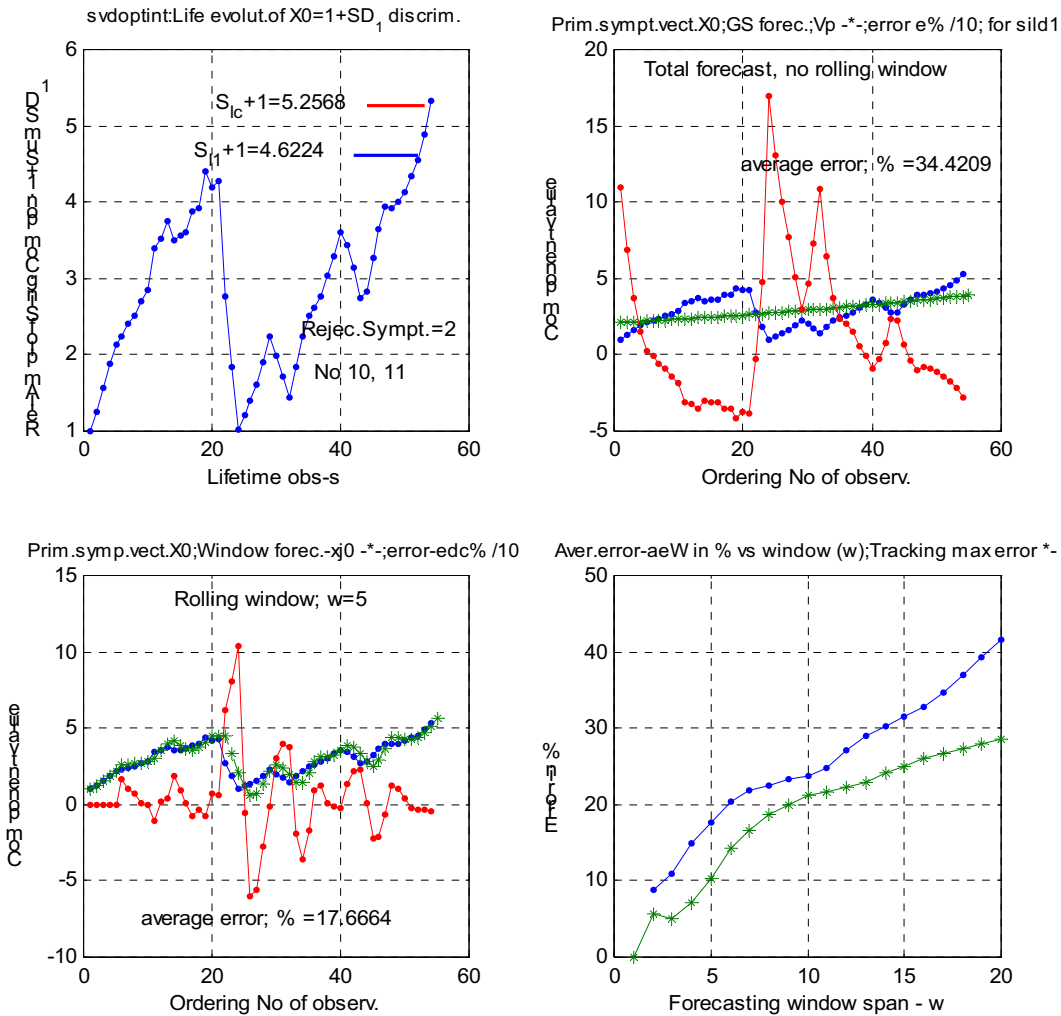


Fig. 7. Dominating fault method and vibration base forecast for the same diesel engine as above (Fig. 6)

Summing up all the results of our illustrative calculation for the two different objects one can say that the idea of calculating two symptom limit values simultaneously; for the global damage symptom $SumSD_i$, and for the first dominating generalized symptom SD_1 has proved its usefulness in increasing the reliability of diagnostic decision. Moreover, this integration of inference seems to be needed both in the main calculation in fault space and observation space optimization (Fig. 1-4), as well as in the grey system forecasting (Fig. 5, 6, 7).

7. CONCLUSIONS

The premise to write this paper was the supposition that the integral inference basing on the first generalized dominating fault symptom SD_1 and the total damage generalized symptom $SumSD_i$ of machine condition, can bring us valuable and reliable diagnostic information. As usually in multidimensional condition monitoring we have used the singular value decomposition to extract the fault information from the symptom observation

matrix. After the first round of calculation it was possible to optimize observation space using some measures of fault space, such as $Frob1$ and $Voll$ and reject some redundant symptoms. Having just mentioned generalized symptoms calculated, the symptom reliability and the symptom limit values S_{lc} , S_{ll} were assessed on that basis for the total damage symptom $SumSD_i$, and for the dominating generalized symptom SD_1 . The last stage of inference was the forecast of the future value of the both symptoms made by grey system theory and $GM(1,1)$ model. As an example we have used the most unstable case of condition monitoring, of the huge fan working in ventilation system of deep copper mine, and the railroad diesel engine. It was shown here that the optimization procedure can reject unstable symptom, and more over we are able to calculate two symptom limit values, and infer more effectively on the basis of such integral software.

It means also the global and partial inference do not exclude each other, both they are valuable expansion of our inference capability.

8. REFERENCES

- [1] Cempel C.: *Innovative developments in systems condition monitoring, Keynote Lecture*. Proceedings of DAMAS'99, Dublin 1999, Key Engineering Materials, Vols. 167-168 (1999), pp. 172-189.
- [2] Cempel C.: *Implementing Multidimensional Inference Capability in Vibration Condition Monitoring*. Proceedings of Conference: Acoustical and Vibratory Surveillance, Senlis - France, October 2004.
- [3] Cempel C., Natke H. G., Yao J. P. T.: *Symptom Reliability and Hazard for Systems Condition Monitoring*. Mechanical Systems and Signal Processing, Vol. 14, No 3, 2000, pp 495-505.
- [4] Korbicz J., et all, (eds.): *Fault Diagnosis – Models, Artificial Intelligence*. Applications, Springer Verlag, Berlin - Heidelberg, 2004, p828.
- [5] Tumer I. Y., Huff E. M.: *Principal component analysis of tri-axial vibration data from helicopter transmission*. 56th Meeting of the Society of Machine Failure Prevention Technology, 2002.
- [6] Jasiński M.: *Empirical models in gearbox diagnostics (in Polish)*. PhD Thesis, Warsaw University of Technology, Warsaw, December 2004.
- [7] Cempel C.: *Vibroacoustic Condition Monitoring*. Ellis Horwood Press, New York, 1991, p212.
- [8] Cempel C.: *Simple condition forecasting techniques in vibroacoustical diagnostics*. Mechanical Systems and Signal Processing, 1987, pp 75 – 82.
- [9] Berry M. W., Drmac Z., Jessup E. R.: *Matrices, Vector Spaces, and Information Retrieval*. SIAM Review, 1999, Vol. 41 No 2, pp 335-362.
- [10] Wen K. L., Chang T. C.: *The research and development of completed GM(1,1) model toolbox using Matlab*. International Journal of Computational Cognition, 2005, Vol. 3, No 3, pp 42-48.
- [11] Zhang L., Wang Z., Zhao S.: *Short-term fault prediction of mechanical rotating parts on the basis of fuzzy-grey optimizing method*. Mechanical Systems and Signal Processing, 2007, Vol.21, pp 856-865.
- [12] Yao A. W. L., Chi S.C.: *Analysis and design of a Taguchi-Grey based electricity demand predictor for energy management systems*. Energy Conversion & Management, 2004, Vol.45, pp 1205-1217.
- [13] Deng J-L.: *Control Problems of Grey Systems*. Systems and Control Letters, Vol. 1, No 5, North Holland, Amsterdam, 1982.
- [14] Deng J-L.: *Introduction to grey system theory*. The Journal of Grey System, 1989, Vol. 1, No 1, pp 1-24.
- [15] Deng J-L.: *The Course on Grey Systems Theory*. Publishing House, Huazhong University of Technology, Wuhan, (in Chinese), 1990.
- [16] Zhang H., Li Z.: Chen Z., *Application of grey modeling method to fitting and forecasting wear trend of marine diesel engines*. Tribology International, 2003, Vol.36, pp 753 – 756.
- [17] Wang T. C.: Liou M. C., Hung H. H., *Application of grey theory on forecasting the exchange rate between TWD and USD*. Internet 2005, pp 1 – 8.
- [18] Tabaszewski M.: *Forecasting of residual life of the fan mill by means of neural nets (in Polish)*. Diagnostyka, vol. 3, (39), 2006, s. 149-156.
- [19] Cempel C., Tabaszewski M.: *Multidimensional condition monitoring of the machines in non-stationary operation*. Mechanical Systems and Signal Processing, Vol. 21, 2007, pp 1233-1247.
- [20] Hall D. L., Llinas J.: *An introduction to multisensor data fusion*. Proceedings of the IEEE, Vol. 85, Jan. 1997, pp 6-23.
- [21] Roemer M. J., Kacprzyński G. J., Orsagh R. F.: *Assessment of data and knowledge fusion strategies for prognostic and health management*. Internet, http://www.impact-tex.com/data/Publications/f054_gjk.pdf
- [22] Will T., *Hanger matrix, two-thirds theorem*, Internet: <http://www.uwlax.edu/faculty/will/svd/svd/index.html>, June 2005; (see also: SVD ingredients Mathematica, April 2004).

EXAMINATION OF THE IMPACT OF AMPLITUDE-MODULATED VIBRATION ON THE COURSE OF A FATIGUE TEST (HCF)

Marcin JASIŃSKI, Stanisław RADKOWSKI

Instytut Pojazdów, Politechnika Warszawska
ul. Narbutta 84, 02-524 Warszawa, ras@simr.pw.edu.pl

Summary

The purpose of this paper is to develop a method of forecasting and analysis of high-cycle (HCF) resistance to fatigue relying on vibroacoustic signal analysis. It proposes using the results of vibroacoustic signal analysis obtained during accelerated fatigue tests conducted in dedicated test bed constructed specially for this purpose and operating in the frequency range of 10 kHz which corresponds to the proper frequency of vibration of samples.

Thanks to the small dimensions and mass, the test bed can be located on the vibration inductor, which enable investigations of the amplitude modulation's influence.

Additionally, it's described a problem of, phenomena oriented, diagnostics information's detection.

Keywords: vibroacoustic diagnosis, high-cycle fatigue processes (HCF), piezoelectric generators, amplitude modulation.

BADANIE WPLYWU AMPLITUDOWO ZMODULOWANYCH DRGAŃ NA PRZEBIEG TESTU ZMĘCZENIOWEGO (HCF)

Streszczenie

Celem pracy jest opracowanie metody prognozowania i analizy wysokocyklowej (HCF) trwałości zmęczeniowej na podstawie badania sygnału wibroakustycznego. Proponuje się wykorzystać wyniki analizy sygnału wibroakustycznego, uzyskiwane podczas przyspieszonych badań zmęczeniowych, prowadzonych na specjalnie do tego celu skonstruowanym i zbudowanym stanowisku badawczym, pracującym w zakresie częstotliwości rzędu 10 kHz, odpowiadającym częstotliwości drgań własnych próbek.

Dzięki małym wymiarom i masie stanowisko badawcze może być umieszczone na wzbudniku drgań, co umożliwia badanie wpływu modulacji amplitudy.

Dodatkowo opisano zagadnienie detekcji informacji diagnostycznej, zjawiskowo zorientowanej.

Publikacja opracowana na podstawie badań wykonywanych w ramach projektu „Monitorowanie Stanu Technicznego Konstrukcji i Ocena jej Żywotności” (MONIT). Projekt współfinansowany ze środków Europejskiego Funduszu Rozwoju Regionalnego w ramach Programu Operacyjnego Innowacyjna Gospodarka (PO IG 1.2)

Słowa kluczowe: diagnostyka wibroakustyczna, wysokocyklowe procesy zmęczeniowe (HCF), generatory piezoelektryczne, modulacja amplitudowa.

1. INTRODUCTION

In 1960's and 1970's solutions which put stress on the possibility of controlling the growth of cracks and faults that initially existed in the material were applied when designing structures subjected to variable loads, which could lead to the effect of fatigue-related damage. Another approach assumed that the existing cracks propagated only until reaching the assumed threshold value. Both methods referred to the principles and methods having origins in the mechanics of cracking. Development of high-speed vehicles and machines with high-speed motors as well as increasingly broader use of new materials, especially the high

performance materials, led to the need for revising the 19th century assumptions regarding the possibility of occurrence of infinite resistance of structural materials to fatigue. Above all it turned out, in the case of such materials the assumption related to the asymptotic run of Wohler's curve after exceeding the limit of 10^6 - 10^7 cycles was not fulfilled, which could have been the reason for occurrence of critical defects and catastrophes with extensive consequences, since in many cases fatigue-related defects of these materials were noted after exceeding 10^8 - 10^9 cycles.

Majority of materials fail to fulfill such assumptions [1], thus there exists the need for looking for new high performance materials, we can

examine in high-cycle fatigue testing (HCF) or gigacycle fatigue testing (VHCF). This aspects was presented in [2]. Much more information about this methods we can find in paper's of Murakami [3, 4].

Authors proposed to develop a method of forecasting and analysis of high-cycle fatigue testing (HCF) or gigacycle fatigue durability (10^8 - 10^9 cycles) for the metal-based, highly resistant materials used in high-speed motors and turbines. The method relies on the results of analyzing the vibroacoustic signal obtained during accelerated fatigue tests performed on a dedicated test bed which operates in the samples' proper vibration frequency range of 10 kHz [2].

Till the present moment there have not existed any norms regarding the method of conducting the tests of gigacycle fatigue processes. Laboratories dealing with such research, e.g. in the USA, Austria, France [1], China, Japan, Slovakia are at the stage of developing their own research procedures. More about that test beds was presented in [2].

It was built a test bed for high-cycle tests of fatigue processes (Fig. 1). We have calculated the initial dimensions of a sample (HxWxL): 10mm x 5mm x 30mm. For the preset maximum deformation from 5 - 40 μm range as well as the generated frequency of 10kHz, we selected a piezoelectric actuator - type PPA80L with parameters: max. no load displacement: 90 μm , blocked force 3500 N, resonance frequency (free-free): 7000 Hz, capacitance: 26,6 μF , height: 97 mm, width: 18 mm. This actuator can be powered with 150V current, which interworks with LA75C amplifier. The typical high-cycle test beds rely on the frames of machines used for testing the fatigue durability and are usually of big dimensions and weight. The authors proposed a small-dimension test bed for diagnosing the high-cycle fatigue processes, with dimensions of usually 0.2x0.2x0.2 m and its weight does not exceed 2 kg, with a titan head mounted directly on the piezoelectric generator. To do away with play, the beam in the head is mounted by means of an eccentric cam (to preventing of moving the beam in the head). Small dimensions result from the proposal of mounting the test bed on TIRA TV 5500/LS shaker. Such an application of the inductor will enable examination of the tested sample's response to an input being a compilation of a carrier frequency and low-frequency modulating function, which will enable examination of more complex mechanisms of initiation and development of fatigue-related cracks [2].



Fig. 1. High-cycle fatigue test bed

In this type of investigation it is problem of measurement amplitude of vibrating beam free end. It's is almost unrealizable to mounting the accelerometer at the vibrating beam, we should use other source of the vibration signal. There were used a microphone Bruel&Kjær type: 4189-A-021, sensitivity 47,4 [mV/Pa], and a laser triangulation sensor MTI Instruments Inc. type: Microtrack II – LTC-050-10, range: 5 [mm], resolution 1 [μm], mounted at the ground-isolated stand. It was done comparison of signals from a laser sensor, and a microphone. The signal from the laser sensor alone might be insufficient (overload for example) at the moment when a fatigue crack is initiated and the amplitude of vibrations is rising very fast. Results received from the acoustic signal will serve to observe the resonant curve changes (the resonance frequency changes), together with the propagation of fatigue crack. Although was measured vibration signal from an accelerometer Bruel&Kjær type: 4507 B 004, sensitivity 10,22 [mV/ms²].

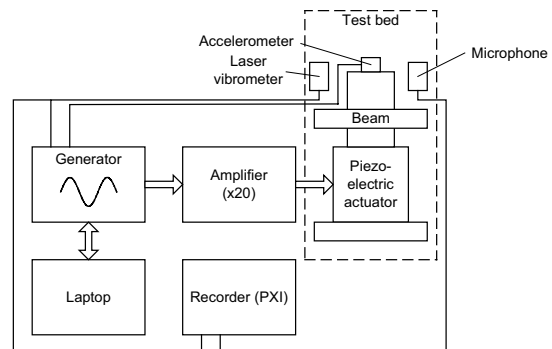


Fig. 2. Non-contact recording-control system

A recording-control program has been developed in the LabView 7.1 environment which has the task of tracking the resonant frequency of a beam based on the spectral analysis of a vibration signal registered by a use of the non-contact measurement system (Fig. 2) and the piezoelectric accelerometer. The frequency value estimated in this way is in the next step was sent to the generator in order to correct the frequency of the signal stimulating the piezoelectric converter. Thus it is

possible to track the changes of frequency (at the resonant curve) of a beam's proper vibration (first mode of bending eigenfrequency) connected with the developing fatigue-related crack. Modes of eigenfrequencies were isolated, more information about it we can find in [5].

This investigations enables not only detection of surface failures, but also detection of failures appearing in the specimen core.

2. THE EXPERIMENT

Fatigue tests were conducted at the aforementioned test-bed. An item which becomes essential from the point of view of the strength of a structure subjected to vibration having a small amplitude is the issue of existence of a notch as well as the shape of such a notch. An experiment was conducted which was intended to define the impact of a notch on fatigue strength of a sample made of copper. We use of displacement amplitude of forced.

The size of the sample (height x width x length) was 10 mm x 5 mm x 40 mm, however there were notches in the sample in the place in which it was mounted (notch dimensions: width: 2 mm, depth: 1 mm). Three types of notches were examined:

- the P-type notch (rectangular) - Fig. 3.
- the V-type notch,
- the U-type notch.



Fig. 3. A specimen with a P-type notch



Fig. 4. View of the fracture of a beam with a P-type notch

The most interesting results were obtained for the sample with a P-type notch. The tests were conducted until the sample broke due to fatigue (Fig. 4), which occurred after around 2 million cycles.

Bispectrum from channel no. 2 (laser vibration meter), which measured the amplitude at the free end of the beam, was calculated during the measurements.

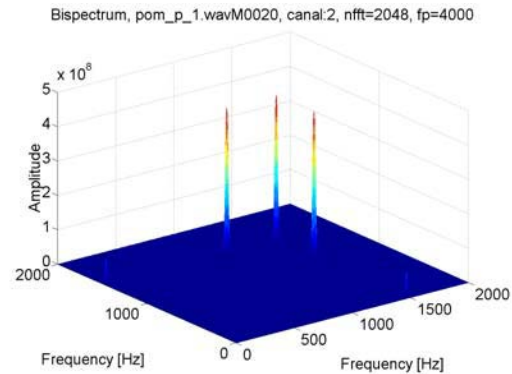


Fig. 5. Bispectrum - channel 2 (laser) at the start of the test

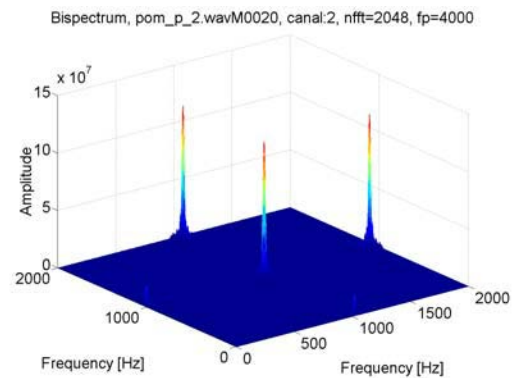


Fig. 6. Bispectrum - channel 2 (laser) after $1 \cdot 10^6$ cycles

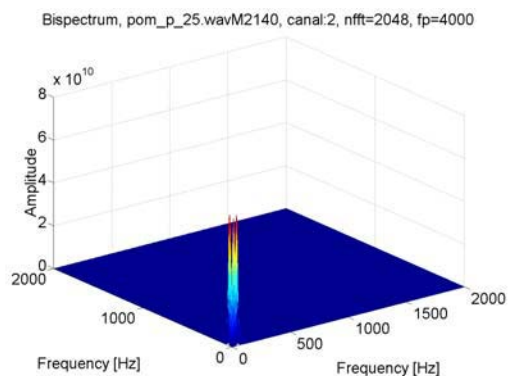


Fig. 7. Bispectrum - channel 2 (laser) after $2 \cdot 10^6$ cycles (close to the specimens break)

Fig. 5 shows the bispectrum drawn at beginning of the test, Figures 6 show the bispectrum during the test while, Fig. 7 shows the bispectrum at the end of the test, after $2 \cdot 10^6$ cycles. After $1,5 \cdot 10^6$ cycles the eigenfrequency was alone. It was caused by develop of nonlinear effect of fatigue crack, that is the

influence of material properties structure. Modulating frequencies appeared at $2 \cdot 10^6$ cycles (Fig. 7), just before the sample broke.

Thus bispectral analysis can be a useful tool for detecting fatigue-related tracks. More informations about this investigations was presented in [6].

A similar effect was observed while building the bispectral measures in the function of change of the loads, including the maximum bispectrum and the diagonal bispectrum. The next step was to create a new measure which would be able to foresee the moment of emergence of a fatigue-related crack in a much better way. Integrals for the entire lifecycle of a sample were calculated based on the graphs of the maximum bispectrum (Fig. 8) and the maximum bispectrum calculated on the basis of a triangular matrix – the residual bispectrum (Fig. 9), which emerged as a result of cutting out the main diagonal which described the impact of modulation phenomena and non-linear effects. In addition the cut-off level for maximum amplitudes was applied at $0.25E8$ [m/s^2] (everything which had a higher value than this level was reduced to this level). Then, the beam's resonant frequency curves, obtained during consecutive measurements (dot-and-dash line), were superimposed over the above graphs).

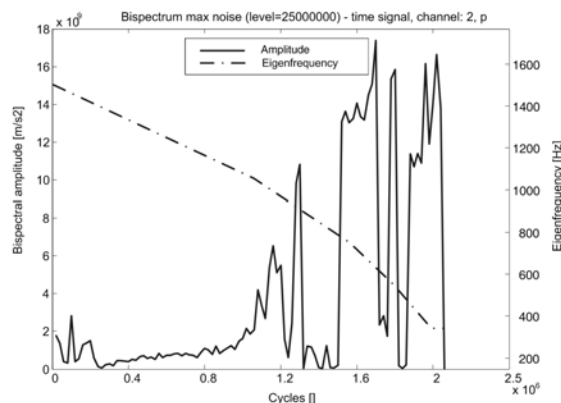


Fig. 8. Integrals from the maximum bispectrum graphs (level of $0.25E8$ [m/s^2]) - full line and eigenfrequency of a beam (dot-and-dash line)

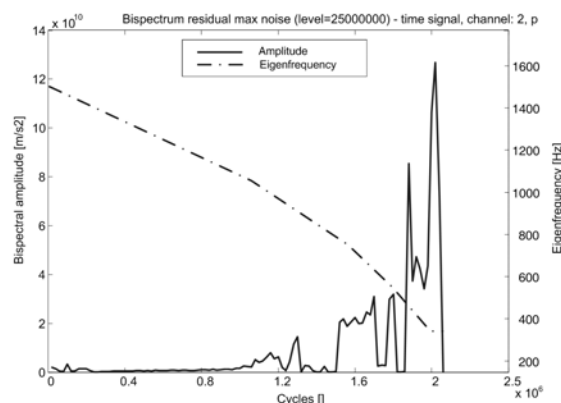


Fig. 9. Integrals from residual bispectrum graphs (level of $0.25E8$ [m/s^2]) - full line and eigenfrequency of a beam (dot-and-dash line)

In both graphs (Fig. 8 and Fig. 9) we can observe an upward trend of the amplitude which accompanies the presumed development of a fatigue-related crack. This trend is similar to falling of beam's eigenfrequency, causing by developing of fatigue crack (changing of beam's cross section) of While by analyzing Fig. 9 it could be concluded that the fatigue-related crack most probably started developing from measurement no. 2500 (1.2 million cycles) and reached the critical (pre-failure) level at measurement no. 4700 (1.9 million cycles). Thus, based on these findings it is possible to build a very sensitive and reliable diagnostic parameter which describes the development of a fatigue-related crack.

Then a test was conducted to see if existence of amplitude modulation would lead to faster destruction of a sample.

3. IMPACT OF MODULATION – TESTS ON A SHAKER

Small dimensions were proposed so as to enable installing the test-bed on the TIRA TV 5500/LS shaker (Fig. 10) which had the following parameters: nominal load – 4000 N, frequency range – $DC \div 3000$ Hz, maximum acceleration – 54 g. Use of the shaker enabled generation of frequencies which modulated the frequency of the beam's proper vibration thanks to which it became possible to examine more complex mechanisms of initiation and development of fatigue-related cracks. The frequency of the input generated by the inductor was by ca. $20 \div 30$ Hz smaller than the frequency of input generated by a piezoelectric stack, thanks to which the phenomenon of beating of the end of the beam occurred (Fig. 11). The dimensions of the beam were the same as in the case of modulation tests and just the same the beam had a P-type notch. We use a use the same the non-contact measurement system (Fig. 2).

Fig. 12 presents change of the value of the beam's resonant frequencies, associated with the development of the degradation process, in the function of subsequent cycles. This time the tests were interrupted after $2,5 \cdot 10^6$ cycles due to occurrence of a visible crack in the beam. Let us note that the monotonous, in its essence, decrease of the proper vibration's value prevents determination of the phase of fatigue-related crack's initiation. Such a possibility is created by the observation of phase coupling, including the analysis of the residual bispectrum. This time we have applied a cut-off level for maximum amplitudes equal to $0.5E8$ [m/s^2] (Fig. 13). While observing the trend, we can note that a qualitative change of the run occurs after ca. 1.8 million cycles. Most probably the change indicates transition to the next phase of degradation – initiation of fatigue-related crack.

Scientific publications devoted to examining the impact of modulation, show that the samples subjected to vibration generated by modulated vibration become destructed after a much smaller

number of cycles. The conducted research did not confirm such results, however one should note that the maximum amplitudes measured at the end of a sample were of the same order as in the case of incitation with a signal having a constant amplitude. This resulted from the limited power of the shaker on which the head containing the sample was mounted. The future investigations require the shaker with much more power.



Fig. 10. High-cycle test bed on TIRA TV 5500/LS shaker

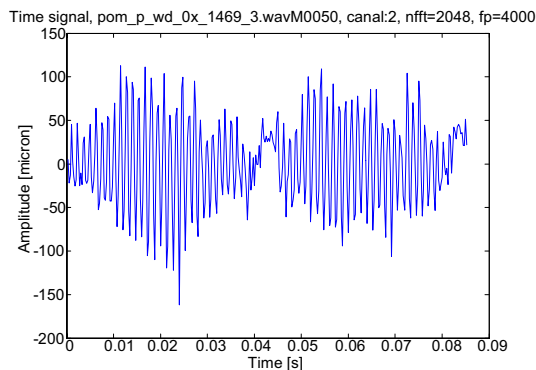


Fig. 11. Time run of the signal – amplitude of vibration at the end of the beam

The authors contemplate additional possibilities of increasing the amplitude of vibration of the examined sample. Such a possibility is created by introduction of coupling of the linear structure with an adaptive non-linear dynamic system and exploitation of the phenomenon of energy transfer to a non-linear system [7]. Occurrence of energy transfer is possible if relevantly big residual energy is supplied and if the non-linear resonance of an oscillator occurs.

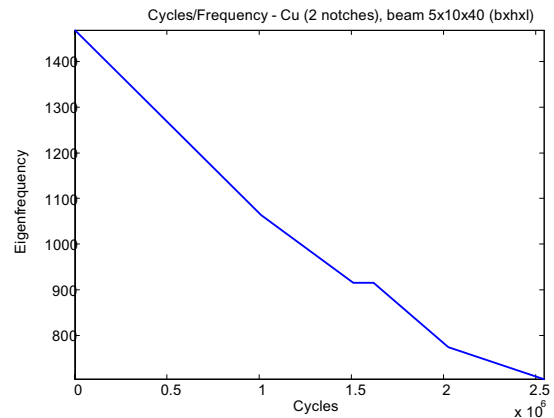


Fig. 12. Eigenfrequency of a beam

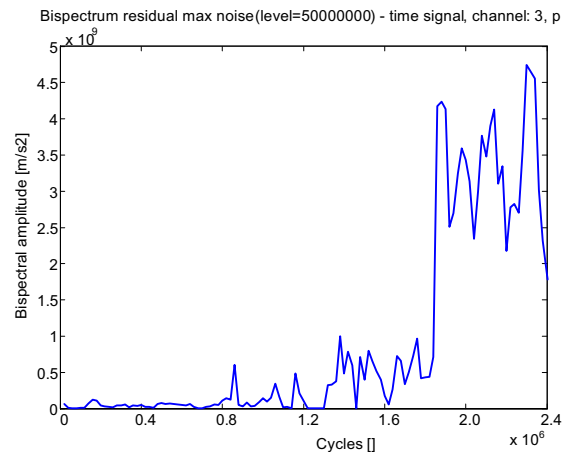


Fig. 13. Integrals from residual bispectrum graphs (level of $0.5E8$ [m/s^2])

4. CONCLUSIONS

A unique, comparatively small-size test-bed has been designed and built. It operates based on the resonance of the examined sample, within the frequency range of up to 10 kHz, has a system for tracking the frequency of a sample's proper vibration and is accommodated to conducting tests in the conditions of combined frequency inputs generated by an additional inductor. It has a head made of titanium which is mounted to a piezoelectric generator. To do away with any play, the sample is mounted in the head by means of a circular cam.

A program has been developed. Its task is to track the resonant frequency of a beam based on the spectral analysis of a vibration signal registered by high frequency acceleration meter. Thus it is possible to track the changes of the beam's proper vibration frequency which are associated with the growing fatigue-related crack.

A contact-free method of vibration measurements has been developed. It relies on two independent sensory-measurement systems – a laser vibration meter and a condense microphone.

A method has been developed for analyzing higher order spectra for forecasting and identification of the degree of degradation of a sample's dynamic

properties. Residual bispectrum has been proposed as a measure enabling determination of initiation of a beam's fatigue-related crack.

One should stress that independently of the type of input, whether it has a constant amplitude or whether the input is modulated, we have been able to confirm the sensitivity of the residual bispectrum to occurrence of consecutive phases of development of a crack in a sample. Bispectral analysis is very sensitive type of analysis. It can detect the structural changes of material's parameters, much more before the organoleptic changes.

The conducted research did not confirm that impact of modulation, show that the samples subjected to vibration generated by modulated vibration become destructed after a much smaller number of cycles. However one should note that the maximum amplitudes measured at the end of a sample were of the same order as in the case of incitation with a signal having a constant amplitude. This resulted from the limited power of the shaker on which the head containing the sample was mounted.

Acknowledgments

The authors would like to thank cordially to the staff of Vibroacoustic Laboratory at IPBM PW for providing access to TIRA TV 5500/LS shaker.

The paper was prepared on the basis of researches conducted within a project „Monitoring of Technical State of Construction and Evaluation of its Lifespan” (MONIT). Project is co-financed by the European Regional Development Fund in the Operational Programme Innovative Economy (PO IG 1.2)

LITERATURA

- [1]. Bathias C., Paris P. C.: *Gigacycle Fatigue in Mechanical Practice*. Marcel Dekker, New York, 2005.
- [2]. Gumiński R., Jasiński M., Radkowski S.: *Small-sized test bed for diagnosing the gigacycle fatigue processes*. *Diagnostyka*, Vol. 45, 2008, pp. 5÷10.
- [3]. Murakami Y., Nomoto T., Ueda T., Murakami Y.: *On the mechanism of fatigue failure in the superlong life regime ($N > 10^7$ cycles). Part I: influence of hydrogen trapped by inclusions*. *Fatigue & Fracture of Engineering Materials & Structures*, Vol. 23, 2000, pp. 893÷902.
- [4]. Murakami Y., Takahashi K.: *Torsional fatigue of a medium carbon steel containing an initial small surface crack introduced by tension-compression fatigue: crack branching, non-propagation and fatigue limit*. *Fatigue & Fracture of Engineering Materials & Structures*, Vol. 21, 1998, pp. 1473÷1484.
- [5]. Jasiński M., Radkowski S.: *Use of the Contactless Measurement Method in the Frequency-Control System of the Gigacycle Fatigue Test*, Proceedings of the Symposium Plasticity 2009, St Thomas, Virgin Islands, USA, 2009.
- [6]. Jasiński M., Radkowski S.: *Use of the higher spectra and the Wigner's analysis in the gigacycle fatigue testing*. Proceedings of the 3rd World Congress on Engineering Asset Management and Intelligent Maintenance Systems Conference (WCEAM-IMS 2008), 27÷30 October, 2008, Beijing, China, pp. 730÷743 (CD-ROM).
- [7]. Gendelman O. V.: *Transition of energy to a nonlinear localised mode In a highly asymmetric system of two oscillators*. *Nonlinear Dynamics*, Vol. 25, 2001, pp. 237÷253.



Marcin JASIŃSKI, Ph.D.
a lecturer in Laboratory of Automotive Mechatronics System of Institute Automotive Engineering of Warsaw University of Technology.
In his scientific work he deals with vibroacoustic diagnosis, empirical models and Automotive Mechatronics.



Prof. Stanisław RADKOWSKI, a professor in Institute of Institute Automotive Engineering of Warsaw University of Technology, manager of Laboratory of Automotive Mechatronics System.
In his scientific work he deals with vibroacoustic diagnosis and technical risk analysis.

ESTIMATION OF WELDING PROCESS STABILITY BASED ON IMAGE ANALYSIS AND RECOGNITION

Anna BZYMEK, Anna TIMOFIEJCZUK

Silesian University of Technology, Department of Fundamentals of Machinery Design
44-100 Gliwice ul. Konarskiego 18a, tel (032) 237 10 63, fax (032) 237 13 60,
anna.bzymek@polsl.pl , anna.timofiejczuk@polsl.pl

Summary

Vision systems are often applied to control the quality of welds or some parameters of welding processes. A review of current applications has shown that such approaches are being used for control of weld geometry, assessment of weld quality, and also for adaptive control of the welding processes. An approach presented in the paper concerns the application of a method based on image analysis and recognition. Estimation of welding process stability has been based on results of the application of this method. Observation of the welding arc with the use of the vision system can provide us with the information about stability of the arc and through this – stability of the welding process and indirectly, the quality of a weld being made. The investigations described in the paper have been carried out within the framework of PW-004/ITE/10/2006 project realized in Department of Fundamentals of Machinery Design of Silesian University of Technology

Presented research has been carried out during observation of selected welding processes. A part of welded samples were correctly prepared, whereas some surfaces and edges were deliberately damaged. These improprieties caused abnormalities of the process. On the basis of performed observations one could state that stability of the arc depended on the quality of a surface that was welded. Moreover, the observations performed during the experiments enabled us to draw some conclusion about correspondence between changes of features of the welding arc and stability of the welding process.

Keywords: process diagnostics, feature selection, image analysis, image recognition.

OCENA STABILNOŚCI PROCESU SPAWANIA Z ZASTOSOWANIEM METOD ANALIZY I ROZPOZNAWANIA OBRAZÓW

Streszczenie

Obecnie systemy wizyjne są stosowane głównie do kontroli jakości połączeń spawanych oraz kontroli parametrów procesu spawania. Zagadnienia, w których stosowane i rozwijane są systemy wizyjne w spawalnictwie to: kontrola geometrii i ocena jakości wykonanych połączeń oraz adaptacyjna kontrola parametrów spawania. Podejście prezentowane w niniejszym artykule dotyczy zastosowania metody bazującej na technikach przetwarzania i analizy obrazów, której celem jest ocena stabilności procesu spawania. Obserwacja obszaru łuku spawalniczego podczas procesu spawania dostarcza informacji na temat stabilności łuku, przez co możliwe jest wnioskowanie o stabilności procesu spawania oraz pośrednio, o jakości wykonywanego połączenia. Badania prezentowane w niniejszym artykule przeprowadzone zostały w Katedrze Podstaw Konstrukcji Maszyn na Politechnice Śląskiej w Gliwicach w ramach projektu badawczego PW-004/ITE/10/2006.

Słowa kluczowe: diagnostyka procesu, wybór cech relewantnych, analiza obrazów, rozpoznawanie obrazów.

1. BACKGROUND OF THE RESEARCH

Nowadays vision systems are often applied to control the quality of welds or some parameters of welding processes. A review of current applications has shown that such approaches are being used for seam tracking [5], control of a weld pool size [6], control of weld geometry and assessment of weld quality [2, 7], and also for adaptive control of welding processes [8].

An approach presented in the paper concerns the application of a method based on image analysis and

recognition. Estimation of welding process stability has been based on results of the application of elaborated algorithms. Observation of the welding arc with the use of the vision system can provide us with the information about stability of the arc and through this – stability of the welding process and indirectly, the quality of a weld being made. The investigations described in the paper have been carried out within the framework of PW-004/ITE/10/2006 project realized in Department of Fundamentals of Machinery Design of Silesian University of Technology.

The elaborated method has been based on the analysis of images acquired during observation of the welding arc with the use of a CCD camera equipped with additional filters. Series of images have been acquired, processed and analysed. The purpose of this analysis is to find out these features that correspond to shape, location, orientation and volume of the welding arc. This information is essential since variations of these features in time functions reflect instability of the process. Presented research has been carried out during observation of welding especially prepared plates. During the experiment one side butt welding was performed. A part of welded samples were correctly prepared, whereas some surfaces and edges were deliberately damaged. These improprieties caused abnormalities of the process, which were a great source of information.

2. LABORATORY STAND CONFIGURATION

A prototype version of the vision system was tested in Laboratory of Welding Research of Silesian University of Technology. A laboratory stand consisted of an infrared camera, which observed the arc and join and two CCD cameras, which observed respectively the arc and join, was presented in Fig. 1. However, in the paper only images acquired by the camera applied to observe welding arc area has been taken into consideration. Results concerning comparison of thermogram and image analysis were presented in [4, 1].



Fig. 1. Laboratory stand configuration

During the laboratory tests plates were moved along the straight line and the device passing filled wire was stationary. Welded plates were made of 0H18N9 of thickness equal to 2 mm and the plate edges were beveled. The following cases of surfaces and edges were taken into consideration: lack proper distance between plates ($S=0\text{mm}$), proper distance ($0 \leq S \leq 0,8 \text{ mm}$), too big distance between plates ($S > 0,8 \text{ mm}$) and varying width of the gap between plates along the weld. In order to simulate abnormality parameters of the welding process were also changed and some impurities (e.g. oil, paint)

were also introduced. Examples of defective welded joint have been presented in Fig. 2.

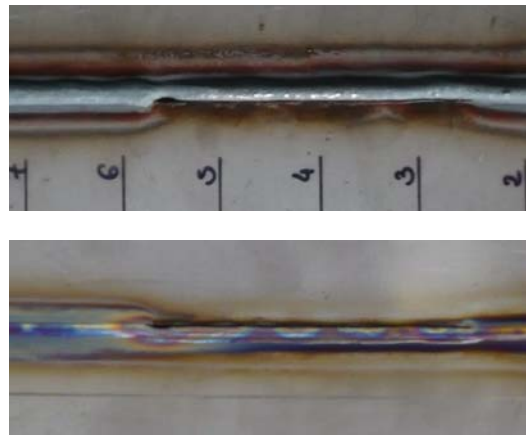


Fig. 2. Example of defective welded joint

The second stage of system testing was performed under industrial conditions. The subject of observation was welding exhaust silencers [1]. The welding process was carried out with the use of welding automata. In that case the device was also motionless but elements to be welded were turned around their axes. The main goal of these tests was to acquire series of images and verify initial assumptions related to placements of cameras, sources of lights as well as parameters of image recording.

3. IMAGE PROCESSING AND ANALYSIS

During the experiments described in the paper images of resolution 786x1024 (ImagingSource CCD camera) were recorded. In order to minimize processing time and focus elaborated analysis on the arc area, the first step of processing algorithm consisting in extraction of ROI (Region Of Interests) was applied [3]. The next step of this algorithm was to trace edges and apply binarization with a fixed threshold. Similarly to numerous applications, the threshold value resulted from series of experiments. After binarization an object (or objects) identified within the ROI were being analysed.

Exemplary images of the welding arc areas have been presented in Fig. 3. ROIs of welding arc areas have been presented in the 1st row, results of edge tracing in the 2nd row and images after binarization in the 3rd row. Images in Fig. 3 represent different shapes of welding arcs that are examples of stable welding process (Fig. 3a) and unstable processes (Fig. 3b,c). In presented examples sources of process instabilities were incorrect process parameters such as: too high wire feeding speed (Fig. 3b) and to low feeding speed (Fig 3c). It is clearly visible that on the basis of dimensions and shapes of the welding arc areas one can draw a conclusion about the state of the welding process.

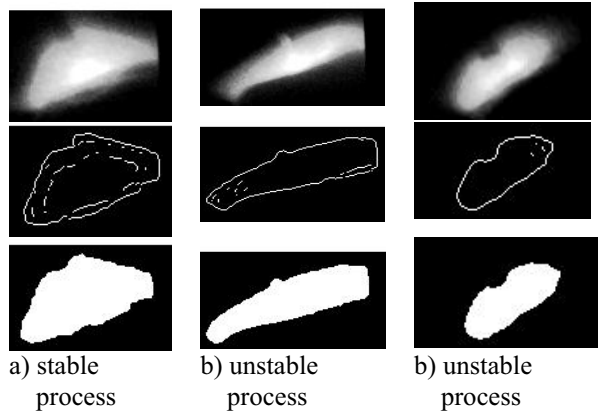


Fig. 3. Examples of different shapes of welding arcs

In order to classify welding processes as a stable or unstable, series of images was necessary to be processed and after that - analysed. The goal of the analysis was to obtain a set of features that could be background for assessment of abnormalities of welding processes and recognition of faults of the welded joint. It has been assumed that a relevant set of selected features provides us with information enabling image classification into one of classes defined a priori. Classes have been defined by means of features estimated on the basis of ROIs distinguished from pattern images.

3.1. Feature estimation and relevant feature extraction

On the basis of elaborated procedures, it was possible to calculate values of numerous features that corresponded to the welding arc. Among geometrical features there were values calculated on the basis of area, perimeter, convexity or concavity, orientation, compactness, elongation and selected geometrical moments. In order to select relevant characteristic values from a set of 81 estimated features, correlation analysis has been performed (Fig. 4).

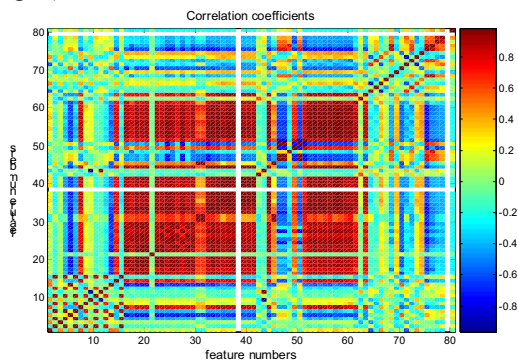


Fig. 4. Features correlation chart

In consequence of correlation analysis 15 relevant values have been distinguished. In Fig. 5 two exemplary features presented together with corresponding arc areas were shown. The features are center of mass and elongation factor that is defined as maximal diameter of identified shape divided by equivalent rectangle short side.

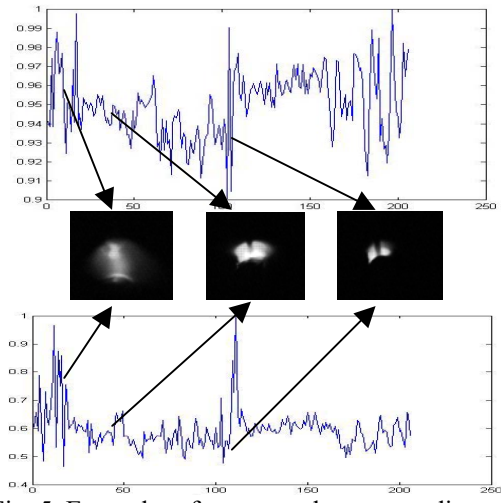


Fig. 5. Exemplary features and corresponding arc areas

4. ESTIMATION OF WELDING PROCESS STABILITY

Stability of the welding process has been estimated on the basis of assessment of images representing welding arcs. In case of correctly prepared edges of welded elements the observed process was stable and deviations of arc and shape dimensions were small.

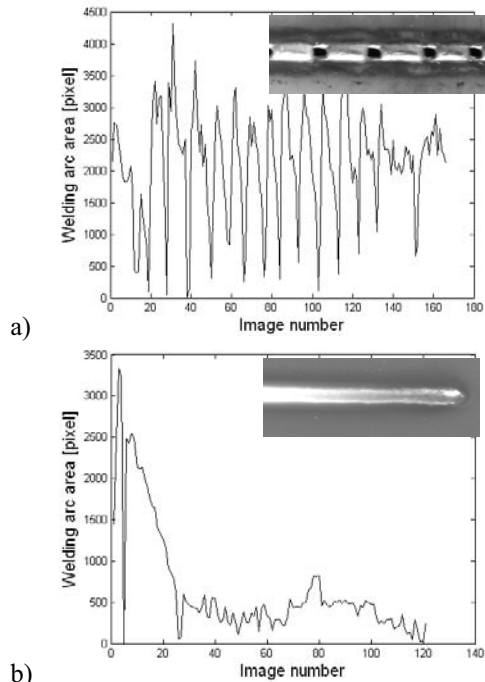


Fig. 6. Changes of arc sizes of for unstable a) and stable b) welding process

During the welding that was not correctly performed, the process was unstable. In order to estimate abnormalities of the process some pattern abnormalities of the process some pattern shapes of arcs were necessary to be determined. They were based on features enumerated above. Exemplary results of estimation of such pattern features (sizes of arc areas) on the basis of images recorded during the observed processes were

presented in Fig. 6. Examples of images presenting stable and unstable arcs were presented in Fig. 3.

Recognition algorithms

The main goal of the application of the system was to recognize state of the process and some selected faults of welded joints. Two separate groups of patterns were necessary to be identified (Fig. 7.). Recognition algorithms have been based on the analysis of features resulting from arc (assessment of the process; dotted red line) and joint (continuous blue line) observation. Features discussed in the paper are results of arc observation (grey fields). However, they constitute only a part of identified patterns. They are processed and considered together with results of thermogram analysis (hatched fields).

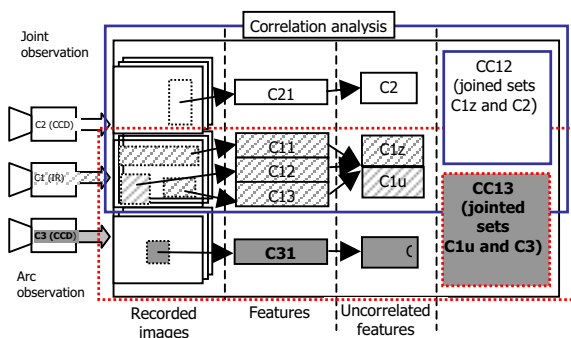


Fig. 7. Procedure of pattern identification

As it was presented in the paper, features resulting from analysis of each image were underwent to correlation analysis. In the next stage some features were being gathered and underwent to correlation analysis once again. Results of this stage made it possible to identify unambiguous patterns of some process states as well as welded joint faults. Patterns were used for building two neural classifiers for process and joint assessment. It is important that patterns had to be identified for each process and welded elements individually since they strongly depend on welding conditions.

5. RESULTS AND CONCLUSIONS

In the paper elements of an approach to automatic control of welding process were presented. Algorithms of image processing consisted in distinguishing ROIs (regions of interests), edge tracing, binarizing and estimation of some characteristic geometrical features. In order to obtain optimal set of these features correlation analysis was employed. A set of relevant mutually not correlated features was distinguished and patterns representing abnormalities of the welding process were identified. On the basis of performed observations correspondence between changes of features of the arc and stability of the welding process has been proved.

REFERENCES

- [1] Bzymek A.: Czupryński A., Fidali M., Jamrozik W., Timofiejczuk A.: *Analysis of images recorded during welding processes*. QIRT2008, 9th International Conference on Qualitative InfraRed Thermography, Kraków, 2008
- [2] Cook G. E., Barnett R. J.: *Automated visual inspection and interpretation system for weld quality evaluation*, Industry Applications Conference, 1995. Thirtieth IAS Annual Meeting, IAS '95., Conference Record of the 1995 IEEE
- [3] E. R. Davies: *Machine Vision Theory Algorithms, Practicalities (3rd ed.)*. Elsevier, 2004
- [4] M. Fidali, A. Bzymek A. Timofiejczuk, A. Czupryński, W. Jamrozik: *Ocena stanu procesu spawania na podstawie analizy obrazów wizyjnych i termowizyjnych XIII Naukowo – Techniczna Konferencja Spawalnicza „postęp, innowacje i wymagania jakościowe procesów spawania”*, Międzyzdroje 2008
- [5] Kim J. S., Son Y. T., Cho H. S., Koh K. I.: *A robust method for vision-based seam tracking in robotic arc welding*, Proceedings of the IEEE International Symposium on Intelligent Control 1995
- [6] Smith J. S., Balfour C.: *Real time top-face vision based control of weld pool size*, An International Journal Industrial Robot, No 32/2/2005
- [7] Xu D., Wang L., Tan M.: *Image processing and visual control method for arc welding robot*, Proceedings of the IEEE International Conference on Robotics and Biomechanics, Shenyang, China, 2004
- [8] Yamamoto M., Kaneko Y., Fujii K., and others: *Adaptive Control of Pulsed MiG Welding Using Image Processing System*, IEEE, 1988



Anna BZYMEK is PhD student in the Department of Fundamentals of Machinery Design. Main area of research are vision systems in diagnostics, machine vision, image processing, analysis and recognition, signal processing.



Anna TIMOFIEJCZUK, PhD, assistant professor in Department of Fundamentals of Machinery Design. Main area of research: time-frequency signal analysis, diagnostic inference, image processing, analysis and recognition.

SYMPTOM LIMIT VALUE: A STATISTICAL APPROACH

Tomasz GAŁKA

Institut Energetyki, Pracownia Diagnostyki Urządzeń Ciepłych Elektrowni
02-981 Warszawa, ul. Augustówka 36, fax (022) 642 8378, e-mail tomasz.galka@ien.com.pl

Summary

Quantitative technical condition assessment may employ a scale provided by symptom baseline and limit values. Prognosis is then based on fitting a suitable function to recorded symptom time history. Such approach assumes the deterministic symptom concept. Due to the influence of factors other than object technical condition, however, symptom often has to be regarded as a random variable. With such approach it is necessary to consider the probability of limit value excess and hence of a false alert. This pertains to the object operation policy. An example is provided by vibration-based symptoms relevant to a steam turbine fluid-flow system. On the basis of experimental data it is shown that this probability can be unacceptably high well before the limit value is attained.

Keywords: technical diagnostics, diagnostic symptom, limit value, prognosis.

WARTOŚĆ GRANICZNA SYMPTOMU W UJĘCIU STATYSTYCZNYM

Streszczenie

Ilościowa ocena stanu technicznego może być oparta na bazowej i granicznej wartości symptomu. Prognozowanie jest wówczas realizowane przez dopasowanie odpowiedniej funkcji do zarejestrowanego przebiegu czasowego symptomu. Zakłada to deterministyczny charakter symptomu. Ze względu na wpływ czynników innych niż stan techniczny symptom musi jednak często być traktowany jako zmienna losowa. Należy wówczas rozważyć prawdopodobieństwo przekroczenia wartości granicznej, a tym samym fałszywego alarmu. Jest to związane z polityką eksploatacji obiektu. Podany przykład dotyczy drganiowych symptomów stanu układu przepływowego turbiny parowej. Na podstawie danych z rzeczywistego obiektu wykazano, że prawdopodobieństwo to może być niedopuszczalnie wysokie na długo przed osiągnięciem wartości granicznej.

Słowa kluczowe: diagnostyka techniczna, symptom diagnostyczny, wartość graniczna, prognoza.

1. INTRODUCTION

Three principal areas of interest in condition monitoring are fault detection, diagnosis and prognosis [1]. Fault detection can be alternatively referred to as qualitative diagnosis, its aim being fault identification and localization. Similarly, diagnosis can be more precisely termed quantitative diagnosis, as it is aimed at determining damage extent [2].

Quantitative technical condition estimation of any object must, by necessity, involve a reference scale. For a given symptom S such scale may be provided by its baseline and limit values (S_0 and S_l , respectively). Interpretation of the baseline value is straightforward, as it refers to a new object with no malfunctions and generalized damage D equal to zero ($D = \theta/\theta_b$, where θ denotes time and θ_b is the time to breakdown). Limit value is the indication of technical condition deterioration to a point where 'some action should be taken'; in other words, $S = S_l$ indicates an 'accelerated wear problem' [3]. It must

not be confused with the maximum admissible value, which pertains to operational safety considerations and should, in principle, be determined by the object manufacturer.

Symptom limit value concept may be based on symptom reliability [3-5]. If we employ the Neyman-Pearson rule, known from the statistical decision theory, we obtain

$$R(S_l) = A/G \quad , \quad (1)$$

where A is the acceptable probability of performing an unnecessary repair (i.e. of the object able for normal operation) and G is object availability. $R(S)$ is the symptom reliability, given by

$$R(S) = P(S > S_e) = \int_{S_e}^{\infty} p(S^*) dS^* \quad , \quad (2)$$

where $p(S)$ is the symptom probability density function. With sufficient database $p(S)$ can be estimated, so that, for given values of A and G , an estimation of S_l can be obtained. Note that A and G are related to the plant operation philosophy and, in

a way, represent acceptable risk level. This is an important issue that shall be recalled later.

Symptom probability density function is estimated from experimental data, so limit value determination inevitably involves some measure of uncertainty. In the following, however, we shall assume that the available database is large enough for this uncertainty to be neglected.

Symptom limit value is particularly important for prognosis. Forecasting technical condition development usually involves some form of symptom time history (trend) analysis and fitting a curve to experimental data [1, 2]. In this manner, it is possible to estimate, at a given moment θ , the 'time to alert' $\Delta\theta$:

$$\Delta\theta = \theta_i - \theta, S(\theta_i) = S_i, \quad (3)$$

so that a subsequent repair can be timed and its extent adjusted. This is important especially for large and critical machines, such as power generating units, aircraft engines etc.

For any real object, especially a large and complex one, we have to keep in mind that a measured symptom value depends not only on object technical condition. In fact,

$$S = S[\mathbf{X}(\theta), \mathbf{R}(\theta), \mathbf{Z}(\theta)], \quad (4)$$

where \mathbf{X} , \mathbf{R} and \mathbf{Z} denote condition parameters, control and interference vectors, respectively. In principle, influence of control parameters can be normalized [6], although procedures may be tedious and their applicability is often limited to a given machine type or even a particular example. In most cases it is reasonable to assume that \mathbf{R} and \mathbf{Z} components have no monotonic trends and can be treated as random variables with parameters that do not change with time. This implies that, for any symptom, its measured value is also a random variable and, in principle, should be dealt with in a statistical rather than a deterministic manner. This immediately brings about a question whether the above approach to symptom limit value excess, based on a deterministic symptom life curve $S(\theta)$, is appropriate.

2. BASIC CONSIDERATIONS

Let us, for simplicity, assume that we are dealing with only one symptom and only one condition parameter. In such case, Eq.(4) takes the form of

$$S = S[X(\theta), R_1(\theta), \dots, R_m(\theta), Z_1(\theta), \dots, Z_n(\theta)]. \quad (5)$$

In many important cases X can be identified with the above-mentioned generalized damage D , so that $X(\theta) = \theta/\theta_b$. If the conditions

$$i \in \hat{(1,m)} \frac{\partial S}{\partial X} \gg \frac{\partial S}{\partial R_i}, \quad (6)$$

$$i \in \hat{(1,n)} \frac{\partial S}{\partial X} \gg \frac{\partial S}{\partial Z_i} \quad (7)$$

are fulfilled, we may assume that recorded symptom time history is dominated by technical condition evolution and influence of other factors may be neglected. This justifies a deterministic approach. If this is not the case, we may infer that a measured symptom value is, to a large extent, influenced by control and/or interference.

In practice, deterministic approach is often acceptable if technical condition deterioration is fast, i.e. when we are dealing with a rapidly developing fault. Example is given in Fig.1a. It is easily seen that, in each life cycle,¹ there is an almost linear increase (in this case caused by increasing rotor bow) and fluctuations are comparatively small. The opposite case is illustrated by another example, given in Fig.1b. Prior to rotor replacement, large fluctuations can be observed, superimposed on a continuous (approximately exponential) curve, related to 'normal' lifetime consumption – a natural damage or 'soft fault' [8, 9]. A deterministic approach in such case may prove inadequate.

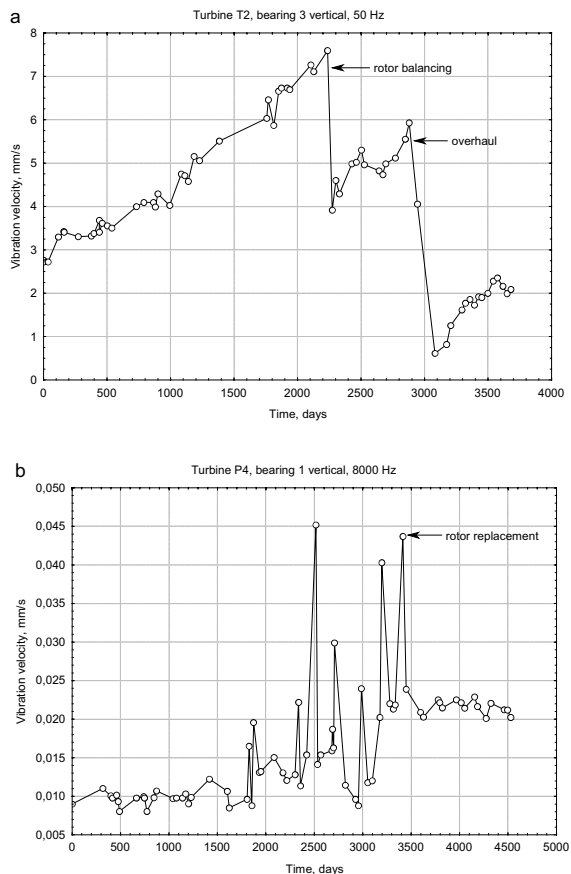


Fig. 1. Examples of vibration time histories, obtained for power steam turbines; a – 13CK230 unit, rear intermediate-pressure turbine bearing, vertical direction, 50 Hz band; b – K-200 unit, front high-pressure turbine bearing, vertical direction, 8 kHz band. See main text for details.

¹ Life cycles are determined by repairs and overhauls; for more details, see e.g. [5, 7].

As already mentioned, R_i and Z_i components can usually be treated as random variables with constant parameters. What we in fact observe, however, is not these components by themselves, but rather the object reaction to their changes. This obviously leads to a question how does the object sensitivity to R_i and Z_i , given by partial derivatives in Eqs. (6) and (7), change with time. This can be estimated only indirectly. Analysis of experimental data for power steam turbines shows [10] that, for vibration-based symptoms, standard deviation determined within a time 'window' changes rapidly as this window moves along the time axis. We may therefore infer that, with D increasing, standard deviation of a symptom, treated here as a random variable, will also increase. Thus, for a fixed S_i , probability of recording a symptom value $S > S_i$ will increase as $\theta \rightarrow \theta_b$, not only as a result of increasing symptom expected value \hat{S} .

There is still no model suitable to account for such processes in a quantitative manner. It seems, however, justified to perform a simulation based on data obtained for real objects. Results turn out to be of importance from the point of view of plant operational policy.

3. OBJECT AND MEASUREMENT DATA

Results dealt with in the following were obtained with a K-200 power steam turbine, operated as a base-load unit in a utility power plant. This turbine had logged about 150,000 hours of operation before investigations started (this particular moment corresponds in the following to $\theta=0$), which for this turbine type means a considerable lifetime consumption degree.² After about nine years the high-pressure rotor was replaced during a scheduled overhaul (Fig.1b refers to this particular turbine).

Data for analysis were obtained from 23% constant-percentage bandwidth (CPB) absolute vibration velocity spectra, recorded on turbine bearings. Amplitudes in individual frequency bands determined from the vibroacoustic model were treated as individual symptoms. More details can be found in references [12, 13]. It seems necessary to recall here that for steam turbines (and in fact for all rotating machines that produce broadband vibration spectra) two frequency ranges can be distinguished. The so-called harmonic or low range contains components generated directly as a result of the rotating motion, while the blade or high range contains those resulting from interaction between fluid-flow system elements and steam flow. The latter range, which is of particular interest for this

study, is in this turbine approximately between 500 and 9000 Hz. It should be noted here that vibration-based symptoms from this range are typically much more sensitive to factors other than technical condition evolution, their typical behavior being similar to that shown in Fig. 1b.

Due to comparatively long period covered by observation it was possible to estimate limit values for the above-mentioned symptoms. Details of relevant procedures are beyond the scope of this study and can be found in references [7, 14].

In the following, two symptoms are analyzed in detail, namely vibration velocity amplitudes in the 6300 Hz and 8000 Hz bands, recorded at the front high-pressure turbine bearing in vertical direction. For brevity these symptoms are hereinafter referred to as S_1 and S_2 , respectively. These frequency bands contain components generated by the high-pressure rotor, which was replaced during the overhaul. Both these symptoms exhibited a marked increase tendency prior to the replacement, which indicates damage acceleration. For obvious reasons, data obtained after the overhaul have not been taken into account.

4. RESULTS AND DISCUSSION

Fig.2 shows raw trends of S_1 and S_2 with exponential fitting; it has been shown, on the basis of experimental data analysis and some model considerations, that this type of $S(\theta)$ function is appropriate for this frequency range [7]. In both graphs limit value is indicated ($S_{1l} = 0.349$ mm/s, $S_{2l} = 0.121$ mm/s). This obviously allows for a prognosis: had it not been for the overhaul, exponential fit of the S_1 would have attained its limit value in about 5,400 days and of S_2 in about 9,500 days, starting from $\theta=0$. As it can be seen in Fig.2a, S_1 actually exceeded its limit value three times before the overhaul.

It seems reasonable to assume, at least as a first approximation, a normal distribution of S_1 and S_2 ; we shall recall this issue later in Section 5. Within the framework of a statistical approach, we may assume that exponential fit represents the time history of symptom expected value \hat{S} . We thus obtain:

$$\hat{S}_1(\theta) = 0.011 \times \exp(0.0006 \times \theta) , \quad (8)$$

$$\hat{S}_2(\theta) = 0.0077 \times \exp(0.0003 \times \theta) , \quad (9)$$

where symptom value is given in mm/s and θ in days. As already mentioned, experimental evidence shows that standard deviation should be expected to increase with θ . We may apply a 'moving window' procedure similar to that described in [10]: standard deviation σ is estimated within a window that includes ten consecutive measurements. Such approach obviously implies the assumption that technical condition deterioration during the period covered by this window can be neglected. Due to the 'accelerated wear' condition, we may also assume

² K-200 turbines had been designed in early 1950s, with a very conservative (by today's standards) service life estimation of about 100,000 hours. In practice service life of thick-walled elements (casings) and rotors has been about 200,000 to 250,000 hours; see e.g. [11].

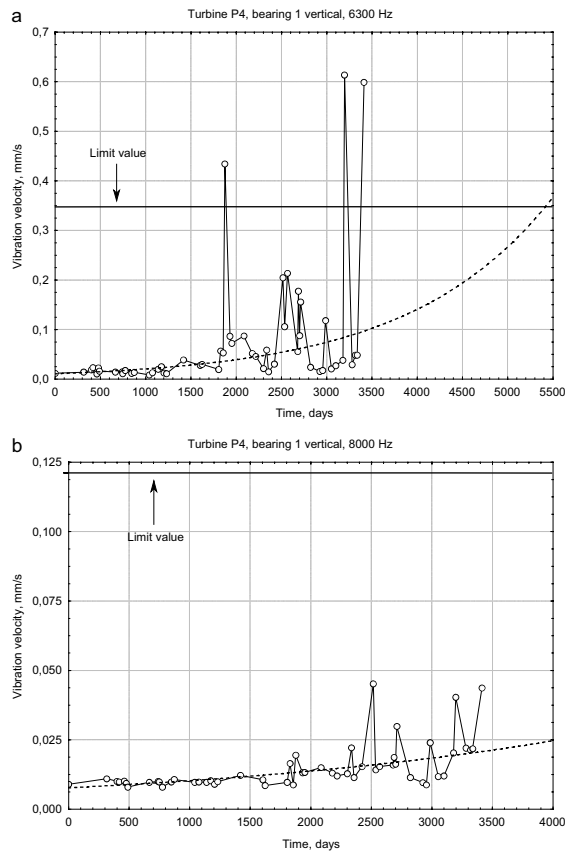


Fig. 2. Time histories of the S_1 (a) and S_2 (b) symptoms; broken line represents exponential fit and horizontal line marks the symptom limit value. Intersection of these lines has not been shown in (b) for clarity (θ is about 9,500 days).

the exponential fit for σ . Corresponding results for symptoms S_1 and S_2 are shown in Fig. 3. It is easily seen that fitting is far from perfect, due to large 'jumps' of the symptom value that cause stepwise changes of σ . This is particularly evident for σ_1 . Exponential increase can nevertheless be seen. For relative standard deviation σ_r ($\sigma_r = \sigma / \hat{S}$) we obtain:

$$\sigma_{r1}(\theta) = 20.51 \times \exp(0.0006 \times \theta), \quad (10)$$

$$\sigma_{r2}(\theta) = 3.50 \times \exp(0.0009 \times \theta), \quad (11)$$

where σ_r is given in percent and θ in days.

Functions given by Eqs. (8 ÷ 11) and estimated values of S_{1l} and S_{2l} allow for numerical simulations of limit value excess probability $P = P(S > S_l)$ as a function of time for both S_1 and S_2 . Results are shown in Fig. 4. It should be noted here that, in order to reduce the influence of randomness, baseline values S_{01} and S_{02} have been determined by averaging first five measurements rather than simply taking the first measured value.

Simulation results shown in Fig. 4 show that for $\theta < 2500$ days and $\theta < 3000$ days for S_1 and S_2 , respectively, limit value excess probability is very low ($P_{1,2} < 0.00001$). At the end of the period covered by observation, i.e. for $\theta \approx 3300$ days, P is still quite low ($P_1 = 0.159$ and $P_2 = 0.017$ for S_1 and S_2 ,

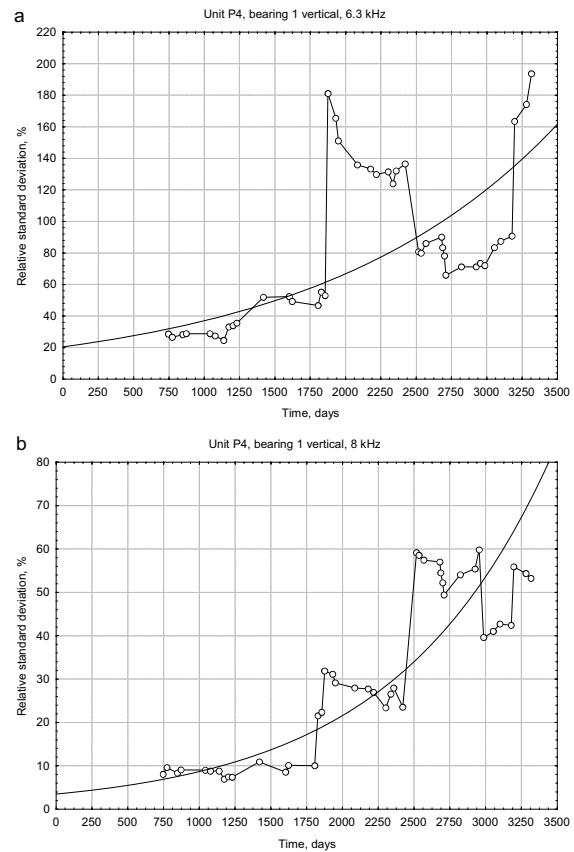


Fig. 3. Exponential fits of σ_{r1} (a) and σ_{r2} (b) time histories.

respectively). It can be easily seen, however, that for $\theta = 5000$ days, i.e. about 400 days before estimated θ , P_1 is only slightly lower than 0.5. From the point of view of unit operation this means that more than a year before symptom limit value is attained the probability of a false alert is almost 0.5. For S_2 initial values of \hat{S} and σ are substantially lower, but due to higher exponential factor the increase is faster. For $\theta = 5000$ days, i.e. over twelve years before estimated θ , P_2 is already over 0.4.

We may note here that $S(\theta)$ fitting and S_l estimation correspond to a 'conventional', or deterministic approach to technical condition development prognosis. Such approach involves some method of symptom limit value determination and hence, as already mentioned, implies a certain plant operation policy. The above considerations show, however, that such policy should also determine the acceptable level of false alert probability. Analysis of data pertaining to real objects clearly shows that this probability is certainly not negligible well before the symptom limit value is attained. With an on-line condition monitoring system, wherein measurements can be taken at arbitrary time intervals, an averaging procedure may be a reasonable alternative: in this way, symptom time history is 'smoothed' and the impact of its statistical nature is reduced. Such systems are, however, usually very costly and their parameters may be limited by the industrial plant environment

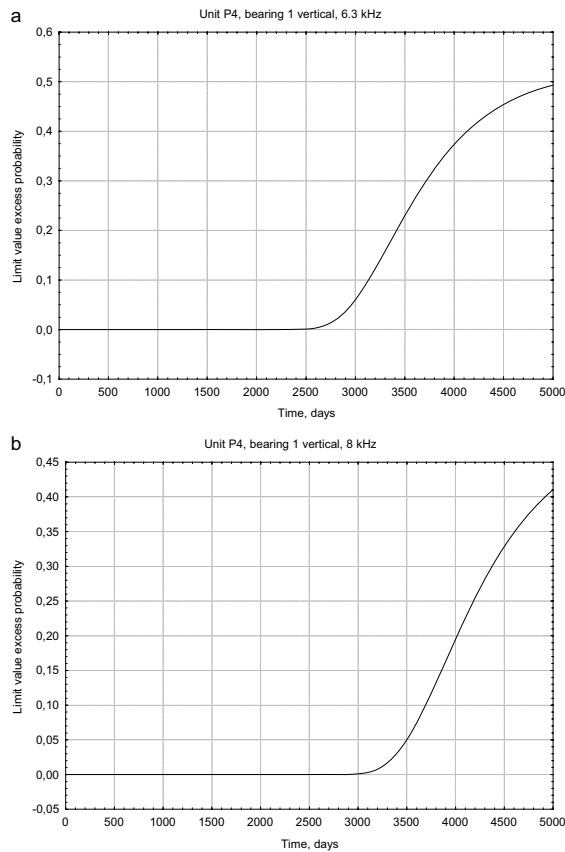


Fig. 4. Symptom limit value excess probability $P(S > S_i)$, calculated for S_1 (a) and S_2 (b).

requirements.³ On the other hand, with an off-line system, wherein measurements are usually performed at certain time intervals, such averaging is not practical and statistical nature of symptoms has to be accounted for.

5. FUTURE PROSPECTS

The example presented in Section 4 immediately raises at least two questions that have to be addressed.

The first one is related to the method of determining statistical parameters involved. It seems reasonable to assume that $\hat{S}(\theta)$ is adequately represented by fitting a curve to experimental results, providing that the function is properly selected and fitting quality satisfactory. Exponential fitting seems justified for objects that approach θ_b , due to the destructive feedback [1]. It has also been shown experimentally that such fitting yields good results for vibration-based symptoms pertaining to the blade frequency range [2]. Fitting a curve to the $\alpha(\theta)$ experimental time histories is, however, more problematic, which is clearly seen in Fig. 3. One

possible reason, and probably the most important one, is the very method of determining σ . Time window should be kept short, in order to fulfill the condition of negligible technical condition change. The shorter the window, however, the worse is the accuracy of estimation. This contradiction is particularly severe if intervals between individual measurements are long, and this is exactly the case in this particular cause. The situation would certainly have been much better if data from a purpose-designed diagnostic experiment had been available. Such experiment should probably be performed with an object characterized by much shorter θ . This opens the field for possible future research.

The other question is whether normal distribution of S is justified. It is well known that many physical phenomena can be described by this type of distribution [14]. In this particular case this implies that, at a given moment θ , with a corresponding expected value $\hat{S}(\theta)$ and an arbitrary ΔS , it is equally probable to record symptom value of $S = \hat{S}(\theta) + \Delta S$ and of $S = \hat{S}(\theta) - \Delta S$. In fact this does not seem to be the case. Figs. 1b and 2 clearly indicate that ‘upward’ jumps are encountered more often than ‘downward’ ones; in other words, influence of control and interference is likely to result in a measured symptom value increase rather than decrease. A right-hand skewed distribution would thus be more appropriate. Weibull distribution, with the probability density function given by

$$p(S) = \frac{c}{b} \left(\frac{S-a}{b} \right)^{c-1} \exp \left[- \left(\frac{S-a}{b} \right)^c \right] \quad (12)$$

(a – threshold, b – scale, c – shape factors, $S \geq a$) might be more suitable. It seems justified to assume $a = 0$, as no lower limit for the symptom value can be determined. Both b and c must in such case be estimated within a narrow time window, which exacerbates the above-mentioned accuracy problem (with the normal distribution only σ is determined in this manner). In the author’s opinion, assumption of a right-hand skewed distribution is very unlikely to change qualitative conclusions presented in Section 4 and render the symptom statistical nature unimportant in technical condition development prognosis. In fact, $P(S > S_i)$ curves might in such case even be steeper than those shown in Fig. 4. Again, a purpose-designed diagnostic experiment might be decisive.

ACKNOWLEDGEMENT

Some of the results used in this paper have been obtained within the framework of a research project, financed by the Ministry of Science and Higher Education (project N504 030 32/2693).

³ On-line vibration measurement systems installed on steam turbines usually have the upper frequency limit of a few hundred Hz, due to sensors used. The entire blade frequency range is thus cut off.

REFERENCES

- [1] Randall R. B.: *State of the art in monitoring rotating machinery*, Sound and Vibration, March 2004, pp.14-20 (part 1), May 2004, pp.10-16 (part 2)
- [2] Gałka T.: *Representation of machine technical condition in evolutionary diagnostic symptoms*, Eksploatacja i Niezawodność, Nr 1(37)/2008, pp. 23-29
- [3] Cempel C.: *Limit value in practice of vibration diagnosis*, Mechanical Systems and Signal Processing, vol.4, No.6, 1990, pp.483-493
- [4] Cempel C.: *Theory of energy transforming systems and their application in diagnostics of the operating systems*, Applied Mathematics and Computer Science, 1993, vol.3, No.3, pp.533-548
- [5] Natke H. G., Cempel C.: *Model-Aided Diagnosis of Mechanical Systems*, Springer, 1997
- [6] Gałka T.: *Influence of turbine load on vibration patterns and symptom limit value determination procedures*, Proceedings of the COMADEM 2001 International Conference. Elsevier, Oxford, 2001, pp. 967-976
- [7] Gałka T.: *Application of energy processor model for diagnostic symptom limit value determination in steam turbines*, Mechanical Systems and Signal Processing, 1999, vol.13, No.5, pp.757-764
- [8] Konieczny J., Olearczuk E., Żelazowski W.: *Elementy nauki o eksploatacji*, WNT, Warszawa, 1969
- [9] Botsaris P. N., Tsanakas J. A.: *State-of-the-art in methods applied to tool condition monitoring (TCM) in unmanned machining operations: a review*, Proceedings of the COMADEM 2008 International Congress, Prague, 2008, pp.73-87
- [10] Gałka T.: *Statistical Vibration-Based Symptoms in Rotating Machinery Diagnostics*, Diagnostyka, Nr 2(46)/2008, pp. 25-32
- [11] Orłowski Z.: *Diagnostyka w życiu turbin parowych*, WNT, Warszawa, 2001
- [12] Gałka T.: *Large Rotating Machines*, in *Encyclopedia of Structural Health Monitoring*, ed. C.Boller, F.Chang and Y.Fujino, John Wiley & Sons, Chichester, UK, 2009, pp. 2443-2456
- [13] Gałka T.: *Normalization of vibration measurements: unnecessary complication or important prerequisite?* Proceedings of the Second International Symposium on Stability Control of Rotating Machinery ISCORMA-2, Gdańsk, 2003, pp. 722-731
- [14] Papoulis A.: *Probability, Random Variables and Stochastic Processes*. McGraw-Hill, New York, 1965



Tomasz GAŁKA, Ph.D graduated from Warsaw University of Technology, Faculty of Electronics. Since 1982 he has been employed at the Institute of Power Engineering. His main professional interests are focused on vibration-based diagnos-

tics of large rotating machines, in particular steam turbines. He has participated in a number of research projects in this field. He has authored or co-authored about 70 publications. His non-professional interests include railways and scuba diving.

APPLICATION OF THE PRESSURE PROCESS DETECTOR FOR DIAGNOSING INJECTION APPARATUS IN MARINE DIESEL ENGINES IN THE INJECTION PIPE

Jan MONIETA*, Karol KROCZYŃSKI

*Akademia Morska, Instytut Technicznej Eksploatacji Siłowni Okrętowych, Zakład Siłowni Okrętowych,
ul. Wały Chrobrego 2, 70–500 Szczecin, fax: (091) 4809 575, email: jmonieta@am.szczecin.pl

Summary

The paper includes results of the preliminary research of the application of the pressure process detector for diagnosing injection apparatus in marine diesel engines in the injection channel during exploitation without its dismantling. The research was conducted on the marine auxiliary engine and on injection analysis probe for shipping engines, which are situated in the Laboratory of the Ship Power Plant at Maritime Academy of Szczecin.

The aim of the research was to select symptoms of the fuel vibration signal in the fuel channel with the use of the pressure detector in a way that the signal is the reflection of the technical condition of the injection apparatus.

Keywords: marine diesel engines, injectors, diagnosis.

ZASTOSOWANIE DETEKTORA PRZEBIEGU CIŚNIENIA W PRZEWODZIE WTRYSKOWYM DO DIAGNOZOWANIA APARATURY WTRYSKOWEJ SILNIKÓW OKRĘTOWYCH

Streszczenie

Referat zawiera wyniki badań wstępnych zastosowania detektora przebiegu ciśnienia w przewodzie wtryskowym do diagnozowania aparatury wtryskowej silników okrętowych w czasie eksploatacji bez jej demontażu. Badania zostały przeprowadzone dla okrętowego silnika pomocniczego, oraz wykorzystaniem próbnika do badań wtryskiwaczy silników okrętowych, znajdującym się w Laboratorium Siłowni Okrętowych Akademii Morskiej w Szczecinie.

Celem było wyselekcjonowanie symptomu sygnału drgań paliwa w przewodzie paliwowym za pomocą czujnika ciśnienia tak, by był on odzwierciedleniem stanu technicznego aparatury wtryskowej. Badania wykazały, że niektóre parametry zarejestrowanych drgań w przewodzie wtryskowym mogą służyć do oceny stanu technicznego aparatury wtryskowej.

Słowa kluczowe: silniki okrętowe, wtryskiwacze, diagnozowanie.

1. INTRODUCTION

Injector nozzle, as an element working in the combustion chamber, is exposed to the highest thermal as well as mechanical load. At the same time precision of fuel dosing has to be very high, because it has significant influence on the quality of work of the whole engine. An injector as well as pumps and injection pipes are the elements, which are most often damaged or worn out during the operation of the engine [2]. Therefore care and proper control of these objects is extremely important.

They were making an attempt at using various methods and signals of pressure, vibration, combustion, etc. to diagnose injectors of diesel engines were made, but the level of their implementation is so far rather low [1, 3, 4, 5, 6]. Measurement of vibration is easier, and the amount of information obtained on the technical condition of injection apparatus is bigger.

2. PURPOSES OF THE RESEARCH

The aim of the work was to work out the method of diagnosing the injection apparatus of marine engines during their operation without their disassembly using the pressure process detector in the injection pipe. The research was conducted using the probe for testing marine injectors and 5BAH22 engine, which can be found in the Laboratory of Marine Power Plants at Maritime Academy in Szczecin.

The aim was also to select the symptom of fuel vibration signal in the fuel pipe, so as it was a reflection of the technical condition. At the same time it was decided to record the basic parameters of the internal combustion engine during its work.

The research is going to assess the usefulness of this method of diagnosing the injectors of marine diesel engines.

3. SCHEDULE OF THE RESEARCH

3.1. Objects of the research

The objects of the research were injectors of medium-speed engines by Sulzer company, type 6AL20/24D and BAH22. Preliminary research was conducted using AL20 probe for testing engine injectors. Principal research was conducted during work of 5BAH22 engine, which is a diesel engine with direct fuel injection. It is an in-line, four-stroke, supercharged, not reversible engine. It works with a constant rotational speed, maintained by rotational speed regulator by Woodward. This kind of engine is usually used for driving electrical generators.

Basic technical details of 5BAH22 engine:

- power for all cylinders 220 kW,
- rotational speed 500 rpm,
- unitary fuel consumption for 100% load 234 g/kWh,
- cylinder's diameter 220 mm,
- piston stroke 320m.

Injection valve of 5BAH22 consists of a frame and a injector nozzle with a needle. The needle opens at the pressure of 220 bar and after the end of the injection it is pressed to the seat by means of a spring. The pressure of needle opening can be adjusted by means of an adjusting screw.

AL 20 injectors' probe is used for dynamic testing, which enables to determine the opening pressure and its dynamic properties along with the quality of spraying and the form of a stream.

3.2. Measurement system

The pressure process detector in the injection pipe is designed for converting the fuel pressure in the injection pipe of marine diesel engines to electric signal. The process of pressure detection consists in integrating the detector with the injection pipe, which becomes a converter of one of the tested quantities. Final pressure conversion to electric signal is carried out by piezoelectric elements.

The measurement was taken at a station with a probe (fig. 1), where AL20 injector was connected to a high-pressure conduit. The injector was attached to the conduit in such a way, that the joint was tight and the injector nozzle remained in a vessel, in which a stream of injected fuel could be observed. A CL 52 sensor was attached to the high-pressure conduit and clipped to the injection pipe.

The measurement circuit with the pressure detector underwent calibration. The signal converted by the sensor, after amplification, was sent to a computer, where by means of a 'System of Signal Analysis' program, basic analysis taking into account time, amplitude and frequency was carried out.

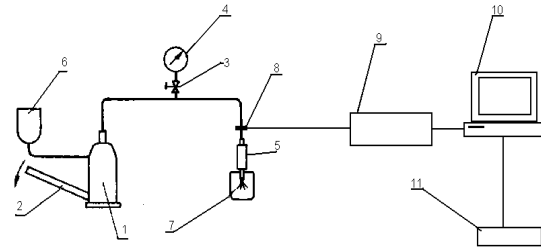


Fig. 1. Workstation with the probe used for measurement: 1 – pump, 2 – lever, 3 – cut-off valve, 4 – manometer, 5 – injector, 6 – fuel container, 7 – transparent vessel, 8 – pressure detector, 9 – signal amplifier, 10 – PC computer, 11 – printer

Measurements were also carried out with the use of 5BAH22 engine (fig. 2), where a clasp sensor was fastened to the high-pressure conduit for particular cylinders, one by one. The signal was sent to an amplifier, and then to a computer, where it was analyzed according to the needs, by means of the 'System of Signal Analysis' program. Measurements were made for various engine loads. The engine was loaded by means of a generator and a water resistor. The load was increased by 25 kW from 0 to 150 kW, so 7 measurements were taken altogether. Previous tests pointed out, that a correct diagnostic symptom, if it is interrelated with the dose of fuel injected, that is with the load, is also interrelated with the technical condition of the injector.

During each measurement basic parameters of the engine's work were recorded. The injection system of cylinder number 3 was in the state of disability.

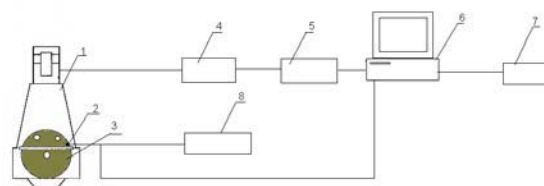


Fig. 2. Scheme of investigated stand: 1 – 5BAH22 engine, 2 – sensor of crankshaft position, 3 – electrical generator, 4 – amplifier, 5 – low-pass filter, 6 – PC computer, 7 – printer, 8 – sensor's power pack

4. RESULTS OF THE RESEARCH

An active experiment, consisting in changing one of the input quantities, such as engines' load, into diagnostic parameter values [3]. The measurement of the course of the injection process was taken for various frequency bands – from 0 to 125 Hz, from 0 to 1 kHz and from 0 to 2,5 kHz. In this article mainly the results for the frequency band from 0 to 1 kHz are presented.

Temporal courses of the signals of the injection process, which were recorded by the system in the real time, were also analyzed. An example of a record of this process is depicted in fig. 3.

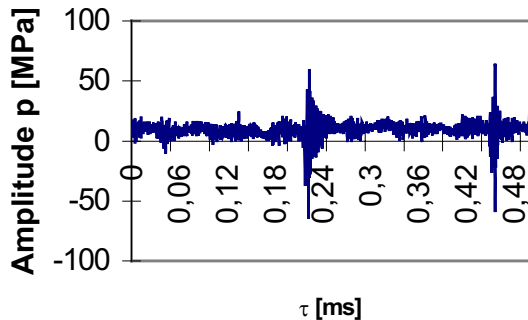


Fig. 3. An example of time course of the injection process for the fifth subsystem of 5BAH22 engine at the load of 75kW

Picture 3 implies, that the impulse from the injection process appears every specific period of time. Depending on the frequency band of the analysis, it was variously interfered.

Analysis in the domain of amplitudes was used, in which the estimates were originally presented in the form of cascades. During the analysis in the domain of the amplitude, estimates were determined [3]:

- root-mean-square value,
- average value,
- peak-to-peak value,
- positive peak value.

During the analysis in the domain of frequency, sequences of signals in various frequency bands were used, where spectrums were originally presented in the form of cascades. The spectrums of pressure pulsation were repeatable in each instance of measurement. In fig. 4 one can see, that the averaging envelope of the spectrum includes many characteristic components for various values of frequency.

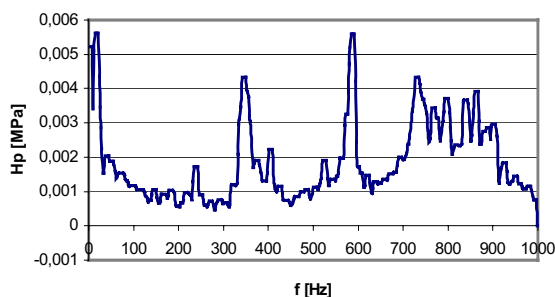


Fig. 4. An example of the envelope of an averaging spectrum of pressure pulsation in the injection pipe

Depending on the band of the analysis, various spectrums were obtained.

During the tests at the workstation with the probe, the results of the measurement were strongly influenced by vibrations caused by attempts to force the injection by means of hand lever and by difficulties with achieving the uniform speed of lever movements.

The influence of the tension of the clamp screw of the sensor was also examined, with the use of a torque spanner. The producer had not given any specific recommendations on this matter.

5. ANALYSIS OF THE RESULTS

The presentation of the results of the conducted tests was given in a form of graphs for various values of pressure pulsation in the injection pipe, resulting from various loads and technical condition of the engine.

During compiling the results in the domain of the amplitude, the influence of the engines' load on the value of amplitude estimates was examined. The examples of the courses of the estimates for tests conducted are depicted in fig. 5. These are the values for the frequency from 0 to 1 kHz. Very promising course can be observed for root-mean-square and average values. In fig. 6 RMS and AVER values for both ranges of frequency were isolated. With an approximation line introduced, linear interdependence of the estimates values along with the increase of load can be observed.

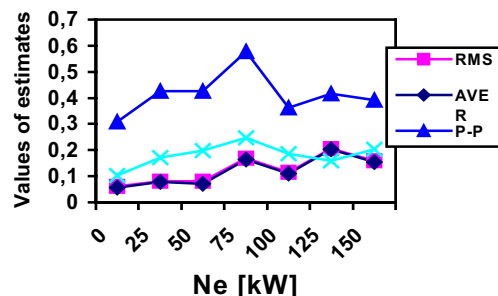


Fig. 5. Interdependence of amplitude estimates for various values of engines' load: $f =$ from 0 to 1 kHz

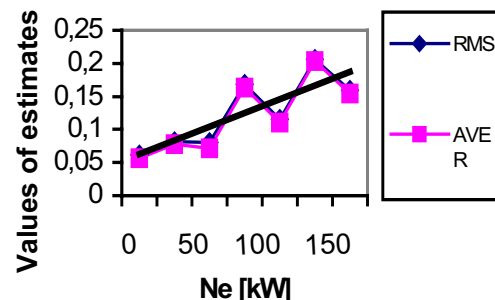


Fig. 6. Interdependence of root-square value (RMS) and average value (AVER) from engines' load, $f =$ from 0 to 1 kHz

The influence of the value of the load for all the values of component amplitudes of pressure pulsation spectrum was examined. In the range for $f =$ from 0 to 2.5 kHz, three components in the lower range, which show an explicit change of value along with the load. These values are depicted in fig. 7.

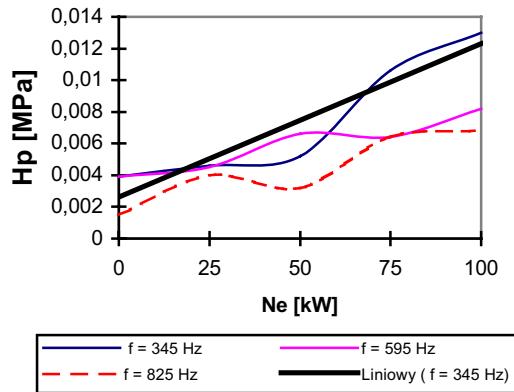


Fig. 7. Influence of engines' load on the values of selected component amplitudes of an envelope of pressure pulsation spectrums in the injection pipe

6. CONCLUSIONS

The following conclusions can be drawn from the conducted research:

- 1) The analysis of the graphs confirmed, that some parameters of the vibrations registered in the injection pipe can serve as symptoms reflecting the technical condition of the injection apparatus.
- 2) The tension of the clamp screw fastening the sensor to the pipe has a significant influence on the measurement, and the producer does not determine the value of this quantity.
- 3) The vibration of the whole engine during its work influenced the interference of the measurement signals with the probe.
- 4) The measurement at the workstation for injection testing was hindered because of considerable vibrations during injection attempts and a non-uniform speed of pumping;
- 5) The tests in the frequency band $f = 0$ to 2.5 kHz are less useful, than $f = 0$ to 1 kHz, where it is easier to isolate the components showing linear interdependence with load and technical condition.
- 6) Root-mean-square value (RMS), as well as average value (AVER), for both frequency bands, are suitable for diagnosing.
- 7) The research has to be verified on a marine vessel.

REFERENCES

- [1] Drozdowski J.: *Diagnostyka eksploatacyjna systemu wtryskowego silników okrętowych*. Budownictwo Okrętowe 1987 nr 3, pp. 27–33.
- [2] Monieta J.: *Choice of most deceptive functional system and sub-assembly of marine diesel engines*. Povyšenie Effektivnosti Raboty Energetičeskich Ustanovok. Meždunarodnyj Sbornik Nayčnych Trudov. Kaliningrad 2002, pp. 141–146.
- [3] Monieta J.: *Metodyka badań diagnostycznych wtryskiwaczy silników okrętowych*. Zagadnienia Eksploatacji Maszyn 2003 nr 1, pp. 169–185.
- [4] Monieta J. Rokicki P.: *Zastosowanie sygnałów prędkości drgań do diagnostyki wtryskiwaczy silników spalinowych*. Diagnostyka'2004 – Vol. 33, pp. 229–234.
- [5] Piaseczny L.: *Technologia naprawy okrętowych silników spalinowych*. Wydawnictwo Morskie Gdańsk 1992.
- [6] Piotrowski L. Witkowski K.: *Eksploatacja okrętowych silników spalinowych*. Wyd. Fundacja Rozwoju WSM w Gdyni. Gdynia 2002.



Dr. Sc. Eng. **Jan MONIETA** is a graduate of Working Machines and Vehicles Department of the Poznań University of Technology. He is employed doctor at the Institute of Ship Power Plant Operation at Maritime Academy of Szczecin. In his research work he deals with the issues of marine power plants operating, particularly internal combustion engines. He is an author or a co-author of 107 reports and articles.



Eng. **Karol KROCZYŃSKI** graduated from the Mechanical Department of Maritime Academy of Szczecin. He gains experience and practical knowledge by serving on ships of English shipowner North Star Shipping Ltd., as a III ship's engineer. Recently he has taken up postgraduate studies at the AGH University of Science and Technology in Cracow at the Kerosene and Gas Drilling Department.

IDENTIFICATION AND VERIFICATION OF SIMULATION MODEL OF GEARS WORKING IN CIRCULATING POWER SYSTEM

Bogusław ŁAZARZ, Grzegorz PERUŃ

Faculty of Transport, Silesian University of Technology
40-019 Katowice, ul. Krasińskiego 8, fax (+48) 32 6034108, email: grzegorz.perun@polsl.pl

Summary

This article presents executed stages of preparing and identification a power circulating gear testing machine. The purposefulness of modelling this test-stand was justified by its popularity and universal character that enabled to apply it in many laboratory research works. It was assumed that property defined and next identified model would be used to analyze dynamic phenomena in meshing and bearings of examined gears and it enabled to optimize their construction, especially to minimize their vibroactivity.

The described model combines advantages of two main modelling directions: it is characterized by very accurate analyzes of a model of toothed wheels pair, that includes nonlinear description of properties of both gears meshing in a test-stand (examined and closing), as well as it includes the influence of remaining system's elements, which enables to examine the dynamics of a system as a whole.

Calculation algorithm additionally includes possibility to simulate faults of wheels in the examined gear, such as chipping of tooth tips, tooth root crack together with possible faults of rolling bearings elements.

The article includes description of the construction of a test-stand, dynamic system model with detailed parameters as well as short characteristics of the simulation program and purposes of its main modules. Next the research works, which aimed at identification of selected parameters of the model, were presented. Afterwards it was verified whether the model was correctly fine tuned by means of measuring the velocity of transversal vibrations at the test-stand using Ometron VH300+ laser vibrometer, and results of laboratory examinations were compared with the results achieved during computer simulation.

Keywords: gearbox, power circulating gear testing machine, dynamic model.

IDENTYFIKACJA I WERYFIKACJA MODELU SYMULACYJNEGO PRZEKŁADNI ZĘBATYCH PRACUJĄCYCH W UKŁADZIE MOCY KRAŻĄCEJ

Streszczenie

W artykule przedstawione zostały zrealizowane etapy opracowywania i dostrajania modelu stanowiska z przekładniami zębatymi pracującymi w układzie mocy krążącej (FZG). O celowości modelowania tego stanowiska zadecydowała jego popularność i uniwersalność, pozwalająca wykorzystać je w wielu badaniach laboratoryjnych. Założono, że poprawnie zdefiniowany a następnie zidentyfikowany model, zostanie wykorzystany do analizy zjawisk dynamicznych w zazębieniach i łożyskach badanych przekładni oraz pozwoli na optymalizację ich konstrukcji, w szczególności w kierunku minimalizacji ich wibroaktywności oraz rozbudowy bazy wiedzy diagnostycznej.

W pracy opisano budowę stanowiska, przedstawiono jego model dynamiczny z wyszczególnieniem uwzględnionych parametrów oraz krótką charakterystykę programu symulacyjnego i przeznaczenie jego głównych modułów. W dalszej części przedstawiono badania, mające na celu identyfikację wybranych parametrów modelu. Poprawność dostrojenia modelu została następnie zweryfikowana poprzez pomiar prędkości drgań poprzecznych wałów na stanowisku doświadczalnym z użyciem wibrometru laserowego Ometron VH300+, a wyniki badań laboratoryjnych zostały odniesione do wyników uzyskanych drogą symulacji komputerowej.

Słowa kluczowe: przekładnia zębata, stanowisko FZG, model dynamiczny.

1. INTRODUCTION

Many research centres deal with modelling of gears, as they are found to be useful tools for designing and for a dynamic analysis of power transmission systems.

The research works, described, inter alia, in [1, 2, 4, 8, 9], are facilitated by continuous development of analytical equipment and software which make it possible to enrich models with further, previously not taken into account, factors.

Creating models of devices already at their designing stage allows meeting the requirement of production cost minimization and, above all, optimizing the construction in terms of its durability, reliability and functionality, optimizing thereby the service costs.

Such direction in designing devices is facilitated by defining the functional changes which result from changes in the condition of the device during its service.

By using models of gears, it is possible to make complicated dynamic analyses to identify symptoms of faults in gears, which analyses could not be carried out in real conditions.

Computer simulations allow us to considerably reduce the time and cost of examination, ensuring, at the same time, stability of the conditions in which the examination is carried out.

The mentioned advantages of using models justify the usefulness of research on models. They also effectively facilitate reduction of the number of stand tests.

The correctness of tests performed with use of a model results from its proper identification. Since a model always constitutes certain simplification of the actual object, which results from the fact that it is impossible to take into account all parameters of the investigated system, those quantities whose influence on the investigated phenomenon is very small, should be left out. This will allow avoiding mistakes, shortening of calculation time and obtaining results which are qualitatively and quantitatively comparable to the results of measurements made on a real object.

The developed model combines the advantages of two main directions in modelling: it is characterized by a precise analysis of a model of a pair of toothed wheels, with taking into account a non-linear description of meshing properties of both gears in a stand (the tested and closing gears). In addition, it takes account of the influence of other elements of the system and enables testing the dynamics of a power transmission system as a whole.

2. DESCRIPTION OF THE TEST STAND

The test stand with gears working in a circulating power system (Fig. 1) consists of an electric motor, which through a belt transmission (1) drives the

closing gear (2) and, connected to it by means of a torsional shaft (3) and coupling shafts (4), the tested gear. The tests may be carried out at different rotational speeds, the change of which is made smoothly by means of a frequency converter through which the motor is powered, and at a load controlled by means of torsional shafts, a tightening clutch (6) and a lever with weights. The closing and tested gears have identical ratios and identical axle bases [2, 4].

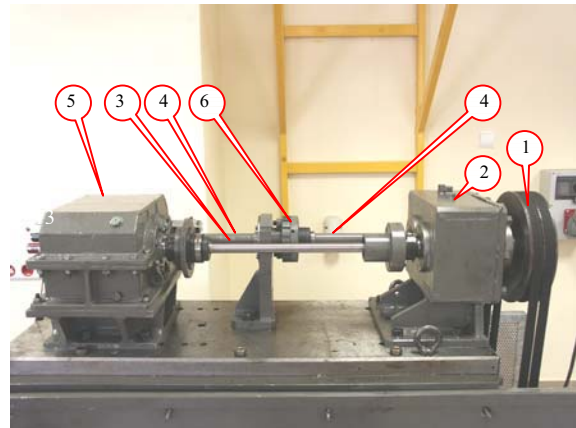


Fig. 1. Test stand

3. DYNAMIC MODEL

In a dynamic model of the test stand, the belt transmission connecting the motor with the closing gear was replaced with a tightening clutch. The model shown in Figure 2 allows taking into account, inter alia:

- the changeable rigidity of gear teeth meshing, friction and damping of vibration of meshing gears, deviations in gear pitches and position of the profile of each tooth, (according to PN-ISO 1328-1:2000), clearance between the teeth (j_{n1}, j_{n2}) – the developed description of meshing properties of the closing and testing gears is in line with the modelling direction proposed in [5, 6, 7],
- operation in conditions of a variable rotational speed and torque $M_s(n_s)$,
- angular displacements of the motor rotor (φ_s), tightening clutches ($\varphi_{sp}, \varphi_{wn}$), pinion and wheel of the closing gear (φ_H, φ_K) and tested gear (φ_B, φ_E) around the axis consistent with the direction of the gear shafts' axis,
- displacements in all system bearings in the direction of forces acting between the teeth ($x_A \div x_L$) and friction in meshing ($y_A \div y_L$),
- torsional rigidity of shafts,
- rigidity of supports $c_A \div c_L$,
- damping in bearings $k_A \div k_L$ and shafts,
- inertial mass and moments of inertia of the modelled elements of the stand ($m_I \div m_d, J_s, J_{sp}, J_{wn}, J_I \div J_d$).

The calculation algorithm additionally takes into account the possibility of simulation of faults in the tested gear, such as a crack at the tooth root or spalling of the tooth crest with possible concurrent occurrence of damage of rolling bearings components.

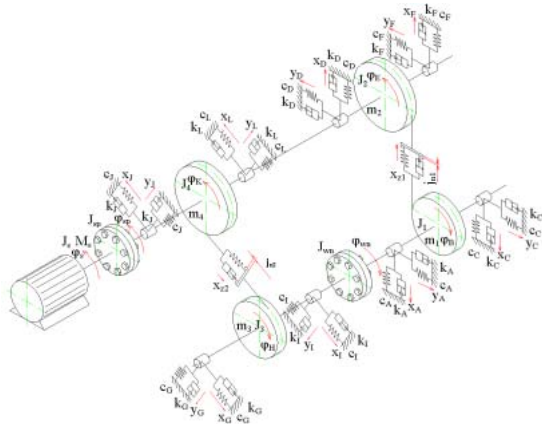


Fig. 2. Dynamic model of the stand

4. SIMULATION PROGRAM

The calculations are carried out using a program developed in the Delphi programming environment. For functional reasons, it has been divided into three parts: entering data and preliminary calculations (Fig. 3) simulation calculations and analysis of results. The stages of carrying out the calculations are schematically shown in Fig. 4.

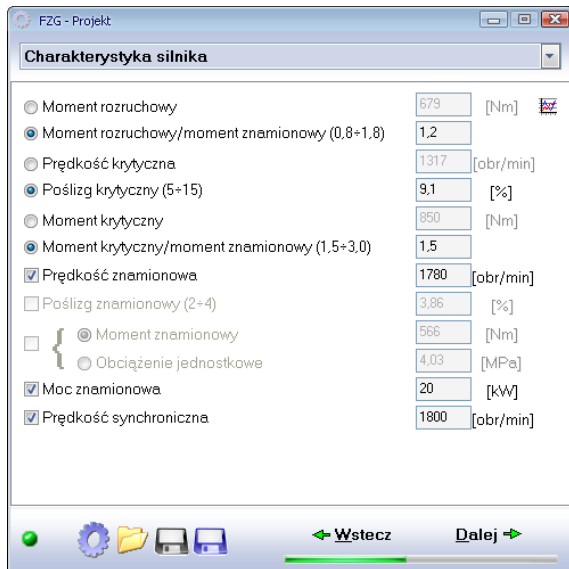


Fig. 3. Module window of data input and preliminary calculations with an active motor characteristics sheet

The Runge-Kutty 4 method was used to solve motion equations. The results of simulation calculations are recorded in a standard format of the Matlab program, what allows their processing using

advanced methods offered by this calculation environment.

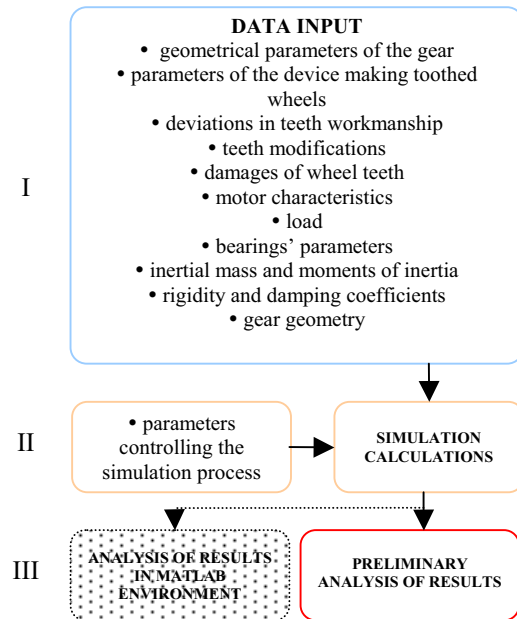


Fig. 4. Stages of simulation calculations

5. MODEL IDENTIFICATION

Application of the model for simulation tests requires previous tuning of its parameters. Only an identified model can be a tool enabling a reduction of the number of stand tests.

The first stage of tuning the model parameters consisted in measuring the geometrical parameters and deviations in pitch of toothed wheels mounted at a laboratory stand and in determining the inertial mass and moments of inertia of the modelled components, as well as torsional rigidity of the stand shafts. Basic geometrical parameters of toothed wheels of the stand-tested gear are compiled in Table 1.

Table 1. Parameters of toothed wheels of the tested gear

Number of pinion teeth, z_1	19
Number of wheel teeth, z_2	30
Angle of tooth line inclination, β	15 °
Addendum modification coefficient for the pinion, x_1	0,500
Addendum modification coefficient for the wheel, x_2	0,295
Nominal module, m_n	3,5 mm
Nominal pressure angle, α_n	20 °
Distance between axes of cooperating wheels, a_w	91,5 mm
Meshing width, b	56 mm
Meshing ratio, ϵ_a	1,32

Using the results of tests presented in [3], the model was tuned in the direction of determining efficiency values similar to those obtained during laboratory tests by means of the heat balance method. Concurrence of the efficiency values obtained from the simulation and from laboratory tests enabled determining the characteristics of friction coefficient in mesh (Fig. 5).

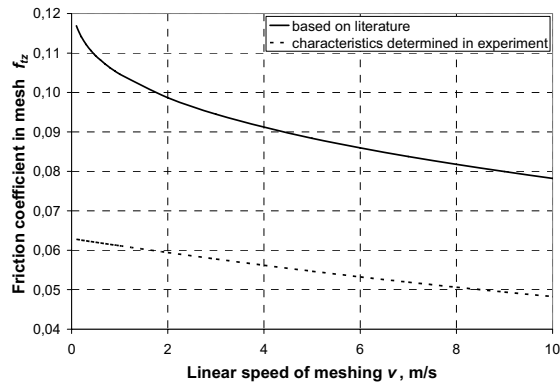


Fig. 5. Characteristics of friction coefficient in mesh

6. VERIFICATION OF THE SIMULATION TEST RESULTS

Verification of the model tuning correctness consisted in comparing the results of measurements of shafts' transverse vibration speed with the results of simulation calculations. The measurements were carried out on FZG stand (Fig. 1) using an Ometron VH300+ laser vibrometer in the direction of force acting between the teeth. Transverse vibration speeds of the pinion and wheel shafts were recorded for both, the tested and closing gear. Measuring points on the tested gear are presented in Fig. 6.

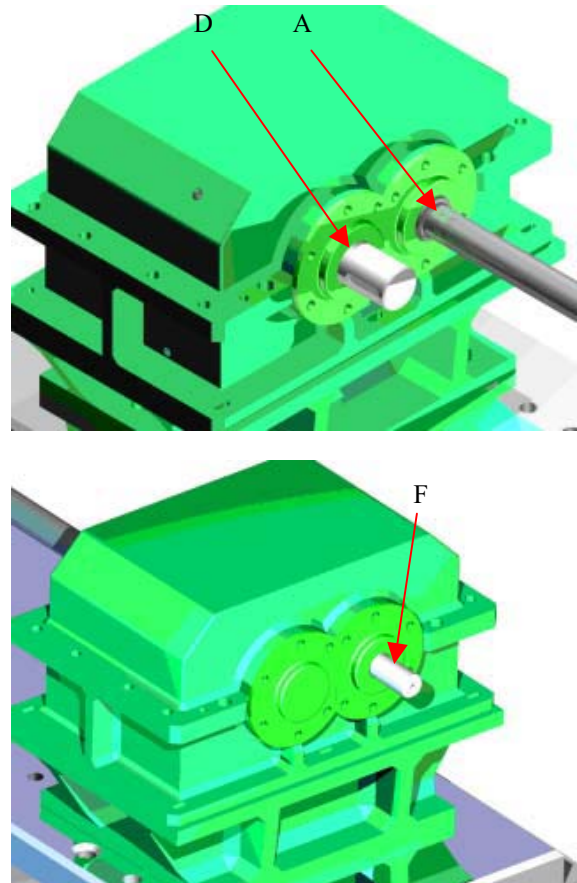


Fig. 6. Measuring points on the tested gear

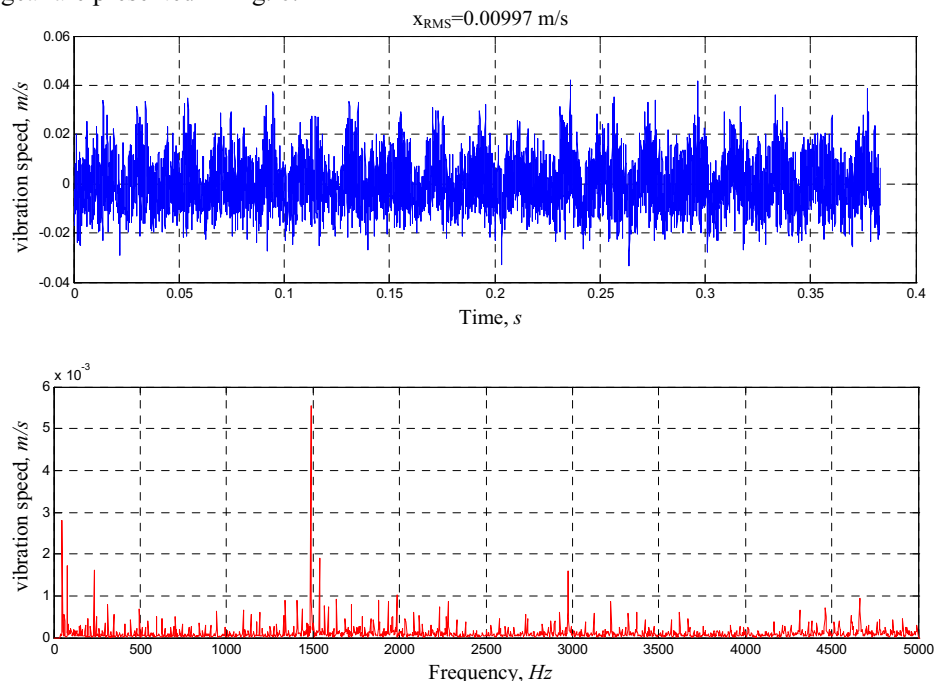


Fig. 7. Time and spectrum of transverse vibration speed of the wheel shaft in tested gear – measurement at a laboratory stand (measuring point F, wheel rotational speed $n_2 \approx 2975$ rpm, load intensity $Q \approx 1.5$ MPa)

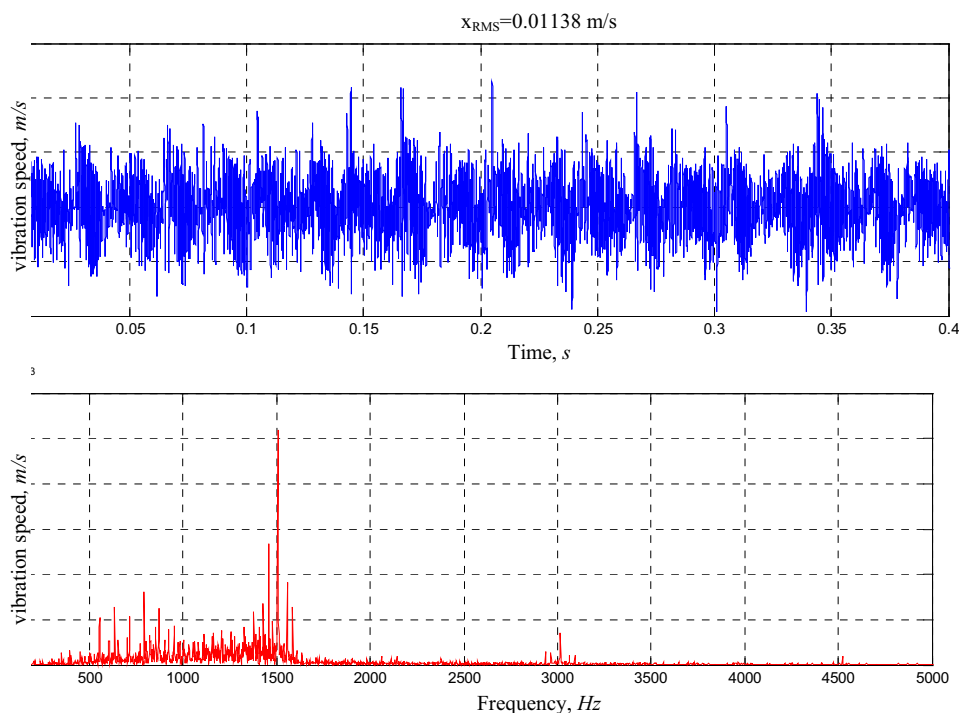


Fig. 8. Time and spectrum of transverse vibration speed of the wheel shaft in tested gear – simulation (measuring point F, wheel rotational speed $n_2 \approx 3013$ rpm, load intensity $Q \approx 1.5$ MPa)

Some examples of the speed and spectra of transverse vibration of the wheel shaft in the tested gear, obtained from laboratory measurements and from the simulation, are presented in Figs 7 and 8, respectively.

7. CONCLUSIONS

The stages of model identification presented using an example of the test stand's testing part more important from the point of view of further research, do not show all difficulties of the process. Obtaining of calculation results qualitatively and quantitatively concurrent with the results of laboratory measurements in a wide range of rotational speeds and loads requires carrying out a number of measurement series.

Since in the model tuning process there was no possibility of making measurement of values most useful for this purpose, e.g. forces acting between the teeth in both gears or forces in the stand bearings, it was necessary to make a large number of simulations, during which a change of selected parameters was applied, until obtaining satisfactory compliance of the results with the measurements made for the same conditions.

Obtaining compliance of the results in time and frequency domains enables taking advantage of the model in further tests and justifies this method of conducting research.

REFERENCES

- [1] Dalpiaz G., Rivola A., Rubini R.: *Dynamic modelling of gear systems for condition monitoring and diagnostics*. Kongres Diagnostyki Technicznej, Gdańsk, 1996.
- [2] Dąbrowski Z., Radkowski S., Wilk A.: *Dynamika przekładni zębatych. Badania i symulacja w projektowaniu eksploatacyjnie zorientowanym*. Warszawa-Katowice-Radom 2000.
- [3] Łazarz B.: *Badania wpływu zużycia zębów kół na obciążenia dynamiczne w diagnostyce przekładni*. Rozprawa doktorska. Politechnika Śląska, Katowice 1996.
- [4] Łazarz B.: *Zidentyfikowany model dynamiczny przekładni zębatej jako podstawa projektowania*. Instytut Technologii Eksploatacji, Katowice-Radom 2001
- [5] Müller L.: *Nowy model dynamiczny przekładni walcowej o zębach prostych*. Przegląd Mechaniczny nr 21/1974.
- [6] Müller L.: *Przekładnie zębate. Badania*. WNT Warszawa 1984
- [7] Müller L.: *Przekładnie zębate. Dynamika*. WNT Warszawa 1986.
- [8] Osiński J.: *Zjawiska dynamiczne w układach z przekładniami zębatymi*. II Ogólnopolski Sympozjum Naukowo – Techniczne „Przekładnie Mechaniczne Specjalne”, Warszawa 1997.
- [9] Wilk A.: *Wpływ parametrów technologicznych i konstrukcyjnych na dynamikę przekładni o zębach prostych*. Zeszyty Naukowe

Politechniki Śląskiej, Mechanika z. 72, Gliwice 1981.



Bogusław ŁAZARZ Ph.D., D.Sc. Eng. professor of The Silesian University of Technology. Scientific interest: modelling of dynamic processes, diagnostics of tooth gear, machine design and vibroacoustic signal processing. Member of

Machines Construction Committee and Polish Society of Technical Diagnostics.



Grzegorz PERUŃ is Ph.D. student in the Department of Automotive Vehicle Construction Silesian University of Technology in Katowice. Scientific interest: modelling of power transmission systems, machine design and vibroacoustic signal

processing.

The results presented in the paper were obtained with the support of the Polish Scientific Committee.

SOME INVESTIGATIONS INTO ULTRASONIC DIAGNOSTICS APPLICABILITY FOR COMPOSITE STRUCTURE

Mirosław RODZEWICZ*, Grzegorz CZERWIŃSKI**

*Institute of Aeronautics and Applied Mechanics, Warsaw University of Technology

00-665 Warsaw, Nowowiejska 24, fax (+22) 628 57 48,

00-665 Warszawa, ul. Nowowiejska 24, fax (+22) 628 57 48, miro@meil.pw.edu.pl

**Telecommunication Research Institute S.A., 04-051 Warsaw, Poligonowa 30, czerwinski@pit.edu.pl

Summary

Authors present results of their investigations into diagnostic applicability of the ultrasonic NDT systems developed by them for composites inspection. The attention was focused on the methods of visualization of the defectoscopy results. There were tested composite specimens, subjected earlier to fatigue or impact loads. Presented results proves effectiveness of ultrasonic NDT methods in detection of such defects as delamination or disglueing, and partly effectiveness in the investigations of fatigue processes of the composite structure reinforced by fibers. A low effectiveness was observed in case of investigating degradation of glue connection type *metal-composite*, which occurs in the whole volume of the glue layer in cohesive way.

Keywords: composites, delaminations, ultrasonic diagnostics.

BADANIA NAD ZASTOSOWANIEM DIAGNOSTYKI ULTRADŹWIĘKOWEJ W BADANIU STRUKTUR KOMPOZYTOWYCH

Streszczenie

Autorzy przedstawiają wyniki prac badawczych z użyciem opracowanych przez nich systemów defektoskopii ultradźwiękowej. Nacisk został położony na metody wizualizacji wyników diagnostyki. Badaniom poddawano próbki kompozytowe stanowiące obiekty badań zmęczeniowych lub udarowych. Zamieszczone przykłady wskazują skuteczność metod ultradźwiękowych w wykrywaniu takich wad jak delaminacje lub rozklejenia, a także częściową przydatność w badaniach procesów zmęczenia struktury kompozytów włóknistych. Małą skuteczność zaobserwowano natomiast w przypadku badań degradacji zmęczeniowej sklejin typu *metal-kompozyt*, zachodzącej całej masie polimeru skleiny w sposób kohezyjny.

Słowa kluczowe: kompozyty, delaminacje, rozwarstwienia, diagnostyka ultradźwiękowa.

1. INTRODUCTION

Trends to maximise the profits of airtransportation companies generate needs for implementation a maintenance model according to the real technical conditions. This model is going to replace still existing, non-economical maintenance model according to a service life, guaranteed by the producer. The maintenance model according to technical conditions is implement able only in case of parallel implementation of the system of regular (or even better, continuous) defectoscopy monitoring of crucial aircraft structural parts. Taking into consideration increasing application of polymer composites in the aircraft, the necessity of fundamental investigations in the field of composite defectoscopy methods is of great importance. Defectoscopy of the composites is generally more difficult then defectoscopy of metal parts, therefore it is necessary to search for effective NDT methods.

2. SYSTEMS OF ULTRASONIC NDT INSPECTIONS AND VISUALISATION OF NDT RESULTS

Investigating the subject of applicability of NDT method for composite structures, the authors developed two systems for ultrasonic NDT inspections. They are based on the Panametrics 9100 ultrasonic flow detector. The first system is stationary with immersion tank (adapted for drowning the specimens in the water to obtain the acoustic coupling), and the second is mobile (US signal coupling by the stream of water). Both systems were described in the proceedings of the 3rd International Diagnostic Congress [1]. The crucial role in those systems has special software, designated for communication with the flow detector and for control of scanning operation.

A special function of this software is visualization of the defects detected in the composite structures.

Generally, the visualization process depends on analysis of analog signal from US probes, and

observation the amplitude of this signal in the optionally chosen gate of the A-scan (case 1), or depends on analysis of the changes in the whole A-scan (case 2) and on generation 2 or 3-dimensional color bitmap (i.e. C-scan) resulting from probe position and signal value (or value of function based on the whole A-scan value).

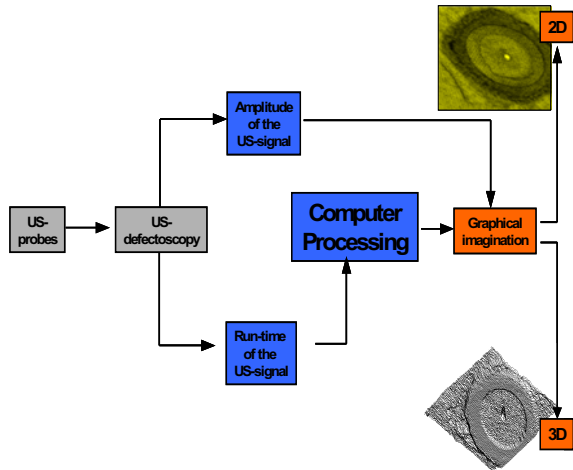


Fig. 1. Ways of flow visualization in ultrasonic defectoscopy systems

Taking into account variability of position and amplitude of the peaks on A-scans, the observation of signal in the gate established on A-scan is connected with the necessity of detection of the active part of A-scan. This gate in the majority of ultrasonic flow detectors is fixed on the A-scan windows and does not follow the movement of signal peaks. The detection of active part of A-scan has been made using differential method or gradiental method. It is possible to establish virtual gate, which follows chosen peaks (or a group of peaks) on the A-scan, and then to link the amplitude value with the color of the pixel on a C-scan.

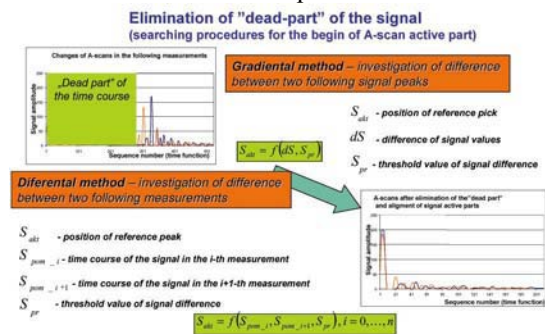


Fig. 2. Detection of active part of an A-scan

An alternative method for it is use of correlation function of the A-scans. The 1st one is so called, “template scan” taken in optionally chosen point of scanned specimen, while the 2nd signal comes from current position of the probe. The maximum value of correlation function is used then for generation of pixel color on a C-scan.

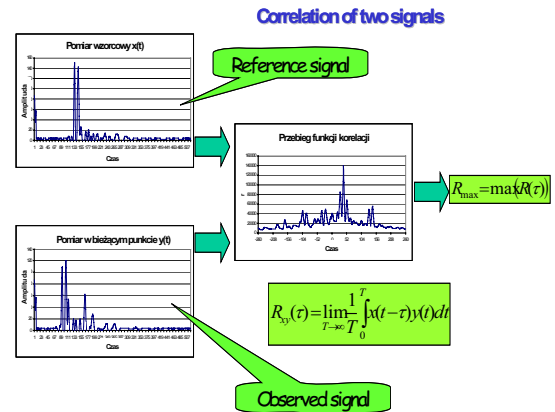


Fig. 3. Explanation of the A-scans correlation function method

In the process of elaboration of the time courses of US signals are used different methods for noise elimination and for data compression. The one of most effective method is application of the wavelet transform. The result of such transform is a set of wavelet coefficients. By eliminating from this set the lowest value coefficients and making reverse transform, it is possible to obtain smooth (unnoised) signal (similarly to the Fourier transform application). This operation facilitates detection of signal changes in consecutive measurement points.

3. APPLICATION EXAMPLES OF DEVELOPED NDT SCANNING SYSTEMS

There are described below a couple examples of application of ultrasonic NDT systems, developed by the authors.

The first example concerns the specimen of composite web spar for a glider (fig. 4). Shear forces load such an element, and the critical zone in which delaminations can occur is a glue connection between the web and spar flanges. The specimen was made from the CFRP composite, and then was fixed in the special 4-joint steel frame, which enables realization of shear loads in composite shell modeling the wing spar web. This shell was subjected to low-cycle fatigue and then to a residual strength test.

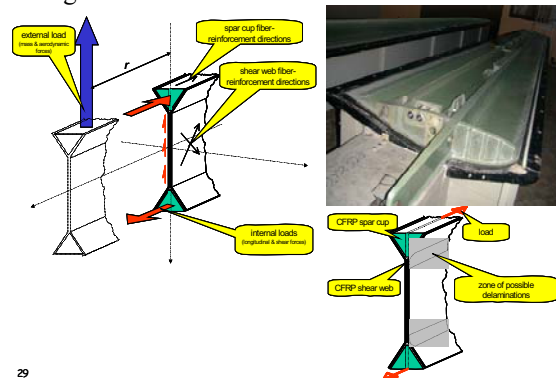


Fig. 4. The loads acting into wing spar and a critical zone in the wing spar web and flanges glue connection

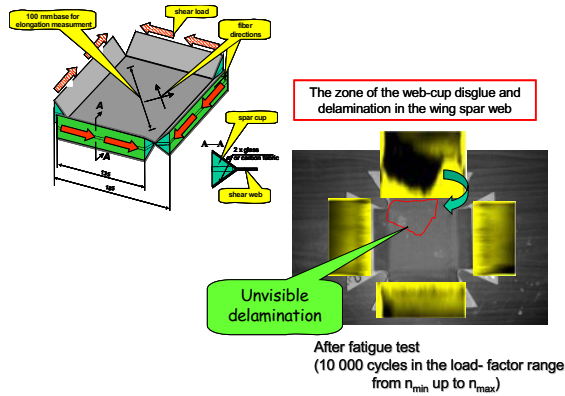


Fig. 5. Specimen modeling interaction between spar web and flanges

Ultrasonic C-scans of the web-flange interfaces after the low-cycle fatigue were shown in figure 5. It is visible, that in one interface occurs a dark area, which indicates serious delamination. This delamination was not detectable by visual inspection.

The next example concerns the specimen modeling a part of main fuselage frame, containing a special joint for wing-fuselage connection, called as a “labyrinth lock”. This was a kind of joint for concentrated force implementation into thin composite shell, which was applied in the gliders build in Warsaw University of Technology. The subject of investigation was a load-bearing capacity. In figure 6 was shown a schema of specimen support and loading. The specimen was subjected into unilaterally fatigue loads (10 000 cycles of a maximum value equal 76% of a static strength). Before the fatigue test and also after each thousand of load cycles the specimen was scanned on the ultrasonic stand. In such a way a structural defect (delamination) occurring in the neighborhood of the “labyrinth lock” was monitored (see fig. 6). The residual strength test result proved that despite this delamination, the residual strength dropped slightly (although one can conjecture that the residual operational life was reduced more significantly).

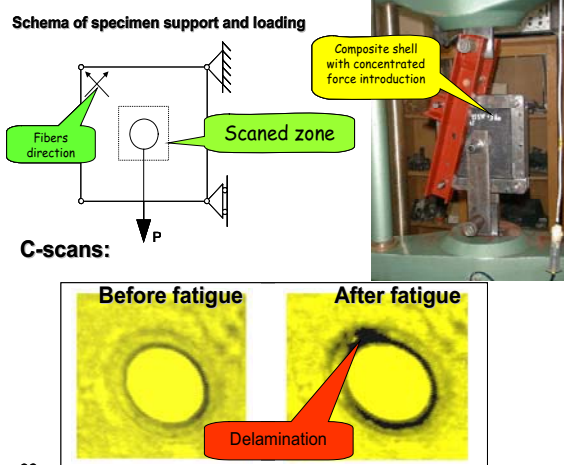


Fig. 6. Specimen with concentrated force implementation into composite shell

The next example concerns monitoring of the defects in the CFRP composite made from fibers of unidirectional orientation (as in the wing spar flanges). The specimens were subjected to impact loads with controlled energy. Some specimens were used for the so called interlayer shear load capacity test, while the rest of specimens were subjected into 1 million of fatigue loads reaching 70% of nonfatigued specimens strength. During the fatigue test the specimens were regularly scanned on the ultrasonic stand, and at the end of experiments the residual strength was examined

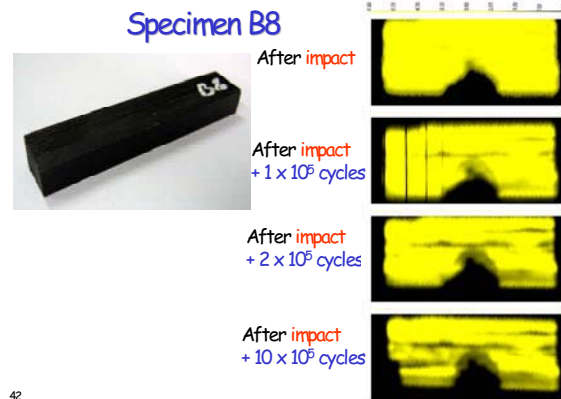


Fig. 7. C-scans of CFRP beams after impact and fatigue loads (black zone shows the defect area)

Examples presented until now show that such structural defects as delaminations or disglueing or fibers crush are easily detectable. The opposite situation occurs in case of diagnostics of a glue connection, in which the fatigue destruction runs inside the glue-layer (in a cohesive way). The example of such a situation in the glue connection between metal and CFRP composite is presented in figure 8.

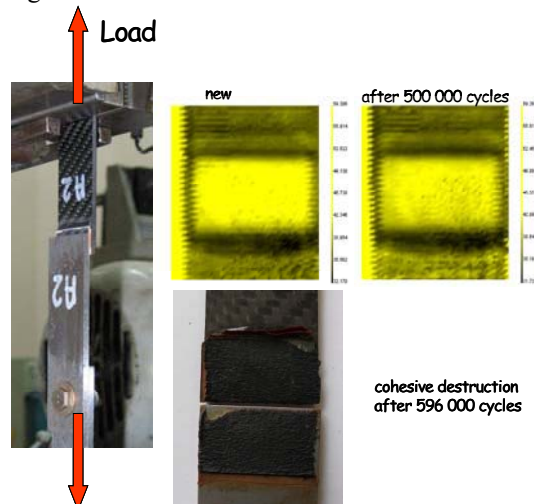


Fig. 8. Testing the glue connection *metal-composite*

On the C-scans which were made at the beginning of fatigue and just before total destruction of the glue joint any changes are not detectable. It is for the reason that in investigated case, the destruction of the glue connection occurred not by

developing of disglue zone, but by micro-cracks in the whole volume of the glue layer (which was proved by later microscope inspection).

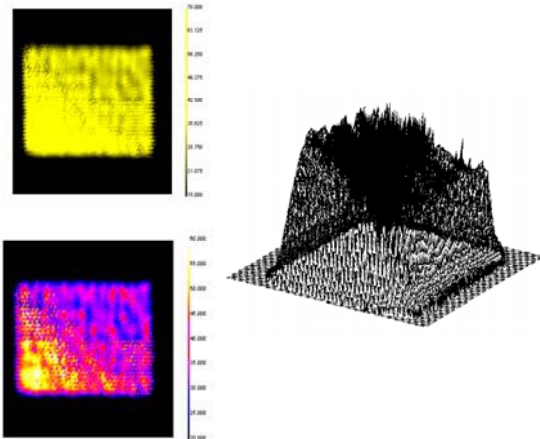


Fig. 9. Examples of different visualization methods of ultrasonic inspections of *metal-composite* glue connection

4. CONCLUSIONS

Examples presented in the paper prove high effectiveness of ultrasonic NDT methods in detection of such defects as delamination or disglueing, and partly effectiveness in the investigations of fatigue processes of the composite structure reinforced by fibers.

A low effectiveness was observed in case of investigating degradation of glue connection type *metal-composite*, which occurs in the whole volume of the glue layer in cohesive way.

LITERATURE

- [1] M. Rodzewicz, G. Czerwiński: *Diagnostyka ultradźwiękowa rozwarstwień w powłokach kompozytowych*. Diagnostyka vol. 30, tom 2, 2004, str.89 – 92.
- [2] G. Czerwiński, M. Rodzewicz: *Zastosowanie ultradźwięków w diagnostyce struktur kompozytowych*. 8-th International Conference „AIRCRAFT AND HELICOPTER DIAGNOSTICS” AIRDIAG’2005, Oct. 27 – 28 2005, proceedings No 5/2005.



Mirosław RODZEWICZ

Ph.D. is currently an assistant professor at the Institute of Aeronautics and Applied Mechanics of Warsaw University of Technology. His primary area of interest is polymercomposite structures applied in aeronautics, experimental mechanics: load

spectra investigation static and fatigue testing of composite aeronautical structures, diagnostic of composite structures.



Grzegorz CZERWIŃSKI.

Ph.D. is currently an assistant profesor at the Telecommunication Research Institute S.A. Research area – development and software implementation in the field of ultrasonic defectoscopy systems, and graphic

visualization of the NDT results.

FAILURE DIAGNOSIS OF THE GAS COMPRESSOR DIAPHRAGM VANE

Zbigniew KOZANECKI, Jakub ŁAGODZIŃSKI, Dorota KOZANECKA

Technical University of Łódź, Institute of Turbomachinery
Wólczańska 219/223, 93-005 Łódź, Poland, e-mail: zkozan@p.lodz.pl

Summary

The goal of this paper was to develop a methodology of explanation of diaphragm vane defects in a two-stage centrifugal compressor which had occurred in during operation of the machine. The methodology consisted of experimental investigations of the disassembled diaphragm, then a dynamical analysis using the finite element method on the 3D diaphragm model, obtained by reversing engineering with an optical photogrammetric camera of the TRITOP CMM measuring system. The final purpose of this research work was to formulate the recommendations to avoid future problems.

Keywords: centrifugal compressor, diaphragm vane, damage, 3D model.

DIAGNOSTYKA USZKODZEŃ ŁOPATEK KIEROWNICY SPREŻARKI PRZEPLYWOWEJ

Streszczenie

Celem pracy było opracowanie metodyki pozwalającej na wyjaśnienie przyczyn uszkodzeń łopatek kierownicy dwustopniowej sprężarki promieniowej, które powstały w okresie eksploatacji maszyny. Zaproponowana metodyka obejmuje badania eksperymentalne oraz weryfikację modelu teoretycznego 3D kierownicy, opracowanego przy wykorzystaniu nowoczesnego systemu optycznej metody skanowania w widmie światła białego TRITOP CMM. Kończącym efektem pracy było sformułowanie zaleceń modyfikacji konstrukcji maszyny dla eliminacji tego problemu.

Słowa kluczowe: sprężarka przepływowa, kierownica, łopatki, uszkodzenia, model 3D.

1. INTRODUCTION

The origins of this paper were diaphragm vane defects, which had occurred after about one-year operation of a large-scale centrifugal compressor. The considered machine was a two-stage compressor working in the natural gas transport line. The subcomponent under analysis was a vaned diaphragm between the first and second stage. The diaphragm guides the gas to the second stage impeller inlet.

The main purpose of this research work was to develop a methodology of explanation of the damage (fig. 1) causes and to formulate the recommendations to avoid future problems.

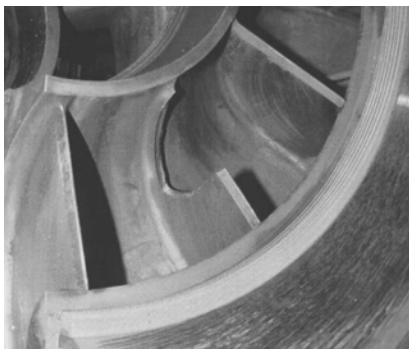


Fig. 1. View of the damaged diaphragm vane

The methodology consisted of experimental investigations of the disassembled diaphragm at the Institute laboratory, then a dynamical analysis using the finite element method on the 3D diaphragm model.

2. THREE-DIMENSIONAL DIAPHRAGM MODEL

A 3D model of the diaphragm was reconstructed using the reversed engineering method. The method is based on the continuous optical scanning of the marked points (fig. 2) with the TRITOP system. Afterwards, the measured point coordinates are transferred to the selected CAD system (fig. 3). The achievable retracing accuracy is about 0.02mm.



Fig. 2. Diaphragm during the optical measurement

2. EXPERIMENTAL VERIFICATION OF THE CREATED MODEL

The investigations were conducted on the lower half of the diaphragm due to its less numerous operational damages than in the upper half. The vibrations were measured by a *Brüel – Kjaer 4375* type accelerometer with a *2635* type preamplifier. The acquisition and vibration data analysis was performed with a *LMS Pimento 5.1* analyzer. During the harmonic response analysis, diaphragm vanes were excited by a *LDS V201* type electrodynamic shaker powered by a *LDS PA25E* type power amplifier and by an impact hammer.

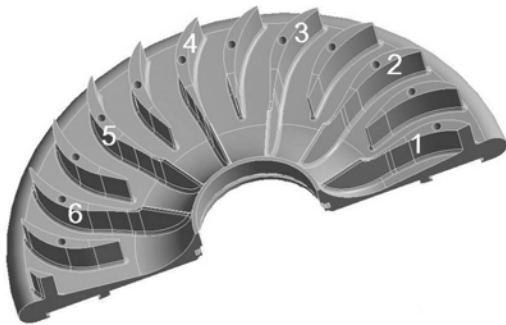


Fig. 3. Numbered vanes of the 3D diaphragm model

Figure 4 shows a *FFT* response spectrum of each vane to the impact hammer. Table 1 contains an interpretation of all response spectra.

For each vane, three natural frequencies, corresponding to three first mode shapes of each vane, were taken down.

Table 1. *FFT* response spectrum interpretation

Vane number	1	3	4	5
1st natural frequency [Hz]	1761	1750	1749	1778
2nd natural frequency [Hz]	3632	3453	3497	3528
3rd natural frequency [Hz]	4762	4449	4555	4509

During the next step, a *FFT* response spectrum for white noise excitation was measured. The purpose was to simulate vane excitation by a fluid flow during the operating conditions. The results of the spectrum response (fig. 5) show a fuzzy nature of the spectrum near the *6kHz* frequency band. Taking this into account, the diaphragm model was verified upon three first natural frequencies, in the bandwidth below *5kHz*.

The natural frequencies acquired from response spectra became a reference for the tuning process of the diaphragm model. By adjusting an algorithm and a structure of the model mesh and other parameters, the model was tuned up to the real object.

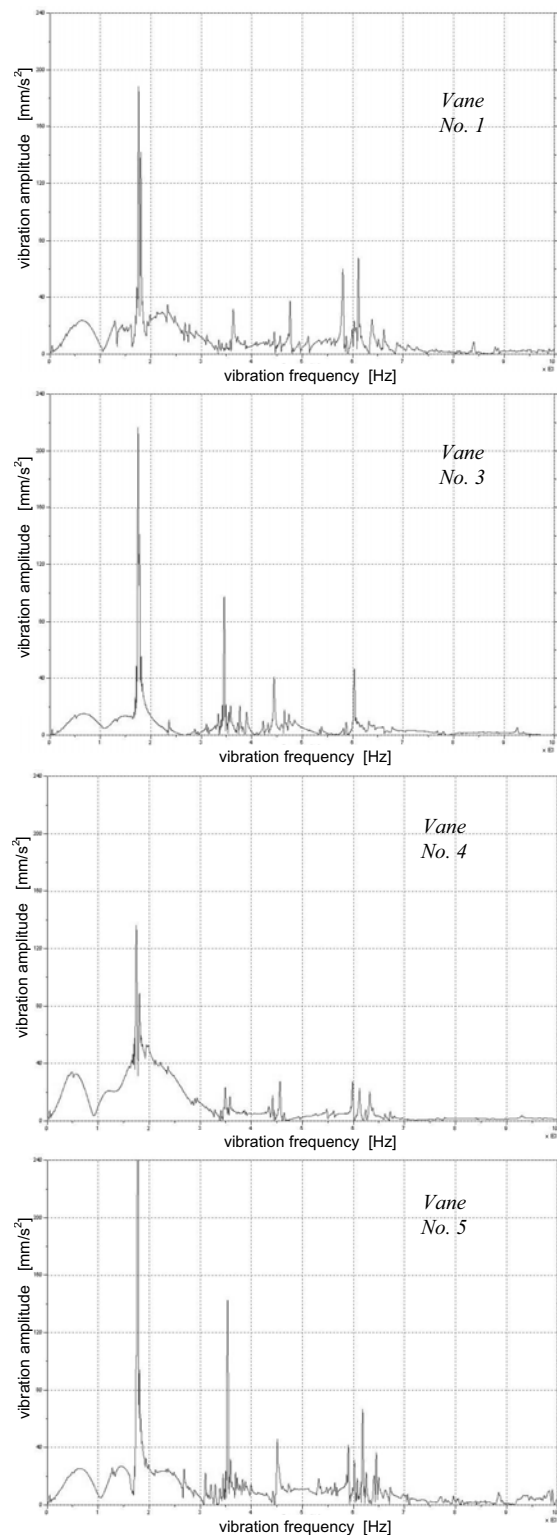


Fig. 4. *FFT* response spectrum in the 0–10 kHz bandwidth of undamaged vanes. The diaphragm cover is dismantled

Table 2 shows frequency differences between the tuned model and the real object. The disagreement did not exceed 3%, which was considered as a good result.

Table 2. Experimental and model natural frequencies of diaphragm vane No.1

Mode shape	f_r (real) [Hz]	f_m (model) [Hz]	$\Delta f = \frac{\Delta f}{f_r} \cdot 100\%$
1st	1761	1782	1,2
2nd	3632	3615	0,5
3rd	4762	4875	2,4

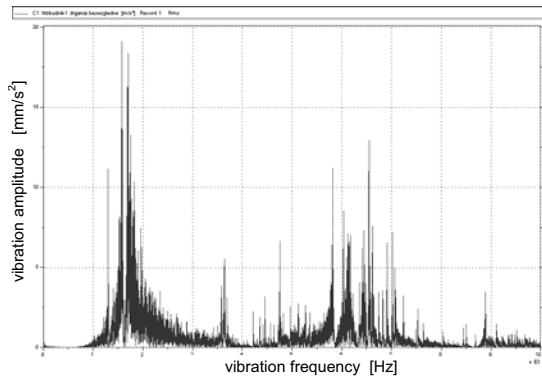


Fig. 5. Diaphragm vane No. 1 response spectrum to the white noise excitation in the 1 – 10 kHz frequency bandwidth

Figure 6 shows theoretical and experimental natural mode shapes of single vane vibrations obtained respectively during calculations and experiments.

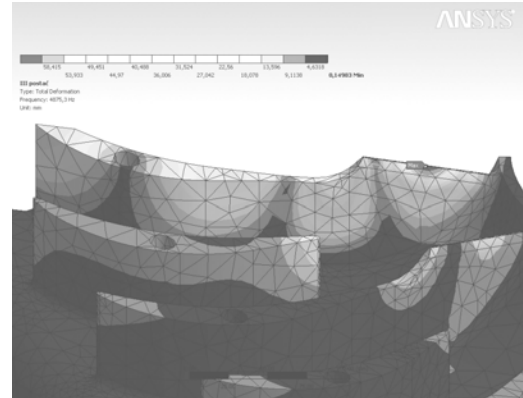
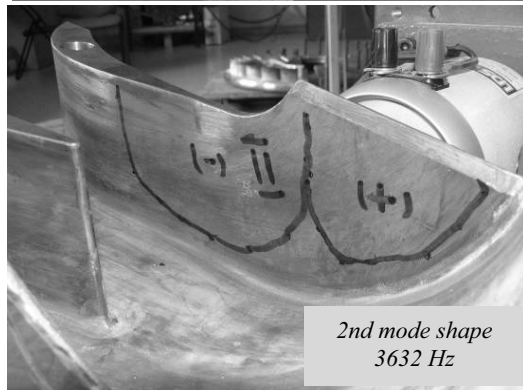
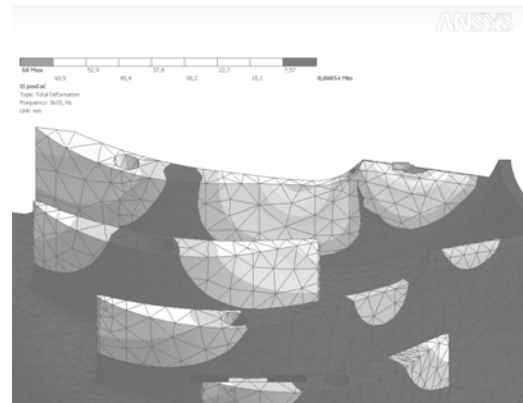
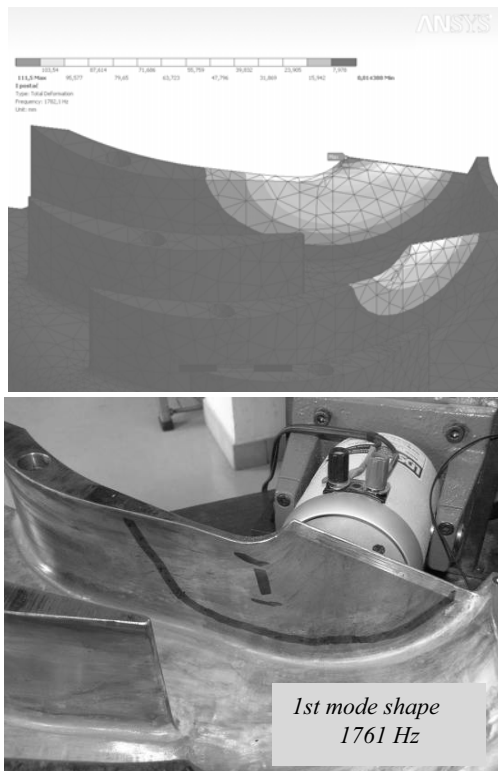


Fig. 6. Experimental and model natural frequencies of diaphragm vane No.1. in response to the white noise excitation

In the next stage, the diaphragm was fastened to the cover (fig. 7) and the impact response spectrum analysis was performed in this state.



Fig. 7. Diaphragm fixed to the cover. A LDS V201 type electrodynamic shaker is visible

Higher foundation stiffness caused an increase of natural frequencies with the fastened cover (fig.8).

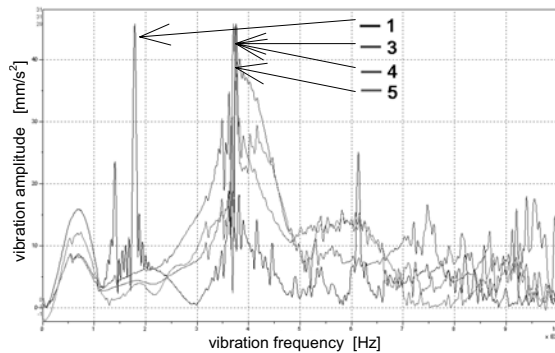


Fig. 8. FFT spectrum responses of vanes No. 1,3,4 and 5 with the fastened cover

From the viewpoint of the stiffness increase of the fixed structure, an interaction between vibrations of the vanes and the diaphragm back plate was considered. Some results are shown in fig. 9.

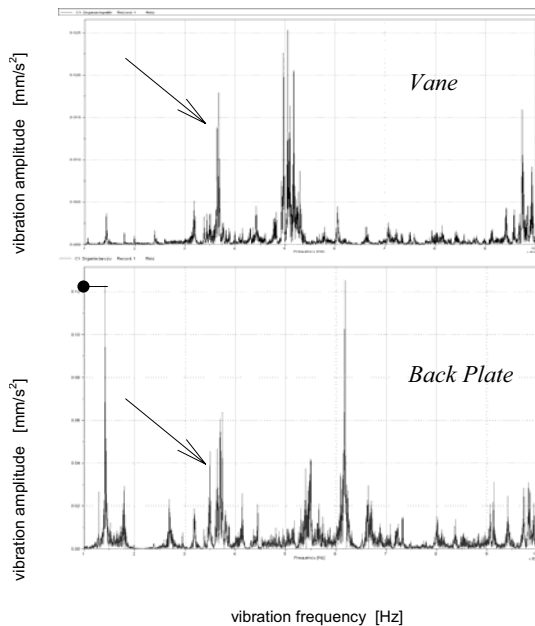


Fig. 9. Vane FFT spectrum response with a shaker whipping up the back plate and vice versa. The frequency interference is marked by arrows

The obtained results are shown in table 3.

Table 3. Interpretation of the diaphragm vanes response spectrum with the cover fastened

Vane number	1	3	4	5
Measured frequency	1801Hz	3705Hz	3748Hz	3766Hz

The band near frequency of 3700Hz (marked by arrows in fig. 9) reveals an interference of the back plate and vane vibrations. It is likely that these natural frequencies amplify one another.

The tuning datum point of the diaphragm model with the fixed cover was to establish the contact surface between the mentioned elements.

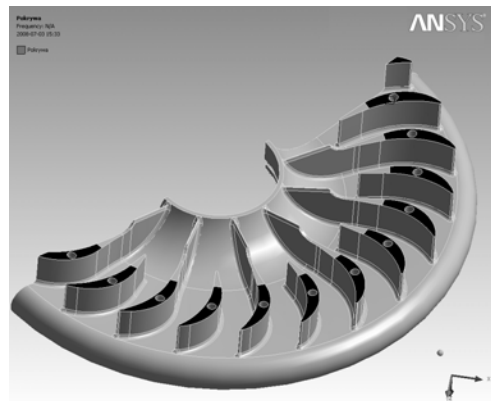


Fig. 10. 3D model of the diaphragm with the fixed cover. The hypothetical contact surfaces are marked in black

Figure 10 shows a theoretical model of the diaphragm with the fixed cover, where the assumed contact surface is marked in black. The contact surface in the real object depends on the assembly technique, surface roughness and was a variable parameter for the tuning process.

4. NUMERICAL APPROACH

In the next stage a numerical modal analysis of the tuned model was performed and a solution was obtained. In fig. 11 mode shapes of the calculated model are shown. They are related to the measured real object natural frequencies, respectively 1410Hz and 1801Hz. A comparison of natural frequencies calculated from the model and measured on the real object is contained in table 4.

Table 4. Natural frequencies of the diaphragm vane with the fixed cover

Mode shape	f_r (measured) [Hz]	f_m (calculated) [Hz]	$\Delta f = \frac{\Delta f}{f_r} \cdot 100\%$
1st	1410	1328	5
2nd	1801	1819	1

Figure 11 shows theoretical mode shapes of the covered diaphragm vibration obtained during calculation in the frequency band below 2kHz .

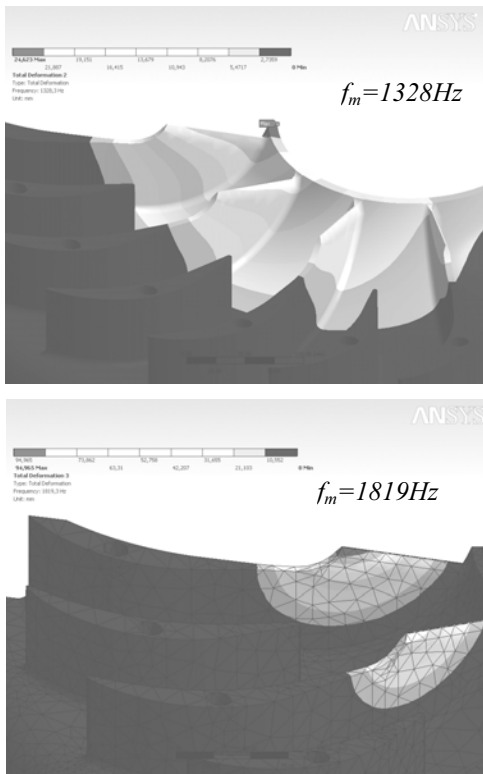


Fig. 11. Mode shapes of the diaphragm with the fixed cover in the frequency band below 2kHz

The mode shape related to the frequency of 1328Hz (fig. 11) is a complex mode of the back plate (marked by point in fig. 9), which definitely has an influence on vibrations of vane No. 1.

Natural frequencies occurring between $2\div 5\text{kHz}$ are related to complex phenomena of the mutual vibration interference among the back plate and the vanes. A few natural frequencies overlap in this range. The white noise excitation response spectrum has a higher resolution, so it allowed for reducing the overlapping bandwidth to $3.5\div 4\text{kHz}$. Calculated mode shapes from this range are shown in fig. 12.

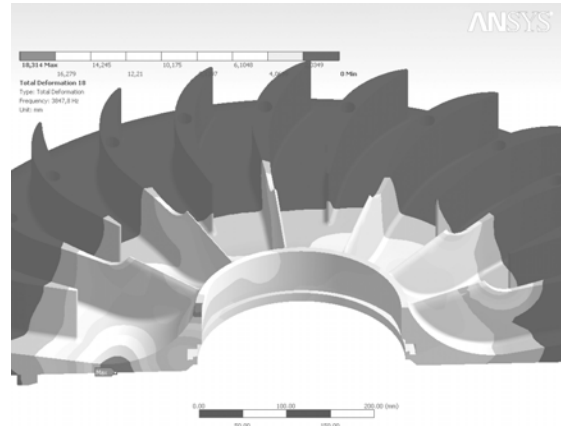
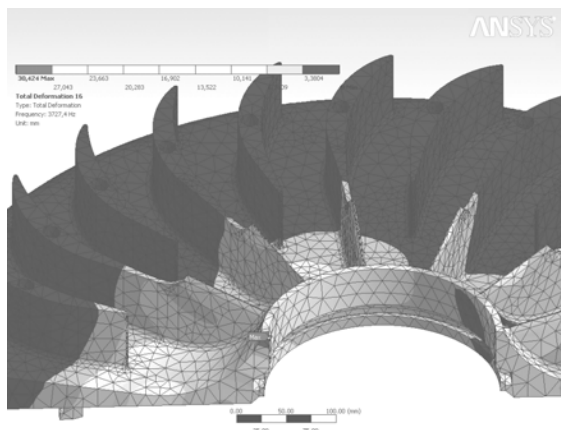


Fig. 12. Mode shapes of the diaphragm with the fixed cover from the bandwidth between $3.5\div 4\text{kHz}$

The obtained model identification results were considered satisfactory, so the model could be used in a further stress analysis. The purpose of the stress analysis was to explain the origin of vane cracking during operation.

5. STRESS ANALYSIS OF VIBRATING COVERED DIAPHRAGM

To approximate real load conditions in the model, the following assumptions were taken:

- Pressure pulsation caused by the transient fluid flow did not exceed 100kPa .
- Pressure pulsation influence area was limited to the elongated part of the trailing edge of the diaphragm vane.

Figure 13 presents load conditions applied to the diaphragm partial model.

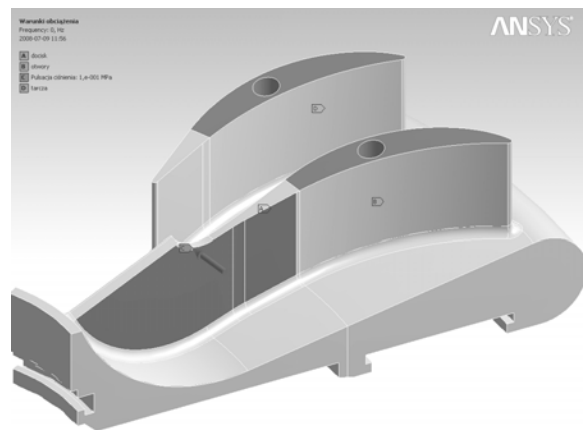


Fig. 13. Load conditions applied to the partial diaphragm model

Assuming that load conditions were only a qualitative approximation of the real fluid pressure pulsation, the obtained results could be also qualitative only.

The analysis performed during this research stage was also qualitative and consisted of the following steps:

1. Calculation of mode shapes and a stress distribution in the present diaphragm partial model.
2. Calculation of mode shapes and a stress distribution in the modified diaphragm partial model.
3. Comparison of the numerical results obtained in steps 1 and 2.

Figure 14 shows a von Mises stress distribution in the vane and a nodal line of the mode shape associated to the load conditions applied to the present structure.

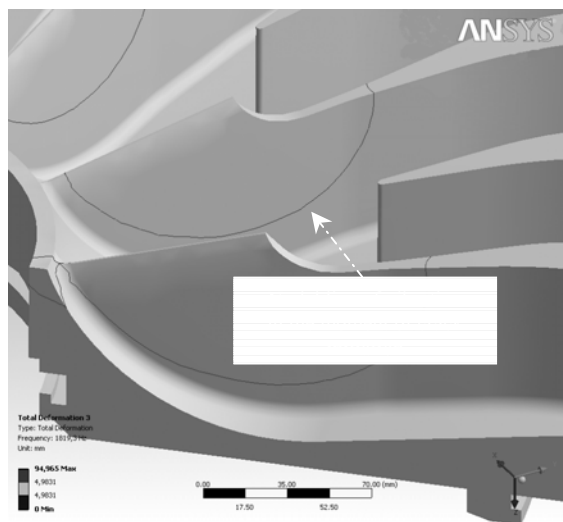
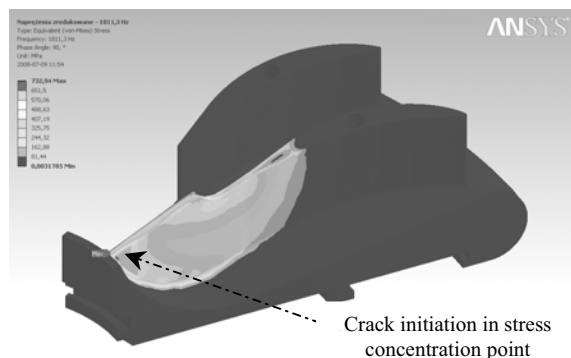


Fig. 14. Von Mises stress distribution in the diaphragm partial model and a nodal line of vane vibration at the moment of the crack initiation

The obtained results show clearly that a stress concentration occurs on the trailing edge of the drawn-out diaphragm vane and the nodal line overlaps the crack propagation lines on the damaged vanes.

Figure 15 shows a theoretical crack propagation caused by the presented phenomena. A crack initiation appears in the same place as in the real object – on the trailing edge of the elongated vane.

During the crack propagation, releasing of the trailing edge causes a change of the initial nodal line to the nodal line of the vibration mode called flutter (black dot line in fig. 15).

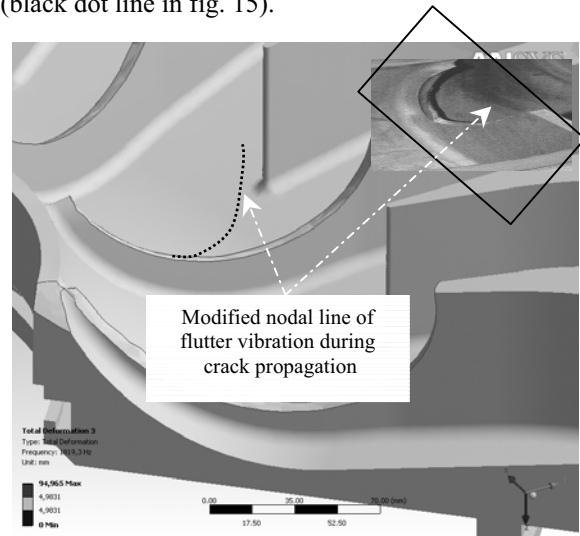


Fig. 15. Nodal line modification during vane crack propagation in comparison with real shape of the crumbled part of the damaged diaphragm

This explains why crumbled fragments are smaller than the parts confined with the initial nodal line of the undamaged vane.

6. RESPONSE ANALYSIS OF THE MODIFIED STRUCTURE

A temporary repair was proposed. In the repair, a part of the vane trailing edge was welded to the diaphragm cover.

In consequence, the diaphragm and the cover became unable to disjoin. Fortunately, the machine assembly procedure allows for this kind of modification.

Figure 16 presents a von Mises stress distribution in the modified diaphragm partial model. This stress distribution is more favorable for the analyzed structure. For the same model load conditions, von Mises stresses in the critical point of the trailing edge are reduced 2.5 times.

It should be pointed out that in the welding point (about 20mm long – assumed in the numerical analysis), a half as high von Mises stress as in the crack initiation point of previous design has appeared. It would be favorable to join the vanes with the cover using a fillet weld with weld penetration to reduce the stresses occurring in the weld.

From a vibration point of view, stiffening the elongated vanes by welding them to the cover improves the dynamic properties of the diaphragm.

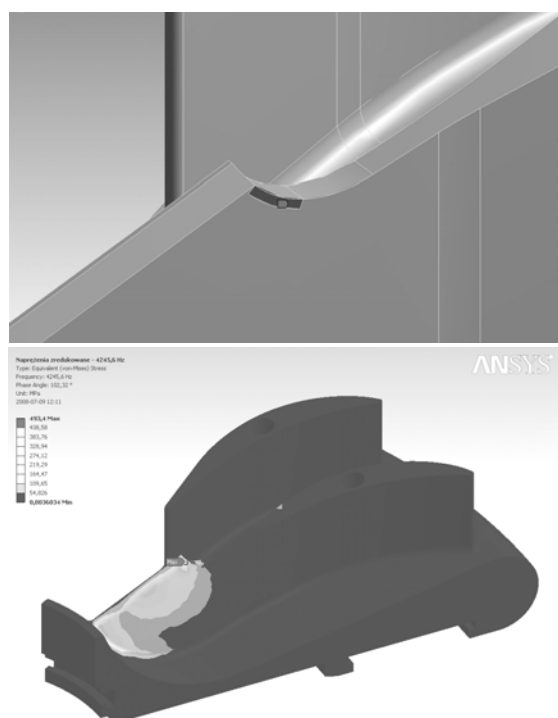


Fig. 16. Altering weld and a von Mises stress distribution in the modified diaphragm partial model

Figure 17 presents a comparison of frequency responses of the free and welded vane under the same load conditions.

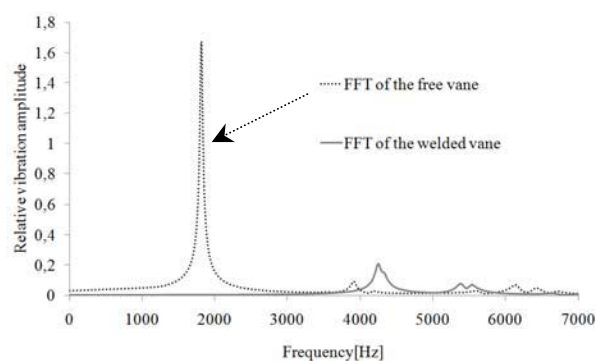


Fig. 17. FFT harmonic spectrum response of the free and welded vane for the applied load conditions

Stiffening the vanes by welding them to the cover eliminates dangerous low-frequency modes being the origin of all operational problems related to the compressor diaphragm.

7. CONCLUSIONS

The elaborated method allowed for explaining the causes of fracture and damage of two-stage gas compressor diaphragm vanes that appeared during the machine operation.

The theoretical model was built and verified by comparing it to the real diaphragm vibration measurement results.

The compatibility between the model and the real object behavior allowed for performing a number of numerical analyses.

Positive results allowed for introducing a modification and expressing the following conclusions:

1. Fracture and damage had a fatigue nature and were caused by a transient flow through diaphragm vane ducts.
2. Tests and numerical approach evaluated positively the proposed modification (repair technology) of welding vane trailing edges to the cover.
3. The results of the presented work applied in industrial practice caused elimination of the mentioned problem of diaphragm vane defects in large centrifugal compressors working in the natural gas transport line.

REFERENCES

- [1] Morel J.: *Drgania maszyn i diagnostyka ich stanu technicznego*, Polskie Towarzystwo Diagnostyki Technicznej, Warszawa 1992.
- [2] *Theory Reference for ANSYS and ANSYS Workbench 11.0*, ANSYS Inc. 2007.
- [3] *The LMS Theory and Background Book: Signal Processing*, LMS International 2004.
- [4] Harris C. M., Piersol A. G.: *Harris' Shock and Vibration Handbook*, 5th edition, MacGraw-Hill, 2002.
- [5] Kozanecki Z.: *Systemy wirujące maszyn przepływowych małej i średniej mocy*, Biblioteka Problemów Eksploatacji, Wydawnictwo Naukowe Instytutu Technologii Eksploatacji, Radom, 2008.
- [6] Osiński Z. i in.: *Thumienie Drgań*, praca zbiorowa pod redakcją Z. Osińskiego, PWN, Warszawa, 1997.
- [7] Eisenmann R. C., Eisenmann R. et al.: *Machinery Malfunction Diagnostic and Correction*, Hewlett-Packard Company 1998.
- [8] Cempel C., *Podstawy wibroakustycznej diagnostyki maszyn*, WNT Warszawa, 1982.
- [9] Wachel J. C.: *Compressor Case Histories, Presented at Rotating Machinery and Controls (ROMAC) Short Course*, University of Virginia, June 8-10, 1983.
- [10] API 617 – *Centrifugal Compressors for Petroleum, Chemical and Gas Service Industries*, American Petroleum Institute – seventh edition, 2002.

IDENTIFICATION OF VIBROACOUSTIC FIELD OF COMPLEX MECHANICAL STRUCTURES ON THE EXAMPLE OF A TOOTHED GEAR

Zdzisław GOLEC, Maria GOLEC, Maciej TABASZEWSKI

Politechnika Poznańska Instytut Mechaniki Stosowanej
Zakład Wibroakustyki i Bio-Dynamiki Systemów
ul. Piotrowo 3, 60-965 POZNAŃ, fax: 061 6652307, email: zdzislaw.golec@put.poznan.pl
maria.golec@put.poznan.pl maciej.tabaszewski@put.poznan.pl

Summary

In the paper global and partial measures of acoustic efficiency including the total and partial values of acoustic power of the sound emitted from definite parts of the considered structure were defined. Usefulness of the above measures of the acoustic efficiency for purposes of investigating the identification of sound sources of complex mechanical structures has been analyzed basing on a study of a single-stage gear transmission model.

Keywords: vibroacoustic diagnostics, noise sources, vibroacoustic efficiency.

IDENTYFIKACJA POLA WIBROAKUSTYCZNEGO ZŁOŻONYCH STRUKTUR MECHANICZNYCH NA PRZYKŁADZIE PRZEKŁADNI ZĘBATEJ

Streszczenie

W pracy zdefiniowano miary globalnej i cząstkowej sprawności wibroakustycznej, które zawierają całkowitą i cząstkowe moce akustyczne dźwięku emitowanego z określonych obszarów analizowanej struktury. Przydatność zdefiniowanych miar sprawności akustycznej do badań identyfikacji źródeł dźwięku w złożonych układach mechanicznych analizowano na podstawie badań pola akustycznego modelu jednostopniowej przekładni zębatej.

Słowa kluczowe: diagnostyka wibroakustyczna, źródła hałasu, sprawność wibroakustyczna.

1. INTRODUCTION

A few measures of acoustic efficiency were proposed for the analysis of vibroacoustic energy distribution in a near external acoustic field of complex mechanical structures. The defined measures include global and partial acoustic powers of the sound emitted from definite areas of the analyzed structure.

The power N of an acoustic wave emitted by a source equals to an integral over a surface S surrounding the source from a dot product of a vector of sound intensity $\vec{I}(\mathbf{r})$ and a related elementary surface vector $d\vec{S}(\mathbf{r})$ [1, 2, 3]:

$$N = \int_S \vec{I}(\mathbf{r}) \cdot d\vec{S}(\mathbf{r}) \quad [\text{W}], \quad (1)$$

where: $dN = \vec{I}(\mathbf{r}) \cdot d\vec{S}$, $\vec{I} = E(p(\mathbf{r},t)\vec{v}(\mathbf{r},t))$, $E(\)$ - is a time-averaging operator, $p(\mathbf{r},t)$ - a value of acoustic pressure, $\vec{v}(\mathbf{r},t)$ - velocity of a particle at the point related to $p(\mathbf{r},t)$.

The acoustic power of the source may be determined basing on measurements of a normal component of sound intensity and acoustic pressure in the middle of every segment of the surface surrounding the source (point by point, one after another - in accordance with PN-EN ISO 9614-1 [1

or by scanning - in accordance with PN-EN ISO 9614-2 [4,5]). Hence, the partial acoustic power N_i is a time-averaged flux of acoustic energy I_m flowing through a segment of the measurement surface S_i :

$$N_i = I_m S_i \quad (2)$$

Thus, the measurement of the sound intensity on the surface surrounding the source of stationary noise enables determination of the acoustic power of the source or partial sources situated inside the space limited by the measurement surface.

The vibroacoustic efficiency η_{WA} is defined as a quotient of vibroacoustic power of a sound source N_{WA} (its mechanical structure) and power N_D delivered to the structure. In the model of power distribution in a mechanical structure it was assumed that the delivered power N_D used in a widely understood technological process consists of the effective power N_U , internally dissipated power N_S and externally dissipated power N_R according to equation (1):

$$N_D = N_U + N_S + N_R \quad , \quad (3)$$

where: $N_R = N_{WA} + N_I$, N_{WA} - the power of vibroacoustic processes, N_I - the power of other accompanying processes, e.g. thermal, diffusion and magnetic processes.

Taking the foregoing assumption into account, the vibroacoustic efficiency may be presented in the form (4):

$$\eta_{wA} = \frac{I}{N_v + N_s + N_l + I} \quad (4)$$

The relationship (4) enables assessment of contribution of the power of residual processes, i.e. the vibroacoustic ones, with respect to the delivered power N_D .

For identification of dominating sources of sound in a given structure and comparative analysis of partial vibroacoustic processes both with reference to characteristic frequencies of the analyzed object and for evaluation of acoustic energy distribution from a spatial perspective a global and partial acoustic efficiencies of mechanical structures were defined.

2. GLOBAL AND PARTIAL ACOUSTIC EFFICIENCIES OF MECHANICAL STRUCTURES

Partial acoustic efficiencies of a sound source – a mechanical structure are defined as follows:

1. The ratio of time-averaged acoustic energy flux in the i^{th} third-octave band flowing through the N_{ijk} measuring surface segment to the averaged acoustic energy flux flowing through the same surface segment N_{jk} :

$$\eta_i = \frac{N_{ijk}}{N_{jk}}, \quad N_{jk} = \sum_i N_{ijk}, \quad (5)$$

where i – is for the i^{th} third-octave band, j, k – coordinates of the middle point of the measurement surface segment,

2. The ratio of time-averaged acoustic energy flux in the i^{th} third-octave band flowing through the N_{ijk} measuring surface segment to the acoustic energy flux averaged in the same i^{th} third-octave band flowing through a certain area or the whole measurement surface N_i (e.g. if the measurement is carried out at a cuboid surface, N_i is the acoustic energy flux averaged in the i^{th} third-octave band flowing through this surface or through one of the walls of this cuboid):

$$\eta_{jk} = \frac{N_{ijk}}{N_i}, \quad N_i = \sum_j \sum_k N_{ijk}, \quad (6)$$

3. The ratio of time-averaged acoustic energy flux in the i^{th} third-octave band flowing through the N_{ijk} measuring surface segment to the averaged acoustic energy flux flowing through a certain area or the whole measurement surface N (e.g. if the measurement is carried out at a cuboid surface, N is the time-averaged acoustic energy flux flowing through this surface or through one of the walls of this cuboid):

$$\eta_{ijk} = \frac{N_{ijk}}{N}, \quad N = \sum_i \sum_j \sum_k N_{ijk} \quad (7)$$

The global acoustic efficiency of a sound source – a mechanical structure is the ratio of time-averaged acoustic energy flux in the whole band of the measured frequencies flowing through the N_{jk} measuring surface segment to the averaged acoustic energy flux flowing through a certain area or the whole measurement surface:

$$\eta_G = \frac{N_{jk}}{N} \quad (8)$$

Thus, determination of the values of the individual measures of acoustic efficiency requires knowledge of acoustic power as a function of frequency of the wave flowing through measurement surfaces and their segments surrounding the investigated structure.

3. IDENTIFICATION OF A VIBRO-ACOUSTIC FIELD OF A TOOTHED GEAR MODEL

Usefulness of the foregoing measures of acoustic efficiency for identification of sound sources in complex mechanical structures was analyzed basing on the investigations of a single-stage toothed gear transmission model.

The research model of a single-stage toothed gear transmission (figure 1) consisted of two straight cylindrical gears, two equal shafts with spacing sleeves of outside diameter $\phi 63$ mm and pins $\phi 40$ mm. The shafts were fixed in ball bearings $\phi 40/\phi 80/18$ mm. The width of the toothed wheel rims amounted to 32 mm.

The welded casing of the gearbox was made of 5 mm thick sheet steel. The rings of the bearing seats were 9 mm thick. The casing lugs were made of 10 mm sheet steel.

During investigations the gearbox casing was not filled with oil and left open – without any cover. The assumption of such research conditions and the disproportion between the dimensions of the shafts and casing walls increased the predominant role of vibrations of the thin casing walls and generation of sound in the range of lower forcing frequencies.

For measurements of the acoustic power of the gearbox using intensity method were used a probe B&K 3584 with a 50 mm separator and an analyzer B&K 2145. The sound intensity level was measured in third octave bands with mid-band frequencies from 31.5 Hz to 1250 Hz. In this frequency range the error of sound intensity level approximation did not exceed 1 dB.

The acoustic power of the gear transmission was determined basing on the measurements of normal component of sound intensity I_{ni} and acoustic pressure p_i in the middle of each segment of the surface surrounding the source (point by point – according to PN-EN ISO 9614-1 [2]). Partial

acoustic power N_i is defined as a time-averaged flux of acoustic energy I_{ni} flowing through a measurement surface segment S_i – relationship (2).

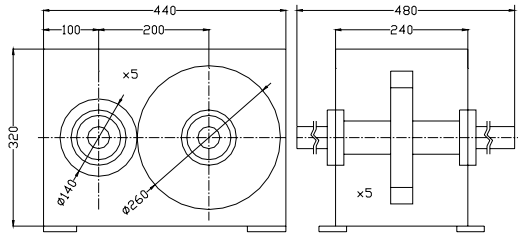


Fig. 1. Main dimensions of the gear transmission model

The measurement surfaces surrounding the gear transmission were parallel to the casing walls (at the distance of 250 mm measured from the middle of the intensity probe). It was defined by the casing walls (wall surfaces A, B, C) (figure 2).

Parameters of the individual measurement nets at the walls A, B i C (measurement surface segments) are listed in table 1.

The acoustic efficiency was investigated for two rotational speeds of the motor: 750 rpm and 1290 rpm (that corresponds to the frequencies $f_1 = 12,5$ Hz and $f_2 = 21,5$ Hz respectively).

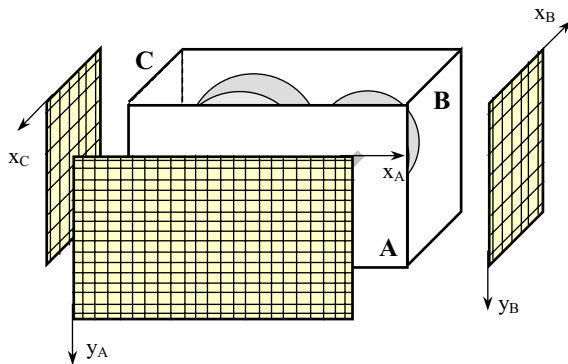


Fig. 2. The model of a gear transmission with the assumed denotations for walls and measurement surfaces which were assigned to them

Table 1. Parameters of the nets of the measurement surfaces surrounding the gear transmission during the measurements of acoustic power using the sound intensity method

Measurement surface dimensions [mm]	Measurement net dimensions [mm]	Distance between net elements and wall edges [mm]
A 440x320	20x20	20 from the left and right 10 from the bottom and top
B, C 240x320	40x40	20 from the left and right; 20 from the bottom and top

The results of the investigations are shown in the form of surface distributions of the global value and partial acoustic efficiencies for the individual third-octave bands. The surface distribution of the global acoustic efficiency η_G for measurement surfaces A, B and C is shown in figure 3.

Because of large sets of test results, figure 4 shows as an example only selected surface distributions of the values of partial acoustic efficiencies for the rotational speed of the motor of 1290 rpm, for three walls A, B and C of the cuboid surrounding the transmission, and for the third octave band with the mid-band frequency of 500 Hz.

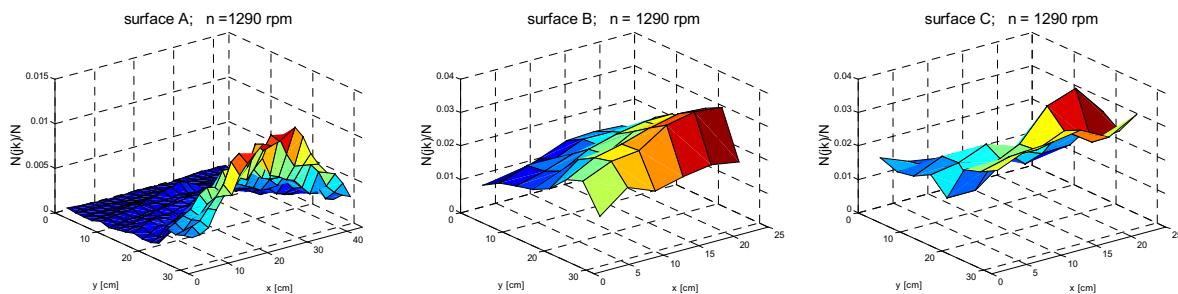


Fig. 3. Global acoustic efficiency η_G for the walls A, B and C of the gear transmission model

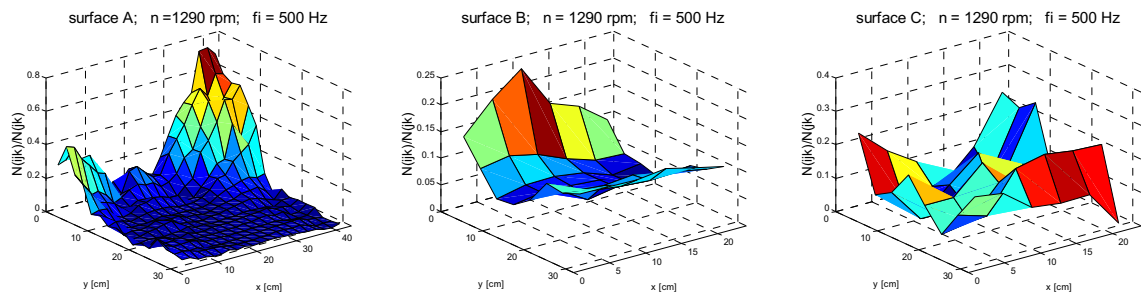
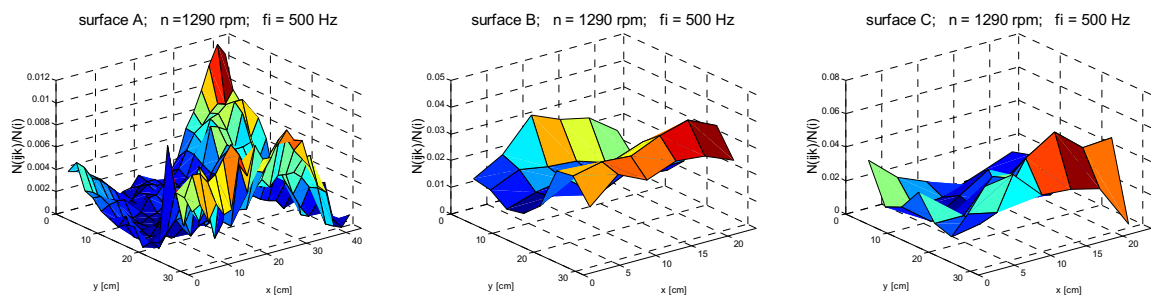
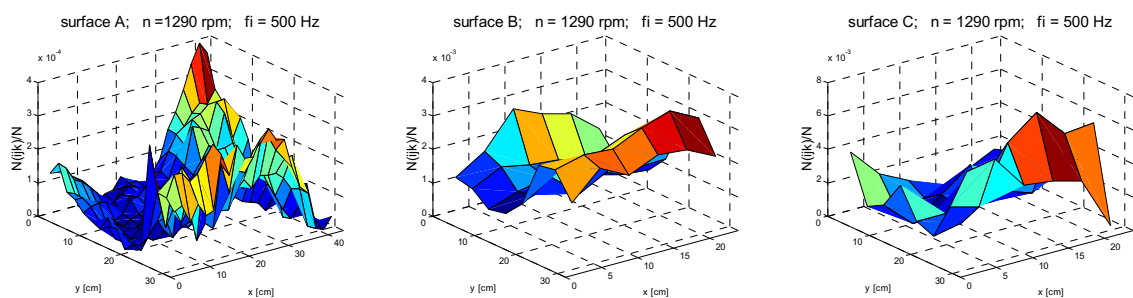
a) – η_i b) – η_{jk} c) – η_{ijk} 

Fig. 4. Surface distributions of partial measure values of acoustic efficiency for the third octave band with mid-band frequency of 500 Hz; walls A, B and C of the gear transmission model; a) – η_i , b) – η_{jk} , c) – η_{ijk}

Both the observed diverse dynamics of the partial measure values of acoustic efficiency for the given third octave band (figure 4) and the measure of the global acoustic efficiency (figure 3) indicate unambiguously that the defined measures carry different diagnostic information about the investigated object.

4. SUMMARY

The analysis of the surface distributions of the acoustic efficiency values as a function of frequency enabled to identify the predominant sound sources in the investigated model of the gear transmission.

REFERENCES

- [1] PN-EN ISO 9614-1: 1999: *Acoustics. Determination of sound power levels of noise sources using sound intensity. Part 1: Measurement at discrete points*. IDT EN ISO 9614-1: 1995; IDT ISO 9614-1: 1993.
- [2] Cz. CEMPEL: *Wibroakustyka stosowana*, PWN Warszawa 1989.
- [3] S. GADE, *Sound Intensity (Part I Theory)*, Technical Review, No 3 /1982, B&K.
- [4] PN-EN ISO 9614-2: 2000: *Acoustics. Determination of sound power levels of noise sources using sound intensity. Part 2: Measurement by scanning*. IDT EN ISO 9614-2: 1996; IDT ISO 9614-2: 1996.
- [5] PN-EN ISO 9614-3: 2003: *Acoustics. Determination of sound power levels of noise sources using sound intensity. Part 3: Precision method for measurement by scanning*. IDT EN ISO 9614-3: 2002; IDT ISO 9614-3: 2002.

DIAGNOSTICS OF THE TURBOGENERATOR SHAFT LINE MISALIGNMENT BASED ON THE BEARING TRAJECTORY PATTERNS

Józef RYBCZYŃSKI

Institute of Fluid-Flow Machinery, Polish Academy of Sciences,
80-952 Gdańsk, Fiszera 14, Tel.: (+48) 058-6995273, E-Mail: ryb@imp.gda.pl

Summary

The paper aims at illustrating effects of computer simulated bearing misalignment defect in a power turbogenerator. The results are presented in the form of journal trajectories of all turbo-set bearings as the effect of displacing two most vulnerable machine bearings. The analysis is limited to misalignment of the bearings in horizontal and vertical directions by the maximum acceptable range calculated with regard to permissible bearing vibration. Shape and dimensions of bearing trajectories are interpreted basing on theory of hydrodynamic lubrication of bearings. It was shown that relative journal trajectories carry much important information about dynamic state of the machine, indicating also the way in which bearings are loaded. The article shows the potential of using trajectory patterns for diagnosing misalignment defects in rotating machines and suggests including sets of trajectory patterns to the knowledge base of the machine diagnostic system.

Keywords: rotor-machine, vibration, misalignment, bearing trajectory, technical diagnostics.

DIAGNOSTYKA ROZOSIOWANIA LINII WAŁÓW TURBOGENERATORA NA PODSTAWIE OBRAZÓW TRAJEKTORII ŁOŻYSK

Streszczenie

W artykule przedstawiono rezultaty komputerowej symulacji defektu rozosiowania łożysk turbogeneratora wielkiej mocy. Wyniki zostały zaprezentowane w formie trajektorii czopów wszystkich łożysk turbozespołu jako skutku przemieszczenia dwu najbardziej newralgicznych łożysk tej maszyny. Analiza jest ograniczona do rozosiowania tych łożysk w kierunku poziomym i pionowym o maksymalną dopuszczalną wielkość obliczoną ze względu na drgania łożysk. Kształt i wymiary trajektorii łożysk są interpretowane na podstawie hydrodynamicznej teorii smarowania. Pokazano, że względne trajektorie czopów niosą wiele ważnych informacji o stanie dynamicznym maszyny, wskazując także na sposób obciążenia łożysk. Artykuł wskazuje na możliwości użycia obrazów trajektorii do celów diagnostyki defektu rozosiowania w maszynach wirnikowych i sugeruje włączenie obrazów trajektorii do bazy wiedzy systemu diagnostycznego maszyny.

Słowa kluczowe: maszyna wirnikowa, drgania, rozosiowanie, trajektoria łożyska, diagnostyka techniczna.

1. INTRODUCTION

Displacing any of turbo-set bearings from its optimum position, defined by the designed shaft catenary, changes conditions of operation of the oil bearings and consequently rotors supported on them. The distribution of the static load of bearings and shafts changes distribution of unbalance along the shaft line and as a following consequence vibrations can be generated [1-4].

The motivation for undertaking the investigations were own observations [5] and the information in the literature on a remarkable effect of bearing misalignment on the dynamic state of a rotating machine with a long shaft line supported in numerous bearings [1-4, 6-9]. According to [7] "Misalignment of multi-bearing rotor systems is one of the most common fault conditions yet it still not fully understood". When the frequency of occurrence is taken into account, bearing

misalignment is the second most common type of failure of a rotating machine, after unbalance [8]. According to [9], misalignment may cause even 70% of vibration problems, which are observed in rotating machines. It is noteworthy, that the literature on bearing misalignment is anyway rather poor. This fact is underlined by majority of authors of papers on the subject [1, 4, 9]. A. Muszynska in [4] stresses it very strongly: "There is, however very little published on misalignment malfunction, its destructive, overloading effects on rotor and bearings, physical phenomena involved, and how to diagnose misalignment by using vibration monitoring". All this can testify to some underestimation of the phenomenon, but also to certain difficulties in analysing it. This situation makes undertaking the research in this area more justified.

The present work aims at illustrating and analysing changes of bearing trajectory attributes, as a result of the appearance of the bearing misalignment defect. The analysis is based on the results of computer simulation of the malfunction in numerical model of the turbogenerator, as this kind of experiments on a real object is, of course, inadmissible. The illustration of effects has a form of complete sets of trajectories of journal centres of all bearings, being the response to a dislocation of one particular bearing. The article interprets relations between scale, location and direction of bearing misalignment on the one hand and shape and dimension of bearing trajectories on the other hand, basing on operational principles of a hydrodynamic bearing. It was revealed, that trajectories of bearings, which express dynamic state of bearings, might play role of an indicator of bearing misalignment in multi-support rotating machine. Specifications of relations between bearing dislocations and the machine state expressed by its vibrations can be treated as sets of diagnostic relations linking bearing misalignment defect with symptoms of the defect [4, 10-12]. The work indicates great potential of using trajectory patterns for diagnosing misalignment defects in rotating machines.

2. RELATIONS BETWEEN BEARING DISLOCATIONS AND BEARING LOADS

The way and scale to which a machine reacts to bearing misalignment depends, first of all, on the type and magnitude of misalignment, but also on many other factors, especially structure of the machine. These are, among others, relative positions of particular bearings, mechanical properties of the bearings, especially stiffness characteristics of the oil film as well as stiffness characteristics of the rotor [3, 4, 11, 13].

If a rotating shaft is supported in two bearings static reaction forces are strictly defined, as the mechanical system description is trivial. A shaft supported in 3 bearings theoretically is statically indeterminate, however the system is simple for analysis and the computational problem disappears after taking into account strains of the shaft and support structure. Considering stiffness and mass of the rotors and the oil film stiffness characteristics it is possible to determine the static shaft shape and load of the bearings. In this situation dislocation of any of the three bearings can be reduced to the same case: to equivalent dislocation of the middle bearing, which then allow to calculate bearing loads.

The situation becomes much more complicated if number of bearings increases. Lets consider the shaft line supported in 4 bearings shown schematically in Fig. 1. If all bearings are positioned on the properly designed catenary line, as shown in Fig. 1a, bearing load distribution and operation

conditions are optimal. Lets assume that bearing No. 2 (denoted as B2) is at certain circumstances relocated up (Fig. 1b). In this situation B2 gets additional load but at the same time neighbouring bearings are unloaded. If the B2 is relocated enough far off, the upper-half of the B1 and B3 can be loaded and also B4 is loaded additionally at its bottom. Fig. 1c presents a different case, when B3 is moved down far enough to load its upper half-shell. In this situation the B2 and B4 are loaded additionally on their low half-shells. Besides the low half-shell of the B1 is unloaded or even is loaded upper half-shell of this bearing. It is easy to note, that bearing load distributions are very similar in the two cases: relocation of the B2 up (Fig. 1b) and relocation of the B3 down (Fig. 1c).

These two cases are really not absolutely equivalent; in some extend for reason of bearing clearances and oil film stiffness characteristics, but first of all because the shaft axis in the base case (shown in Fig. 1a) is not a straight line. Preliminary displacement of the bearings 2 and 3 down with respect to the geodesic line results in lack of symmetry in the shaft shape after displacing the bearing 2 up and after displacing the bearing 3 down. Although the shaft shapes are not identical in the two cases, their effects on the bearing load distributions are very similar. Since the vibration effects can be also similar and this fact will be shown in par. 5. Degree of similarity of the effects depends also on homogeneity of shaft stiffness and on mutual bearing distances, anyway the observation is true in principle. The above analysis is adequate also in relation to horizontal bearing dislocations and is even easier because of lack of the gravitational shaft deflection. Corresponding conclusions regarding similarity of the effects, however with more limitations, can be drawn with reference to dislocations of the terminal bearings: B1 and B4.

3. INVESTIGATION PROCEDURE

The analysis presented in the paper is limited to displacing only two most vulnerable bearings in the machine, i.e. displacing bearings 5 and 6 with respect to their base position on the catenary. These bearings were selected because the turbo-set turned out to be very sensitive to misalignments of the two bearings. What is more, their misalignments are extremely dangerous, as the ranges of acceptable dislocations of these bearings are small. The graphical illustration of the analysis is limited to the effects of the two bearing dislocations in the horizontal direction to the right and to the left, and in the vertical direction up and down and additionally were limited to only one dislocation range in every of the four direction: to a maximum acceptable distance.

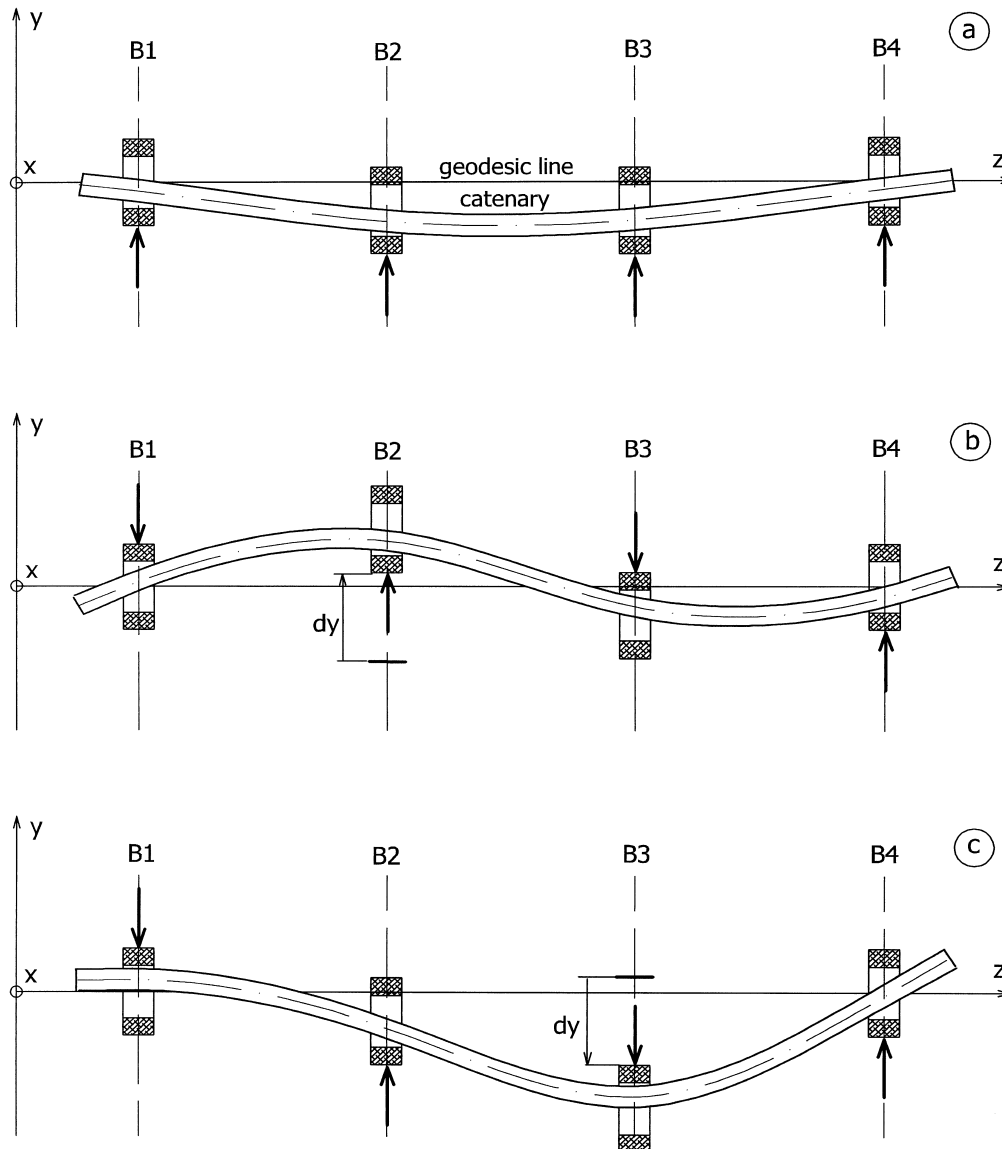


Fig. 1. Scheme of a shaft line bow and bearing loads depending on bearing dislocations:
 a – the bearings in catenary line; b – bearing 2 moved upward by dy ; c – bearing 3 moved down by dy

The ranges of acceptable bearing dislocations were determined taking into account the adopted criteria, which determine turbo-set operation as permissible [12, 14]. The criterion, which allows the state of the entire turbo-set to be assessed as permissible, is simultaneous meeting of two vibration conditions in all seven turbo-set bearings:

- relative journal-bush vibrations, expressed by the p-p displacement amplitudes A in two directions, inclined by 45° to the vertical:

$$A < A_{lim} = 165 \mu\text{m},$$

- absolute bearing vibrations, expressed by the RMS vibration velocities V in horizontal and vertical directions:

$$V_{RMS} < V_{RMS\ lim} = 7,5 \text{ mm/s}.$$

The limiting vibration parameters, values and directions of their measurements, were taken from ISO standards: relative vibration amplitudes from the standard 7919-2, while the absolute vibration velocities – from the standard 10816-2. The limits

correspond to the „warning state” for the turbo-set. It is noteworthy that the two conditions in the two directions are to be met in all seven bearings, and not only in the bearing in which the defect took place. The ranges of tolerable bearing dislocation in horizontal and vertical direction have been determined by author and are subject of the papers [15, 16]. The calculated values of tolerable misalignment of bearings 5 and 6 to the right, to the left, upward and downward are collected in Tab. 1.

All calculations were performed using a set of computer codes composing the system MESWIR. It is a package of codes developed and used in the Institute of Fluid-Flow Machinery for calculating dynamics of rotors supported on oil bearings. Its more detailed description and features are published e.g. in [10-12, 14, 15].

Table 1. The calculated maximum tolerable displacement ranges of bearings 5 and 6 in horizontal and vertical directions

No. of bear.	Direction of dislocation	Permissible dislocations $\Delta x, \Delta y$ [mm]	Vibration exceeded in:
5	right →	$\Delta x_R = 1.4005$	B 4 – dir. u
	left ←	$\Delta x_L = -1.0352$	B 6 – dir. u
	up ↑	$\Delta y_U = 0.8694$	B 4 – dir. u
	down ↓	$\Delta y_D = -1.0841$	B 5 – dir. u
6	right →	$\Delta x_R = 1.2918$	B 4 – dir. u
	left ←	$\Delta x_L = -1.7913$	B 4 – dir. u
	up ↑	$\Delta y_U = 1.2334$	B 5 – dir. u
	down ↓	$\Delta y_D = -0.8706$	B 6 – dir. u

The research consisted in calculating the dynamic state of a turbo-set numerical model with simulated dislocations of selected machine bearings, i.e. with a defect implemented to the base model of the machine. The essential calculations of the machine dynamic condition give at first the time-dependent dislocations of selected nodes, which then allow the trajectories of these nodes to be drawn. The trajectories are composed of instantaneous node positions and can be analysed with respect to their shape and dimensions.

The starting point for the calculations and for further analyses of the results is the “base case” – the numerical model of the machine free of defects [12, 14-16]. The model was created and tuned based on the results of measurements done in a power plant by turbogenerator diagnostic system in steady state, nominal conditions of operation. The data correspond to nominal rotational speed 3000 rev/min and full power output 211 MW. Tuning the numerical model consisted in selecting secondary machine properties and parameters, for instance, residual unbalance distribution, or material damping, in such a way that the results of calculations of the base case were the closest to the turbo-set characteristics measured in the power plant.

The object of examination was a large power turbogenerator 13K215, most commonly used in Polish power industry. The turbo-set consists of a 200 MW turbine and a generator. The turbo-set is a four-body machine, the rotors of which are supported on seven oil bearings. Four shaft segments are linked together by three rigid couplings. Noteworthy is distribution of two pairs of machine bearings, namely bearings 3 and 4 located between the MP and LP turbine parts, and bearings 5 and 6 located between the LP turbine case and the generator. The two bearings composing each pair are located close to each other and are supported on a common foundation block, as a result of which the dislocation of one bearing significantly affects the operation of both of them. Since the presented results and conclusions are

adequate for the pair of bearings 3 and 4, although the analysis in this paper is limited to the pair of bearings 5 and 6. All bearings are of hydrodynamic type, with elliptical clearance and two lubricating pockets in the horizontal division plane.

4. PRESENTATION OF THE MACHINE DYNAMIC STATE BY MEANS OF BEARING TRAJECTORIES

Figs 2 and 3 present tables containing sets of trajectories of journal centres of all bearings for the turbo-set with bearings dislocated from their base position and, for comparison, with bearings in the base position. Fig. 2 refers to misalignment of the bearing 5, while Fig. 3 refers to misalignment of the bearing 6. These diagrams are based on data recorded during 12 rotor revolutions. Successive rows in each table contain graphs of trajectories observed in seven consecutive turbo-set bearings. The first column in each table present a collection of trajectories for the base case, which characterise the state of the turbo-set without defects. They are a reference for further analysis. It results from Figs 2 and 3 that in the base case vibrations of journals and bushes in all bearings are much smaller than the permissible values stated in par. 3. Vibrations in a certain direction are represented by a projection of the trajectory on this direction. The columns 2, 3, 4, 5 present analogous trajectories for the cases when bearings are dislocated to the right, left, upward and down by maximum acceptable distance calculated with respect to permissible bearing vibration. The distances are collected in Tab. 1.

A general remark resulting from these diagrams is negligible effect of misalignment of bearings 5 and 6 on the trajectories of bearings 1, 2, and 3, and small effect on the trajectory of bearing 7. This tendency can be explained by a relatively large distance of those bearings from the displaced bearings, and relatively big shaft flexibility between those bearings. At the same time, the trajectories of bearings 4, 5, and 6 significantly increase in case of bearing 5 or bearing 6 dislocations in an arbitrary direction. A characteristic feature is that in the majority of cases the trajectories of those bearings stratify. In particular the bush trajectories do not coincide with each other during 12 shaft revolutions, which suggests significant contribution of subharmonic components and an analysis reveals that there are the 1/3X and 1/2X subharmonics. The bush vibrations are forced vibrations, which depend on the resonance frequency of the bush and supporting structure. The vibrations in the bearings are excited by forces generated by rotating shaft and by oil film reactions. More precise explanation of the nature of these vibrations requires more detailed analysis based on the vibration spectrum and modal analysis of the turbo-set structure but this problem will be the object of author's future investigations.

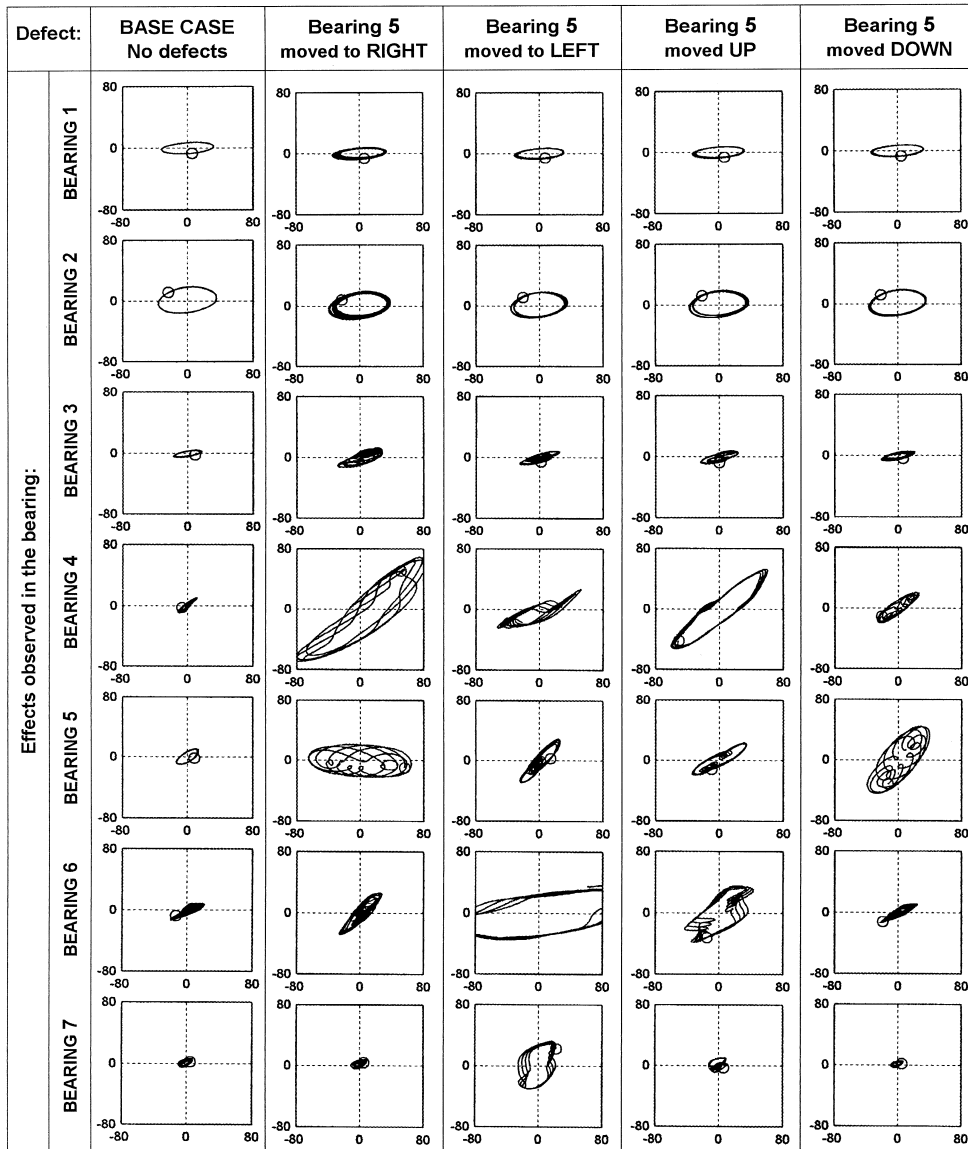


Fig. 2. Changes in relative trajectories of all bearing journals as the effect of dislocation of the bearing 5 by maximum tolerable distance in horizontal and in vertical direction

The diagrams in Figs 2 and 3 reveal that it is bearing 4, which is most sensitive to misalignment with respect to relative journal vibrations, although it is not the bearing to which the defect was introduced. It results from the Tab. 1 that in as many as 4 cases in this particular bearing took place exceeding of the permissible level of relative vibrations. At the same time the bush of this bearing does not get in high vibration. Bearing 5 behaves in an opposite way, characterised by moderate relative journal vibrations accompanied by very high bush vibrations in almost each case of misalignment of bearings 5 and 6. It is characteristic that in 75% of the examined cases the vibration limits are exceeded in the bearing next to the displaced one and not in this bearing itself.

5. INTERPRETATION OF BEARING TRAJECTORY FEATURES AND RELATIONS

Diagrams of the bearing journal trajectories shown in Fig. 2 and 3 reveal close symmetry of the effects of dislocation of the neighbouring bearings 5 and 6 to opposite directions. For instance, displacing bearing 5 down produces similar effect as displacing bearing 6 up. In both cases the pattern of vibrations observed in the two bearings is almost identical and exceeding of the permissible vibration level takes place in the same bearing 5. Also displacing bearing 5 right produces in both bearings identical effects as displacing bearing 6 left, and displacing bearing 5 left results in the same effects as displacing bearing 6 right. In the latter case exceeding of the permissible vibrations does not take place in the same bearing, and vibration amplitudes.

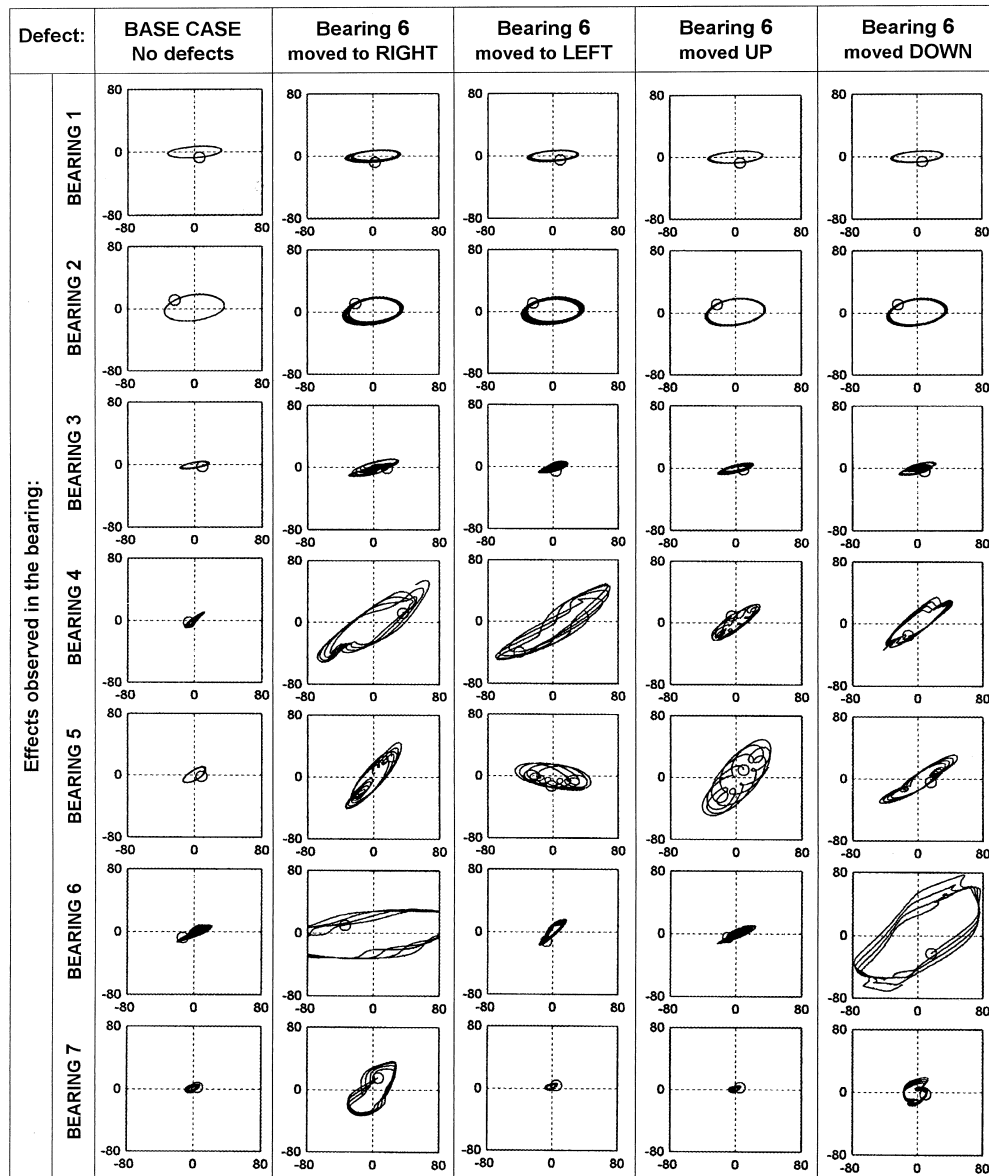


Fig. 3. Changes in relative trajectories of all bearing journals as the effect of dislocation of the bearing 6 by maximum tolerable distance in horizontal and in vertical direction

also differ, but still the diagrams of journal trajectories preserve geometrical similarity. Even in the pair of cases: dislocation of bearing 5 up and dislocation of bearing 6 down, we can observe certain similarities in the trajectory shape in every bearing, although the amplitude values of journal and bush vibrations differ considerably.

The described above similarity of the effects of dislocation of bearings 5 and 6 in opposite directions indicates that the operation of those bearings is closely related and cannot be analysed individually. This similarity also testifies to the same nature of phenomena taking place in the rotor-bearings system in the both cases. The opposite dislocations of the neighbouring bearings produce similar shaft deflection, and, as a consequence, similar change of bearing static load accompanied by similar rotor unbalance change, i.e. similar

dynamic load of the bearings. The symmetry in the bearing load and in the shaft deflection effects generated by displacing the neighbouring bearings to opposite directions was illustrated in the Fig. 1 and was discussed in par. 2.

The shape and dimensions of relative journal trajectories in particular cases of bearing misalignment can be explained basing on the hydrodynamic theory of lubrication and on the resultant mechanism of force generation in oil bearings [17]. Fig. 4 shows the scheme of a hydrodynamic bearing operation in the same coordinate system as implemented for the trajectories in Figs 2 and 3. The direction of rotor revolution (here, counterclockwise) makes the journal centre in the working bearing move to the right, as shown in Fig. 4. In these conditions the the bearing misalignment, which has the form of bush

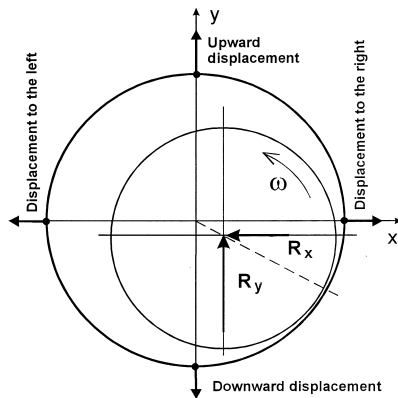


Fig. 4. Effect of the bearing bush dislocations on oil film reaction forces

displacement to the right, is equivalent to relative displacement of the bearing journal centre towards the bush centre. As a result, the main horizontal component of the bearing reaction decreases and the bearing has “more space” for horizontal vibrations. In this situation the neighbouring bearings must take over additional load from this unloaded bearing and it is the cause that horizontal journal vibrations in those bearings are likely to decrease.

The discussed situation is clearly illustrated by trajectories of bearings 5 and 6 after their horizontal dislocation. Displacing the bush of bearing 5 to the right (Fig. 2) removes some load from this bearing in horizontal direction, as a result of which its trajectory in horizontal direction enlarges. At the same time bearing 6 is given extra load as it takes over part of force previously carried by bearing 5, and, consequently, the dimensions of the journal trajectory of bearing 6 decreases. But displacing bearing 5 left pushes the journal towards the bush in this bearing, thus giving it extra load, which stabilises horizontal vibrations in this bearing and, at the same time, enlarges horizontally trajectory of the bearing 6 due to reduction of its load. Similar effects are generated while displacing bearing 6 (Fig. 3). Its dislocation to the right results in enlarging the trajectory of this bearing in the horizontal direction and stabilisation of horizontal vibrations in bearing 5. Similarly, displacing bearing 6 left leads to almost entire disappearance of vibrations in this bearing, accompanied by simultaneous horizontally enlarged journal trajectory in the neighbouring bearing 5.

Relations between the bearing trajectories and misalignment in vertical direction are similar, but even easier for interpretation. Fig. 2 reveals that displacing bearing 5 up extends the bearing trajectory in the horizontal direction and makes it narrower in vertical direction. At the same time dimensions of the journal trajectory of bearing 6 increase. Opposite effects are generated by moving bearing 5 down. The journal trajectory in bearing 5 becomes high, while that in bearing 6 - low. It is

quite understandable, as the dislocation of bearing 5 up gives it extra load, at the same time unloading the neighbouring bearings. The effects of vertical misalignments of the bearing 5 are shown in Fig. 3. Relations between trajectories and vertical misalignment of the bearing 6 can be interpreted in the same way as misalignment of the bearing 5.

6. UTILISATION OF BEARING TRAJECTORY FOR TURBO-SET DIAGNOSTICS

Understanding of the above-described mechanism of change of journal trajectory dimensions and shapes can be useful in using the trajectories for diagnosing large, multi-support and multi-rotor machines, in which particular rotors are linked by means of rigid couplings. The relations between bearing dislocations and machine vibration characteristics represented by bearing trajectories can be considered diagnostic relations and included to the base of diagnostic knowledge of the machine of concern. The concept of the present article was shown based on sample set of trajectories obtained after introducing to a machine the misalignment defect in the form of displacing two bearings by the maximum acceptable range. Similar data sets can be prepared also for misalignments introduced to bearings in an arbitrary range and even in arbitrary direction. Moreover, the analysis can be extended to dislocation of all bearings. However, it would result in great extending the amount of data and then increasing the base of knowledge of a diagnostic system.

Another limitation of possibility of diagnostics based on trajectories is the problem discussed in paragraph 6. There was found, that bearing trajectories and then vibration patterns are very similar in the two cases: dislocation of one bearing creating the pair in a certain direction and dislocation of the other bearing in opposite direction. The similarity results in situation that an attempt to identify a reason of observed vibration can lead to two alternative diagnoses: it can testify to the dislocation of one bearing in one direction, or to the dislocation of the other bearing in the opposite direction.

It is necessary to remember that the trajectory shape is not a characteristic symptom of misalignment of particular bearing. Therefore the diagnostics based on individual trajectories is hard or even not possible in practice. Chances for an accurate diagnosis increase with the number of available trajectories that can be analysed altogether. Also noteworthy is fact, that the presented defect-symptom type relations are strictly valid only for the machine for which the calculation model was worked out and tuned. However, certain remarks and conclusions can be generalised and applied to other similar machines. Such generalized deductions are set up in “conclusions”.

7. CONCLUSIONS

- The effect of misalignment of a bearing on trajectories of distant bearings is negligible, while the effect on trajectories of bearings located close is strong. In the majority of cases the permissible vibration level is exceeded not in the displaced bearing but in a neighbouring bearing.
- Symmetry exists between the effects of dislocations of two neighbouring bearings composing the pair in opposite directions. This testifies to the similarity of phenomena generated in the rotors-bearings system as a result of dislocation of two neighbouring bearings in opposite directions. This effect can be explained by similarity of bearing loads and resulting similar shaft deflection in the both cases.
- Mechanism of changes of journal trajectory shape and dimensions due to bearing misalignment can be explained based on the hydrodynamic theory of lubrication. Bearing trajectory patterns depend on direction and range of displacement and on relation of bearing displacement and direction of shaft revolution.
- Dimension and shape of a trajectory carry important information on the dynamic state of the machine: on the way in which the bearings are loaded and on the location and direction of bearing misalignment. A set of trajectories can be used for diagnostic purpose, however with limitations resulting from similarity of dislocation effects of neighbouring bearings to opposite directions.

REFERENCES

- [1] Piotrowski J.: *Shaft Alignment Handbook*, CRC Press Taylor & Francis Group, Boca Raton, London, New York, 2007.
- [2] Rao J. S.: *Vibratory Condition Monitoring of Machines*, Narosa Publishing House, New Delhi, Chennai, Mumboi, Calcuta, London, 1999.
- [3] Sekhar A. S., Prabhu B. S.: *Effects of coupling misalignment on vibrations of rotating machinery*, Journal of Sound and Vibration, 185 (4), (1995), 655-671.
- [4] Muszynska A.: *Rotordynamics*, CRC Press Taylor & Francis Group, Boca Raton, London, New York, Singapore, 2005.
- [5] Rybczynski J.: *Attempts of explanation of the reasons of vibrations of three-support rotor recorded on the research rig for investigations of rotor dynamics*, in: Proceedings of II International Congress of Technical Diagnostics, 2000, Warsaw, Vol. 2, p. 219.
- [6] Sudmersen U., Stegemann D., Reimche W., Liu Y.: *Vibrational diagnostic of rotating machinery in power plants*, in: Proceedings of ISROMAC-7 Conference, 1977, Honolulu, USA.

- [7] Lees A. W.: *Misalignment in rigidly coupled rotors*, Journal of Sound and Vibration, vol. 305, (2007), 261-271.
- [8] Rao J. S., Sreenivas R.: *Dynamic analysis of misaligned rotor systems*, Proceedings of VETOMAC-1 Conference, 2000, Bangalore, India.
- [9] Bognatz S. R.: *Alignment of critical and non-critical machines*, Orbit, (1995), 23 – 25.
- [10] Rybczynski J.: *Maps of vibrational symptoms of bearing misalignment defects in large power turboset*, in: Proceedings of ASME Turbo Expo 2008, Berlin, No. GT2008-50558.
- [11] Rybczynski J.: *Vibrational effects of bearing misalignment defect expressed in the form of bearing displacement maps*, in: Proc. of ISROMAC-12, Int. Symposium on Transport Phenomena and Dynamics of Rotating Machinery, Honolulu, 2008, No. ISROMAC12-2008-20026.
- [12] Kicinski J., Drozdowski R., Materny P.: *The non-linear analysis of the effect of support construction properties on the dynamic properties of multi support rotor systems*, Journal of Sound and Vibration, 206 (4), (1997), 523-539.
- [13] Hu W., Miah H., Feng N. S., Hahn E. J.: *A Rig for testing lateral misalignment effects in a flexible rotor supported on three or more hydrodynamic journal bearings*, Tribology International, No. 33, (2000), 197-204.
- [14] Kicinski J., Drozdowski R., Materny P.: *Nonlinear model of vibrations in a rotor - bearings system*, Journal of Vibration & Control, vol. 4, No. 5, (1998), 519 - 540.
- [15] Rybczynski J.: *Acceptable dislocation of bearings of the turbine set considering permissible vibration and load of the bearings*, Key Engineering Materials, 293-294, (2005), 433-440.
- [16] Rybczynski J.: *Evaluation of tolerable misalignment areas of bearings of multi-support rotating machine*, in: Proceedings of ASME Turbo Expo 2006, Barcelona, Spain.
- [17] Hamrock B. J.: *Fundamentals of Fluid Film Lubrication*, McGraw-Hill Inc, New York, 1994.



Dr inż. **Józef RYBCZYŃSKI**. Graduated from Gdansk University of Technology at Mechanical Engineering Faculty in 1971 in technical science. PhD since 1988 in mechanics. Employed since 1972 at The Institute of Fluid Flow Machinery, PASci in Gdansk. Area of interest:

dynamics of rotors, oil bearings, machine diagnostics, experimental investigations into rotor and foundation vibrations, measurement techniques. Member of Polish Association of Technical Diagnostics and American Society of Mechanical Engineers.

USE OF HILBERT-HUANG TRANSFORM OF A VIBROACOUSTIC SIGNAL IN THE RESEARCH RELATED TO THE GIGACYCLE FATIGUE PROCESS

Szymon GONTARZ, Marcin JASIŃSKI, Stanisław RADKOWSKI

Institute of Automotive Engineering, Warsaw University of Technology
ul. Narbutta 84, 02-524 Warsaw, ras@simr.pw.edu.pl

Summary

The purpose of this paper is to develop, for highly-resistant materials, a method of forecasting and analysis of gigacycle fatigue durability (10^8 - 10^9 cycles) relying on vibroacoustic signal analysis. The proposed method involves use of results of vibroacoustic signal analysis obtained during accelerated fatigue tests conducted in dedicated test bed constructed specially for this purpose and operating in the frequency range of 10 kHz which corresponds to the resonance frequency of vibration of samples. Let us note that the process of defect formation may lead to both, the intensification of non-linear phenomena as well as the occurrence of non-stationary effects even if during the early stages the intensity of defects is small while the growth of the level of vibration and noise is negligible, as contrasted with emergency states. A useful method is to test the higher order spectra, which respectively define the non-linear effects. The conducted analyses point to high usability of Hilbert spectrum through the EMD examining the non-stationary character of signals.

The main goal of these investigations is to examine the signal processing method for gigacycle fatigue durability and impact of dynamic stress. Efficient signal analysis would be especially important for high frequency loading which dominates in rotating machinery diagnosis.

Keywords: Vibroacoustic diagnosis, gigacycle fatigue processes, piezoelectric generators, bispectrum, Empirical Mode Decomposition, Hilbert Huang Transform.

ZASTOSOWANIE TRANSFORMATY HILBERTA-HUANG SYGNAŁU WIBROAKUSTYCZNEGO W BADANIACH GIGACYKLOWEGO PROCESU ZMĘCZENIA

Streszczenie

Celem pracy jest opracowanie, dla materiałów o wysokiej wytrzymałości, metody prognozowania i analizy gigacyklowej trwałości zmęczeniowej (10^8 - 10^9 cykli) na podstawie badania sygnału wibroakustycznego. W metodzie proponuje się wykorzystać wyniki analizy sygnału wibroakustycznego, uzyskiwane podczas przyspieszonych badań zmęczeniowych, prowadzonych na specjalnie do tego celu skonstruowanym i zbudowanym stanowisku badawczym, pracującym w zakresie częstotliwości rzędu 10 kHz, odpowiadającym częstotliwości drgań własnych próbek. Zauważono, że proces kształtowania się uszkodzenia może prowadzić zarówno do nasilenia zjawisk nieliniowych jak również do wystąpienia efektów niestacjonarnych nawet wtedy, kiedy podczas wczesnych stadiów uszkodzeń ich intensywność jest mała a wzrost poziomu drgań i szumu jest pomijalny, porównując go z poziomem przy stanach zagrożenia. Użyteczna jest w tym wypadku metoda widm wyższego rzędu, która odpowiednio definiuje efekty nieliniowe. Zamieszczone w publikacji analizy wskazują na dużą użyteczność widm Hilberta a w szczególności empirycznej dekompozycji sygnału (EMD), która pozwala na analizę niestacjonarnego charakteru sygnału.

Głównym celem badań było znalezienie skutecznej metody przetwarzania sygnałów dla gigacyklowych wytrzymałościowych procesów zmęczeniowych oraz zbadanie wpływu obciążeń dynamicznych. Efektywny sposób analizy sygnału jest szczególnie ważny w diagnostyce maszyn obrotowych gdzie występują wysoko częstotliwościowe obciążenia.

Słowa kluczowe: diagnostyka wibroakustyczna, gigacyklowe procesy zmęczeniowe, generatory piezoelektryczne, bispektrum, dekompozycja sygnału EMD, transformata Hilberta Huang.

1. INTRODUCTION

The publication presents the possibilities of extracting diagnostic information while relying on the methods which use the results of analysis of a vibroacoustic signal obtained during accelerated fatigue tests performed in a dedicated test bed which operates in a 20 kHz frequency range. This frequency corresponds to the proper frequency of vibration of the samples. Due to the difficulties associated with carrying such long tests on classical testing machines (which offer input frequencies in the range of 30 Hz), research of such a type has not been conducted in Poland and hence no attempts have been made of formulating the assessment of the process while relying on the information contained in vibroacoustic signal. Non-familiarity with phenomenon as well as lack of possibilities of conducting qualitative, and especially quantitative measurements of the process in whose case the predominant part of defect formation period is associated with the crack nucleation phase and it brings the threat of occurrence of catastrophic defects. If a fact is taken into account that the situation concerns modern means of transport (airplanes, ship, fast trains) as well as equipment in conventional electrical power plants and while taking into account the contemplated strategic plans of development in Poland of nuclear power plants whose failures could have catastrophic consequences, then carrying out such research as well as undertaking the task of developing the algorithms which will forecast the useful life become a necessity for the Polish scientific and technical community.

At the same time the researchers who indulge in attempts of conducting such research point out that crack nucleation period accounts for 90% of the time of development of the process of gigacycle material fatigue [1, 2]. For obvious reasons, determining a clear boundary between crack nucleation and propagation phase is not simple. In addition, the relationships between growth of a crack and intensity of the stress as well as the value of stress, which have so far been applied in mechanics, have not gained full acceptance in the conditions of gigacycle fatigue and at the present stage of the research they are subject to verification. From this point of view an urgent need exists for developing new research methods, adequate diagnostic models as well as for selection of the right methods of diagnostic information detection [3].

The purpose of the research was to demonstrate the possibility of reaching the diagnostic information by means of such methods of signal processing as: bi-spectral analysis, Hilbert Huang transform in order to analyze the gigacycle fatigue durability (10^8 - 10^9 cycles), for highly durable materials, while relying on examination of a vibroacoustic signal. The method uses the results

of analysis of vibroacoustic signals obtained during accelerated fatigue tests which are conducted on a dedicated test-bed operating in the frequency range of the samples' proper vibration.

2. TEST-BED AND EXPERIMENT DESCRIPTION FOR EXAMINING GIGACYCLE FATIGUE-RELATED PROCESSES

The authors have designed and performed a small-size test-bed for diagnosing the gigacycle fatigue-related processes (Fig. 1) [4]. The test-bed has the form of a cube with dimensions of 0.2 x 0.2 x 0.2 m and its weight does not exceed 2 kg. The head is made of titanium and mounted directly in the piezoelectric generator. The beam is mounted with the use of an circular cam (in order to do away with play).

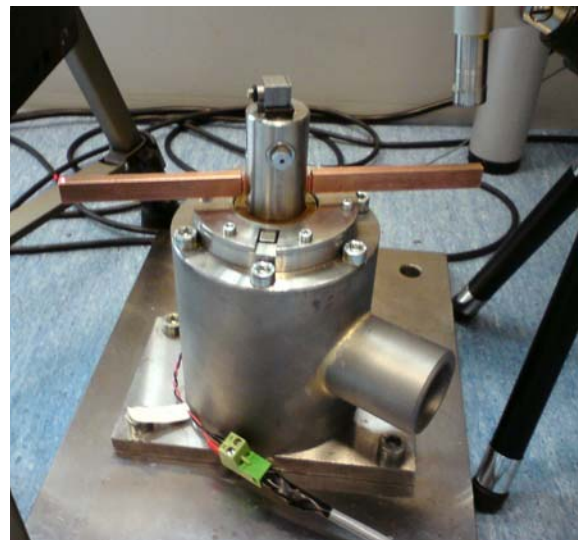


Fig. 1. Small-sized gigacycle fatigue test bed together with the specimen

A recording-control program has been developed in the LabView 7.1 [5] environment which has the task of tracking the resonant frequency of a beam based on the spectral analysis of a vibration signal registered by a use of the non-contact measurement system and the piezoelectric accelerometer. The frequency value estimated in this way is in the next step sent to the generator in order to correct the frequency of the signal stimulating the piezoelectric converter. Thus it is possible to track the changes of frequency (at the resonant curve) of a beam's proper vibration connected with the developing fatigue-related crack.

Fatigue tests were conducted in the aforementioned test bed. It is the existence of a notch as well as the shape of that notch that become essential from the point of view of durability of the structure. An experiment was conducted, which was intended to determine the

impact that a notch has on fatigue durability of a sample. The assumptions of the experiment are presented more extensively in [6].

The dimensions of a sample were as follows (height x width x length): 10mm x 5mm x 40mm, however notches have been introduced, in a P-type (rectangular) sample, at the location of the mounting. The research was conducted until fatigue-related fracture of the sample occurred, which happened after ca. 2 million cycles.

3. SIGNAL PROCESSING FOR FATIGUE RELATED PROCESS DATA ANALYSIS

The paper focuses on use of bi-spectral metrics for evaluating and monitoring the evolution of a fatigue process. A different approach to the problem of extraction of information-carrying features of a signal is presented by the adaptation methods which rely on empirical data. These methods are exemplified by the Hilbert-Huang (HHT) transform [7] and they constitute the basis of this paper.

The Hilbert-Huang transform consists of two techniques of signal analysis. The first one is the so-called empirical decomposition of the EMD signal while the other is the Hilbert's spectral analysis. The complex method can be successfully used in the case of both non-linear and non-stationary signals and as a matter of fact it is its time-and-frequency representation which can serve this purpose. The key part of the transform, and at the same time its advantage which consists of the ability to adapt to a real-life signal, is the so-called sifting process which leads to obtaining of individual components of the original function. Compared to majority of other methods, the EMD method is intuitive and simple, it operates without any information whatsoever about the analyzed function, and it is executed directly on the basis of the original time signal.

EMD relies on the assumption that each complex signal consists of intrinsic functions which are a representation of simple forms of vibration. Each of such forms, linear or non-linear, will contain the same number of extremes and zero places. In each point in time the function can have many various co-existing forms of vibration which are in super-position to each other. The decomposition of a given series of data relies directly on isolation of energy runs (functions) which are contained within the time run of the entire analyzed sample and it can be presented as propagation of information which corresponds to subsequent internal IMF's - intrinsic mode functions, however each such a function has to meet the following requirements:

- in the entire scope of the signal the number of extremes and zero places must be equal or must differ by one,

- at each point the average value of the envelope defined by local maximums and of the envelope defined as local minimums is equal to zero.

The ability to analyze and detect even momentary changes in the signal and adaptability are necessary for analyzing the non-linear and non-stationary runs. Each inherent IMF function represents a simple form of vibration which is considered to be identical to a single harmonic of a function. The obtained local sequences of energy changes and of momentary frequency, obtained from consecutive inherent functions, can be used for constructing the full energy-time-frequency distribution of analyzed data [8].

With the use of the theory of empirical decomposition of the EMD signal, each signal can be decomposed in the following way.

In the first step one should identify all the local extremes and then approximate two functions: one function which passes through the local minima and the other which passes through the local maxima. The obtained curves will be respectively the bottom and the top envelope of the analyzed signal. The average function between the envelopes will be marked as m_1 , while the difference between the original signal $x(t)$ and $M1$ will be the first component of h_1 :

$$x(t) - m_1 = h_1 \quad (2)$$

In the ideal case, if h_1 meets requirements for an IMF inherent function, then h_1 is the first component of function $x(t)$.

If h_1 is not an IMF, then it is treated as the original signal and the above procedure is repeated:

$$h_1 - m_{11} = h_{11} \quad (3)$$

Various criteria of the alloy were developed to guarantee the physical sense of the function which emerges in the process of sifting. [9]. It can be, for example, expressed in the following way:

$$\sum_t \frac{[h_{k-1}(t) - h_k(t)]^2}{h_{k-1}^2(t)} < SD \quad (4)$$

where $h_k(t)$ is the signal obtained as a result of k-th sifting iteration, while SD (standard deviation) is usually assumed at around 0.2-0.3.

Then the identified form becomes a component:

$$c_1 = h_{1k} \quad (5)$$

The first component is obtained from the original signal and that is why it will have the biggest scale and the shortest period.

By isolating c_1 from the original signal (t), we get:

$$r_1 = x(t) - c_1 \quad (6)$$

Where r_1 is treated as the original signal and the whole above describe process of sifting is repeated for r_1 . The second component of $x(t)$ function should be obtained this way.

The whole process is rerun n times and thus IMF inherent functions can be obtained and then:

$$\begin{aligned} r_1 - c_2 &= r_2 \\ &\vdots \\ &\vdots \\ r_{n-1} - c_n &= r_n \end{aligned} \quad (7)$$

The decomposition process can be stopped when r_n becomes a monotone function from which no inherent IMF function can be obtained anymore (Fig. 2).

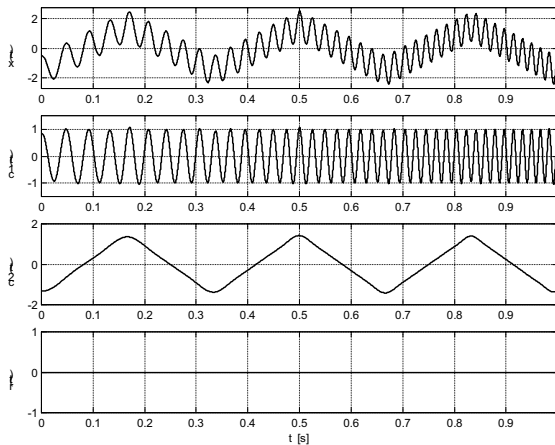


Fig. 2. An example of operation of the method of signal distribution to EMD empirical modes

To recapitulate the whole process:

$$x(t) = \sum_{j=1}^n c_j + r_n \quad (8)$$

This way (as in Fig. 3) we can obtain decomposition of a signal into n empirically obtained functions and residue r_n , which is the average trend of function $x(t)$. Subsequent IMF $c_1, c_2, c_3, \dots, c_n$ contain further varied frequency bands of the original signal, from the band with the highest to the band with the lowest frequency.

Empirical decomposition of signals, as proven by many publications [10, 11, 12], is a method which introduces a new quality and possibilities to analysis of complex non-stationary as well as non-linear signals. It has been tested in a wide scope of diagnostic tasks, i.e. in diagnosis of bearings, toothed gears as well as complex technical systems. EMD is capable of adapting to the signals coming from the above listed technical objects and to

effectively identify the processes taking place in a signal's structure which correspond to changes of a machine's technical condition. The presented properties of Hilbert Huang transform have induced us to try to use this technique of signal processing to analyze the vibroacoustic signal in a gigacycle experiment.

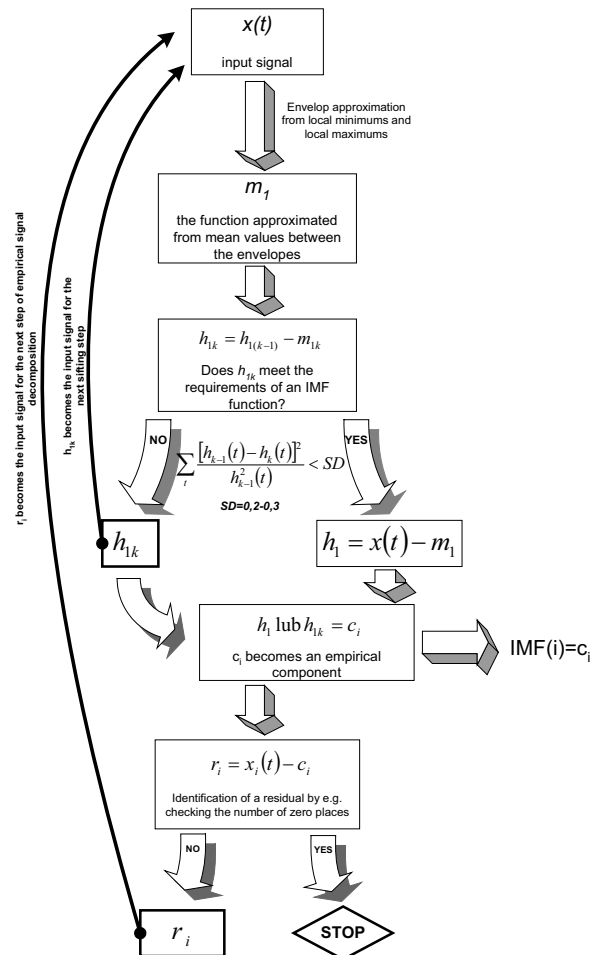


Fig. 3. Block diagram of the EMD shifting algorithm

4. THE EXPERIMENT

During the experiment a laser vibration meter was used to measure the vibration of the end of a beam. In the case of the analyzed test, the beam broke after ca. 2 million of vibration input cycles. Analysis of vibration signals by means of the Hilbert Huang transform enabled detection of a signal's features and the changes occurring in the signal, which are of key importance for analyzing the condition of an object in the case of examination of fatigue processes.

It turned out that the resonant frequency of the beam's vibration carries the information on the wear of the beam. As the number of cycles increased, the resonant frequency decreased. The analysis of the form of signals following the EMD (Empirical Mode Decomposition) decomposition

for the beam's vibration signals enables tracking and shows how the resonant frequency changes after a certain number of input cycles. The graphs (Fig. 5÷8) show the spectra of relevant components of the signal which have been obtained by applying the Hilbert Huang Transform (HHT), which consecutively correspond to the measurements: a – at the beginning of the experiment, b – after 1 million cycles, c - after 1.5 million cycles, d – after 2 million cycles. It is clearly visible how rapidly the resonant frequency decreases along with the growth of the number of cycles which have direct impact on crack development (Fig. 4) – it is the physical symptom of a defect. Such observation is in line with the course of the experiment and the general knowledge on development of fatigue processes.

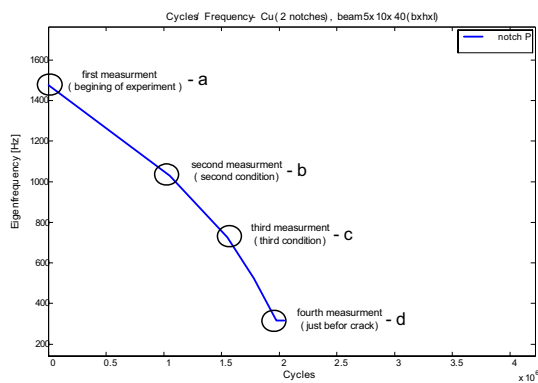


Fig. 4. The beam's resonant frequencies as a function of consecutive cycles, with the places marked at which HHT was calculated

Further graphs present the spectra for respective decompositions of time signals developed for the signals registered in various phases during the fatigue-related experiment (Fig. 5-8). Subsequent components of the signal, which correspond to various frequency bands, are obtained as a result of "sifting" while using the HHT method.. First the highest frequencies are discovered, which are followed by further lower frequencies corresponding to a band which is by half smaller than the preceding one. While analyzing a series of spectra obtained this way in our fatigue experiment, we can see how the resonant frequency, which contains diagnostic information, changes its position to one corresponding to a lower frequency but it also changes the position related to obtaining its pattern in a different empirical component. This can be seen in the figure, where for the third stage the measurement was performed after 2.5 million cycles, and we do not find any resonant frequency in the spectrum of the first component – the resonant frequency can be discovered only after the next operation of empirical decomposition of the signal. This additional relation between crack development stage and the property of Hilbert Huang transform can prove useful for diagnostic inference.

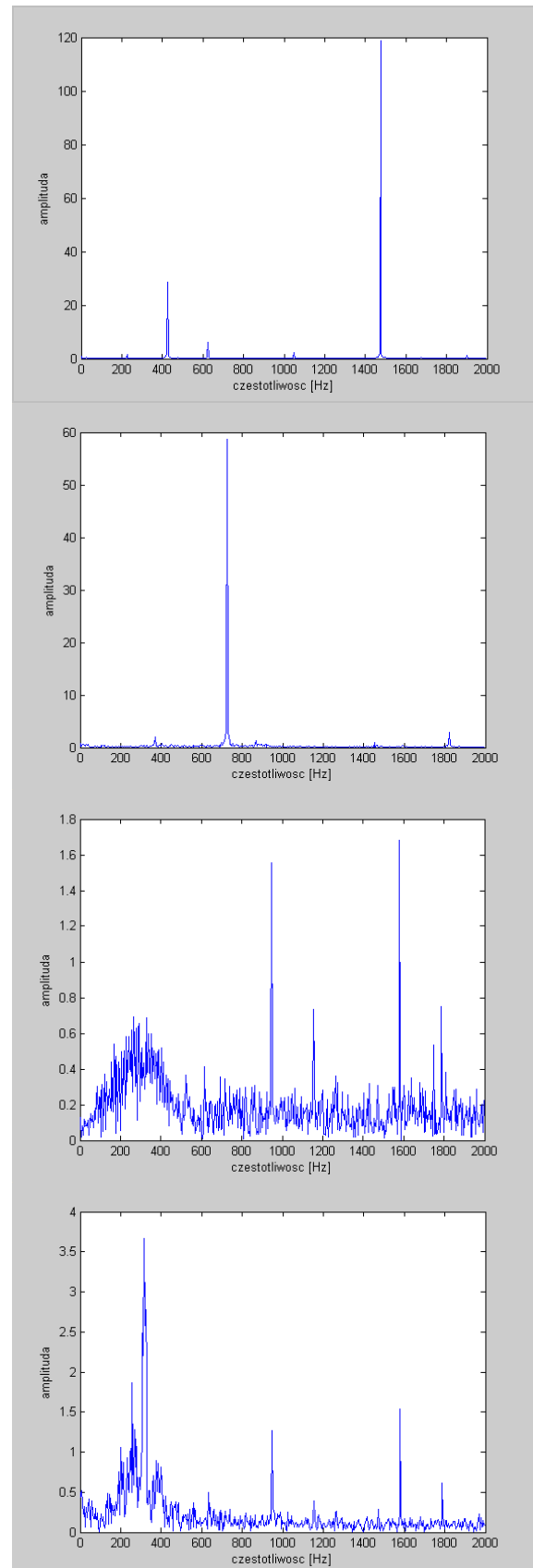


Fig. 5. Entire spectrum – obtained from the first form of the signal after EMD – further states which correspond to the measurement points on the graph

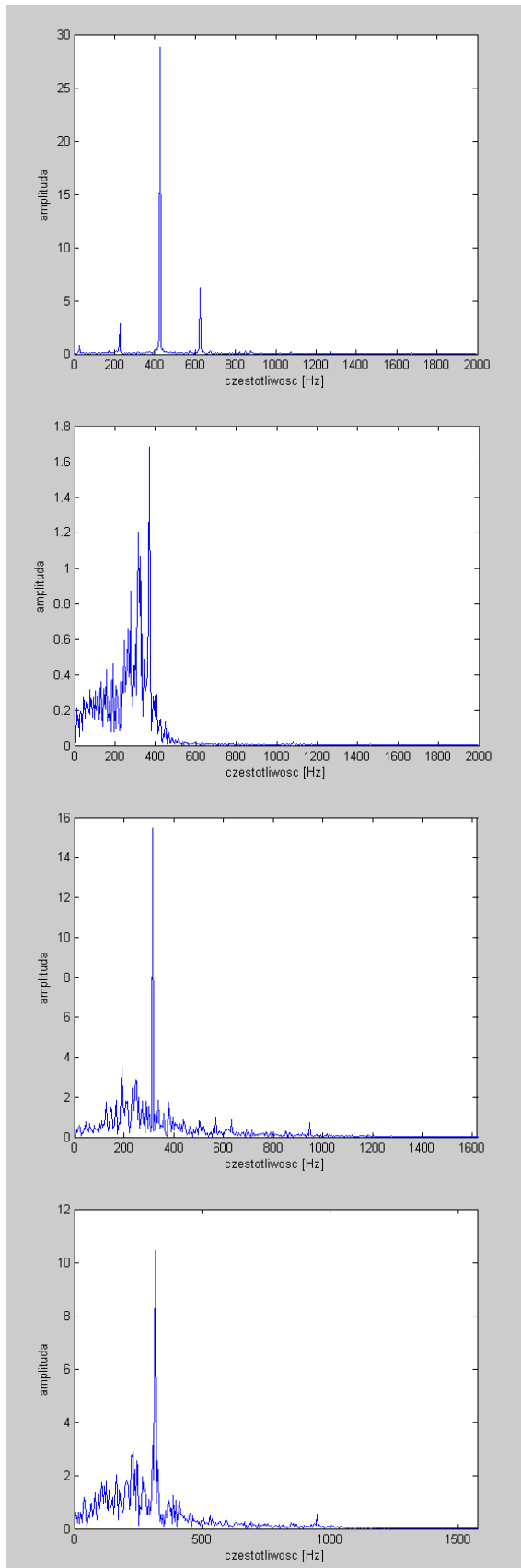


Fig. 6. 1/2 of spectrum – obtained from the second form of the signal after EMD – further states which correspond to the measurement points on the graph

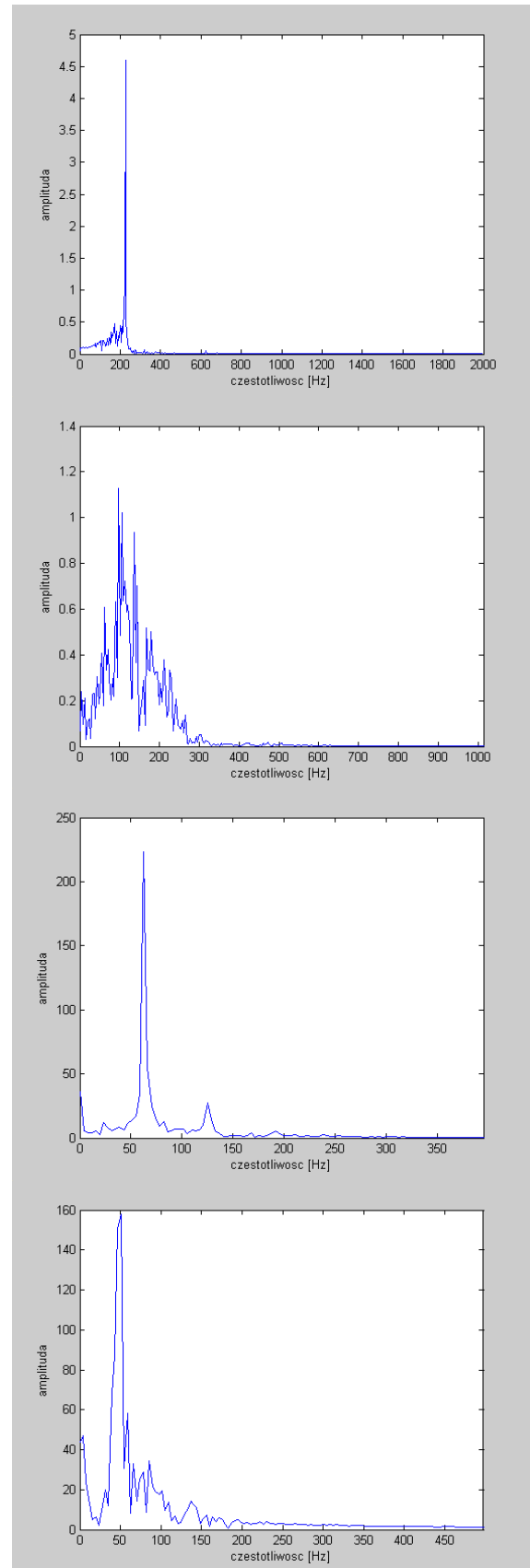


Fig. 7. 1/4 of spectrum – obtained from the third form of a signal after EMD – further states which correspond to the measurement points on the graph

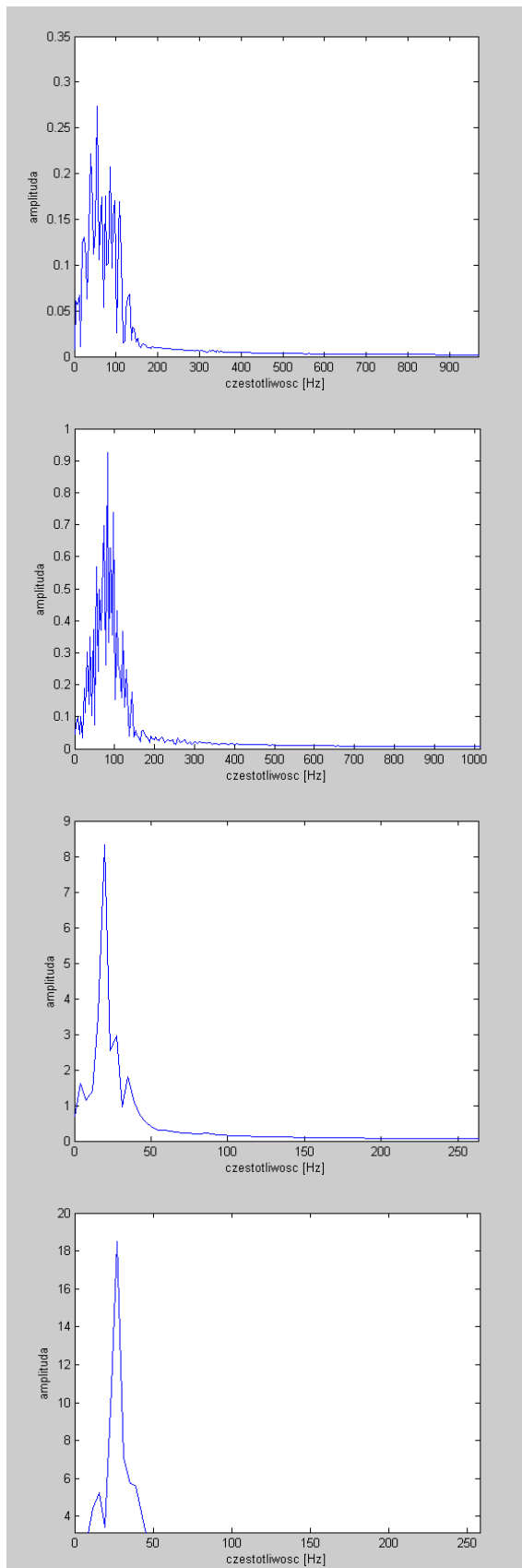


Fig. 8. 1/8 spectrum – obtained from the fourth form of a signal after EMD – further states which correspond to the measurement points on the graph

As we have already demonstrated, development of degradation processes leads to decrease of frequency of an object's proper vibration. In our case the object was a vibrating beam. Use of the Hilbert Huang transform has enabled discovery of the fact that the dynamics of decrease of resonant frequency depend on the phase of crack of development. In the early phases of fatigue the resonant frequency changes significantly as a function of consecutive cycles and then the dynamics of its decrease become reduced as the critical values of cracking are approached. In the case of the analysis relying on HHT, this property leads to exposition of amplification of low frequency bands (respectively for $\frac{1}{4}$ and $\frac{1}{8}$ of the spectrum (Fig. 6 and 7)) – a relevant level of signal decomposition has to be reached in order for this to be observed. To recapitulate, observation of spectra for further components of empirical signal decomposition ($\frac{1}{8}$, $\frac{1}{16}$ spectrum) and to be more precise the growth of energy which occurs in low frequency bands, offers information on the approaching stage of fatigue-related crack emergence (Fig. 8).

4. CONCLUSIONS

The paper proposes development of assessment of the phases of fatigue-related defect development while relying on the defect-oriented analysis of a vibroacoustic signal's parameters. The results of the research, which has been conducted to-date in the Laboratory of the Mechatronics System of Vehicles and Construction Machinery of Warsaw University of Technology, confirm the possibility of developing, on such basis, of both qualitative and quantitative measures of fatigue-related defects' development.

It has been demonstrated that Hilbert spectrum obtained after applying signal sifting with the use of HHT method is a good measure of degradation process development while selection of a relevant level of decomposition enables determination of the degradation phase. The quantitative and the qualitative analysis of a vibroacoustic signal processed this way enables construction of relevant diagnostic measures which define the phase of defect development.

The obtained results of research, which involved an experiment conducted at a unique test-bed for gigacycle analysis of fatigue-related processes as well as use of relevant research procedures, which included unique worldwide attempts of exploiting the vibroacoustic signals' features for forecasting of gigacycle fatigue strength, point to the big possibilities offered by such a method of research and analysis, and they should be continued.

The paper was prepared on the basis of researches conducted within a project „Monitoring of Technical State of Construction and Evaluation of its Lifespan” (MONIT). Project is co-financed by the European Regional Development Fund in the Operational Programme Innovative Economy (PO IG 1.2).

BIBLIOGRAPHY

- [1] Marines I., Bin X., Bathias C.: *An understanding of very high cycle fatigue of metals*. International Journal of fatigue, Vol. 25, 2003, str. 1101÷1107.
- [2] Bathias C., Paris P.C.: *Gigacycle Fatigue in Mechanical Practice*. Marcel Dekker, New York, 2005.
- [3] Radkowski S.: *Wibroakustyczna diagnostyka uszkodzeń niskoenergetycznych (Vibroacoustic diagnosis of low-energy defects)*. Instytut Technologii Eksploatacji, Warszawa-Radom, 2002.
- [4] Gumiński R., Jasiński M., Radkowski S.: *Small-sized test bed for diagnosing the gigacycle fatigue processes*. Diagnostyka, nr 45, 2008.
- [5] Jasiński M., Radkowski S.: *Use of the Contactless Measurement Method in the Frequency-Control System of the Gigacycle Fatigue Test*, Proceedings of the Symposium Plasticity 2009, St Thomas, Virgin Islands, USA, 2009.
- [6] Jasiński M., Radkowski S.: *Use of the higher spectra in the low-amplitude fatigue testing*. Submitted to International Journal of Plasticity, September 2009.
- [7] N.E. Huang, Z. Shen, S.R. Long, M.L.C. Wu, H.H. Shih, Q.N. Zheng, N.C. Yen, C.C. Tung, H.H. Liu: *The empirical mode decomposition and the Hilbert spectrum for nonlinear and non-stationary time series analysis*, Proceedings of the Royal Society of London Series A – Mathematical Physical and Engineering Sciences 454 (1998) 903-995.
- [8] B. Liu, S. Riemenschneider, Y. Xu: *Gearbox fault diagnosis using empirical mode decomposition and Hilbert spectrum*, Mechanical Systems and Signal Processing 20 (2006) 718-734.
- [9] Norden E. Huang: *Introduction to the Hilbert-Huang transform and its related mathematical problems*. Goddard Institute for Data Analysis, Code 614.2, NASA/Goddard Space Flight Center, Greenbelt, MD 20771, USA
- [10] Dejie Yu, Junsheng Cheng, Yu Yang: *Application of EMD method and Hilbert spectrum to the fault diagnosis of roller bearings*, Mechanical Systems and Signal Processing 19 (2005) 259–270
- [11] S.J. Loutridis: *Damage detection in gear systems using empirical mode decomposition*, Engineering Structures 26 (2004) 1833–1841
- [12] Dan-Jiang Yua, Wei-Xin Ren: *EMD-based stochastic subspace identification of structures from operational vibration measurements*, Engineering Structures 27 (2005) 1741–1751



Szymon GONTARZ, M.Sc., a Ph.D. student in SiMR Department of Warsaw University of Technology. In his scientific work he deals with vibroacoustic analysis, security of technical systems, signal processing and non destructive techniques for technical diagnosis.



Marcin JASIŃSKI, Ph.D. a lecturer in Laboratory of Automotive Mechatronics System of Institute Automotive Engineering of Warsaw University of Technology. In his scientific work he deals with vibroacoustic diagnosis, empirical models and Automotive Mechatronics.



Prof. Stanisław RADKOWSKI, a professor in Institute of Institute Automotive Engineering of Warsaw University of Technology, manager of Laboratory of Automotive Mechatronics System. In his scientific work he deals with vibroacoustic diagnosis and technical risk analysis.

FAILURE ORIENTED DIAGNOSTIC MODELS IN CONDITION MONITORING

Stanisław RADKOWSKI*, Maciej ZAWISZA**

*The Institute of Automotive Engineering, Warsaw University of Technology
Narbutta Str. 84, 02-524 Warsaw, Poland, ph. +48-22-234-8118, ras@simr.pw.edu.pl

**Institute of Machine Design Fundamentals, Warsaw University of Technology
Narbutta Str. 84, 02-524 Warsaw, Poland, ph. +48-22-234-8276, mzawisza@simr.pw.edu.pl

Summary

Main aim of paper is to present problems of use of physical probabilistic models in task of decreasing of uncertainty of prognosis of raise and evolution of failure. Presented considerations are supported by example of fatigue analysis of tooth breaking in gearbox.

Keywords: diagnostic, physical probabilistic models, fatigue failure of tooth in gearbox.

USZKODZENIOWO ZORIENTOWANE MODELE DIAGNOSTYCZNE W MONITOROWANIU STANU OBIEKTÓW TECHNICZNYCH

Streszczenie

Głównym celem pracy jest przybliżenie problematyki zastosowania fizykalnych modeli probabilistycznych w zadaniu zmniejszenia niepewności prognozy odnośnie powstawania i ewolucji uszkodzenia. Prezentowane rozważania oparte są na przykładzie zmęczeniowego wyłamania zęba w przekładni zębatej.

Słowa kluczowe: diagnostyka, modele diagnostyczne, zmęczeniowe wyłamanie zęba.

1. INTRODUCTION

The extension of equipment lifetime is the main purpose of maintenance strategy. Correct maintenance strategy can extend mean time to the failure, reduce the frequency of service interruptions and allow to avoid the undesirable consequences of catastrophic damages.

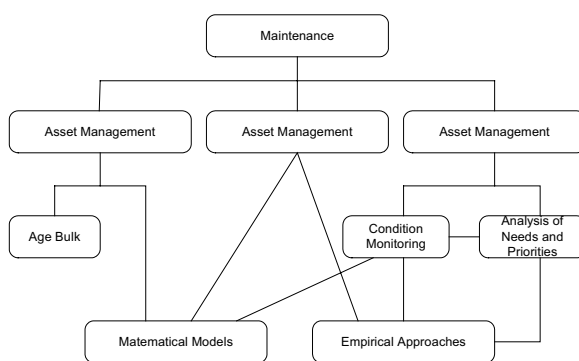


Fig. 1. Schedule of maintenance approaches

In other words, maintenance has relevant impact on components and system reliability. Therefore many companies replaced their scheduled maintenance with more flexible procedures based on a study of information obtained through condition monitoring and predictive maintenance strategy. Figure 1 presents a specification of the various maintenance activities.

Maintenance models range from very simple to quite sophisticated. The simple rigid maintenance schedule defines activities that are carried out at fixed time intervals. The maintenance intervals are evaluated on the long-term experiences. For a complete evaluation one would have to know how the monitoring will extend the lifetime of component. To find this out the deterioration process of components have to be modeled.

2 MODELING OF CHANGES IN PROBABILITY DISTRIBUTIONS

In models that have been analyzed up to now probability of defect occurrence with assumption of invariability of examined distributions in operation time was determined. In reality, as a result of occurrence of wear and tear processes and the associated changes of the conditions of mating of elements and kinematic pairs, the evolution of probability distribution can be observed, both in quantitative terms (change of the parameters of probability density function) as well as in qualitative terms (change of the function describing the distribution). In addition, the degradation processes which accompany performance of the functional task can cause similar variation of probability distributions describing the load-carrying capacity. In this case it can be expected that location of the separating line and the probability of defect occurrence will be dependent on the operating time. Recently numerous methods of examination and

analysis of time-dependent reliability functions have been developed [1, 2, 3]. Examples of such changes are presented in Figure 2.

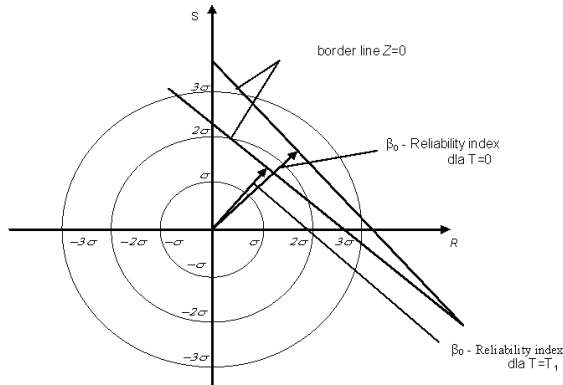


Fig. 2. Illustration of impact of wear and tear on the value of the reliability index

In general random nature of additional load resulting from environmental impact is assumed, however the basic load associated with realization of functional tasks remains a determined value. Still, in the models which take into account relation between the load as well as manufacturing and assembly errors and also for the impact of wear and tear, also this type of load will have random nature. For example, the analysis of the process of emergence of tooth defects in toothed gears points to the fact that the growth of disturbance of contact conditions is accompanied by the phenomenon of amplitude-and-frequency modulation of a signal's parameters [3]. This means that the diagnostically-essential information in such a case is contained in a restricted frequency band where the structure of distribution of power among respective components depends on the type and size of modulation. Assuming the random nature of the input signal $x(t)$ (normal distribution), the probability density of the envelope takes the form which is compatible with Rayleigh distribution [2]:

$$f(A, \sigma) = \frac{A}{\sigma^2} \exp\left[-\frac{A^2}{2\sigma^2}\right] \quad \text{dla } A > 0 \quad (1)$$

where:

$A(t)$ - signal envelope,
 σ^2 - variance of the analyzed narrowband process.

The form of probability density, as described by relationship (1) does not cover the disturbance associated with the occurrence of additional non-linear adjoints, what is connected with the necessity of analysis of third and fourth order moments (2) (Fig. 3).

Thus to extract the information on the type and size of disturbance one must first select the frequency band and apply relevant signal demodulation techniques. The difficulties which occur when using the more complex method of

evaluating defect probability result in more interest shown in the attempts of updating the values of strength and load distribution parameters in time of observation and measurements. Assuming that the distribution parameter is a random variable, which defines the a priori form of the probability density function, the a posteriori distribution upon conducting an experiment (observation) can be determined. It is often assumed that the obtained distribution is conditional, which enables Bayes theorem to be applied. Another example of a method of updating the value of parameters is to determine the a posteriori distribution with the use of credibility function.

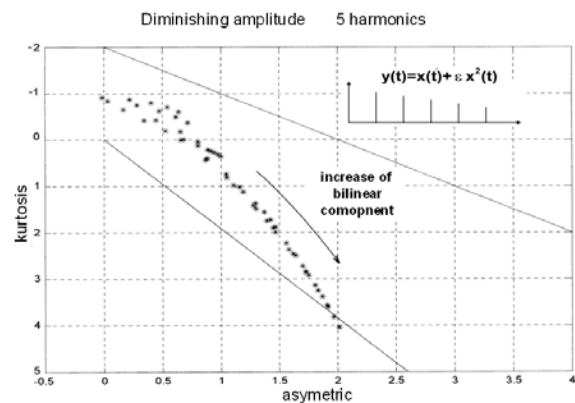


Fig. 3. Example of changes of higher moment values caused by non-linear disturbance

In any approach the main issue is extraction of the relevant diagnostic information. The results of the research confirm that as a result of wear and tear the quality of mating of individual elements and kinematic pairs changes, leading to evolution of load probability distribution. The observation concerns both, the changes of the values of density function's parameters as well as the class of the distribution itself. Similarly, the occurring degradation processes can cause changes in distribution of probability of permitted load capacity. Research [3] confirms the possibility of occurrence of such disturbance.

3. EXAMINATION OF RELIABILITY IN THE FIELD OF STANDARDIZED VARIABLES

The basis for conducting such analyses is such a knowledge of basic parameters and architecture of the system so that it is possible to define the sources and the types of uncertainty. This enables us to contemplate the models of designed objects while accounting for future behavior, state of knowledge of operational processes in the conditions of load which varies in time. In such a case the basic tool is the assessment of reliability while using probabilistic models. To present these problems closer, let us put the formula which defines the possibility of defect occurrence in the following way [4]:

$$Z = f(X_1 \dots X_n) = R - S \quad (2)$$

where:

$f(X_1 \dots X_n)$ - the function of random variables which defines the difference between the loads and the load-carrying capacity. Generally it depends on numerous structural, technological, assembly, operational and environmental factors,

R - load-carrying capacity, e.g. strength,
 S - load, e.g. stress.

Assuming that both, load S and load-carrying capacity R are random variables, we can determine their functions of probability distribution density $f_r(x)$, $f_s(x)$.

The method of determining the function is schematically presented in figure 4 where the striped area denotes the possibility of occurrence of $z < 0$, which is interpreted as the probability of failure occurrence.

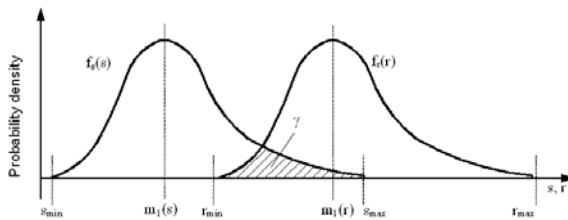


Fig. 4. Exemplary functions of density of load and load-bearing capacity probability

Let us note that the probability depends on the following parameters:

- Relative location of both curves – the expected values and standard deviations of stress and resistance are the parameters which can represent the location;
- In the function of probability density, for non-Gaussian distributions, one should account for the impact of skewness and flatness.

Minimization of probability of defect occurrence is one of the elements of the procedure of reducing the risk level. Determination of the probability of defect p_f can be presented in various ways, for example [1]:

$$P_f = \int_{-\infty}^{s_{max}} \int_{r_{min}}^{+\infty} f_{R,S}(r,s) dr ds \quad (3)$$

where:

r, s – the relevant variables.

Making an assumption that f_s and f_r are independent and taking into account the technical restrictions related to minimum loads and maximum load-carrying capacity, relationship (3) shall be noted as follows:

$$P_f = \int_{s_{min}}^{s_{max}} \int_{r_{min}}^{r_{max}} f_r(r) f_s(s) dr ds \quad (4)$$

Thus an event corresponding to a defect will occur when

$$Z = (R, S) \Rightarrow P_f = P(Z(R, S)) \leq 0 \quad (5)$$

On the assumption that the variables describing load capacity and load have normal distributions, let us now consider the possibility of determining a curve separating the area threatened with the defect from the remaining areas:

$$Z = 0 \quad (6)$$

Let us note that thanks to introduction of standardized variables (2):

$$R' = \frac{R - \mu_R}{\sigma_R} \quad S' = \frac{S - \mu_S}{\sigma_S} \quad (7)$$

the equation of the boundary line $Z=0$, defined by the formula (2), while assuming that the contemplated variables have normal distribution, shall take the following form:

$$Z = \sigma_R R' - \sigma_S S' + \mu_R - \mu_S \quad (8)$$

In analyzed case of standardized variables plane, it will be obtained:

$$p = \beta = \frac{\mu_R - \mu_S}{\sqrt{\sigma_R^2 + \sigma_S^2}} \quad (9)$$

where:

β - reliability index in n-determined spaces.

Hence

$$P = \Phi\left(-\frac{\mu}{\sigma}\right) \quad (10)$$

Thus, we have obtained a measure which indicates, in the (S', R') system, that as the boundary line moves away from the beginning of the coordinate system, hence the probability of a failure decreases.

Referring now to the relationship which defines the distribution function of the standardized normal distribution:

$$\Phi(x) = \frac{1}{2\pi} \int \exp\left[-\frac{1}{2}t\right] dt \quad (11)$$

as well as the probability densities for such distribution (5), the relation defining the probability of a defect (10), as defined by β reliability indicator, shall finally take the following form:

$$P(Z \leq 0) = P = 1 - \Phi(\beta) \quad (12)$$

which in turn enables using the values of the distribution function $\Phi(x)$, found in a table for $x > 0$, or the standardized programs for calculating the probability of normal distribution. Tables containing the values of the distribution function are found in majority of handbooks related to probability calculus and mathematical statistics.

This means that regarding the methods of calculating the probability of a defect, which were mentioned in the first part of the paper, we can use iteration procedures of increasing forecast precision by updating probability density function for permitted load and load-capacity. The specific method depends on the scope of the adopted diagnosis as well as the type of the observed defect. In general one can note that the biggest possibilities of correct solving the problem formulated this way are connected with the fact of reaching of such a diagnostic information for which diagnostic model can be built, which in its essence refers to the process of defect origin and development.

In task outlined this way it becomes important to select the threshold values which will define the selection of ranges and variability classes, respectively for the parameters of distribution and the probability density function.

Summarizing attention can be drawn to the fact that the main reasons of uncertainty of evaluations and analyses are:

- the procedures determining the values of parameters, e.g. small size of samples can have influence on the width of confidence intervals, extrapolation of data from one facility to another, disturbances in observation of data;
- modeling procedures which are focused on determining the essential variables and usually take into account their mutual detailed relations in an unsatisfactory manner;
- the nature of the phenomenon; the status of knowledge that does not always enable to take into account all the important factors, especially the course of defect-generation processes.

Higher credibility of forecasts can be obtained by including the changes of the diagnostic parameter resulting from wear and tear processes. As a result, when forecasting the probability of an emergency situation it becomes necessary to introduce the information about these material changes.

Authors traced such a procedure while analyzing the phenomenon of fatigue-related tooth fracture in a toothed gear. An assumption was made of variability of parameters of load distribution without change of its form and in addition the disturbance of their changes, resulting from defect initiation and propagation, was taken into account. For this purpose information was used from an experiment in which changes of stress at the foot of a tooth in the course of accelerated fatigue tests of a toothed gear (Fig. 5) was traced.

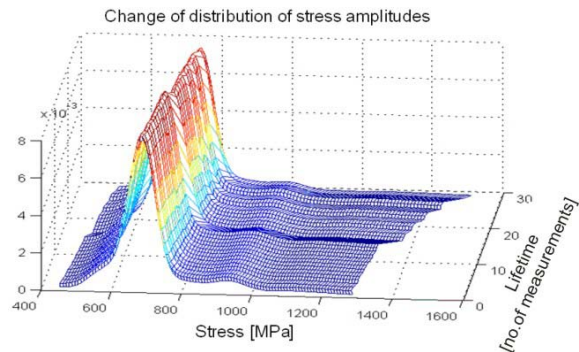


Fig. 5. Change of distribution of stress amplitudes at the foot of a tooth during the experiment

The values of these parameters were standardized in such a way so that they were adequate to the changes of undisturbed distribution. The reliability indicator was the parameter that was observed.

It turned out that if changes of material properties, resulting from wear and tear fatigue-related tooth fracture, were not taken into account, forecasting of the emergency state of a toothed gear is burdened with too big error (Fig. 6).

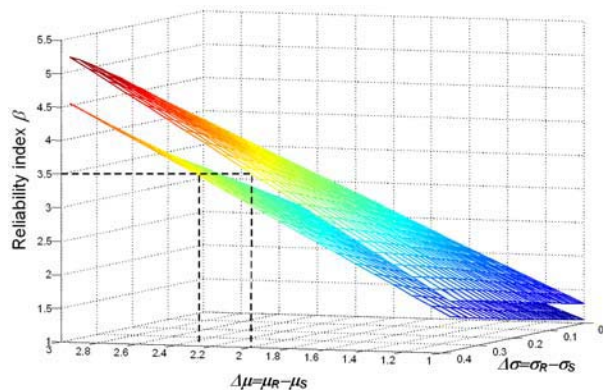


Fig. 6. Change of reliability indicator while not including and while including the wear and tear processes.

4. CONCLUSIONS

Presentation of a relatively simple example was aimed at demonstrating the use of physical probabilistic models in the tasks of reducing the uncertainty of forecasting related to emergence and evolution of defects. The direct application of the presented approach may call for applying, at least, the transformation of probability distribution, procedures of system, linearization and examination of the degree of variables correlation. Still, the main proceedings will preserve their nature.

REFERENCES

- [1] T. A. Cruse: *Reliability Based Mechanical Design*, Marcel Dekker Inc., New York 1997.
- [2] S. Radkowski: *Estimation of failure development basing on envelope analysis of vibro-acoustic signal*, XXV SDM, Węgierska Górka, 1/98, pp 165-178, 1998.
- [3] S. Radkowski: *Usage of vibration signal in assessment of technical risk of fatigue break of tooth*, *Network methods in reliability engineering*', XXVII Zimowa Szkoła Niezawodności, vol II, str. 109-118, Szczyrk 1999.
- [4] B. M. Ayyub, (ed): *Uncertainty Modeling and Analysis in Civil Engineering*, CRC Press LLC, 1998.
- [5] W. Kryszewski, J. Bartos, W. Dyczka, K. Królikowska, M. Wasilewski: *Theory of probability and mathematical statistics*, part I, Wydawnictwo Naukowe PWN, Warszawa 2001.



Prof. **Stanisław RADKOWSKI**, a professor in the Institute of Automotive Engineering of Warsaw University of Technology, manager of the Technical Diagnosis and Risk Analysis scientific team, Chairman of Polish Society of Technical

Diagnosis. In his scientific work he deals with vibroacoustic diagnosis and technical risk analysis.



PhD Eng **Maciej ZAWISZA** Employed at Institute of Machine Design Fundamentals, Warsaw University of Technology; Faculty of Automotive and Construction Machinery Engineering, Member of PTDT. In his scientific work he deals with vibroacoustic diagnosis.

KOMPUTEROWE PRZETWARZANIE SYGNAŁÓW ULTRADŹWIĘKOWYCH

Marcin STARNACKI

Przemysłowy Instytut Telekomunikacji S.A.
ul. Poligonowa 30 04-051 Warszawa, fax. 22 813 0205, email: mstarnacki@pit.edu.pl

Streszczenie

Właściwości użytkowe materiałów wykorzystywanych w przemyśle zbrojeniowym ulegają obniżeniu pod wpływem warunków eksploatacji takich jak temperatura, środowisko pracy oraz naprężenia. Zjawisko to określane jest mianem degradacji materiału i spowodowane jest wieloma procesami zachodzącymi w strukturze eksploatowanego materiału. Efektem tego jest konieczność stosowania metod umożliwiających rozpoznanie i ocenę stopnia degradacji materiału w celu jego dalszego bezpiecznego użytkowania. Ważnym elementem podjętego problemu są komputerowe możliwości oceny badanych struktur kompozytów. Wykorzystano w tym celu wybrane metody sztucznej inteligencji. Wyniki pomiarów powstają na podstawie elementów, które poddawane są systematycznej ocenie poprzez badania nieniszczące, w których wiodącą metodą są pomiary ultradźwiękowe. Badaniom poddawano próbki kompozytowe polimerowe.

Słowa kluczowe: ultradźwięki, defektoskopia, sztuczna inteligencja.

COMPUTER ULTRASOUNDS PROCESSING

Summary

As a result of exploitation of materials in industry their properties are reduced. The reason for which it occur are temperature, environment when it works and stress. This situation is called material degradation. As a result of this it is necessary to use method which makes possible detection and assessment degree of material degradation. It is necessary to qualify further abilities of the material to be used safely. The most important part of this problem are computer based abilities assessment examined of composite structures. To achieve this, selected methods of artificial intelligence (AI) were used. The results of measurement are generated on the basis of elements, which are systematically assess in non destructive testing (NDT). In NDT, among others ultrasonic testing methods are used. In testing polymer composite samples were used.

Keywords: ultrasound, defectoscopy, artificial intelligence.

1. WPROWADZENIE

Potrzeba zwiększenia precyzyjności otrzymywanych wyników monitorowania stanu struktury materiałów kompozytowych jest związana przede wszystkim z uwarunkowaniami ekonomicznymi, bezpieczeństwem ludzkim oraz ekologią środowiska naturalnego. W tym celu przeprowadzane jest wiele badań nad rozwojem metod nieniszczących używanych do testowania wykonanych kompozytów, w których najbardziej efektywną są pomiary ultradźwiękowe [2].

Wymagane jest aby badania ultradźwiękami elementów kompozytowych wykonywane były okresowo tak jak to ma miejsce w przemyśle lotniczym oraz wszędzie tam gdzie materiały eksploatowane są w szczególnych warunkach. W przypadku niektórych samolotów pasażerskich w około 25% składają się one z materiałów kompozytowych, których niekontrolowana degradacja mogłaby doprowadzić do katastrofy

w przypadku braku polityki bezpieczeństwa wykonanego produktu.

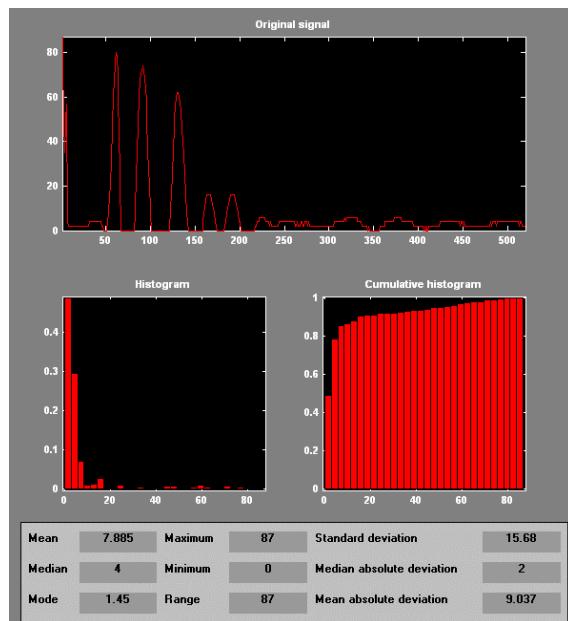
Jednym z najważniejszych etapów badania materiału ultradźwiękami jest późniejsza interpretacja otrzymanych wyników w postaci dyskretnych wartości sygnału dźwiękowego. Sygnały te przesyłane są on-line z głowicy przetwornikowej do komputera i poddawane są przetwarzaniu i wizualizacji. Badanie kompozytów wspieranych przy pomocy opracowanego programu UTracker umożliwia na bieżąco śledzić wady wykryte w materiale od początku jego przechwycenia. Powoduje to szybsze i dokładniejsze wskazanie całego obszaru defektu materiału.

Wykrywane przez program wady są bazą danych dla sztucznej sieci neuronowej, która otrzymuje je w postaci wektorów liczbowych i dokonuje na nich samoorganizacji. Powstają dzięki temu skupiska obiektów w przestrzeni dwuwymiarowej nazywane grupami. Są one charakterystyczne dla poszczególnych grup wad materiałów, które każdy musi określić sam.

Celem niniejszego artykułu jest raport z przeprowadzonych testów rozpoznania poprawności wykrywania wad w wybranych materiałach kompozytowych wspieranych technologiami komputerowymi.

2. ULTRADŹWIĘKI W DEFEKTOSKOPII

Głównym problemem w defektoskopii jest wykrycie lub zlokalizowanie obszarów w testowanym obiekcie. W tym przypadku jest to płytka kompozytu polimerowego. W większości przypadków wady materiału nie są wykrywalne gołym okiem tylko są skumulowane w wewnętrznej strukturze obiektu. W celu oceny jakości struktury materiału możemy wykonać dowolnym narzędziem do przetwarzania obrazów histogram tego obiektu. Wizualnie możemy ocenić różnice w statystycznym rozkładzie składowych otrzymanego sygnału oraz kolejnych sygnałów z przetwornika jak pokazane jest na rys. 1. Jest to najprostszy sposób wykazania nieprawidłowości w materiale.



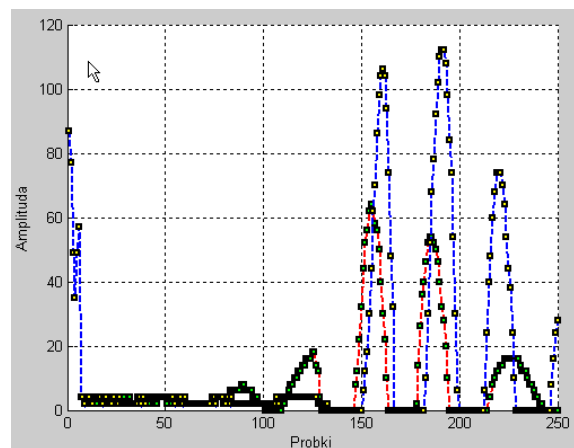
Rys.1. Przebieg sygnału oraz jego histogramy

Ludzkie ucho umożliwia odbieranie dźwięków o częstotliwości 20 – 20 000 Hz. Ultradźwięk jest dźwiękiem [5], którego częstotliwość jest większa niż 20 000 Hz. Ultradźwięk diagnostyczny operuje w zakresie od 1 do 10 MHz. Kierunek w jakim podąża fala ultradźwiękowa jest taki sam jak ruch cząstki. Fale są wytwarzane przez przetwornik ultradźwiękowy. Cechą jaką posiada fala ultradźwiękowa jest przenikania przez dane medium, które jest ograniczone przez właściwości tego medium; te właściwości obejmują gęstość i elastyczność. Określają one impedancję akustyki dla danego medium. Przenikanie fali jest także ograniczone przez częstotliwość przetwornika: wyższe częstotliwości mają krótsze długości fali

oraz mniejsza zdolność penetracji materiału niż niższe częstotliwości.

Ponieważ ultradźwięk napotyka warstwy w materiale o różnej impedancji akustycznej, tak więc prędkość fali przechodzącej przez medium ulega modyfikacji tak że wracające echa są odbierane przez przetwornik w różnych czasach oraz zmiennej intensywności. Komputer odbiera tylko dyskretne dane z każdego wykonanego kroku wysłania fali ultradźwiękowej oraz odebrania echa. Właściwość przenikania fali przez materiał pozwala zbudować diagnostyczny obraz na monitorze.

Problem jaki się pojawia to błędy pomiaru a raczej przesunięcia pozycji prążków wynikające z niedoskonałości głowicy jedno przetwornikowej, która wykonuje ruch w określonym czasie. Może powodować to zmiany pomiaru obszaru martwego oraz przesunięcia względem siebie pomiaru właściwego jak pokazano na rys. 2. Dlatego też opracowano metodę testową śledzenia wybranej próbki będącej elementem piku sygnału. W założeniu metoda ta śledzi położenie próbki w kolejnych sygnałach co umożliwia śledzenie defektu w materiale na bieżąco.



Rys. 2. Widmo przebiegu dwóch sygnałów w kolejnych punktach pomiarowych

3. BADANIE KOMPOZYTÓW

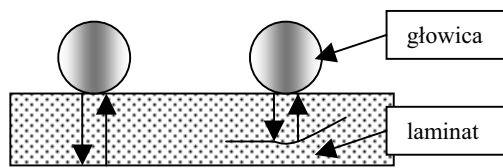
Zwiększone zapotrzebowanie na materiały kompozytowe w przemyśle lotniczym wynika z faktu, że pod wieloma względami przewyższają tradycyjne materiały konstrukcyjne. Wysokie parametry wytrzymałościowe, mała gęstość a co za tym idzie niższa waga w stosunku do tradycyjnych materiałów powoduje tak dużą popularność kompozytów w tym obszarze gospodarki.

Ogólnie kompozytem nazywamy materiał składający się z co najmniej dwóch komponentów o odmiennych właściwościach fizykochemicznych, którego całość zawiera lepsze bądź inne właściwości niż osobno każdy z komponentów. Kompozyt polimerowy badany w tym przypadku składa się z żywicy, która jest bazą dla włókien wzmacniających nadających kompozytowi wytrzymałość i sztywność. Ponieważ składa się

z wielu cienkich warstw połączonych spoiwem nazywany jest laminatem. Można go porównać do naturalnego laminatu jakim jest drzewo.

Pośród różnych metod nieniszczących przeznaczonych do badania kompozytów można wymienić m.in. „Tap test”, „Metoda rezonansowa”, „Metody termowizyjne i interferometryczne” oraz „Metody radiograficzne i ultradźwiękowe”. W przeprowadzonym eksperymencie użyto metody ultradźwiękowej typu A-mode.

Tryb amplitudy (A) wyświetla amplitudy indywidualnych ech jako funkcję dystansu w czasie. Technika ta stosowana jest głównie do badań monolitycznych struktur laminatowych. Jej przeznaczeniem jest głównie wykrywanie wad materiału typu rozwarstwienie, posiadanie ciała obcego oraz porowatość.



Rys. 3. Badanie laminatu techniką A-mode. Głowica badająca laminat bez wad oraz laminat z rozwarstwieniem

Opisana powyżej metoda sprawdza się najlepiej podczas produkcji laminatu kiedy można testować proces spajania warstw w kompozycje. W rozpatrywanym przypadku przeprowadzono wiele testów laminatu w punkcie na całej powierzchni jak pokazano na rys. 3. Na podstawie przeprowadzonych testów zebrano dane liczbowe, które poddawane były obróbce gdzie opisane jest to w kolejnych rozdziałach.

4. PORÓWNYWANIE SYGNAŁÓW PRZY POMOCY FALI ELEMENTARNEJ

Na potrzeby przeprowadzenia eksperymentu stworzono program o nazwie USTracker opracowany całkowicie w języku wysokiego poziomu Matlab. Program ten służy do analizy sygnałów ultradźwiękowych oraz powstałych na ich podstawie tzw. falek (ang. wavelet). Falka jest rodzajem fali skończonej [1] lub inaczej funkcją dążącą do zera, która przekształca reprezentację sygnałów nieskończonych na ograniczonych w czasie. Czyli jest swojego rodzaju filtrem. W artykule przedstawiono sposób śledzenia prążka, który jest elementem piku z wykorzystaniem ciągłej transformaty falkowej (ang. Continuous Wavelet Transform) według funkcji (1).

$$\text{cwt}(S, \text{SCALES}, 'wname') \quad (1)$$

gdzie:

S – sygnał analizowany wektorowy,
 SCALES – skala analizy sygnału,
 wname – skrócona nazwa z rodziny z jakiej pochodzi falka.

Przekształcenie falkowe CWT opiera się na schemacie, w którym falkę podstawową poddaje się skalowaniu i przesuwaniu pozycji wzdłuż badanego sygnału według wzoru (2).

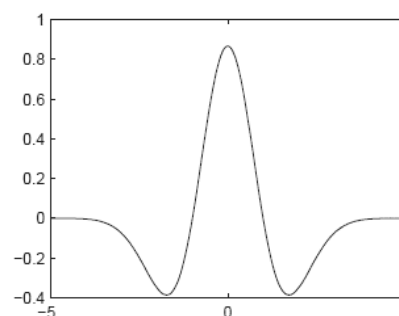
$$C(\text{scale}, \text{position}) = \int_{-\infty}^{\infty} f(t)\psi(\text{scale}, \text{position}, t)dt \quad (2)$$

gdzie:

ψ – falka podstawowa.

Jedną z przyczyn dlaczego wybrano ten rodzaj przekształcenia jest to iż ma ona tę wyższość nad tradycyjną analizą fourierowską, że wyniki analiz podawane są w dziedzinie czasu i częstotliwości, co jest szczególnie przydatne przy analizie sygnałów sporadycznych i nieciągłych.

Falka podstawowa nie jest zawsze sztywno określona, musi jednak spełniać pewne kryteria. Musi mieć m.in. skończoną energię oraz wartość średnią równą zero. Natomiast funkcja skalująca danej falki ma wartość średnią różną od zera. Te wymagania sprawiają, że falka ma postać krótkotrwałej charakterystycznej oscylacji jak na rys.4, stąd wywodzi się jej nazwa. Rozróżniamy wiele typów rodzin falek, które można stosować do analizy sygnałów jednowymiarowych ale także analizy obrazów takich jak dekompozycję oraz kompresje. W przeprowadzonych badaniach poddano transformacji sygnały przy pomocy falek tj. Haar, Daubechies, Coiflets, Morlet oraz Mexican hat. Ich wspólnymi cechami są mianowicie dokładna rekonstrukcja skompresowanego sygnału czy transformacja ciągła. W zależności od użytej falki podstawowej można określić różne cechy sygnału. Falka Mexican hat nadaje się do oceny rozkładu ekstremów sygnału, a falka Morleta do rozkładu amplitud częstotliwości składowych sygnału.

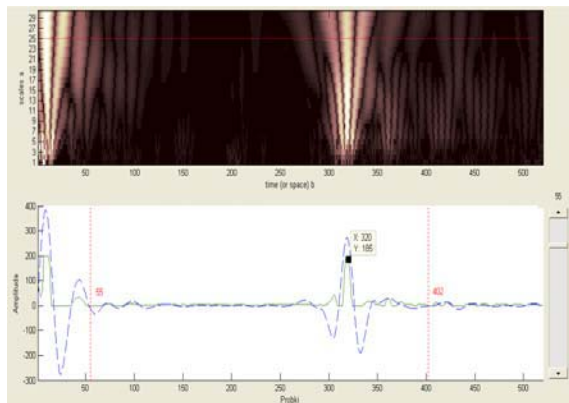


Rys. 4. Falka podstawowa Mexican hat

Posiadanie dodatkowych cech takich jak symetryczność pozwoliło ocenić funkcję falkową Mexican hat jako najlepiej reprezentującą charakter badanych sygnałów.

W eksperymencie na bieżąco kolejne sygnały były poddawane przekształceniom falkowym w skali z przedziału od 1 do 30 według funkcji (1). Jest to przedział wystarczający aby zostały wykryte wszystkie ekstrema sygnału. W wyniku transformaty CWT powstaje widmo parametryczne sygnału stworzone w programie USTracker jak na rys. 5.

Chociaż stworzenie widma współczynników wydaje się trywialne to wstępna interpretacja stawia wiele pytań. Wartości skali w jakiej analizowany jest sygnał określa szerokość falki oraz pozycje na których nastąpi wyliczenie wzajemnej korelacji falki z sygnałem. Mała skala na widmie odzwierciedla lokalne analizy sygnału, natomiast duża skala opisuje globalną analizę.



Rys. 5. Widmo współczynników sygnału dla różnych skal oraz jego wykres oryginalny (kolor zielony) i wykres współczynników dla skali 25 (kolor niebieski)

Nawiązując do rys. 5 na którym przedstawiona została transformata CWT dla sygnału numer 55. Program USTracker ma za zadanie wczytywanie kolejnych sygnałów z bufora oraz przedstawienie ich w postaci graficznej. Operator ma możliwość zweryfikowania widma sygnału widocznego w górnej części rys. 5. Kolor białej jasny oznacza najlepsze dopasowanie falki *Mexican hat* do sygnału czyli posiada najwyższą wartość współczynnika korelacji zawierającej się w przedziale -1 do 1. Korelacja może być dodatnia lub ujemna tak jak przestawia to niebieski wykres na rys. 5. Czerwona pozioma linia informuje, w której skali osiągnięto najlepszą korelację falki i badanego sygnału.

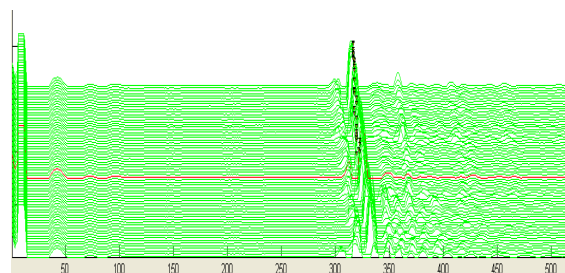
Na dolnej części wykresu na rys. 5 widoczne są dwie pionowe czerwone linie w danych punktach pomiaru. Mają one za zadanie oddzielić strefę martwą sygnału po lewej stronie wykresu oraz zbędne dane, które nie mają znaczenia także w kolejnych pomiarach. Powoduje to oddzielenie zakłóceń jakie wprowadza strefa martwa do naszych obliczeń oraz zmniejszenie wykonywanych operacji obliczeniowych co ma duże znaczenie podczas przesyłu danych w trybie on-line z dużą częstotliwością. W celu śledzenia konkretnego punktu próbki w pikcie zaznaczamy na oryginalnym wykresie współrzędne, które są wyświetlane na bieżąco. Następnie uruchamiany jest proces analizy, który rozpoczyna pobieranie kolejnych sygnałów oraz ich porównywanie. Efektem czego jest wyznaczenie przybliżonego położenia próbki we wszystkich sygnałach pochodzących z badanego materiału.

4.1. Gradient generalizacji

Gradientem generalizacji czyli uogólniania można nazwać wzmocnienie pewnej reakcji na dany układ sygnałów wzmacniającej tendencję do takiego samego reagowania na inne układy sygnałów tym bardziej im bardziej są one do siebie podobne. Czyli należałoby znaleźć wzorce w podstawowym sygnale i próbować znaleźć podobne w kolejnych sygnałach.

Szukanie pików odbywa się według następującej procedury. Fragmenty analizowanego sygnału są kolejno skanowane pod kątem wartości współczynnika transformaty CWT. Stała zmiana gradientu oznacza początek pikcie. Czyli przed osiągnięciem szczytu możemy uznać, że jesteśmy na lewym skrzydle pikcie. Natomiast poza punktem szczytu wstępnie możemy uznać pomiar za prawe skrzydło pikcie.

Powyższy słownie opisany algorytm może rozpoznać jako pikcie pewien fragment analizowanego widma, który pikcie nie jest a tylko częstymi zmianami amplitud. Należy wprowadzić więc warunki przybliżonej ilości liczby próbek na szczycie pikcie co dałoby podstawy sądzić, że są one pikcie. W znalezionym pikcie należy znaleźć odwzorowanie szukanej próbki. Nie zawsze jest to pikcie jeżeli poszukujemy próbki w wadzie materiału. Wynik symulowanej ścieżki szukanej próbki w wadzie pokazano na rys. 6.



Rys. 6. Wykres sygnałów wraz z śledzonym położeniem próbki w defekcie badanego materiału

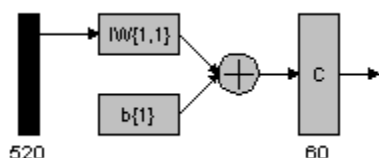
5. MODEL SZTUCZNEJ SIECI NEURONOWEJ

Generalnie sztuczna sieć neuronowa [6], która ma odzwierciedlać pracę ludzkich neuronów zachowuje się najbardziej szczególnie w dwóch kluczowych przypadkach. Po pierwsze wtedy gdy sieć czerpie wiedzę z wydzielonej części świata, którą mu dostarczamy. Wtedy to następuje etap postrzegania cech, które w jakiś sposób opisują badane środowisko. Następuje formowanie pewnych wag będących wskaźnikami przyswajania wiedzy przez sztuczną sieć neuronową. Po etapie nauki możemy wprowadzić sieć w inne środowisko i kazać jej się adaptować na podstawie posiadanej bazy wiedzy. Oczywiście im bardziej złożony problem mamy do rozwiązania tym bardziej doświadczona musi być sieć neuronowa.

Jedną z metod sztucznej inteligencji (ang. Artificial Intelligence) są sztuczne sieci neuronowe. Ich ważną cechą jest możliwość manipulowania

obiektami z bazy zapisanych jako dyskretne struktury danych.

W przeprowadzonym eksperymencie wykorzystano sieć Kohonen-a [3], która została nazwana przez jego twórcę samoorganizującym odwzorowaniem (ang. Self-Organizing Map - SOM). W sieci tej mamy do czynienia z uczeniem konkurencyjnym. Oznacza to, że mamy do dyspozycji jedynie wzorce wejściowe, nie posiadamy natomiast żadnych wzorców wyjściowych. Zadaniem sieci w trakcie procesu uczenia jest wytworzenie takich wzorców oraz utworzenie takiej struktury, która w najlepszy sposób będzie odwzorowywała zależności w przestrzeni wektorów wejściowych. Dla sieci SOM przygotowano do przetwarzania danych wejściowych, którymi są współczynniki CWT obliczane tak jak w rozdziale 4. Schemat obrazowy sztucznej sieci samoorganizującej się przedstawiono na rys. 7. Przedstawia on liczbę 520 kanałów wejściowych oraz wyjście zawierające mapę 60 neuronów pozwalających reprezentować odwzorowanie cech danych wejściowych, a także sumator wag wejść układu.



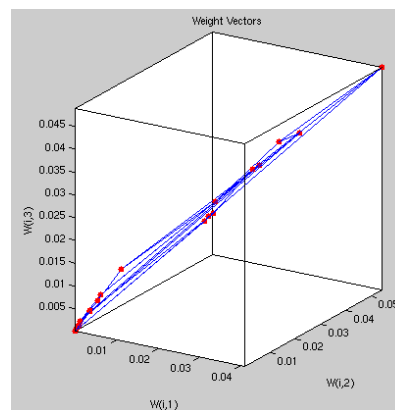
Rys. 7. Widok schematu sztucznej sieci samoorganizującej się

Niezależnie od mechanizmów uczenia sieci samoorganizujących się, ważną rolę odgrywa nadmiarowość (redundancja) danych uczących, bez której nie byłoby możliwe uczenie. Szerokie spektrum danych uczących zawierające wielokrotne powtórzenia podobnych wzorców stanowi "bazę wiedzy" dla sieci, z której za pomocą odpowiednich skojarzeń wyciągane są wnioski decyzyjne po przyłożeniu na wejście sieci określonego wzorca poddawanego klasyfikacji.

Wiadomo, że algorytm SOM równocześnie realizuje dwa zadania - wektorowej kwantyzacji (kompresja danych) oraz zadanie odtwarzania przestrzennej organizacji danych wejściowych.

Przeprowadzono testy dla trzech topologii sieci SOM. Trenowano takie struktury sieci jak heksagonalna (Hextop), prostokątna (GridTop) oraz losowa (Randtop).

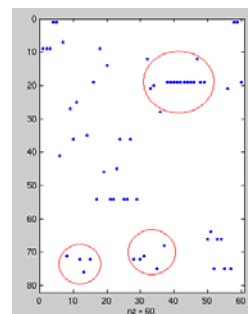
Na rys. 8 wykazano strukturę odległości pomiędzy otrzymanymi wagami neuronów. W tym przypadku nawet otrzymanie topologii sieci prostokątnej o zbliżonych odległościach wag neuronów była trudna. Objawiało się to wyłączeniem niektórych neuronów z rywalizacji o możliwość adaptacji swoich wag a przez co generowanie martwych bezużytecznych neuronów.



Rys. 8. Wyniki trenowania sieci SOM - wektory odległości wag neuronów

Porównując otrzymane wyniki w poszczególnych eksperymentach można zauważyć, że rozwój sieci neuronowej SOM przebiega w bardzo zróżnicowany sposób w zależności od przyjętych parametrów. W wyniku obserwacji trenowania sieci neuronowej możemy dojść do wniosku, iż na rezultaty uczenia główny mają wpływ: liczba i rodzaj parametrów wejściowych jak również parametry uczenia sieci takie jak ilość epok oraz funkcja odległości sąsiedztwa neuronów. Podobnie jak w rzeczywistym systemie zmiana parametrów pracy powoduje zmianę charakterystyki tak i przy trenowaniu sieci zmiana określonych wartości powoduje odmienny jej rozwój.

Faktem jest iż do tej pory nie zdefiniowano wzorców, które opisują w jednoznaczny sposób typowych wad w materiale poddanym badaniu. Ważne jest aby zbierać jak najwięcej danych, które m.in. udostępnia program UTracker przetwarzający dane z przetwornika i podający je na wejście sieci Kohonen-a. W obecnej fazie zdiagnozowano kilka płytek kompozytowych zawierających różne wady struktury. W wyniku samoorganizacji otrzymano różne rozmieszczenie cech wejść sieci neuronowej w przestrzeni dwuwymiarowej. Mapę zwycięskich neuronów dla blisko 80 pomiarów pokazano na rys.9.



Rys. 9. Mapa zwycięstw neuronów uzyskana w wyniku eksperymentu

5.1. Wnioski z symulacji SOM

Wprowadzając dane jako parametry wejściowe do sieci neuronowej samoorganizującej się SOM

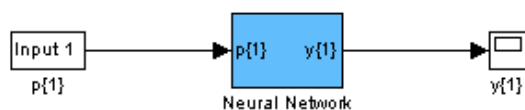
można zauważyć pewne występujące w nich prawidłowości. Okazało się, że system zachowuje się bardzo stabilnie z występowaniem regularnych map cech istotnych. Można zauważyć pewne obszary, w których powtarza się pewien schemat jak na Rys.9 występowania określonych grup parametrów.

Neurony zazwyczaj grupują się wokół innych neuronów zwycięzców. Jeśli pewne zdarzenie porządkujące ma miejsce [6], to warunkiem pojawienia się samoorganizacji jest, by oddziaływanie rozbijające porządek w systemie, było słabsze od porządkującego. W przeprowadzonych eksperymentach nie udało się uzyskać pełnej sprawności sieci.

6. SYMULACJA MODELU SYSTEMU USTRACKER W SIMULINK-U

Simulink jest programowym narzędziem do modelowania, symulacji i analizy systemów dynamicznych [4]. Program umożliwia budowanie modeli dla systemów liniowych, nieliniowych, ciągłych w czasie lub dyskretnych, mieszanych czyli dyskretno - ciągłych (hybrydowych) oraz dyskretnych ze zmiennym czasem próbkowania. Ważną zaletą programu jest jego interaktywność, co oznacza, że można zmieniać parametry układu podczas symulacji i na bieżąco obserwować rezultaty wprowadzanych zmian.

Model systemu USTracker wykonano w postaci hierarchicznego schematu blokowego, czyli graficznego. Schemat blokowy USTracker zawiera bloczki stanowiące wejście systemu odpowiedzialne za pobieranie danych oraz bloczki odpowiedzialne za przetwarzanie i wizualizację wyników. Jeden z podsystemów przetwarzających dane pokazano na Rys.10. Każdy z podsystemów zawiera jedno lub więcej wejść, wyjść oraz stanów.



Rys. 10. Schemat blokowy podsystemu dla sztucznej sieci neuronowej

Tak więc na potrzeby badań stworzono model systemu w Simulink-u podobny do programu analizującego USTracker. Jego głównym zadaniem jest możliwość tworzenia wymuszeń na wejściach systemu i obserwowanie jak zachowują się wyjście wzorcowe sztucznej sieci neuronowej. Symulacja tych wymuszeń przebiega z wykorzystaniem całkowania numerycznego. Wybór algorytmu symulacji zależy od zdolności modelu do obliczania pochodnych jego stanów ciągłych.

Obliczanie pochodnych składa się z dwóch etapów. Najpierw jest wyznaczany sygnał wyjściowy każdego bloczka, w kolejności wynikającej z sortowania przeprowadzonego

podczas etapu inicjalizacji. Następnie w każdym bloczku są obliczane wartości pochodnych na podstawie aktualnego czasu oraz wartości wejściowych i stanu bloczka. Powstały w ten sposób wektor pochodnych jest wprowadzany do algorytmu numerycznego, który jest używany do obliczenia nowego wektora stanu w następnym punkcie czasowym.

Powyższy system jest w fazie rozwojowej i jego zadaniem jest poprawa efektywności klasyfikacji wykrywanych wad w materiałach kompozytowych.

7. WNIOSKI

Metody komputerowego przetwarzania sygnałów ultradźwiękowych jakie przedstawiono w tym artykule pozwalają na dokładniejszą ocenę stanu struktury materiału kompozytowego. Ze względu na dużą różnorodność warunków badań ultradźwiękowych brak jest jakichkolwiek uniwersalnych wzorców oraz reguł regulujących ten obszar badań.

LITERATURA

- [1] Lee Fugal D. *Conceptual wavelets in digital signal processing*. San Diego, Space & Signals Technologies, 2006.
- [2] Stephane M. *A wavelet tour of signal processing*. San Diego, Academic Press, 1999.
- [3] Kohonen T. *Associative Memory: A System – Theoretical Approach*. Berlin, Springer – Verlag, 1982.
- [4] Brzózka J., Dobroczyński L. *Programowanie w Matlab*. Warszawa, Mikom, 1998.
- [5] Morse P. M., Ingard K. U. *Theoretical Acoustics*. New York, McGraw-Hill, 1968.
- [6] Osowski S. *Sieci neuronowemu w ujęciu algorytmicznym*. Warszawa, WNT, 1996.
- [7] Zimmer A.. *Identyfikacja obiektów i sygnałów - Teoria i praktyka dla użytkowników MATLABA*, Kraków, Politechnika Krakowska, 1998.



Marcin STARNACKI urodzony w 1980 r. w Siedlcach. Posiada tytuł magistra w dziedzinie projektowania sieci i systemów komputerowych. Pracownik PIT S.A. w Warszawie na stanowisku programisty. Od roku 2007 doktorant w Instytucie Badań Systemowych PAN w Warszawie. Od 2005 roku członek polskiej sekcji IEEE.

DIAGNOZOWANIE ZMIAN KLIMATU AKUSTYCZNEGO NA ODCINKU AUTOSTRADY A2 KOMORNIKI – KRZESINY

Małgorzata ORCZYK, Franciszek TOMASZEWSKI

Politechnika Poznańska, Instytut Silników Spalinowych i Transportu
Zakład Pojazdów Szynowych, 60-965 Poznań, ul. Piotrowo 3
fax: (061) 665-2204, Malgorzata.Orczyk@put.poznan.pl

Streszczenie

W artykule przedstawiono wyniki pomiarów oraz modelowania hałasu środowiska autostrady obwodnicy miasta Poznania, Komorniki – Krzesiny. Zaprezentowane rezultaty badań związane były z monitoringiem (diagnostowaniem) poziomu hałasu wokół autostrady, w miarę włączania do eksploatacji kolejnych odcinków płatnej autostrady A2. Badania podzielone zostały na trzy etapy. Na podstawie uzyskanych wyników badań przeanalizowano wpływ autostrady na klimat akustyczny sąsiadujących z nią terenów oraz opracowano model prognozowania hałasu wokół odcinka Komorniki – Krzesiny.

Słowa kluczowe: hałas drogowy, autostrada, klimat akustyczny.

DIAGNOSIS OF ACOUSTIC CLIMATE CHANGES AT A2 MOTORWAY DISTANCE FROM KOMORNIKI TO KRZESINY

Summary

The article presents the results of noise measurement investigated at the motorway ring road of Poznań at the distance from Komorniki to Krzesiny. The presented results of research dealt with monitoring (diagnosis) of the level of noise surrounding the motorway, as the following parts of payable A2 motorway were put into commission. The works were divided into three stages of research. On the basis of the received results of research, the influence of motorway on the acoustic climate of its surrounding areas was analyzed.

Keywords: traffic noise, motorway, acoustic climate.

1. WPROWADZENIE

Hałas stał się obecnie jednym z ważnych czynników decydujących o jakości życia w dużych aglomeracjach. Natężenie hałasu jego zmienność w czasie, pochodzenie i rodzaj, odniesione do charakteru rozpatrywanego obszaru określamy mianem klimatu akustycznego.

Problemy związane z zakłócaniem środowiska przez hałas komunikacyjny – szczególnie drogowy, nabierają aktualnie coraz większego znaczenia wobec stałej presji motoryzacji, wyrażającej się dynamicznym wzrostem liczby pojazdów. Szacuje się, że w Polsce liczba osób zagrożonych hałasem zawiera się pomiędzy 13 ÷ 15 milionów, a w porze dziennej średni równoważny poziom dźwięku w centrum miast wynosi około $L_{Aeq,dzień} = 72$ dB [4]. Przeprowadzony w 2005 r. generalny pomiar ruchu drogowego w Polsce wykazał, że średnio dobowy ruch pojazdów samochodowych na sieci dróg krajowych wynosił ponad 8 000 poj./dobę i był wyższy o około 18 % w porównaniu z badaniami przeprowadzonymi w 2000 r. [3]. Wzrost liczby poruszających się samochodów oprócz niewątpliwych problemów związanych z notowanymi wysokimi poziomami dźwięku

pociąga również problem braku w Polsce dróg o właściwym standardzie. Pod koniec 2001 r. Polska dysponowała siecią dróg krajowych o łącznej długości 18 036 km, z czego 398 km stanowiły autostrady i 206,2 km drogi ekspresowe, jedynie 7% dróg (346 km) spełniało wymogi Unii Europejskiej w zakresie dopuszczalnych nacisków 11,5 tony na oś [6]. Wobec powyższych przesłanek poprawa warunków drogowych stała się obecnie w Polsce jednym z priorytetowych zadań. Przyjęcie programu budowy autostrad i zamiar wybudowania na terenie Polski czterech płatnych autostrad o łącznej długości ponad 2000 km wiąże się z przeprowadzeniem oceny ich wpływu na środowisko. W przypadku hałasu konieczna jest ocena klimatu akustycznego przed uruchomieniem inwestycji oraz diagnostowanie poziomu dźwięku podczas jej eksploatacji.

2. OBIEKT BADAŃ

Autostradowa obwodnica miasta Poznania to odcinek o długości 13,3 km leżący w ciągu płatnej autostrady A2 Świecko – Kukuryki. Obwodnica Poznania, pomimo, iż jest częścią płatnej autostrady A2 dostępna jest dla użytkowników poprzez węzły: Komorniki, Dębina i Krzesiny – bez wnoszenia

opłat. Badany odcinek autostrady przechodzi w przeważającej części w głębokim wykopie (część zachodnia i środkowa) – wzdłuż terenów ogródków działkowych i terenów zabudowy mieszkaniowej wielorodzinnej, a także na nasypie i poziomie terenu – poprzez ujęcie wody pitnej Dębina i tereny rolnicze (część środkowa i wschodnia).

Ochrona klimatu akustycznego wokół omawianego odcinka autostrady zapewniona jest poprzez zieleń izolacyjną (ok. 150 tys. drzew i krzewów), wały przeciwhałasowe, 4 km ekranów akustycznych oraz wymianę w pobliskich domach ok. 520 m² okien na dźwiękoizolacyjne.

Obecnie udostępnionych jest do eksploatacji 5 odcinków tej autostrady o łącznej długości ponad 250 km:

- Września – Konin; 47,7 km,
- Obwodnica miasta Poznania; Komorniki – Krzesiny; 13,3 km,
- Września – Krzesiny; 37,5 km,
- Nowy Tomyśl – Komorniki; 50,4 km,
- Konin – Strzyków; 105 km.

3. METODYKA BADAŃ

Badania hałasu na autostradowej obwodnicy miasta Poznania prowadzono w oparciu o założenia eksperymentu czynno-biernego. Polegały one na pomiarze hałasu na odcinku Komorniki – Krzesiny w trzech kolejnych etapach eksploatacji płatnej autostrady A2 (w miarę włączania do ruchu nowych odcinków tej autostrady). Etap pierwszy badań dotyczył pomiaru hałasu, gdy odcinek Komorniki – Krzesiny nie był jeszcze oddany do eksploatacji (pomiar tła akustycznego). Etap drugi wiązał się z pomiarem hałasu po włączeniu do eksploatacji odcinka Września – Krzesiny a trzeci etap badań obejmował pomiar hałasu po włączeniu do ruchu odcinka Nowy Tomyśl – Komorniki.

Na odcinku obwodnicy miasta Poznania Komorniki – Krzesiny wybrano łącznie 23 punkty pomiarowe (rys. 1÷3), które znajdowały się w różnych miejscach otoczenia autostrady:

- 16 punktów na osiedlach w pobliżu, których przebiega autostrada,
- 3 punkty w węzłach autostradowych,
- 4 punkty, które uwzględniały różną głębokość wykopu.

Punkty na osiedlach zostały wybrane na podstawie wskazanych w dokumentacji technicznej autostrady jako miejsca szczególnie zagrożone hałasem. Punkty w węzłach autostradowych (Komorniki, Dębina, Krzesiny) były wybrane w celu oceny rzeczywistego poziomu dźwięku przy jezdni autostradowej i węzłach o potencjalnym wysokim poziomie hałasu związanym ze zmianą parametrów ruchu pojazdów. Punkty na różnych głębokościach wykopu wybrano, ze względu na opracowanie modelu, umożliwiającego prognozowanie hałasu w środowisku autostrady, przy takim jej usytuowaniu.

Ogólnie przyjęto lokalizację punktów pomiarowych na osiedlach w pobliżu, których przebiega autostrada zgodnie z zaleceniami Polskiej Normy PN-ISO 1996-1 w odległości 1 m od płotu posesji lub ściany zewnętrznej budynku na wysokości 1,2÷1,5 m od powierzchni gruntu. W przypadku pomiarów, które uwzględniały różną głębokość wykopu badania prowadzono według następującego algorytmu: pomiar pierwszy w odległości 1 m od krawędzi jezdni autostrady, pomiar drugi 1 m od krawędzi skarpy, kolejne punkty pomiarowe były oddalane od pasa rozdziału pomiędzy jezdniami autostrady i zawierały się w przedziale od 10 m do 100 m. Do badań wybrano trzy głębokości wykopu (usytuowania autostrady): 2,5 m, 4,3 m i 7,1 m. Uzyskane w ten sposób wyniki pomiarów stanowiły podstawę do opracowania modeli hałasu w środowisku.

Pomiary hałasu na autostradzie wykonano całkującym miernikiem poziomu dźwięku typu 2238 MediatorTM firmy Brüel & Kjær [1, 5, 7].

4. ANALIZA WYNIKÓW BADAŃ

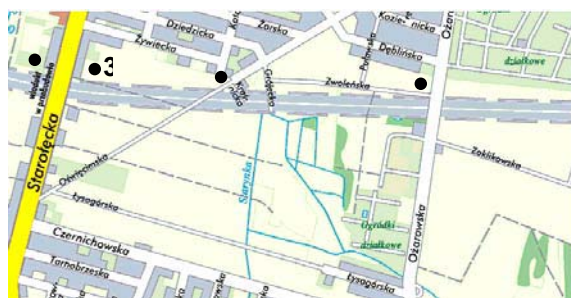
W pracy przedstawiono wyniki analizy pomiarów hałasu na autostradzie w wybranych punktach pomiarowych podczas trzech etapów badań. Punkty te zaznaczono na mapkach fragmentów autostrady zamieszczonych na rysunkach 1÷3.



Rys. 1. Punkty pomiarowe znajdujące się w obrębie węzła Komorniki



Rys. 2. Punkty pomiarowe znajdujące się w obrębie węzła Dębina



Rys. 3. Punkty pomiarowe na osiedlu Poznań – Starołęka

Po zakończeniu każdego z etapów badań obliczono na podstawie uzyskanych wyników dla każdego punktu pomiarowego zgodnie z zaleceniami rozporządzenia Ministra Środowiska z dnia 2.10.2007 r, w sprawie wymagań w zakresie prowadzenia pomiarów poziomów w środowisku substancji lub energii przez zarządzającego drogą, linią kolejową, linią tramwajową, lotniskiem, portem średni równoważny poziom dźwięku, który odpowiadał 16-godzinom dnia.

Na podstawie uzyskanych wyników pomiarów w pierwszym etapie badań (pomiar tła akustycznego) ustalono dla całego odcinka Komorniki – Krzesiny poziom tła akustycznego wynoszący $L_{Aeq,TLA} = 51$ dB.

W tabelach 1÷3 zestawiono przykładowe wyniki pomiarów hałasu z trzech etapów badań na odcinku autostrady A2 Komorniki – Krzesiny. W tabeli 1 zestawiono wyniki pomiarów uzyskanych dla głębokości wykopu $h = 4,30$ m, tabela 2 zawiera wyniki dotyczące pomiarów hałasu w węźle autostradowym Dębina, a tabela 3 odnosi się do pomiarów wykonanych na osiedlu mieszczącym się w pobliżu autostrady.

Tabela 1. Wyniki pomiarów hałasu dla głębokości wykopu $h = 4,30$ m

Okres badań	Etap badań	Poziomy dźwięku L_{Aeq} odpowiadające różnym położeniom punktów pomiarowych				
		jezd- nia	ska- rpa	22 m	37 m	100 m
I okres	I etap	46	48	49	51	47
	II etap	74	70	57	55	49
	III etap	80	74	60	60	53
II okres	I etap	48	55	54	55	57
	II etap	75	69	60	55	54
	III etap	79	74	63	59	53
III okres	I etap	48	55	54	55	50
	II etap	71	62	56	53	50
	III etap	78	73	62	59	53
$L_{Aeq,16T}$	I etap	47	54	52	54	53
	II etap	73	68	58	54	52
	III etap	79	74	61	59	53

Tabela 2. Wyniki pomiaru hałasu L_{Aeq} w węźle Dębina

Etap badań	Okresy pomiarowe			$L_{Aeq,16h}$
	I okres	II okres	III okres	
I etap	45	45	50	46
II etap	74	74	74	74
III etap	77	78	77	77

Tabela 3. Wyniki pomiarów hałasu L_{Aeq} na osiedlu

Etap badań	Okresy pomiarowe			$L_{Aeq,16h}$
	I okres	II okres	III okres	
I etap	48	49	49	48
II etap	58	55	53	56
III etap	58	55	57	57

5. MODELOWANIE HAŁASU W ŚRODOWISKU AUTOSTRADY

Punktem wyjścia do opracowania modelu były zmierzone w trzech etapach badań równoważne poziomy dźwięku w różnych odległościach od jezdni autostrady. Opracowany model dotyczy przypadku, w którym jezdnia autostrady przebiega w wykopie. Dla modelu przyjęto następujące założenia:

- pojazdy poruszają się po prostym odcinku drogi w jednym kierunku, ze stałą prędkością,
- w modelu nie uwzględnia się podziału na pojazdy osobowe i ciężarowe,
- odległości poszczególnych odcinków pomiarowych r_1, r_2, \dots, r_n dobierano licząc od skraju skarpy, tak aby długość ostatniego odcinka r_n wynosiła 100 m od autostrady. Ma to związek z tym, że przy odległościach większych od 100 m zaczynają odgrywać rolę zjawiska związane ze stanem atmosfery tj. pochłanianie dźwięku przez powietrze, rozpraszanie na turbulencjach i refrakcja spowodowana wiatrem i gradientem temperatury [2],
- w każdej przyjętej odległości r_n uwzględniono także głębokość wykopu w którym przebiega jezdnia autostrady,
- elementami wejściowymi modelu są następujące parametry: natężenie ruchu będące sumą wszystkich pojazdów, które przejechały przez autostradę w danej godzinie w obu kierunkach Q [poj/godz] i odległość od jezdni autostrady r [m].

Dla opracowywanego modelu przyjęto założenia klasycznego modelu regresji. Było to podyktowane faktem, że prognozowana wartość równoważnego poziomu dźwięku miała zależeć od następujących parametrów: natężenia ruchu na autostradzie i odległości od jezdni autostrady. Po sprawdzeniu poprawności i adekwatności danych użytych do budowy modelu zależność ogólna według, której prognozuje się hałas na autostradzie przyjęła postać:

$$L_{Aeq}(Q, r) = \beta_3 \log_{10} + \beta_1 \log(r+1) + \beta_2 \log(Q+1)$$

gdzie:

$L_{Aeq}(Q, r)$ – równoważny poziom dźwięku zależny od natężenia ruchu na autostradzie i odległości od autostrady,

β_1 – współczynnik związany z odległością od źródła dźwięku,

β_2 – współczynnik związany z natężeniem ruchu,

β_3 – wyraz wolny równania regresji,

Q – natężenie ruchu na autostradzie [poj./godz.],

r – odległość od autostrady [m].

Do wyznaczenia współczynników regresji wielokrotnej i związanych z tym statystyki regresji oraz analizy wariancji wykorzystano aplikację Microsoft Excel. Model umożliwiający prognozowanie poziomów dźwięku w środowisku autostrady A2 na odcinku Komorniki – Krzesiny ostatecznie przyjął postać:

$$L_{Aeq}(Q, r) = 10,13 \cdot \log(Q+1) - 16,46 \cdot \log(r+1) + 52,93$$

gdzie:

Q – natężenie ruchu na autostradzie [poj./godz.],

r – odległość od autostrady [m].

Mając wyznaczone na podstawie danych eksperymentalnych, współczynniki regresji β_1 , β_2 , β_3 oraz zweryfikowane hipotezy dotyczące wpływu zmiennych na zmienną zależną wykonano weryfikację modelu. W losowo wybranych dniach i godzinach dokonano pomiarów hałasu w różnych odległościach od autostrady. Dla danego dnia i godziny pomiarów hałasu dokonano odczytu z liczników autostradowych liczbę przejeżdżających samochodów przez odcinek autostrady Komorniki – Krzesiny. Uzyskane dane o natężeniu ruchu podstawiono do modelu i dokonano szacowania hałasu dla określonych warunków (głębokości wykopu i odległości). W tabeli 4 przedstawiono wybraną weryfikację opracowanego modelu z rzeczywistymi pomiarami hałasu przeprowadzonymi na autostradzie dla głębokości wykopu $h = 2,85$ m.

Tabela 4. Porównanie wyników pomiarów z wynikami uzyskanymi z modelu dla głębokości $h = 2,85$ m

Natężenie ruchu Q [poj./godz]	Odległość [m]	Pomiary [dB]	Model [dB]	Błąd wzgl. aprosymacji
822	1	76	78	2%
	8	73	67	8%
	32	59	58	2%
	37	58	57	3%
	62	57	53	7%
	100	53	49	7%
1589	1	78	80	3%
	8	76	70	8%
	32	58	60	4%
	37	56	59	6%
	62	54	56	3%
	100	55	52	5%

6. PODSUMOWANIE

Wykonane pomiary hałasu na odcinku autostrady A2 Komorniki – Krzesiny wykazały, że uruchomienie omawianego odcinka autostrady spowodowało wzrost równoważnego poziomu dźwięku przy jezdni o około 30 dB a przy krawędzi wykopu o około 20 dB w stosunku do pomiarów wykonanych w pierwszym etapie badań.

Rozpatrując wpływ autostrady A2 na klimat akustyczny osiedli położonych wzdłuż odcinka Komorniki – Krzesiny stwierdzono, że zmierzone w trzech etapach pomiarowych równoważne poziomy dźwięku na osiedlach nie przekroczyły w ciągu dnia poziomu 60 dB. Otwarcie autostrady spowodowało wzrost równoważnego poziomu dźwięku na osiedlach znajdujących się w odległości 100 m od autostrady o około 8 dB w stosunku do pomiarów wykonanych w pierwszym etapie pomiarowym (pomiar tła akustycznego autostrady).

Weryfikacja opracowanego modelu wykazała, że błąd względny aproksymacji szacowania poziomu dźwięku na omawianym odcinku autostrady nie przekracza 10%. Opracowany model można stosować do szacowania poziomu hałasu w otoczeniu autostrady.

LITERATURA

1. Akustyka *Opis i pomiary hałasu środowiskowego. Podstawowe wielkości i procedury*. Polska Norma PN-ISO 1996-1.
2. Embelton T. F. W.: *Tutorial on sound propagation outdoors*. Journal of the Acoustical Society of America, 1996, nr 100(1), s. 31 – 48.
3. Generalna Dyrekcja Dróg Krajowych i Autostrad. *Generalny pomiar ruchu 2005. Synteza wyników*. Komunikat internetowy: www.gddkia.gov.pl, kwiecień 2006.
4. Kucharski R. J., Chyla A., Koszarny Z., Kraszewski M., Szymański Z., Sakowska P., Taras A.: *Stan klimatu akustycznego w kraju w świetle badań WIOŚ*. Biblioteka Monitoringu Środowiska, Warszawa 2002.
5. Orczyk M.: *Analiza i ocena wpływu natężenia ruchu drogowego na poziom hałasu w otoczeniu autostrady A2 na odcinku Komorniki – Krzesiny*. Praca doktorska, Politechnika Poznańska, Poznań 2007.
6. Raport z realizacji Programu Budowy Dróg Krajowych i Autostrad. Biuletyn Informacyjny Drogownictwa. Warszawa 2004.
7. Rozporządzenie Ministra Środowiska z dnia 23 stycznia 2003 roku w sprawie Wymagań w zakresie prowadzenia pomiarów poziomów w środowisku substancji lub energii przez zarządzającego drogą linią kolejową, linią tramwajową, lotniskiem, portem. Dz. U. 2003 nr 35 poz. 308.

**SPRAWOZDANIE
Z VII KRAJOWEJ KONFERENCJI
DIAG'2009
"DIAGNOSTYKA TECHNICZNA URZĄDZEŃ
I SYSTEMÓW"**

W dniach 19 ÷ 23 października 2009 r., w ORW „Muflon” w Ustroniu, odbyła się VII Krajowa Konferencja **DIAG'2009**.

Organizatorem konferencji był – podobnie jak wszystkich wcześniejszych – Instytut Systemów Elektronicznych Wydziału Elektroniki Wojskowej Akademii Technicznej, a stowarzyszeniami wspierającymi – także tradycyjnie: Polskie Towarzystwo Diagnostyki Technicznej oraz Zespół Diagnostyki Sekcji Podstaw Eksploatacji Komitetu Budowy Maszyn PAN. Patronat nad tegoroczną konferencją sprawował Naczelny Metrolog Wojska Polskiego.

Prace organizacyjne realizował zespół pod kierunkiem przewodniczącego Komitetu Naukowego DIAG'2009 dr. hab. inż. Tadeusza Dąbrowskiego, sekretarza Komitetu Naukowego dr. inż. Krzysztofa Kwiatosa oraz przewodniczącego Komitetu Organizacyjnego mgr. inż. Romana Wrony.

Komitet Naukowy konferencji – pod przewodnictwem Honorowych Przewodniczących w osobach: prof. Lesław Będkowski (WAT), prof. Czesław Cempel (PPoz.) i prof. Zbigniew Engel (AGH) – stanowił elitarny zespół pracowników naukowych reprezentujących wszystkie ważniejsze krajowe ośrodki zajmujące się badaniami, nauczaniem i stosowaniem diagnostyki technicznej w praktyce eksploatacyjnej.

Charakter i zasięg terytorialno-naukowy konferencji opisują poniższe dane.

1. Liczba nadesłanych referatów: **45**, liczba wygłoszonych referatów: **38**.
2. Rozkład nadesłanych referatów w aspekcie wyróżnionych obszarów tematycznych (tab.1).

Materiały konferencyjne zostały wydane w postaci tomu o objętości 230 str.

Nadesłane referaty poddane zostały recenzowaniu przez członków Komitetu Naukowego – i w przypadku pozytywnej recenzji – są kierowane do druku w postaci artykułów w periodykach naukowych: „Przegląd Elektrotechniczny” oraz „Biuletyn WAT”.

Konferencja DIAG'2009 pozwoliła uczestnikom wymienić aktualne doświadczenia i informacje w sferze badań i osiągnięć naukowych oraz w sferze praktyki eksploatacyjnej.

W trakcie dyskusji „okrągłego stołu” zwrócono uwagę na pilną potrzebę włączenia do obszaru badań diagnostyczno-eksploatacyjnych problematyki metod i narzędzi diagnozowania operatorów obiektów

technicznych. Z naciskiem podkreślano, że tylko systemowe ujęcie procesów diagnozowania (dozorowania) stwarza możliwość racjonalnej eksploatacji współczesnych, na ogół znacznie zelektronizowanych i z informatyzowanych, obiektów i systemów.

Uczestnicy konferencji powszechnie wyrażali uznanie Organizatorom za dobrą organizację, miłą atmosferę i atrakcyjne imprezy towarzyszące w postaci wycieczki do pałacu w Pszczynie oraz uroczystej kolacji o charakterze integracyjnym.

Tabela 1.

Lp	Nazwa obszaru	Udział referatów w [%]
1	Metody i narzędzia pomiarowo-diagnostyczne	36
2	Komputerowe wspomaganie procedur pomiarowo-diagnostycznych	11
3	Metody i narzędzia techniczne w diagnostyce medycznej	2
4	Diagnostyka bezpieczeństwa systemów antropotechnicznych	15
5	Diagnostyka projektowo-wytwórcza	7
6	Diagnostyka eksploatacyjna	29
	<i>Suma</i>	100



Foto 1. Przedstawiciele Komitetu Organizacyjnego w oczekiwaniu na uczestników konferencji:
Od lewej: Roman Wrona, Amelia Chocholska,
Ewa Budna

3. Statystyka uczestników DIAG'2009 w aspekcie geograficznym (tab.2)

Tabela 2.

MIEJSCOWOŚĆ	INSTYTUCJA	LICZBA UCZESTNIKÓW z instytucji	LICZBA UCZESTNIKÓW z miejscowości
Gdańsk	Wyższa Szkoła Bankowa	1	2
	Politechnika Gdańska	1	
Gdynia	Akademia Marynarki Wojennej	1	2
	Akademia Morska	1	
Katowice	Politechnika Śląska	6	6
Kielce	Politechnika Świętokrzyska	1	1
Kraków	Akademia Górniczo-Hutnicza	9	11
	EC Test Systems Sp. z o.o.	2	
Mikołów	GEDORE Polska Sp. z o.o.	2	2
Olsztyn	Uniwersytet Warmińsko-Mazurski	4	4
Piła	Wojewódzki Ośrodek Ruch Drogowego	2	2
Radom	Politechnika Radomska	1	1
Rzeszów	Politechnika Rzeszowska	1	1
Szczecin	Politechnika Szczecińska	1	1
Warszawa	Instytut Techniczny Wojsk Lotniczych	4	39
	Politechnika Warszawska	6	
	Wojskowa Akademia Techniczna	24	
	Wojskowe Centrum Metrologii	3	
	Wyższa Szkoła Technologii Informat.	2	
Wrocław	Politechnika Wrocławska	1	1
Ukraina - Lwów	Politechnika Lwowska	2	2
RAZEM		75	75



Foto 2. Widok sali obrad

W imieniu Komitetu Naukowego
Przewodniczący

dr hab. inż. Tadeusz Dąbrowski
prof. nadzw. WAT



Piotr DEUSZKIEWICZ
Stanisław DOBROCIŃSKI
Jacek DZIUDŹ
Leszek FLIS
Andrzej GRZĄDZIELA
Radosław PAKOWSKI
Cezary SPECHT

*Diagnostyka
wibroakustyczna
okrętowych turbinowych
silników spalinowych*

ITE Radom – 2009

Zadania stawiane okrętom wojennym wymagają stałej gotowości siłowni do uruchomienia oraz długotrwałej pracy w ekstremalnych warunkach środowiskowych. Konstrukcje okrętowych układów napędowych (OUN) powinny ponadto utrzymać zdolność do ruchu w warunkach bojowych, przy powstaniu uszkodzeń będących efektem oddziaływania środków walki przeciwnika. Oznacza to konieczność wdrożenia systemów diagnozowania *on-line* i *off-line* OUN jako trwałego elementu obrony przeciwwarjacyjnej okrętu. Możliwość prognozowania zmian stanu technicznego podstawowych elementów OUN pozwala na podjęcie szybkiej i optymalnej decyzji eksploatacyjnej, co w przypadku działań na morskim obszarze przekłada się na utrzymanie zdolności bojowej okrętu.

Książka zawiera 10 rozdziałów dotyczących metodyki diagnozowania okrętowych turbinowych silników spalinowych z wykorzystaniem metod wibroakustycznych. Po krótkim wprowadzeniu Czytelnika w poruszaną w monografii tematykę oraz charakterystyce obiektu badań, Autorzy przedstawiają w sposób syntetyczny informacje dotyczące obecnie stosowanych drganiowych metod diagnostycznych. W rozdziale tym, Autorzy charakteryzują zakres stosowalności metod pomiarowych typu *free – run* jak i z wykorzystaniem synchronizmu sygnałów. W rozdziale 3 przedstawiono metodę przygotowania i wykorzystania w diagnostyce technicznej charakterystyk drganiowych zarówno w stanach ustalonych jak i nieustalonych. Zaproponowano metody pozyskiwania wiedzy o układzie wirnikowym silnika turbinowego z zastosowaniem badań podczas wybiegu silnika oraz jego zimnego rozruchu. Kolejny rozdział przedstawia wyniki badań pilotażowych na modelu laboratoryjnym symulującym wirnik silnika turbinowego. Analiza porównawcza wyników modelowania w MES oraz pomiarów z wykorzystaniem młotka modalnego zidentyfikowała przyjęty model, pozwoliła określić błędy modelowania a w konsekwencji umożliwiła przygotowanie metodyki badań na obiekcie

rzeczywistym. W rozdziale 5 przedstawiono propozycję modelu diagnostycznego układu wirnikowego silnika turbinowego, zaś w rozdziale 6 przeprowadzono identyfikację modelu. Badania identyfikacyjne przeprowadzono z założeniem konieczności uzyskania zgodności symptomów drganiowych w dziedzinie częstotliwości oraz amplitud. Ze względu na przyjęte uproszczenia wprowadzono do modelu transmitancję mechaniczną, która w zakresie prędkości eksploatacyjnych wirnika dopasowywała model do wartości symptomów pozyskiwanych z obiektu rzeczywistego. Kolejny rozdział książki przedstawia wykorzystanie MES do określenia postaci drgań własnych całego wirnika jako jego podstawowych elementów. Rozdział 8 prezentuje bazę danych parametrów drganiowych dla systemu monitoringu typu *on-line*. Autorzy do tego celu wykorzystali wyniki wieloletnich badań realizowanych w trybie *off-line* oraz wyniki pomiarów pilotażowych wykonanych zgodnie z przyjętą w książce metodyką. W rozdziale 9 zaproponowano metodykę sterowania eksploatacją okrętowych układów napędowych z turbinowymi silnikami spalinowymi eksploatowanymi w Marynarce Wojennej RP. Diagnostykę wibroakustyczną umieszczono w szerokim zbiorze dysponowanych metod diagnostycznych jako przydatny element w diagnozowaniu wielosymptomowym. Rozdział 10 przedstawia analizę możliwości opisu matematycznego dynamiki okrętowego układu napędowego z turbinowymi silnikami spalinowymi typu LM 2500. Prezentowane wyniki badań z wykorzystaniem typowej aparatury badawczej wspomaganą przez system GPS umożliwiają określenie charakterystyk okrętowych układów napędowych w procesie akceleracji i deceleracji.

Warto podkreślić, że zawartość książki w zdecydowanej większości oparta jest na oryginalnych wynikach modelowania oraz pomiarów przeprowadzonych na poligonach morskich. Zaprezentowana identyfikacja uzyskanych modeli uwiarygodnia wyniki badań, co podnosi wartość książki i czyni ją jeszcze bardziej atrakcyjną dla czytelnika. Należy podkreślić, że prezentowane w książce wyniki prac zostały wdrożone do systemu diagnozowania okrętowych turbinowych silników spalinowych eksploatowanych na okrętach Marynarki Wojennej i stanowią istotny element obecnie realizowanej polityki eksploatacyjnej.

Diagnostyka

Obszar zainteresowania czasopisma to:

- ogólna teoria diagnostyki technicznej
- eksperymentalne badania diagnostyczne procesów i obiektów technicznych;
- modele analityczne, symptomowe, symulacyjne obiektów technicznych;
- algorytmy, metody i urządzenia diagnozowania, prognozowania i genezowania stanów obiektów technicznych;
- metody detekcji, lokalizacji i identyfikacji uszkodzeń obiektów technicznych;
- sztuczna inteligencja w diagnostyce: sieci neuronowe, systemy rozmyte, algorytmy genetyczne, systemy ekspertowe;
- diagnostyka energetyczna systemów technicznych;
- diagnostyka systemów mechatronicznych i antropotechnicznych;
- diagnostyka procesów przemysłowych;
- diagnostyczne systemy utrzymania ruchu maszyn;
- ekonomiczne aspekty zastosowania diagnostyki technicznej;
- analiza i przetwarzanie sygnałów.

Topics discussed in the journal:

- General theory of the technical diagnostics,
- Experimental diagnostic research of processes, objects and systems,
- Analytical, symptom and simulation models of technical objects,
- Algorithms, methods and devices for diagnosing, prognosis and genesis of condition of technical objects,
- Methods for detection, localization and identification of damages of technical objects,
- Artificial intelligence in diagnostics, neural nets, fuzzy systems, genetic algorithms, expert systems,
- Power energy diagnostics of technical systems,
- Diagnostics of mechatronic and antropotechnic systems,
- Diagnostics of industrial processes,
- Diagnostic systems of machine maintenance,
- Economic aspects of technical diagnostics,
- Analysis and signal processing.

Wszystkie opublikowane artykuły uzyskały pozytywne recenzje wykonane przez niezależnych recenzentów.

All the published papers were reviewed positively by the independent reviewers.

Druk:

Centrum Graficzne „GRYF”, ul. Pieniężnego 13/2, 10-003 Olsztyn, tel. / fax: 089-527-24-30

Oprawa:

Zakład Poligraficzny, UWM Olsztyn, ul. Heweliusza 3, 10-724 Olsztyn
tel. 089-523-45-06, fax: 089-523-47-37



Dynamique des Systèmes, des Matériaux
et des Structures

22 - 24 Mars 2010, Djerba - TUNISIE



www.impact2010.ec-lyon.fr



XXXVII

**Ogólnopolskie Sympozjum
DIAGNOSTYKA MASZYN**

Wisa 08.03. ÷ 13.03.2010 r.

organizatorzy:

Wydział Transportu Politechniki Śląskiej

Polskie Towarzystwo Diagnostyki Technicznej

Zespół Diagnostyki Sekcji Podstaw
Eksploatacji KBM PAN

KOMUNIKAT NR 2

e-mail: diagmasz@polsl.pl

Wszystkie opublikowane w czasopiśmie artykuły uzyskały pozytywne recenzje, wykonane przez niezależnych recenzentów.

Redakcja zastrzega sobie prawo korekty nadesłanych artykułów.

Kolejność umieszczenia prac w czasopiśmie zależy od terminu ich nadesłania i otrzymania ostatecznej, pozytywnej recenzji.

Wytyczne do publikowania w DIAGNOSTYCE można znaleźć na stronie internetowej:

<http://www.uwm.edu.pl/wnt/diagnostyka>

Redakcja informuje, że istnieje możliwość zamieszczania w DIAGNOSTYCE ogłoszeń i reklam.

Jednocześnie prosimy czytelników o nadsyłanie uwag i propozycji dotyczących formy i treści naszego czasopisma.

Zachęcamy również wszystkich do czynnego udziału w jego kształtowaniu poprzez nadsyłanie własnych opracowań związanych z problematyką diagnostyki technicznej. Zwracamy się z prośbą o nadsyłanie informacji o wydanych własnych pracach nt. diagnostyki technicznej oraz innych pracach wartych przeczytania, dostępnych zarówno w kraju jak i zagranicą.